UNIVERSITÁ DEGLI STUDI DI MESSINA

DIPARTIMENTO DI INGEGNERIA

Dottorato di Ricerca in

"Ingegneria e Chimica dei Materiali e delle Costruzioni"

XXIX ciclo

Catalytic Hydrogenations for Energy Applications and Chemical Productions

Processi di Idrogenazione per Applicazioni Energetiche e Produzione di Chemicals

Tutor: Prof. Gabriele Centi

Co-Tutor: Dr. Salvatore Abate

PhD Student: Gianfranco Giorgianni

ANNO ACCADEMICO 2015-2016

PhD Director: Prof Signorino Galvagno

Table of Contents

Figures

Tables

Preface

Hydrogenation reactions are one of the most widespread class of reactions in industrial chemistry. This field is huge and plenty of articles, reviews and books have been written about this topic. In this thesis three relevant examples of hydrogenation reactions have been discussed, namely:

- The direct synthesis of H_2O_2 from the elements
- The hydrodeoxygenation and hydrocracking of microalgae oils finalised to the production of green diesel and jet fuel
- The hydrogenation of furfural to 2-methylfuran

All these reactions have been conducted in liquid phase, in presence of a solvent by using several kinds of reactors. This thesis was divided into four chapters by topic. Each chapter can be read independently from each other and was written in the form of a self-standing article.

In the first chapter, hydrogenation reactions have been discussed in general, focusing mainly on hydrogenation in presence of a solvent. Furthermore, various reactor design alternatives widely used in the industry and novel reactor concepts for conducting hydrogenation reactions in multiphase systems have been discussed, focusing specifically on slurry reactors and catalytic membrane reactors, in line with the objectives of this work.

The second chapter was completely devoted to the direct synthesis of H_2O_2 by using a catalytic membrane reactor (catalytic diffuser / contactor concept). In the case of the direct synthesis of H_2O_2, catalytic membrane reactors together with microreactors have been recently proposed for their intrinsically safe features, which as will be discussed in the first chapter, is particularly advantageous for conducting highly exothermic reactions in the presence of possible runaway phenomena or even in the presence of explosive mixtures. In this study, several procedures for preparing catalytic membranes have been reported. The sol-immobilization technique, in line with the literature, has been identified as one of most interesting procedures for maximising Pd dispersion and achieving high selectivity. However, severe deactivation phenomena limit its use. Furthermore, the effect of the calcination has been analysed and correlated to an increase in selectivity. Therefore, the main focus of this chapter are: 1) understanding the role of the size of Pd nanoparticles (NPs), 2) the nature of the active sites and their redox behavior, 3) the promotion effect of polyvinyl alcohol (PVA), used as a capping agent in the sol-immobilisation technique (SI) for obtaining colloidal Pd NPs and 4) on the deactivation mechanism of the catalysts prepared by SI. All these phenomena were studied by using several original kinetic models and supported by several characterization techniques. Specifically, the first objective of this study is filling the gap in the literature between researchers reporting oxidised palladium as more active and selective and researcher reporting metallic palladium as the only active site. The second goal of this study is getting further insights into the promotion effect of PVA on the mechanism of the direct synthesis and its leaching correlated to the deactivation of the catalyst and loss of its promotion effect. Part of this chapter has been already published, while the other part will be presented for the first time.

The third chapter was devoted to the hydrodeoxygenation/hydrocracking of microalgae oils by using hierarchical based zeolite systems. In this chapter, the better performances of mesoporous Ni-based

zeolite catalysts were demonstrated for the conversion of methyl palmitate, used as a model compound, to biofuels in the jet fuel fraction. Furthermore, the role of the proper design of the catalysts for conducting this kind of reactions is evidenced and some conclusions about the mechanism of the early stages of reactions have been provided. Part of this chapter has already been published and presented at the 2nd international conference on biomass (IConBM2016) held in Taormina, Italy, in 2016.

The fourth chapter is about the hydrogenation of furfural to 2-methylfuran, recently identified as a potential high-quality biofuel for its high research octane number, energy density and low miscibility with water. Currently, 2-methylfuran is mainly produced as a by-product in the hydrogenation of furfural to furfuryl alcohol. Its industrial production, however, is not sufficient for meeting a possible increase in the demand for its use as a biofuel. Therefore, the main aim of this research was finding a good catalyst for obtaining, selectively, 2-methylfuran. However, most of the products potentially obtainable from the hydrogenation of furfural by using multifunctional catalysts are highly valuable. Therefore, the interested reader can take full advantage of this chapter for getting a concise idea about the chemistry of the hydrogenation of furfural. The latter has been recently identified as a high-value platform molecule for producing several useful compounds used as intermediate, solvents and so on. This reaction, in the literature, has been mostly studied in the gas phase by using several catalysts, mostly homemade. However, deactivation phenomena in the gas phase are often important. Using a solvent, therefore, could be a useful mean for improving the catalyst life. Furthermore, as widely reported in the literature, using a solvent is the most powerful tool for tuning the selectivity in multistep reactions. Therefore, the effect of three solvents was evaluated. In addition, to achieve a comprehensive view of the furfural hydrogenation chemistry with respect to different active metals, the effect of several catalysts has been evaluated at 60, 120 and 180 °C, keeping the H_2 pressure and catalyst amount constants. For achieving this objective, the reaction has been evaluated by using a high throughput approach by using several mini-batch reactors operating with the catalyst in slurry phase. The effect of the metals has been discussed, and the effect of the solvent correlated to its thermodynamic properties in relation to the substrates/intermediates/products to be hydrogenated. The content of this chapter has not been published yet.

Potentially useful catalysts for the industrial exploitation of this reaction has been found and also the effect of several promoters has been evaluated. The patentability of these systems is still being evaluated. Therefore, in this case, only a small selection of the obtained results will be presented and discussed.

Acknowledgements

First of all, I would like to express my sincere gratitude to my tutor Prof. Gabriele Centi for his support, comments and for giving me this great opportunity.

In particular, I would like to express my sincere gratitude to Dr. Salvatore Abate for his great enthusiasm, support, motivational guidance, instructional comments and for believing in my potential. Without his mentoring experience, this research would not have been like this.

My sincere thanks also go to all the people in Avantium who welcomed me in The Netherlands. More specifically, Dr. Jan Kees Wan der Waals who mentored me and to Dr. Robert-Jan van Putten for checking the manuscript, Paula Claassens-Dekker for helping to organize the experimental activity, and finally Imko Juffermans and the whole analytical team for their professional support.

Furthermore, there are many people to whom I am greatly indebted and which have been precious for completing this work. Among these people: Prof. Siglinda Perathoner, Antonio Troia, Giuseppe Romeo, Giuseppe Italiano, Katia Barbera and Paola Lanzafame.

I would also like to thank all my old and new friends for supporting me and for the pleasant time spent together, namely, Giorgia Papanikolaou, Giovanni Sidoti, Mariarita Santoro, Serena Gentiluomo, Chiara Genovese, Roberto Pizzi, Carlo Angelici and Jorge Bueno Moròn.

Special thanks go to my family and my sister for motivating me to do my best and for their sincere support and help.

Finally I want to acknowledge the National Interuniversity Consortium of Materials Science and Technology (INSTM) by which my PhD was financed, the European Union (Integration of Nanoreactor and multisite CAtalysis for a Sustainable chemical production “INCAS”, FP7-NMP-2009-LARGE-3 and the BIOpolymers and BIOfuels from FURan based building blocks “BIOFUR”, FP7-PEOPLE-2012-IAPP) and the Italian government (Innovative downstream processing of conversion of algal biomass for the production of jet fuel and green diesel, prot. 2010H7PXLC) for financing these researches.

This work is dedicated to my family

which supported me in this adventure with love

“Imagination is more important than knowledge.

Knowledge is limited.

Imagination encircles the world.”

Albert Einstein, What Life Means to Einstein (1929)

Chapter 1
Hydrogenations Generalities: Chemistry, Catalysis and Rector Engineering Concepts

1. Introduction

Hydrogen is one of the most important chemicals produced in the chemical industry. Its presence on the earth crust as an element is very widespread. However, it is mostly present in its oxidised form. Molecular hydrogen conversely is present in the atmosphere only at a very low concentration (0.1 ppm) [1]. Therefore, for exploiting hydrogen as a chemical, its production is of paramount importance. This increased interest in hydrogen has speeded up the development of technologies for its production, e.g. electrolyzers, solar thermal cycles, and for its efficient use both as a fuel and as a chemical. However, currently, most of the hydrogen is used in the industry as a chemical and most of the production is still carried out by steam reforming and gasification of fossil resources or as a by-product of other reactions [1,2]. The industrial uses of hydrogen are very widespread. The refining, petrochemical and chemical sectors are largely dependent on H_2 [1]. The most important reactions involving the use of hydrogen are a synthesis of ammonia and methanol, hydrogenations, hydrogenolysis reactions, hydrocracking reactions. Furthermore, since the 70's, the concept of *hydrogen economy* has triggered the research toward its use as an energy carrier, e.g. as a fuel in fuel cells application, and toward its production from renewable sources, such as biomass, solar and wind as primary energy sources [1].

The object of my PhD thesis is about the use of hydrogen for the production of chemical and fuels, essentially as hydrogenation reactant. In this framework, 1) the direct synthesis of hydrogen peroxide, 2) the hydrodeoxygenation/hydrocracking of microalgae oils, and 3) the hydrogenation of furfural for producing 2-methylfuran was studied. All of these reactions involve the use of hydrogen for various reactions, such as hydrogenation, hydrodeoxygenation and hydrocracking reactions and can be considered as special cases of hydrogenation reactions.

In this chapter, a brief introduction to hydrogenation reactions, their chemistry and on the mainly used reactors will be given. Hydrogenations, as previously underlined are widely used in the industry and for laboratory synthesis, and the topic is huge. Therefore, a comprehensive review of hydrogenation

reactions is out of the scope of the chapter. Consequently, in this chapter, only preliminary and common concepts about hydrogenations will be discussed with a particular emphasis toward the studied reactions.

2. Hydrogenations

Hydrogenation is one of the most widely used class of reactions in the industry both for the production of bulk and fine chemicals. Some interesting reviews, book chapters and books can found in [3–22] and references therein. This kind of reaction is defined as the addition of hydrogen to a substrate, usually in the presence of a catalyst [3]. Generally, Hydrogen can be added to double, triple bonds, even in the presence of heteroatoms [3]. Another specific case of reactions involving hydrogen is given by the cleavage of C-C or C-X bonds after reaction with hydrogen, where X is a heteroatom. These reactions are referred as hydrogenolysis reactions [3].

Hydrodeoxygenation (HDO), hydrodesulfurization (HDS), hydrodenitrification (HDN), hydrodemetallation (HDM) reactions, Hydrocracking and dewaxing [23], widely used in the petrochemical industry and for the production of bulk and fine chemicals, belong to this class of reactions [3]. Other specific cases of reactions which can be classified as hydrogenations are, e.g. the synthesis of methanol, ammonia, and the (direct) synthesis of H_2O_2, of which the latter is treated in this work. A schematic representation of hydrogenation reactions of importance for this work is given in Scheme 1.

2.1 Hydrogenation Strategies

Catalytic hydrogenation in the presence of a catalyst and molecular hydrogen is the most widely used strategy for hydrogenation. Behind catalytic hydrogenation in the presence of H_2, hydrogenation reactions can be run in the presence of an organic substrate acting as a source of hydrogen and a hydrogenation catalyst. These reactions are referred as *hydrogen transfer reactions* [24,25]. Hydrogenation reactions can also be conducted by using standard organic chemistry procedures involving 1) the use of stoichiometric hydrogenating reactant, such as $NaBH_4$, $LiAlH_4$, formic acid, hydrazine 2) Na, Zn, Al, and so on, in presence of a solvent/acidic solution/NH_3 as hydrogen donor or 3) electro-catalytic methods [25]. An example of the latter kind of reactions is the electrocatalytic hydrogenation of furfural to furfuryl alcohol and 2-methylfuran [26]. Regarding the use of hydrogenating reactant (stoichiometric strategy) such as $NaBH_4$, $LiAlH_4$, this is very popular for laboratory scale production and/or the production of fine chemicals, however, this kind of hydrogenation strategy, because of the high costs of the hydrogenating reactant, high production of by-products, safety and purity constraints, is not widely employed in the chemical industry. The electrochemical strategy, although studied for several years it's still in its infancy and not widely used in the industry also because of the high costs/environmental impact associated with the production of electric energy and low energy efficiency. Furthermore, currently, electricity is mostly produced by using fossil resources, which make the process not very sustainable from the environmental point of view. However, in the future, the availability of electric energy from renewable sources such as wind, solar and geothermal will probably change the current hydrogen production scenario [26].

Another difference regarding the addition of hydrogen to an organic substrate regards its reduction state. Because of its intermediate electronegativity with respect to the other elements in the periodic table, hydrogen can be added as H^-, H or H^+ (after initial addition of electrons) [25]. Usually, heterogeneous catalysts add atomic hydrogen; metallic hydrides add hydrides ions and electrochemical methods and

some catalysts protons. In the case of hydrogen transfer reductions the reduced state of hydrogen is not always obvious [25].

Hydrogenation Reactions

$$H_2 + A \rightleftarrows B$$

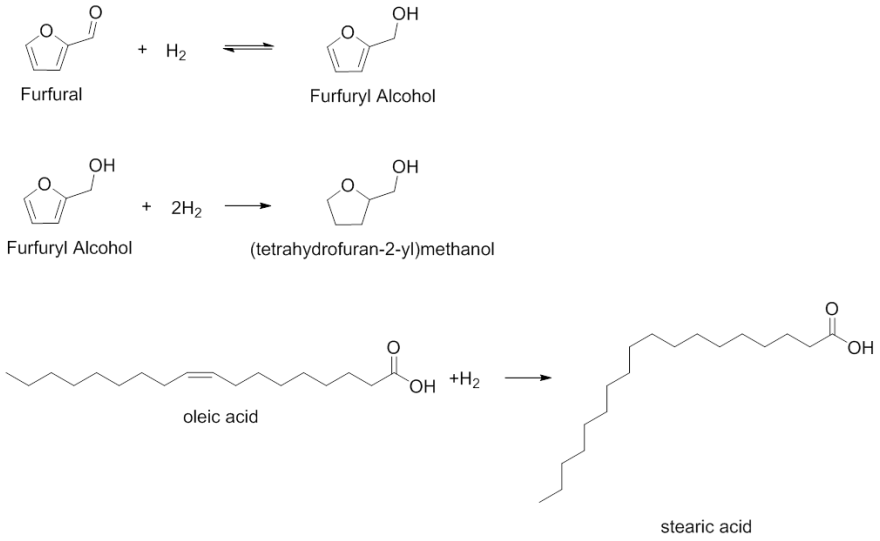

Hydrogenolysis Reactions (Hydrodeoxygenation, HDO)

$$H_2 + R_3C - X \rightarrow R_3CH + H_2X$$

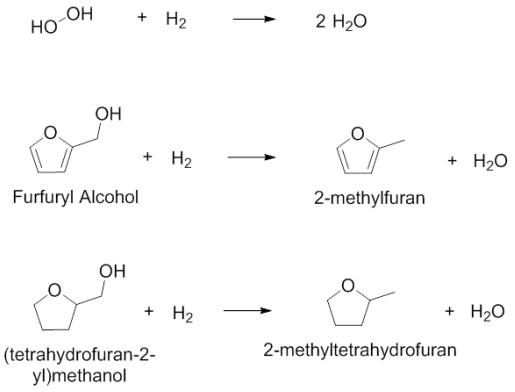

Hydrocracking Reactions

$$H_2 + R_3C - CR_3 \rightarrow 2R_3CH$$

Scheme 1 – Hydrogenation Reactions

2.2 Thermodynamics

Hydrogenation reactions are generally limited by the thermodynamic equilibrium, exothermic and favourite at moderate temperature and high H_2 pressures [3,27]. At higher temperatures, conversely, on the same kind of catalysts, dehydrogenation reactions are favoured. Generally, for using H_2 as hydrogenation agent, given the high strength of H-H bond, using a catalyst is of paramount importance. Although the reaction is thermodynamically favoured, the addition of hydrogen without a catalyst, according to orbital symmetry rules, is a forbidden process [6]. Similarly, dehydrogenation reactions cannot proceed easily without a catalyst [28]. In this case, indeed, the strength of the C-H bond is much higher than the C-C strength. Therefore, dehydrogenation cannot be simply achieved thermally without a significant thermal cracking of the substrate [28]. Furthermore, for hydrogenation reactions, although an increase in temperature increases the rate of reaction this might have a negative effect on conversion and also on the catalyst life and selectivity [3]. In addition, given the high exothermicity of the reaction, the control of the temperature is very important, especially for thermally unstable compounds. Consequently, several strategies are in use to mitigate this effect.

2.3 Operative Parameters

The most important parameters for conducting hydrogenation reactions, behind the temperature, are H_2 pressure, reactor engineering, fluid dynamics, catalyst metal and loadings [3]. Generally speaking, increasing the turbulence of the system and hydrogen partial pressure increase the concentration of H_2 on the catalyst surface and therefore the rate of hydrogenation [3]. However, the influence of the operative conditions should be evaluated case by case, with respect to the specific targets.

2.4 Solvent Effect

Hydrogenation reactions, with respect to the phase of the substrate/substrates, are generally conducted in liquid or in gas phase. Solvents, usually are used for hydrogenating solid substrates and for mitigating hotspots [3]. However, it should be taken into account that in the presence of a solvent, the space-time yield is usually lower, there is a cost for separating the product from the solvent. Furthermore, the solvent itself represent a cost because of the need of integrating the solvent lost in the process [3]. However, the presence of a solvent can be considered as one of the most powerful tools to tune the selectivity of the reaction, to control the temperature and improve the catalyst life [8,13,15,29–32]. Solvents often present a dramatic effect on selectivity and activity of organic reactions [33]. The effect of the solvent for catalytic hydrogenations as widely reviewed in [8,13,15,29–32] might: 1) influence the availability of hydrogen on the active sites by limiting its solubility/activity/transport, 2) influence the kinetics by its polarity, 3) compete with the substrate to be hydrogenated for active sites 4) influence the mechanism by participating in the reaction, e.g. acting as H-donor or reacting with a substrate/intermediate, 5) stabilize/destabilize transition states, and so on [30]. Convenient solvents might be the product itself or solvents used before or after the hydrogenation stage [3]. All the reactions conducted for this work have been conducted in liquid phase in the presence of a suitable solvent. Some examples of solvent effect were reported for the direct synthesis of H_2O_2 and for the hydrogenation of furfural. In the first case, the hydrogen solubility and the availability of protons by the solvent have been correlated with the observed activity [34,35]. Regarding the effect of the solvent polarity on the selectivity of hydrogenation of furfural, a specific example will be given in chapter 4.

2.5 Catalysts for Hydrogenation Reactions

Catalytic hydrogenations can be classified as heterogeneous and homogeneous catalytic reactions. Heterogeneous catalysts are solid and not miscible with the solvent/substrates [3]. Homogeneous catalysts, conversely, dissolve in the same phase with the reactant in the liquid medium [3] or in a supercritical medium such as for the direct synthesis of H_2O_2 in supercritical CO_2 using a catalyst soluble in the supercritical solvent [36]. In this chapter, the use and applications of homogeneous catalysts, given the topic of this thesis were not covered. However, several comprehensive reviews and books are available in the literature, see for example ref. [6] and references therein. At the border between heterogeneous and homogeneous catalysts, also homogeneous immobilised catalysts, exploiting the advantages of easy recovery by heterogeneous catalysts and the high selectivities and catalyst efficiency typical of homogeneous catalysts are exploited [14]. The latter kind of catalysts is especially employed for niche applications such as asymmetric hydrogenations, although also heterogeneous catalysts were developed for this scope. The main disadvantage of using homogeneous hydrogenation catalysts, although very efficient from the point of view of catalyst atom utilisation and very selective for many reactions, is represented by the separation of the catalysts from the products. Nonetheless, till now, heterogeneous catalysts are the most widely used class of catalysts in the industry for hydrogenation reactions.

Active metals for hydrogenation reactions span from noble metals like palladium, platinum, rhodium, ruthenium (platinum group metals), to base metals like nickel, copper, cobalt, molybdenum [3]. Platinum group metals are particularly active as catalytic materials. Base metals conversely are economical alternatives, but present lower activity with respect to the previously reported noble metals. Also, gold catalysts have been used. However, these are much less active because of their electronic configuration, and a similar behaviour is normally shown by copper and silver, belonging to the same periodic group. The activity of the catalysts for hydrogenation reactions is indeed strongly influenced by the ability to dissociate hydrogen and absorbing the substrates. These properties, in turn, are a function of the position of the *d* band with respect to the Fermi level, their degree of extension and filling and of the surface structure of the given metal [7,37]. Activity and selectivity are influenced by changes in the coordination sphere of the active phase surface, similarly to homogenous catalysts [3]. Hydrogenation reaction, indeed, most of the times, are structure-sensitive reactions [3]. This is the case for example for the hydrogenation of furfural [38,39] and for the direct synthesis of H_2O_2 [34]. The selectivity of a hydrogenation reaction, especially for reaction in series (like $A \rightarrow B \rightarrow C$) can be classified as thermodynamic selectivity and mechanicistic selectivity [3]. Thermodynamic selectivity is dependent on the extent of adsorption of A and B. if the desired product is B, then it is desirable that A is preferentially adsorbed on the catalyst in order to avoid the conversion of B to C. With the term mechanistic selectivity, conversely, the difference in selectivity is given by the preferential route followed by the adsorbed intermediates, e.g. if A can be directly hydrogenated to C, without desorption of B on the surface of the catalyst [3]. Probably, both thermodynamic and mechanistic selectivity can be found for different catalysts for the hydrogenation of furfural, where 2-methylfuran as suggested in the literature [40], can be formed directly from the hydrogenation of furfural or furfuryl alcohol. Selectivity can be further influenced by the support as a consequence of interaction with the active metal or by the presence of specific active sites [3]. Regarding the mechanicistic aspects, hydrogenation on heterogeneous catalysts has been demonstrated to follow the Horiuti–Polanyi type mechanism, which considers the hydrogenation reaction via a step addition of adsorbed hydrogen to the

adsorbed substrate [3]. Therefore, the ability of the catalyst to dissociate hydrogen is of paramount importance.

The choice of the metal and supports is usually a function of the functional group which has to be reduced. Several examples regarding the choice of active metals and supports have been given by [3,4,24,27]. A comprehensive and schematic overview is further given by the Johnson Matthey in the "Catalytic Reaction Guide" [41]. The preparation of typical catalysts for hydrogenation is reported in [4] and references therein.

Heterogeneous catalysts for hydrogenation reactions are usually employed as supported and unsupported catalysts and in the reduced state or oxidised or sulfided state [4]. The preferred catalysts in the industry are usually the supported ones, with the exception of Raney catalysts. Supports are normally used in order to increase the metal surface areas of the active components and as structural promoters in order to avoid sintering during the activation and during the reaction [4]. This is especially true for Platinum group metals. In this case, given the high costs of the metal, it is very important to maximise the efficiency of use of the metal. Supports, further, increases the resistance of catalysts against deactivation due to the formation of coke or poisons, often present as impurities in the reacting mixture [4,42]. Furthermore, supports often influence the kinetics of the reaction by making available additional catalytic sites (e.g. bifunctional catalysts), interacting electronically with the support, modifying the structure of the active phase, by shape selective catalysis as in the case of zeolites or by steric effects [9], creating other active sites at the border of the catalytic particles, participating in the reaction by hydrogen spillover mechanism, and so on. The most widely used supports are carbon and alumina [5]. Although, several kinds of supports are in use, and the optimum choice of the support is strictly connected to specific applications. For example, in the case of hydrodeoxygenation reactions, the use of acidic supports can increase the rate of elimination of water from alcohol and, therefore, the subsequent hydrogenation [43]. For hydrocracking and dewaxing, the presence of acidic sites and hydrogenating/dehydrogenating function together with a shape selective support is of paramount importance [23]. Another example in which the effect of the support was found to be important is for the selective hydrogenation of α,β-aldehydes [9]. In this latter example, the higher selectivity observed with Pt and Ru on graphite with respect to the same metals on other supports was attributed to an electron donating effect from the support to the surface of the metal [9].

Unsupported catalysts, conversely, are widely used in laboratory scale synthesis [4]. This class of catalysts might be distinguished as "blacks" or colloidal particles. Colloidal particles are usually more active and, often, also more selective [4]. The high activity reported by using these catalysts can be ascribed to the high dispersion of the active metal. The high selectivity, on the other side, can be ascribed to impurities related to the used reducing agents or to protective capping agents [4], as will be discussed for the direct synthesis of H_2O_2 regarding the use of PVA as a capping agent. The main disadvantage of colloidal catalysts is the separation of the catalysts from the products [4].

The use of multi-metallic catalysts is a useful tool for tuning the selectivity and the literature about the use of second metal as alloys and ad-atoms are huge. Specific examples in the literature for the direct synthesis of H_2O_2 are the use of Pd-Au and Pd-Sn catalysts. In the case of hydrogenation of alpha-beta unsaturated aldehydes supported Pt-Sn catalysts, for example, have been reported to increase the selectivity to the unsaturated alcohol by favouring the absorption of the carbonyl moiety [7,9]. The use of

bimetallics to improve the selectivity to furfuryl alcohol have been reported [44]. Promoters are other components in use to tune the catalyst selectivity and activity. Some examples of promoters are bromide ions for the direct synthesis which as will be discussed allow decreasing direct combustion kinetics [45], or organic thiolates [46,47] and acids [48] for the hydrogenation of furfural.

2.6 Catalyst Safety

Heterogeneous catalysts, depending on the specific materials are generally classified as harmful, irritating or even carcinogenic, even in the oxidised form. This problem is even worse in the presence of chromite as support, which up to now is widely used in the industry, e.g. with copper as active metal for the reduction of furfural to furfuryl alcohol [49]. Therefore, in order to avoid direct contact or inhalation of powders, special care should be used for handling e.g. reactor loading, discharge, manipulation. Extreme care should be used when heterogeneous catalysts are in the reduced state. These materials, especially when the active metals are based on base metals, are pyrophoric, and carbon supports are easy to ignite. These problems are amplified when the catalysts are in powdered form. In this case, in the presence of carbon as support and mixture containing oxygen or air could give rise to dust explosions and therefore should be avoided. Noble metals are generally not pyrophoric, but when freshly reduced in the presence of chemisorbed hydrogen, oxygen containing mixtures could ignite the catalysts or in the presence of organic vapours could give rise to explosive mixtures. In the industrial practice, therefore, hydrogenation catalysts are reduced in situ or, if necessary in the reduced form, are usually stored in oils, water, alcohols [50]. Alternatively, heterogeneous catalysts, after reduction, can be passivated by using diluted oxygen mixtures and then reactivated in situ with hydrogen or other reducing mixtures [51,52]. Storage in an oxygen free environment is very important for base metals also because oxygen, chemisorbing on the active metal, is often a poison for the reaction.

The absence of oxygen is very important in the reaction environment also because in the presence of hydrogen, given the very wide limit of explosivity for the latter, and dry catalysts, could give rise to explosions. Similar problems were encountered for the direct synthesis of H_2O_2 analysed in this work [53]. Because of these risks, several reactor designs have been suggested in this case, e.g. microreactors [54] and membrane reactors [55].

3. Hydrogenation Reactors

The design of reactors has a determining role for running hydrogenation reactions. Hydrogenation reactions, with the exception of the direct synthesis, are devices used in the industry and in laboratory practice for contacting hydrogen, catalyst, and a substrate in an oxygen-free environment [3]. In the presence of molecular hydrogen, heterogeneous catalysts and a liquid solvent, hydrogenation reactors can be classified as heterogeneous gas-liquid-solid reactors. This kind of reactors can be classified as fixed bed reactors and suspended catalysts reactors [56].

- Slurry reactors (stirred tank reactors)
- Bubble column reactors (packed bed, slurry bubble columns)
- Ebullated flow reactors (fluidised beds)
- Trickle-bed reactors (fixed bed)

In the last decades, novel reactor concepts capable of handling three-phase systems have been conceived, between these:

- Catalytic membrane reactors
- Microreactors
- Microstructured falling film reactors [57]
- Microstructured mesh contactor [57]

Choosing between these reactors is not a trivial task, and frequently heuristic strategies are used in practice. Generally, these criteria are a function of the catalyst, reactant and hydrodynamic regimes [56].

3.1 Slurry Reactors

Slurry reactors are used for hydrogenating liquid substrates directly without the presence of a solvent or for hydrogenating solid, liquid or gaseous substrates in the presence of a solvent. Catalysts are used in solid form (heterogeneous catalysts) as Raney, Blacks or more frequently as supported metals. Supported metals are easier to handle and easier to separate by common filtration procedures. Catalysts are present as particles with catalyst particles are often between 5-50 μm, but even bigger particles have been used [58]. In this kind of reactors, the catalysts are suspended in the liquid. Therefore, the presence of turbulent flow conditions for the liquid is essential. The presence of turbulence is often ensured by using stirring devices, external recirculation systems and gas induced fluid motion [56]. The presence of turbulent conditions has also the effect of minimising the effect of transport phenomena, minimising thermal and concentration gradients, end ensuring a uniform concentration of the catalyst in the liquid. The compatibility between the liquid/solvent and the catalysts is important in order to avoid agglomeration of the catalyst. This kind of reactors can be used as a batch, semi-batch and continuous reactors and can be described by two ideal flow reactors, namely perfectly stirred batch reactors and continuous-flow stirred tank reactor (CSTR). The fluid regime is generally a function of the chosen reactor type. Examples at the extreme are stirred reactors and bubble columns. In the first case, the fluid regime can be approximated to perfectly stirred reactors, in the second case with the plug flow regime, even though back-mixing is often important [56,58]. For slurry reactors, with respect to fixed bed reactors, catalysts are easily added to the system and removed for compensating the presence of deactivating phenomena in order to keep the productivity between acceptable/economic limits. Hydrogen is usually bubbled within the liquid, and its transport through the solution is often ensured by using gas spargers and custom designed stirrers. For stirred reactors, stirrers can be in the in the form of magnetic or mechanical stirrers. Magnetic stirrers are easier to operate, but their use is limited to laboratory reactors and generally not recommended in the presence of highly viscous liquids. In the latter situation, the use of mechanical stirring devices is required. The use of stirrers, further, is limited by the size of the reactor and often in laboratory reactors with limited volumes shaking devices are often employed.

For heterogeneous catalytic hydrogenations often transport limitations are very important and can have a significant role in both selectivity and activity. For hydrogenation reactions in the liquid phase, the main transport limitations might be related to the transport of hydrogen from the gas phase and thermal gradients [8]. In order to study the kinetics of hydrogenation reactions, therefore, all these effects should be minimised. When hydrogenation are conducted in liquid phase, hydrogen, before reacting with the substrate on the catalyst surface, must diffuse from the gas phase, solubilize in the liquid and then diffuse

toward the catalyst surface. The main steps for a hydrogenation reaction in the liquid phase can be summarised as follows [59]:

1. Diffusion from the gas phase to the liquid at the bubble interface
2. Solubilization at the gas-liquid interface
3. Diffusion from the gas interface (bubble surface) throughout the bulk of the liquid to the surface of the catalyst (external diffusion)
4. Diffusion through the pore system (internal diffusion)
5. Chemisorption on the active metal surface
6. And finally reaction with the adsorbed substrates/intermediates within the porous system

The reaction product, depending on its phase follow the opposite sequence of events. Thermal capacity and thermal conductivities in the liquid phase are about one order of magnitude higher with respect to the corresponding values in the gas phase. Therefore, the effect of thermal gradients for hydrogenation reactions in the liquid phase is generally not taken into account [8]. The concentration gradients for hydrogen for hydrogenation reactions in the liquid phase can be represented as in Figure 1, as suggested by Fogler [59]. From the same figure, a total of five resistances in series for hydrogen transport from the gas phase to the catalytic sites is reported. The resistance of mass transfer from the bulk of the gas phase to the liquid interface can be considered as negligible when in the presence of pure H_2 in the gas phase. The concentration of hydrogen at the gas-liquid interface is generally proportional to the Henry constant for its adsorption in the pure liquid ($c^*_{H_2} = H \cdot P_{H_{2,gas}}$) [59]. The resistance in the liquid film surrounding the gas bubbles can be minimized by increasing the interface areas of gas bubbles. This is generally achieved by using advanced gas spargers or by increasing the stirring speed. The resistance in the liquid phase (R3) is generally achieved by minimizing the distance between the gas bubbles and catalyst particles and ensuring a homogenous concentration of catalyst within the liquid. For slurry reactors, generally increasing the stirring speed can minimize this resistance (R3), and as well also the external resistance to mass transfer on the outer side of the catalyst particle (R4). This resistance can be further minimized by increasing the liquid-solid interface. Using finely divided catalyst particles has further the beneficial effect of decreasing the pore transport resistance (R5). Therefore, the amount of catalyst and its activity, together with the stirring speed, catalyst particle size and pore diameters are the most important parameters governing transport phenomena.

The most important criteria/tests for minimising/taking into account the effect of transport limitations for hydrogenation reactions in liquid solvents, as suggested by Singh et. al. [8], can be summarised as:

1. Invariance of the rate of hydrogenation with respect to the increase in the stirring speed and decrease of the catalyst particle size (test for internal and external transport limitations)
2. Madon–Boudart test (a variation of the Koros–Novak criterion) which is valid both for structure-sensitive and structure-insensitive reactions (test for internal and external heat and mass transfer limitations)
3. Weisz-Prater criterion (test for internal transport limitations)
4. Thiele modulus (test for internal transport limitations)

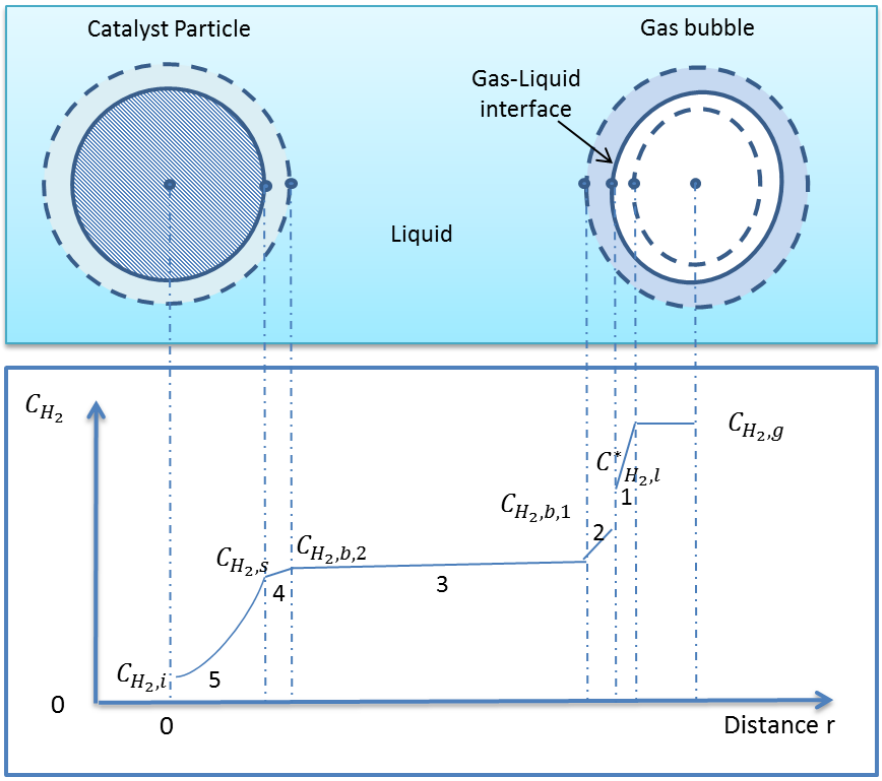

Figure 1 – Hydrogen transport resistances (numbers in figures) for catalytic hydrogenation reactions in slurry reactors (adapted from [59,60])

For studying the kinetics, slurry reactors are often used in the laboratory practice. In order to study the kinetics of a hydrogenation reaction the CSTR configuration, with respect to data analysis is the easier one. However, in practice, because of the need to ensure an ideal stirring in the liquid phase, separation of the catalyst and continuous addition of reactants and withdrawal of liquids this configuration is not used often. Hydrogenation reactions are often used in batch or semi-batch configuration, with liquid and catalysts operated in batch mode. This kind of configuration can be used in differential mode (conversion lower than 5%) or integral mode. In batch mode, the rate of hydrogenation is often monitored by the decrease of the total pressure or in semi--batch with dead end configuration by the consumption of hydrogen by using a gas burette. For semi-batch configuration, a continuous flux of hydrogen is often ensured by using thermal gas mass flow controllers. For monitoring the pressure both analogic manometers and digital gas pressure transducers are in use. The latter devices are easier to handle and allow a continuous registration of the pressure.

Hydrogenation reactions, further, as previously underlined, are exothermic reactions and often are conducted at high temperature, depending on the target functional group to be hydrogenated. Therefore, hydrogenation reactors are often equipped with external heaters. For controlling the temperature and ensuring isothermal conditions, of paramount importance for kinetic studies, hydrogenation reactors are often equipped with internal coils for cooling the liquid, operated externally through the circulation of suitable refrigerating liquids. Water and ethylene glycol are often used for cooling. The temperature is controlled by using thermocouples immersed in the liquid equipped with PID controllers acting on the flow of cooling liquids and on the power of the external heating device.

The safety of hydrogenation reactors, often operated at high pressures (100-200 barg) is ensured by using rupture disks mounted on the head of the reactor and electrical devices designed for operating in explosion environments. Furthermore, in order to avoid the direct exposure of the operators, in laboratory practice, this kind of reactors should be operated in certified fume-hoods, behind safety glasses and using gas sensors able to track potential leaks of hydrogen.

For laboratory practice, semi-batch and batch reactors are easier to build in-house or available from a number of manufacturers (Parr Inc., Autoclave engineers). The most widely used reactors in laboratory practice for hydrogenations are the stirred autoclaves or shaker type reactors. The latter type of reactor is used for operating at moderate temperatures and low pressures (below 60 psig and 80°C). For achieving high pressures, gas tanks are often used, while for low pressures the use of H_2 generators is recommended. Gas tight operations are often achieved by using PTFE, Viton, Kalrez or graphite gaskets, depending on the final temperature.

Materials of construction for the body of the reactor are very important in order to avoid corrosion problems and other parasitic phenomena influencing the kinetics or the analysis of the catalysts. Normally stainless steels are used, but the materials should be chosen as a function of the reaction environment. A summary of the most frequently used materials is given in [61].

For kinetic studies, in order to study the reaction at a constant temperature in the presence of a heterogeneous catalyst the use of internal catalysts addition device or external devices for adding the substrate once a constant temperature has been achieved is recommended. Liquid sampling is a further complication for reactions conducted at high temperature. This problem is usually circumvented by using a sampling line immersed in the liquid, often equipped with a filter in order to avoid the sampling of the catalyst and by using a cooling device on the sampling line.

In this study, a 300 ml autoclave reactor fully equipped for hydrogenation reactions has been used for screening several Ni/zeolite catalysts for the hydrodeoxygenation/hydrocracking of microalgae oils in batch mode. Further details have been given in Chapter 3. For the hydrogenation of furfural to 2-methylfuran, conversely small reactors (7ml) equipped with a magnetic stirrer organised in a battery of twelve parallel reactors have been used in batch mode for the high throughput screening of a set of commercial catalysts (see Chapter 4 for further details). In all these studies the minimization of transport phenomena with respect to the gas phase has been ensured by stirring at high speed (1000 rpm) and using finely divided powdered catalysts. Further details about slurry reactors can be obtained in the following reviews [58,60,62].

3.2 Trickle bed reactors

Trickle bed reactors are fixed bed reactors generally used for continuous processes for gas-liquid-solid reactions. This kind of reactors are widely used for hydrogenation reactions, hydrocracking, hydrodenitrogenation, hydrodesulfurization and are extensively used in the petroleum refining industry [3,23,63]. In this case, the liquid and gas are fed concurrently downward over the catalyst. Although, also applications in which the gas flow is in the upward direction are in use [64]. The liquid flow, however, is always in the downward direction [63]. Generally, in the downward flow concurrent configuration the liquid and gas flow through the packed bed with residence time distribution similar to a plug flow reactor,

consequently, with respect to a CSTR reactor, the rate of reaction is always high and very high conversions can be achieved [3]. This feature is very important e.g. for hydrodesulfurization processes where very low sulphur concentration are desired at the exit. The liquid trickles through the catalytic bed(s) forming a film of the catalyst particles. For achieving a good liquid distribution across the catalytic bed, achieving a good catalyst utilisation efficiency and avoiding preferential paths several solutions have been proposed [3,63]. Catalysts are generally in forms of randomly packed pellets, although also different structured beds are in use, e.g. monoliths [63]. The fluid dynamics in this kind of reactors is quite complex, making scale up or scale down a difficult task [63].

In the presence of highly exothermic reactions, the catalyst is organised in multiple beds of different length, while, cold hydrogen is fed between each bed for lowering the temperature at the exit of each catalytic bed [3].

This kind of reactors, although often used in the industrial practice and laboratory scale, are not the ideal ones for obtaining kinetic data [65]. This is because, kinetics, fluid dynamics and mass transport of the reactants are often complexly interlinked. Therefore more advanced treatments are needed in order to interpret/infer the kinetics [64,65]. Good reviews about trickle-bed reactors were given in [56,63,64,66–70].

3.4 Microstructured reactors

Microreactors are a relatively new technology, still in its infancy [71]. The first publications of this kind of reactors appeared only in the 1990's [71] and only a few attempts to bring this technology to industrial scale have been attempted [57]. Although, commercial units are already available for laboratory scale synthesis. An example is the H-cube developed by ThalesNano, which is usually employed for screening and small productions [72]. In this case, a set of catalyst cartridges has been developed. This solution further allows intrinsically safe operations, reliable and flexible catalytic systems. By this name, several conceptually different kind of miniaturised reactors with open channels between 0.1µm and 1mm usually realised by microtechnology techniques are generally described [71,73]. By similar techniques also other micro-devices have been produced. Between these: micro-mixers, micro-heat exchanger, micro-separation systems and micro-analytical modules [73]. This kind of devices is generally used for highly exothermic reactions and/or in the presence of explosion risks. Gas-phase, liquid-phase, and gas–liquid–solid reactions are easily handled [57,73]. Several examples of microreactors have been recently reported by [57]. Techniques for the production of these micro-devices have generally been reviewed by [73] and for conciseness will not be reported here. The main advantages: high surface-to-volume ratios (10,000–50,000 m^2/m^3), high heat and mass-transfer coefficients, improved energy efficiency, narrow residence time distribution (RTD), inherently safe because of the low inventory of reactants/intermediates/products, useful for distributed production units, easy scale-up [57]. Catalysts are generally in the form of packed beds, wash coated on the walls, metallic wires, metallic grids or wash-coated on grids [57,74]. The last option particularly can be considered as a micro-structured contactor and can be useful for feeding hydrogen through the walls. Specifically for hydrogenation reactions micro-structured falling film reactors and micro-structured mesh contactor have been proposed [57]. Further details are available in [57] and references therein.

Generally, this kind of reactors, for gas-liquid applications, operate in laminar flow conditions [57]. Hydrogen can be solubilized in the liquid phase or continuously fed in a biphasic flow (Taylor flow [57]). The

peculiar characteristics of the flow regimes and the high mass transfer rates for gases in liquids make these devices very useful for studying the kinetics of hydrogenation reactions. Further, these systems are also useful for high-throughput experiments [75].

Some examples of hydrogenation in liquid phase conducted by using microreactors are: hydrogenation of benzalacetone using Pd-immobilized on the walls of micro-channel reactors [74], hydrogenation of furfural realised in parallel microreactors packed with several commercial catalysts [76], the direct synthesis of H_2O_2 [77–83]. In the latter case, the use of microreactors is particularly interesting because, behind increasing mass transfer rates of O_2 and H_2, the high surface to volume ratios ensures safe operations in the presence of possible run-away reactions [84]. Further examples regarding the application of microstructured reactors were reported in [72,73].

3.2 Catalytic Membrane Reactors

By the IUPAC definition, "*a membrane reactor is a device combining a membrane-based separation and a chemical reaction in one unit*" [85,86]. Recent advances in the field of inorganic membranes, highly resistant to high temperatures and pressures normally used in the industrial practice, has triggered the interests of academia and industry toward catalytic membrane reactors [85]. The membranes used for this kind of applications are generally classified as dense perm-selective and porous non-perm-selective membranes. Palladium and polymeric membranes are examples of dense and generally perm-selective membranes. Porous inorganic membranes, like asymmetric alumina membranes, conversely are not perm-selective. Selective microporous membranes are at the frontier between dense and porous membranes.

The definition of catalytic membrane reactors, however, is often used in practice for identifying several reactor configurations involving the use of a membrane. Accordingly, membrane reactors can be classified with respect to the features of the membrane as [85,87]:

1. *Extractor membrane reactor*
2. *Forced through-flow catalytic membrane reactor*
3. *Distributor membrane reactor*

For a more extensive classification of membrane reactors see ref[85,88–90]. The first type of catalytic reactors are generally used for dehydrogenation reactions, therefore were not taken into account. In the following paragraph, only some of the most important catalytic reactors in configurations used for hydrogenation reactions in liquid phase will be presented.

Forced through-flow catalytic membrane reactors use catalytically active membranes, which might be the result of the intrinsic composition of the membrane, e.g. containing acidic sites, or the result of catalytic particles dispersed thereon. Membranes, in this case, are porous and often asymmetric. Generally, reactants flow throughout the membrane from the same side in a forced manner. The difference in pressure between each side of the membrane is used as a driving force, and the flow inside the membrane is not in diffusive regime, as commonly observed for most of the membrane driven processes, but in forced convection regime. In this way, very short contact time can be achieved [85], and therefore the whole system can be intended as a battery of parallel nano-reactors. This flow regime has

as a major effect the improvement of transport phenomena inside the membrane. This set up has also been used for hydrogenation reactions in gas-liquid systems [89].

Distributor membrane reactors, together with *extractor membrane reactors* are the most widely used membrane reactors. In the first case, with respect to the latter, the primary function of the membrane is the carefully dosing of one or more reactants along the reactor in order to keep its concentration constant through the longitudinal side of the membrane, while other reactants flow from the internal side. For this kind of configurations, both dense perm-selective membranes and porous non-perm-selective membranes can be used. Extractor membrane reactors are generally used for improving the thermodynamic yields of equilibrium limited reactions, e.g. dehydrogenation reactions, by separating selectively H_2. Other applications of this kind of concept are in use also for different kind of reactions.

Taking into account the position of the catalyst, in this kind of reactors, the catalyst is present inside the separation module, generally a tubular membrane, as catalytic pellets, coated on the wall of the membrane or can be constituted by the membrane itself. The latter two cases are generally strictly known as catalytic membrane reactors.

3.2.1 Distributor membrane reactors – dense membranes

Generally, perm-selective membranes can be used with both gas-liquid-solid reactions and gas-solid reactions, while non-perm-selective membranes are generally used for gas-liquid-solid reactions. A typical setup used for hydrogenation reactions using perm-selective membranes is reported in Figure 2 for the direct synthesis of H_2O_2, although in this case the role of the membrane is separating H_2 and O_2 physically. The main advantage of using perm-selective membranes, further, is the possibility of using non-pure reactants, e.g. hydrogen containing impurities by exploiting dense palladium membranes. In this case, further, the catalytic membrane can be exploited as a catalyst directly for some reactions. However, the kinetic coupling between the transport of hydrogen inside the membrane and the catalytic reaction should always be considered with care. Often one of the main limitation for the productivity of these reactors is given by the diffusive transport of hydrogen inside the Pd membrane. The transport mechanism of hydrogen through the membrane can be described by the following series of steps [88]:

1. H_2 dissociative chemisorption on the surface of Pd
2. Solubilization of atomic hydrogen in the lattice of palladium
3. Diffusion of atomic hydrogen in the lattice through the thickness of the membrane
4. Recombination of hydrogen on the surface of the Pd membrane
5. H_2 desorption

In this case, H_2 transport through the membrane is generally described by equation 1.

$$1)\ J_{H_2} = \frac{Pe_{H_2}}{\delta} \cdot \left(p^n_{H_2 Retentat} - p^n_{H_2 Perm}\right)$$

Where, J_{H_2} is the flux of H_2 across the membrane $[mol/s]$, Pe_{H_2} is the permeability of the membrane $[mol \cdot m^{-1} \cdot Pa^{-n}]$, δ the thickness $[m]$, $\frac{Pe_{H_2}}{\delta}$ the permeance $[mol \cdot m^{-2} \cdot Pa^{-n}]$. The *driving force* is given by the difference between $p^n_{H_2 retentat}$ and $p^n_{H_2 perm}$ $[Pa]$, respectively the pressure of the retentate and permeate side of the membrane. The n parameter, presents usually values between 0.5-1 and by this parameter is possible to discriminate which step is limiting. When the transport of hydrogen through the membrane is the rate limiting step, then, $n = 0.5$ and equation 1 reduces to equation 2:

$$2)\ J_{H_2} = \frac{Pe_{H_2}}{\delta} \cdot \left(p^{0.5}_{H_2\ retentato} - p^{0.5}_{H_2\ permeato}\right)$$

Known as Sievert or Sievert-Fick law.

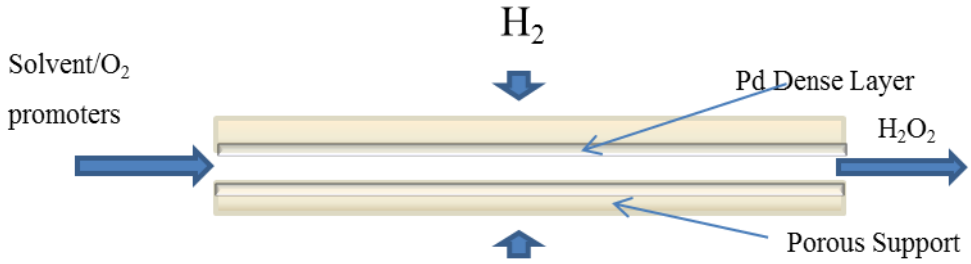

Figure 2 – Catalytic distributor with a dense membrane reactor used for the direct synthesis of H_2O_2 in liquid phase [91–94].

Other examples of hydrogenation reactions beyond the direct synthesis of H_2O_2 are the selective hydrogenation of several unsaturated hydrocarbons, alcohols, and hydroxylation reactions by using in-situ produced H_2O_2 [85].

This kind of catalytic membranes is usually prepared by using standard procedures like electroless plating deposition. One of the main limits in using this kind of membranes is the working temperature. Below 300°C and already 2MPa of H_2, there is a phase transition from the α to the β phase. The $\beta - Pd - H$ phase, present a lattice constant which is about 3% higher with respect to the α phase [88]. The expansion of the lattice is the main cause of hydrogen ambritlement and failure of the membrane. Several solutions have been studied for overcoming this phenomenon. Between these the addition alloying elements like Ag [88,94–97] and Au [98]. This phenomena, although mitigated by introducing alloying elements is one of the main problems for the direct synthesis of H_2O_2, although in this case the presence of some holes and pits in the catalytic membrane are not a special concern as the liquid solvent fills the free pores as described for the contactor concept described in the following paragraph.

3.2.1 Distributor membrane reactors – Contactors

Using mesoporous and macroporous membranes, compared to dense membranes, can improve the transport of hydrogen significantly and avoiding hydrogen embrittlement. Furthermore, for reactions not requiring a selective membrane, this concept can further minimise the costs associated with the preparation of the catalytic membrane. In this case, asymmetric membranes are generally used. These kinds of membranes are prepared by depositing several layers of support with different porosity as depicted in Figure 3. The porous membrane can be further used as a support for depositing the active

phase. The latter kind of reactor is strictly known as *Catalytic Membrane Contactor* [85] or "*Catalytic Diffuser*" [87]. This concept is generally exploited also for hydrogenations in liquid phase [85]. In this case, two possible alternatives can be distinguished depending on the wetting features of the surface of the pores of the membrane [89]. In the first alternative, the liquid does not wet the membrane, a condition achieved by using solvent and support of opposite polarity, e.g. using H_2O as a solvent and a hydrophobic membrane [89] (see Figure 4). When the membrane and solvent have similar polarity, the solvent wets the membrane (see Figure 5). For hydrogenation reactions, the first situation can be desired when in the presence of a catalyst physically separated from the membrane in order to increase the transport of hydrogen through the membrane [89]. Conversely, in the presence of a catalytic diffuser, with the catalyst dispersed as nanoparticles on the catalytic membrane, the second alternative is often desired. In the latter case, asymmetric membranes are often used.

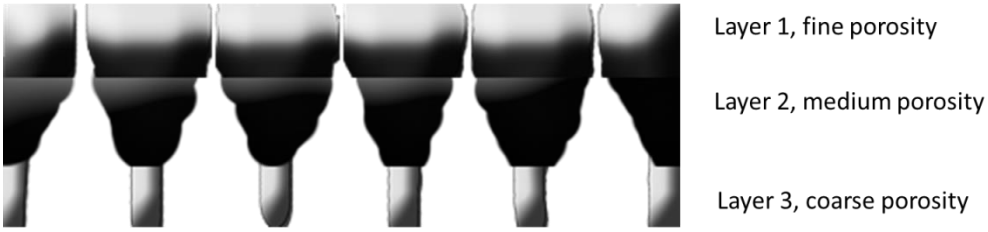

Figure 3 - Asymmetric Membrane Concept (layer 3 is usually intended as a mechanical support for the medium and fine porosity layers)

The gas-liquid interface position across the thickness of the catalytic membrane is a function of the capillary forces acting between the liquid and the support, and the applied pressure for the reactant through the catalytic membrane, e.g. H_2, and can be modelled by the Laplace equation [99,100]:

$$\Delta P = 2\frac{\sigma_L \cos \alpha}{r_p}$$

Where σ_L is the gas-liquid surface tension, α the wetting angle of the solvent on the membrane interface (often assumed to be zero), and r_p the pore diameter, which for asymmetric membranes varies across the membrane thickness.

The direct synthesis of H_2O_2 is an example of a reaction which has been proposed for exploiting the concept of distributor membrane reactors, and both dense membranes and porous contactor type membranes have been proposed. Further details about the application of these membrane reactor concepts will be given in Chapter 2.

In this case, the transport of hydrogen and/or other reactants through the pores of the membrane are governed by the Fick's law of diffusion. This kind of reactor concept, as reported in Figure 5 is characterised by a stagnant zone of liquid inside the pores of the membrane. In the same zone, catalytic particles are deposited.

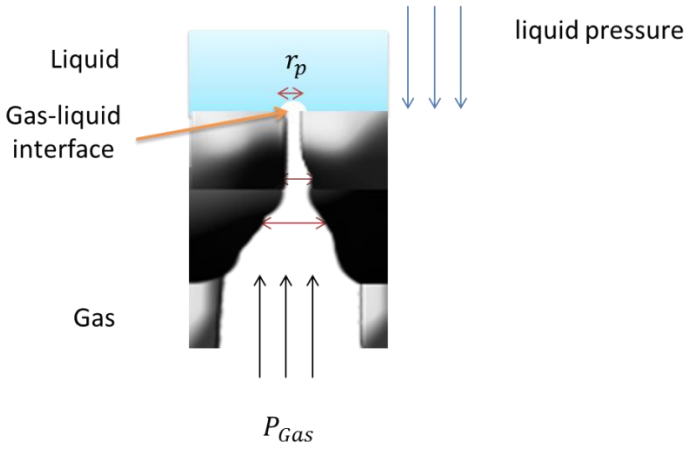

Figure 4 – Schematization of contactor concept in the case the liquid do not wet the membrane.

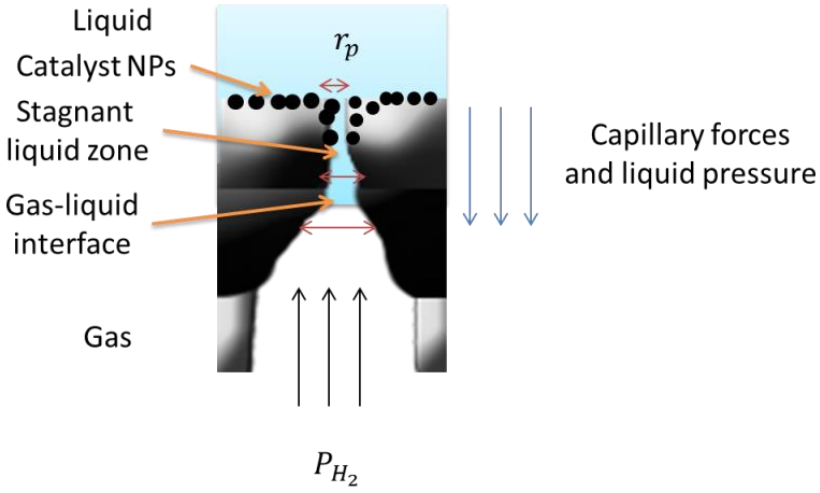

Figure 5 – Schematization of contactor concept. In the same figure the equilibrium position for the gas-liquid interface inside a single pore of an asymmetric membrane, variation of the pore radius across the membrane thickness, directions of capillary forces and applied pressure (arrows indicate the direction of the applied forces and their magnitude)

Generally, the procedures used for preparing this kind of catalytic supports make use of the typical procedures for preparing eggshell catalysts. In this way, internal diffusion phenomena are mitigated. The transport of hydrogen is further influenced by its conversion kinetics in the catalytic layer. Of course, the relative kinetics of consumption of the reactants should be taken into account, and also the fluid dynamic regime of the liquid should be considered in order to avoid external diffusion phenomena.

This kind of membranes has been used for several hydrogenation reactions in the liquid phase. Between these the direct synthesis and the hydrogenation of nitrates [55,87,89].

Several procedures have been used for depositing various metals. Some of these procedures have been given in Chapter 2 for the case of Pd for the direct synthesis of H_2O_2.

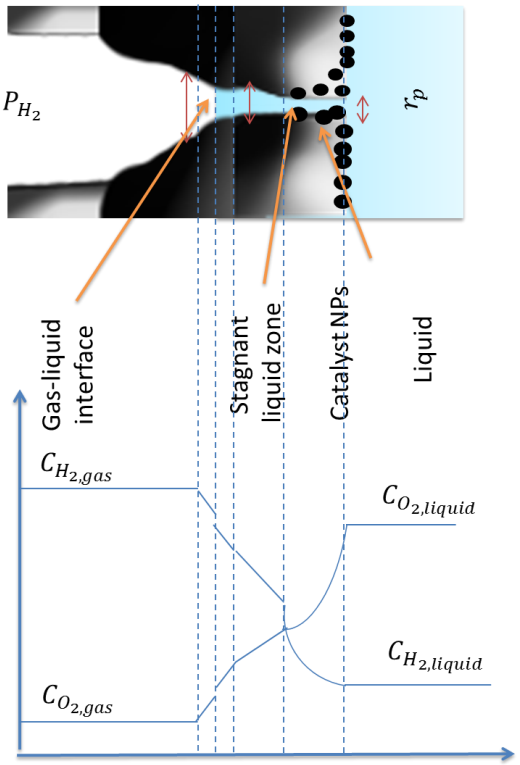

Figure 6 – Typical gradients present through the pores of a catalytic contactor for the direct synthesis of H_2O_2 (Gradients were deliberately exaggerated), see also ref. [99].

References

1. W. F. Baade, U. N. Parekh, and V. S. Raman, in *Kirk-Othmer Encyclopedia of Chemical Technology*, John Wiley & Sons, Inc., Hoboken, NJ, USA, 2001, vol. 13.

2. P. Häussinger, R. Lohmüller, and A. M. Watson, in *Ullmann's Encyclopedia of Industrial Chemistry*, Wiley-VCH Verlag GmbH & Co. KGaA, Weinheim, Germany, 2000.

3. D. Sanfilippo and P. N. Rylander, in *Ullmann's Encyclopedia of Industrial Chemistry*, Wiley-VCH Verlag GmbH & Co. KGaA, Weinheim, Germany, 2009, vol. 1, pp. 131–139.

4. S. Nishimura, *Handbook of Heterogeneous Catalytic Hydrogenation for Organic Synthesis*, 2001.

5. P. Rylander, *Catalytic Hydrogenation in Organic Syntheses*, 1979.

6. L. A. Oro and D. Carmona, in *Encyclopedia of Catalysis*, John Wiley & Sons, Inc., 2002.

7. P. Mäki-Arvela, J. Hájek, T. Salmi, and D. Y. Murzin, *Appl. Catal. A Gen.*, 2005, **292**, 1–49.

8. U. K. Singh and M. A. Vannice, *Appl. Catal. A Gen.*, 2001, **213**, 1–24.

9. P. Gallezot and D. Richard, *Catal. Rev.*, 1998, **40**, 81–126.

10. P. N. Rylander, *Hydrogenation methods*, Academic Press, 1985.

11. Y. Nakagawa, M. Tamura, and K. Tomishige, *ACS Catal.*, 2013, **3**, 2655–2668.

12. P. N. Rylander, *Acad. Press inc.*, 1967.

13. R. A. Rajadhyaksha and S. L. Karwa, *Chem. Eng. Sci.*, 1986, **41**, 1765–1770.

14. L. Cerveny, *Catalytic Hydrogenation*, 1986, vol. 27.

15. L. Červený and V. Růžička, *Catal. Rev.*, 1982, **24**, 503–566.

16. G. R. List and J. W. King, *Hydrogenation of Fats and Oils: Theory and Practice*, Elsevier Science, 2016.

17. H.-U. Blaser, A. Schnyder, H. Steiner, P. Baumeister, F. Rössler, P. Baumeister, F. ROssler, and P. Baumeister, in *Handbook of Heterogeneous Catalysis*, Wiley-VCH Verlag GmbH & Co. KGaA, Weinheim, Germany, 2008, pp. 3284–3308.

18. H. Arnold, F. Döbert, J. Gaube, D. Frank, and J. Gaube, in *Handbook of Heterogeneous Catalysis*, Wiley-VCH Verlag GmbH & Co. KGaA, 2008, pp. 3266–3284.

19. P. Claus, Y. Önal, and A. Tungler, in *Handbook of Heterogeneous Catalysis*, Wiley-VCH Verlag GmbH & Co. KGaA, 2008, pp. 3308–3329.

20. B. Gutsche, H. Rößler, S. Würkert, and E. Production, in *Handbook of Heterogeneous Catalysis*, Wiley-VCH Verlag GmbH & Co. KGaA, 2008.

21. J. W. Veldsink, M. J. Bouma, N. H. Schöön, and A. a. C. M. Beenackers, *Catal. Rev.*, 1997, **39**, 253–318.

22. R. L. Augustine, *Catal. Rev.*, 1976, **13**, 285–316.

23. J. A. R. van Veen, J. K. Minderhoud, L. G. Huve, and W. H. J. Stork, in *Handbook of Heterogeneous Catalysis*, Wiley-VCH Verlag GmbH & Co. KGaA, Weinheim, Germany, 2008, vol. 634, pp. 2778–2808.

24. P. N. Rylander, *Hydrogenation Methods*, .

25. R. a. W. Johnstone, A. H. Wilby, and I. D. Entwistle, *Chem. Rev.*, 1985, **85**, 129–170.

26. Y. Kwon, K. J. P. Schouten, J. C. van der Waal, E. de Jong, and M. T. M. Koper, *ACS Catal.*, 2016, **6**, 6704–6717.

27. P. Gallezot, in *Encyclopedia of Catalysis*, John Wiley & Sons, Inc., 2002.

28. D. E. Resasco, in *Encyclopedia of Catalysis*, John Wiley & Sons, Inc., 2002, pp. 1–52.

29. C. Reichardt and T. Welton, *Solvents and Solvent Effects in Organic Chemistry*, Wiley, 2011.

30. P. J. Dyson and P. G. Jessop, *Catal. Sci. Technol.*, 2016, **6**, 3302–3316.

31. V. Fajt, L. Kurc, and L. Červený, *Int. J. Chem. Kinet.*, 2008, **40**, 240–252.

32. H. S. Lo and M. E. Paulaitis, *AIChE J.*, 1981, **27**, 842–844.

33. D. Y. Murzin, *Catal. Sci. Technol.*, 2016, **6**, 5700–5713.

34. N. M. Wilson and D. W. Flaherty, *J. Am. Chem. Soc.*, 2016, **138**, 574–586.

35. Y. Yi, L. Wang, G. Li, and H. Guo, *Catal. Sci. Technol.*, 2016, **6**, 1593–1610.

36. D. Hâncu, J. Green, and E. J. Beckman, *Acc. Chem. Res.*, 2002, **35**, 757–764.

37. K. W. Kolasinski, in *Surface Science*, John Wiley & Sons, Ltd, 2012, pp. 115–183.

38. V. V Pushkarev, N. Musselwhite, K. An, S. Alayoglu, and G. a Somorjai, *Nano Lett.*, 2012, **12**, 5196–5201.

39. Q.-X. Cai, J.-G. Wang, Y.-G. Wang, and D. Mei, *AIChE J.*, 2015, **61**, 3812–3824.

40. R. Mariscal, P. Maireles-Torres, M. Ojeda, I. Sádaba, and M. López Granados, *Energy Environ. Sci.*, 2016, **9**, 1144–1189.

41. Johnson Matthey, 2016.

42. R. J. Farrauto and C. . Bartholomew, *Fundamentals ofIndustrial Catalytic Processes*, Blackie Academic & Professional, 2nd edn., 2010.

43. G. Li, N. Li, X. Wang, X. Sheng, S. Li, A. Wang, Y. Cong, X. Wang, and T. Zhang, *Energy and Fuels*, 2014, **28**, 5112–5118.

44. S. Lee and Y. Chen, *Ind. Eng. Chem. Res.*, 1999, **38**, 2548–2556.

45. C. Samanta, *Appl. Catal. A Gen.*, 2008, **350**, 133–149.

46. S. H. Pang, C. A. Schoenbaum, D. K. Schwartz, and J. W. Medlin, *ACS Catal.*, 2014, **4**, 3123–3131.

47. S. H. Pang, N. E. Love, and J. W. Medlin, *J. Phys. Chem. Lett.*, 2014, **5**, 4110–4114.

48. M. J. Gilkey, P. Panagiotopoulou, A. V. Mironenko, G. R. Jenness, D. G. Vlachos, and B. Xu, *ACS Catal.*, 2015, **5**, 3988–3994.

49. K. J. Zeitsch, *The Chemistry and Technology of Furfural and its many By-Products, Volume 13*, Elsevier Science, Amsterdam, 1st edn., 2000.

50. P. Mars, T. v. d. Mond, and J. J. F. Scholten, *Ind. Eng. Chem. Prod. Res. Dev.*, 1962, **1**, 161–164.

51. F. Huber, Z. Yu, S. Lögdberg, M. Rønning, D. Chen, H. Venvik, and A. Holmen, *Catal. Letters*, 2006, **110**, 211–220.

52. A. Gil, A. Diaz, and M. Montes, 1991, **87**, 791–795.

53. D. Dissanayake, *J. Catal.*, 2003, **214**, 113–120.

54. T. Inoue, M. A. Schmidt, and K. F. Jensen, *Ind. Eng. Chem. Res.*, 2007, **46**, 1153–1160.

55. G. Centi, R. Dittmeyer, S. Perathoner, and M. Reif, *Catal. Today*, 2003, **79**–**80**, 139–149.

56. A. K. Saroha and K. D. P. Nigam, *Rev. Chem. Eng.*, 1996, **12**.

57. L. Kiwi-Minsker and A. Renken, *Catal. Today*, 2005, **110**, 2–14.

58. S. Nedeltchev and A. Schumpe, in *Handbook of Heterogeneous Catalysis*, Wiley-VCH Verlag GmbH & Co. KGaA, Weinheim, Germany, 2008, pp. 2132–2156.

59. H. S. Fogler and N. M. Gurmen, in *Elements Of Chemical Reaction Engineering*, Pearson Education Inc., Upper Saddle River, NJ, 4th edn., 2005, pp. 596–610.

60. R. V Chaudhari and P. A. Ramachandran, *AIChE J.*, 1980, **26**, 177–201.

61. M. Picciotti, Ed., *Petrochemical Catalysts: Catalysts, Applications and Bench-Scale Reactors*, National Petrochemical Company, Roma, Teheran, 2005.

62. D. Stern, A. T. Bell, and H. Heinemann, *Chem. Eng. Sci.*, 1983, **38**, 597–605.

63. V. V Ranade, R. Chaudhari, and P. R. Gunjal, *Trickle Bed Reactors: Reactor Engineering and Applications*, Elsevier Science, 2011.

64. G. Mary, J. Chaouki, and F. Luck, *Int. J. Chem. React. Eng.*, 2009, **7**, 1–15.

65. G. Biardi, *Catal. Today*, 1999, **52**, 223–234.

66. J. D. Silva and C. A. M. Abreu, *Brazilian J. Chem. Eng.*, 2012, **29**, 567–576.

67. A. Gianetto and V. Specchia, *Chem. Eng. Sci.*, 1992, **47**, 3197–3213.

68. M. Herskowitz and J. M. Smith, *AIChE J.*, 1983, **29**, 1–18.

69. M. H. Al-Dahhan, F. Larachi, M. P. Dudukovic, and A. Laurent, *Ind. Eng. Chem. Res.*, 1997, **36**, 3292–

3314.

70. M. P. Duduković, F. Larachi, and P. L. Mills, *Catal. Rev.*, 2002, **44**, 123–246.

71. W. Ehrfeld, V. Hessel, and V. Haverkamp, in *Ullmann's Encyclopedia of Industrial Chemistry*, Wiley-VCH Verlag GmbH & Co. KGaA, Weinheim, Germany, 2000.

72. M. Irfan, T. N. Glasnov, and C. O. Kappe, *ChemSusChem*, 2011, **4**, 300–316.

73. W. Ehrfeld, V. Hessel, and H. Löwe, *Microreactors: New Technology for Modern Chemistry*, 2000.

74. J. Kobayashi, *Science (80-.).*, 2004, **304**, 1305–1308.

75. F. Schuth, in *Handbook of Heterogeneous Catalysis*, Wiley-VCH Verlag GmbH & Co. KGaA, Weinheim, Germany, 2008, vol. 37.

76. A. J. Garcia-Olmo, A. Yepez, A. M. Balu, A. A. Romero, Y. Li, and R. Luque, *Catal. Sci. Technol.*, 2016, **6**, 4705–4711.

77. Y. Voloshin, R. Halder, and A. Lawal, *Catal. Today*, 2007, **125**, 40–47.

78. Y. Voloshin and A. Lawal, *Chem. Eng. Sci.*, 2010, **65**, 1028–1036.

79. T. Inoue, K. Ohtaki, S. Murakami, and S. Matsumoto, *Fuel Process. Technol.*, 2012, 1–4.

80. J. F. Ng, Y. Nie, G. K. Chuah, and S. Jaenicke, *J. Catal.*, 2010, **269**, 302–308.

81. Y. Voloshin and A. Lawal, *Appl. Catal. A Gen.*, 2009, **353**, 9–16.

82. S. Maehara, M. Taneda, and K. Kusakabe, *Chem. Eng. Res. Des.*, 2008, **86**, 410–415.

83. *Focus Catal.*, 2011, **2011**, 6.

84. G. Veser, *Chem. Eng. Sci.*, 2001, **56**, 1265–1273.

85. R. Dittmeyer and J. Caro, in *Handbook of Heterogeneous Catalysis*, eds. G. Ertl, H. Knözinger, F. Schüth, and J. Weitkamp, Wiley-VCH Verlag GmbH & Co. KGaA, Weinheim, Germany, 2008, pp. 2198–2249.

86. W. J. Koros, Y. H. Ma, and T. Shimidzu, *J. Memb. Sci.*, 1996, **120**, 149–159.

87. M. Reif and R. Dittmeyer, *Catal. Today*, 2003, **82**, 3–14.

88. A. Basile and F. Gallucci, Eds., *Membranes for Membrane Reactors: Preparation, Optimization and Selection*, John Wiley & Sons, Singapore, 2011.

89. R. Dittmeyer, K. Svajda, and M. Reif, *Top. Catal.*, 2004, **29**, 3–27.

90. E. Fontananova, E. Drioli, and M. Technology, in *Comprehensive Membrane Science and Engineering, Volume 3*, 2010, vol. 3, pp. 110–133.

91. S. Abate, G. Centi, S. Perathoner, and F. Frusteri, *Catal. Today*, 2006, **118**, 189–197.

92. S. Abate, G. Centi, S. Perathoner, S. Melada, F. Pinna, and G. Strukul, *Top. Catal.*, 2006, **38**, 181–

193.

93. S. Abate, S. Melada, G. Centi, S. Perathoner, F. Pinna, and G. Strukul, *Catal. Today*, 2006, **117**, 193–198.

94. V. R. Choudhary, A. G. Gaikwad, and S. D. Sansare, *Angew. Chem. Int. Ed. Engl.*, 2001, **40**, 1776–1779.

95. S. Abate, G. Centi, S. Perathoner, and F. Frusteri, *Catal. Today*, 2006, **118**, 189–197.

96. V. Choudhary, S. Sansare, and A. Gaikwad, *US Pat. 6,432,376*, 2002.

97. L. Shi, A. Goldbach, G. Zeng, and H. Xu, *Int. J. Hydrogen Energy*, 2010, **35**, 4201–4208.

98. L. Shi, A. Goldbach, G. Zeng, and H. Xu, *Catal. Today*, 2010, **156**, 118–123.

99. A. Pashkova, K. SVAJDA, and R. Dittmeyer, *Chem. Eng. J.*, 2008, **139**, 165–171.

100. M. Vospernik, A. Pintar, G. Berčič, and J. Levec, *Catal. Today*, 2003, **79**–**80**, 169–179.

Chapter 2
Direct Synthesis of H_2O_2

Abstract

Three families of catalytic membranes have been prepared by dispersing Pd on asymmetric alumina membranes. By using 1) reduction with hydrazine in an ultrasonic bath, 2) impregnation-decomposition and 3) sol-immobilisation techniques, Pd nanoparticles (NPs) with different particle size distributions were prepared. The prepared catalytic membranes were tested for the direct synthesis of H_2O_2 in a membrane reactor operating in semi-batch in the presence of H_2SO_4 and, eventually, KBr as promoters. All the catalytic membranes were tested in the fully reduced state and/or after pre-oxidative treatments (calcination). The catalytic membranes have been characterised before, and after testing by using transmission electron microscopy (TEM), Temperature-programmed reduction (TPR) and diffuse reflectance infrared Fourier transform spectroscopy (DRIFT). Sol-immobilisation and impregnation-decomposition have been identified as promising preparation techniques.

Compared to other reported procedures, catalytic membranes prepared by using the sol-immobilisation technique have shown the greatest selectivities and productivities in their reduced form. This was related to promotion effects active in the presence of polyvinyl alcohol, the capping agent used for obtaining colloidal Pd NPs in the case of the sol-immobilisation. However, during the tests, by using this technique, extensive deactivation phenomena were observed. In line with the extensive literature about the direct synthesis of H_2O_2, the calcination pretreatment led to improved selectivity and productivity. However, the results have shown a marked dependence on the Pd NPs size. The experimental results have been analysed by using several kinetic models in order to understand the origin of the deactivation phenomena observed for SI membranes, obtaining insights on the promotion effect of PVA and analysing the nature of the active sites for pre-oxidised catalytic membranes.

1. Introduction

Hydrogen peroxide (H_2O_2) represent one of the most important and efficient available green oxidant [1–5] and, also because of these properties, nowadays it is in the top 100 chemicals in the world [6]. Compared to all the available oxidants, it contains the highest concentration of active oxygen (47.1 wt%) and water

is the only by-product of its reaction [5]. Therefore, its use in substitution of other oxidants is environmentally desired. Examples of new industrial routes exploiting H_2O_2 as a green oxidant are the production of propylene oxide, caprolactam and phenol [6–10]. However, about 95% of the H_2O_2 is currently produced by the anthraquinone oxidation (AO) process [5,11–14], which because of its multi-step nature and production of a series of by-products, is not a green process [12]. This, of course, reduces the environmental benefit of using H_2O_2 [5]. The main advantage of this process is the avoidance of direct contact between oxygen and hydrogen, circumventing the formation of explosive mixtures [15,16]. Because of its multi-step nature and the necessity of separating the obtained H_2O_2, this process requires a high degree of integration, and therefore it is economical only for large scale productions. Consequently, nowadays the production of H_2O_2 is centred in a few big plants in the world, producing at high production costs [4,17,18]. Furthermore, the transport and handling of H_2O_2 generates other environmental and safety issues, limiting the development of new processes using H_2O_2 only in the proximity of big production facilities. Therefore, new processes for the production of H_2O_2 are currently studied [5,6,16,19–22]. Between the new emerging processes for the production of H_2O_2, the direct synthesis of H_2O_2 from the elements is probably the most promising one [5,6,14,16,20,23]. The direct synthesis, indeed, because of the intensification of the process, with respect to the AO process, could determine a drop of about 50% in the actual investment costs and a drop of about 20% in its production costs [1,13,24]. Moreover, the only by-product associated with the direct synthesis is, indeed, only water. Therefore, this route could decrease drastically the environmental impact associated with this bulk chemical. The lower investment costs associated with the process, also, could make its *on-site* production feasible and, in turn, increase its use for the production of greener chemicals or for bioremediation applications. The feasibility of this route is further demonstrated by several competitors active in this area and by several pilot plants [14,25–30], even though, until now, no commercial plant has been realised [31].

The main issues associated with the direct synthesis are safety and the low reported selectivity. These aspects are related to the problem of working within the explosion region for H_2 for obtaining an acceptable selectivity. Furthermore, the target concentration needed for some commercial applications, e.g. the production of propylene oxide, has not been achieved yet. Therefore, research in this area is mainly focused on improving the above-reported aspects.

Focusing on safety, in the literature for the direct synthesis, several approaches were reported in order to address this issue: 1) using diluted mixtures of O_2 and H_2, e.g. by using CO_2 as ballast [32], 2) the use of microreactors [23,33–40], 3) the use of membrane reactors [23,41–43], and 4) other alternatives [20,23,44]. By using microreactors and membrane reactors, it could be possible to work within the explosion limits, in an intrinsically safer way. Particularly, using microreactors is advantageous because of the large surface to volume ratio make possible the scavenging of radicals and, therefore, avoiding runaway reactions [45]. Conversely, by using of membrane reactors, the reactant, H_2 and O_2 get in contact with each other only on the catalytic layer of the membrane, in the liquid phase, while are physically separated in the gas phase [23,41,42]. In the past, our research group has studied several aspects of this reaction associated with membrane reactors, both using dense membranes and by the catalytic contactor concept [42,46–48]. The two reported approaches differ with each other with respect to the way in which the active phase is deposited. Specifically, with dense membranes, a thin film of palladium is deposited, while with the catalytic contactor, the active phase is deposited in the form of tiny particles, at the interface between the

membrane and the solvent [49]. In the first case, preferable in terms of safety, the transport of hydrogen is limited by the metallic Pd membrane. In the second case, the efficiency of use of the active metal and reliability are higher, and the production cost lower with respect to the first case. Therefore, most of the research was focused on the contactor concept. In agreement, this chapter is focused only on the use of the catalytic contactor concept.

Another critical issue is the low selectivity because of the parallel and consecutive reaction of hydrogen, oxygen and hydrogen peroxide giving water as a by-product, all catalysed by the active metal. Additionally, as reported by several studies, the reaction is probably structure-sensitive [50–54], with corners and edges active in the direct combustion and decomposition of H_2O_2 [55]. For improving the selectivity, the main used strategies have been: 1) the use of acidic and halides as promoters, 2) the use of alloy with gold [56] or other non-noble metal like tin [57]. The mechanism of the reaction, in particular, has been the object of many studies and reviews [5,14,16,20,23,58,59]. Unfortunately, the nature of the active sites involved in the reaction is still unclear. Specifically, in the literature, there is still uncertainty about the oxidation state of the active sites [56] with some authors reporting metallic Pd as active phase and other suggesting PdO. Furthermore, during the reaction, catalysts changes dynamically together the changing conditions inside the reactor under the influence of the redox potential of the reacting solution [60], a factor which has been limitedly considered [32,60–64]. Deactivation has been reported [65,66], but not treated in details. Mechanisms for catalyst deactivation has been reported and attributed to: the formation of H_2O_2 oxidising the catalyst [67–69], leaching [23,70], poisoning [23,71–73] and sintering [53].

All these factors make more complicated giving an answer about the nature of active sites, especially when the reaction is run under harsh conditions. However, studying the reaction in mild conditions, as in the present case, can simplify the study of the reaction. Further, several preparation techniques have been reported, with the sol-immobilisation often reported as a promising technique for obtaining selective and productive catalysts. However, also in this case, deactivation of the catalyst, given by loss of PVA and particles sintering, limit its application [60,61,64]. Therefore, the objectives of this study are: 1) studying the dynamics of catalysts prepared by sol immobilisation, in order to access the underlined deactivation mechanism, and 2) studying the effect of the oxidation of Pd on the reactivity of the catalyst, in order to access the nature of the active phase.

To achieve the first goal, the time on stream and recyclability of catalysts prepared by Sol Immobilization (SI) technique was studied by kinetic analysis and transmission electron microscopy. By using the developed kinetic model, the effect of PVA, used as a capping agent and often reported as a promoter [64,74], was analysed.

For studying the nature of the active sites, a similar kinetic analysis was used to access the oxidation degree of several catalysts during their time-on-stream. Specifically, the kinetic of as prepared, calcined and reduced catalysts was analysed by using several models, by using the initial redox state of Pd particles as a reference. The initial state of Pd, indeed, is a function of the redox pretreatment [61]. Therefore, the analysis of the dynamic changes of the oxidation degree of Pd during the initial stage of reaction as a function of the pretreatment could provide indications about the influence of the reaction medium on the nature of the active sites and on the features of the nanoparticles.

Studying these effects from a kinetic point of view, could, in principle, give some quantitative information, otherwise hardly accessible, with respect to other techniques. Although several kinetic models have been reported for this reaction, similar treatments were never attempted. Additionally, for a more comprehensive treatment, the effect of several preparation techniques giving different particle size distributions, all compared with the same loading level, was studied. Therefore, several catalytic membranes were prepared, tested and characterised. The catalytic membranes were prepared by using the following techniques: 1) hydrazine reduction in an ultrasonic bath (NR), 2) impregnation decomposition (ID) and 3) sol-immobilisation technique (SI). By using these techniques, we were able to obtain Pd nanoparticles (NPs), respectively, of 12, 5.4 and 3.27 nm.

2. Experimental

2.1 Preparation of the Catalysts

2.1.1 Features of the Ceramic supports, quality check and pretreatment

The catalytic membranes used in this work were prepared by depositing Palladium nanoparticles on the internal side of Asymmetric α-Al_2O_3 tubular membranes (AAM) provided by INOPOR, Germany (see Figure 7). The main features are reported in Table 1.

Table 1 –Features of the AAS Membranes used in this work

φin	**0.7cm**
φext	**1cm**
L	**13cm**
$L_{membrane\ layer}$	**10cm**
Location of the mesoporous layer	**Internal**
Porosity of the macroporous support and thickness	**3µm, 1.5mm**
Porosity of the mesoporous layer and thickness	**70nm, 10 µm**
ε	**40-55%**

Before Pd deposition, to exclude the presence of possible macro-defects, the tubular membranes were tested by the bubble point method. This testing method is based on the wetting of the internal side of the membrane in an ethanol-water solution by using a support holder similar to the one used for the testing setup. Then the external side of the membrane was pressurised at 5 barg with N_2, a pressure much greater than the one used for testing, monitoring the nucleation of bubbles which is used to evidence cracks and holes[31]. The ceramic supports, before the active metal deposition were washed with 2-propanol in a sonic bath for 10 min and dried for 1 h at 110 °C.

The active metal was deposited on the inner side of the supports, in the mesoporous layer (see Table 1 and Figure 7). The selective deposition of the active metal in the thin mesoporous layer was favoured by the strong capillary forces during palladium deposition (wet procedures). This deposition strategy ensures the best selectivity in the studied experimental conditions and that all the active metal is used in in the testing stage [75]. Other catalytic membranes with the mesoporous layer on the outer side of the ceramic support (external membranes) and/or depositing palladium either on the external side of the membrane were prepared, but the best results in terms of reliability, selectivity and productivity were obtained in the above-described configuration. Therefore, only the results obtained for internal membranes were reported.

The catalytic membranes used in this work were prepared by 1) hydrazine reduction in ultrasonic bath (NR), 2) impregnation decomposition (ID) and 3) sol immobilisation technique (SI).

2.1.2 Hydrazine Reduction (NR)[31]

This procedure starts with the preparation of two solutions (named P and R). The precursor solution (P) is an aqueous HCl solution (0.25ml/50ml HCl 37 %wt) containing 0.1 %wt $PdCl_2$. The reducing agent solution (R) is a 0.25ml/50ml aqueous N_2H_4 solution containing NH_4OH (0.35ml/50ml of 25% NH_4OH solution). The ceramic support, in this case, was protected by a Parafilm layer from the external side, to avoid palladium deposition in the macroporous layer. The membrane was, then, immersed in a cylinder containing solution P for 3 minutes and in solution R for the same time in an ultrasonic bath, to create the appropriate mixing, with intermediate washing in distilled water. This procedure was repeated for 5 cycles, in order to get a final loading of 3.5mg of Pd. At the end of the procedure, the catalytic supports were washed and dried at 110°C for 1h. The final Pd loading, in this case, was estimated by weight difference. By this procedure, several catalytic supports were prepared, both for testing and characterization. The membranes were tested as prepared and after calcination at 450 °C for 6 h with a ramp of 1°C/min. The samples prepared by this procedure were named, respectively, NR (as prepared) and NRC (after calcination).

2.1.2 Impregnation – decomposition (ID)

The impregnation-decomposition procedure was originally proposed Pashkova et. al. [66] and subsequently modified in order to simplify the experimental setup and improve the dispersion of the active metal. By the modified procedure, the palladium precursor (Palladium-(II)-acetate) was dissolved in acetone and poured in a graduate cylinder. The ceramic support was connected on both ends by using teflon tubing, and N_2 was fed on the internal side of the membrane by using a thermal mass flow controller. The other side of the membrane was fitted in the same way and sent to a vent system. Then, the support was immersed in the palladium acetate solution. The solution, wetting the membrane from the macroporous side (external side of the support), penetrates into the pores and gets concentrated in the inner side of the supports by a 2.5 L n.c./min nitrogen flow. The amount of solution to be deposited is calculated at the beginning of the procedure. The procedure stopped when the amount of solution to be evaporated reached the target value, to achieve a final Pd loading of 4 mg, confirmed by weighting. At the end of the procedure, the ceramic tube was pre-dried at room temperature with the same flow of N_2 and, then, dried at 50°C in a natural convection oven overnight. Afterwards, the support was placed in a tubular oven and heated up for 3h to 250 °C in N_2 flow to achieve the precursor decomposition. The reproducibility

of this preparation technique was quite good. The catalytic membranes prepared by this procedure were named as ID. After testing, the same membrane was calcined at 450°C for 6h by using a 1°C/min ramp and reduced in pure H_2 at 100°C. This membrane was, then, named IDCR. The same membrane was tested and calcined again and indicated as IDC. Several catalytic membranes were prepared by this procedure for testing and characterization.

2.1.3 Sol immobilisation

The original procedure for this preparation technique was originally reported by Prati et. al. [76,77] and slightly modified in order to deposit palladium on ceramic membranes. By this procedure, 100ml aqueous solution of PVA (2.8g/L, Mw=13000–23000, 87–89% hydrolyzed, Sigma Aldrich) and Na_2PdCl_4 ($1.49 \cdot 10^{-3}$ mol/L, Sigma Aldrich) was prepared. Then, under vigorous stirring, 0.028g $NaBH_4$ in solid form ($7.4 \cdot 10^{-3}$mol/L, Sigma Aldrich) was added. After the addition of the reducing agent, the solution turned from yellow to dark brown, indicating the formation of Pd nanoparticles. The solution was kept under stirring for 30 minutes and then acidified with an H_2SO_4 solution to obtain a final pH of 2. Then, by using a membrane holder with recirculation of the liquid, a similar apparatus to the one used for testing, and applying an external pressure of 2.5 barg (N_2), the obtained sol was deposited on the internal side of the membranes. This method is based on the Laplace equation, describing the wetting of the membrane under the effect of a counter pressure. The peculiar characteristics of this method make it possible to prepare catalytic membranes with a specified egg-shell geometry by tuning the N_2 pressure. By this procedure, four catalytic membranes were prepared, both for characterization and for testing purposes. In the following text, the prepared catalytic membranes were indicated as Si-fresh, SI-used(2) and SI-used(12), with the number under bracket indicating the number of tests performed. All the above-indicated membranes were tested in the presence of only H_2SO_4 as promoter. The fourth catalytic membrane was calcined at 450°C for 6h by using a 1 °C/min ramp and tested in the presence of KBr and H_2SO_4 (SIC-KBr).

All the prepared catalytic membranes were tested for recyclability for a number of tests (see Scheme 3 for an overview of the experimental plan).

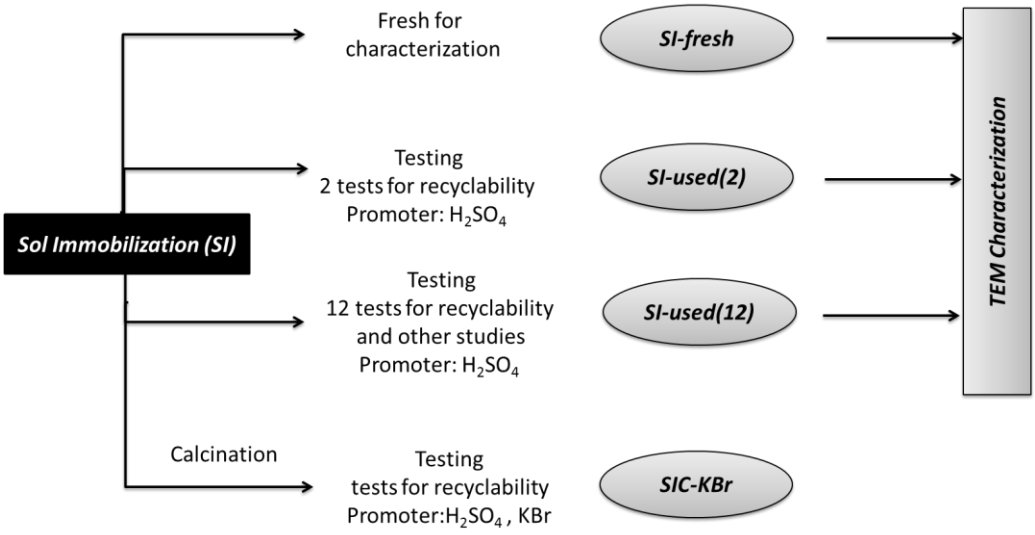

Scheme 2 – Experimental flow chart for catalytic membranes prepared by SI technique

2.2 Testing

2.2.1 Experimental apparatus

All the catalytic tests were carried out in a semi-batch recirculation membrane reactor at room temperature. The experimental apparatus consisted in:

- A four-neck flask,
- A tubular membrane holder (membrane reactor)
- A peristaltic pump connected by special Tygon MH tubing.
- A gas frit used for dispersing oxygen inside the four neck flask
- A gas septum installed in one of the four-neck flask
- A thermal mass flow controller for O_2 (Brooks ® instruments)
- A thermal mass flow meter for H_2 (Bronkhorst ®)
- A pressure regulator for setting the pressure on the external side of the membrane
- A 0-4 barg manometer

The experimental apparatus was accurately dried to keep a moisture free environment and assembled. The typical experimental setup used for this work is depicted in Figure 7, with the membrane reactor arranged in vertical position. In the typical configuration, hydrogen was fed from the external side of the membrane reactor and oxygen in the solution, through the depicted four-neck flask. The membrane holder used for this work was built in stainless steel with removable ends. The catalytic membranes were held by the two glass coated ends by using viton o-rings. In order to avoid H_2O_2 decomposition during the tests, due to the contact, with stainless steel, the ends of the reactor in contact with methanol solution were built in Teflon. All the parts of the catalytic contactor are home-made.

2.2.2 Testing Procedure

All the tests were performed by using an anhydrous methanol solution as a solvent. The starting solution of methanol (100 ml) was prepared by using 100 µl of H_2SO_4 96 wt% and eventually adding also 6 mg KBr as promoters, depending on the chosen experimental conditions. The ceramic membrane was tested for macro-defects by a bubbling test with N_2 under a static pressure of 3 barg. Two gas feeding configurations were tested (see Figure 7), but the best performances were achieved by using configuration A. Before the beginning of the tests, in order to pre-saturate the methanol solution and mildly pre-oxidize the catalyst (see Figure 7, configuration A), oxygen was bubbled through the methanol solution with a flow of 75 ml n.c./min and the solution recirculated through the membrane in a H_2 free environment for 20 minutes (O_2 pre-saturation stage, p_{O_2}=1.013 barg) with a liquid recirculation flow of 44 ml/min. This step has been shown to be important, both in order to keep the oxygen concentration constant with time during the tests and to improve the selectivity and productivity to H_2O_2 [78]. After the pre-saturation stage, a sample was taken and analyzed for the starting initial concentration of water (blank sample). Finally, the

external side of the membrane reactor was purged with nitrogen and then with hydrogen, setting its pressure at 2 barg. The last step was considered as the time zero of the experiment. Subsequently, the solution was sampled with regular time intervals. Each experiment lasted for 4 hours. After each test, the catalytic supports were washed with methanol, dried at room temperature and stored in a moisture free environment.

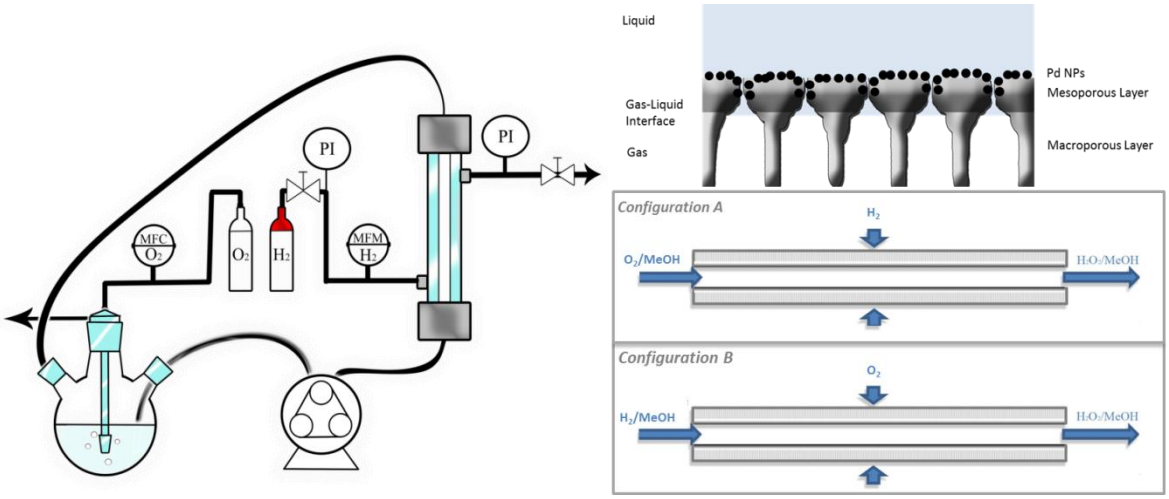

Figure 7 – Experimental setup, gas feeding configurations and AAS Catalytic Membrane schematization

Table 2 – Experimental conditions, configuration A

Experimental conditions	
KBr concentration	0 - 0.06 g/100ml
H_2SO_4 concentration	0.018M
Solution volume	100ml
Solution recirculation flow	44ml/min
Temperature	r.t.
O_2 presure	1.013 bar
O_2 flow	75 ml/min *n.c.*
H_2 pressure (external side of the membrane)	2 barg

The estimated O_2/H_2 ratio during the catalytic tests, based on the gas solubility, is about 0.88 in the inner side of the membrane.

Other tests varying the H_2 partial pressure on the external side of the membrane (*Configuration A*, $p_{H_2}^{ext}$= 0.3-4 barg) were performed. However, in the range of the experimental conditions tested, feeding H_2 on the external side of the catalytic membrane at 2 barg has shown the best performances. Therefore, only the results of the tests performed by using *configuration A* with H_2 fed at 2 barg will be reported. A summary of the used experimental conditions in each test is reported in Table 2.

2.2.3 Analytical procedures

H_2O_2 concentration was monitored by iodometric titration by using an automatic titration apparatus (Metrohm, 794 Basic Titrino) and a standard $Na_2S_2O_3$ solution. Water concentration was determined by using a Karl Fischer coulometer (Metrohm 831 KF coulometer). The H_2O results were corrected by the initial water content in the anhydrous methanol solution and by subtracting the water adsorbed from the flowing gas, determined by independent tests without catalyst (blank tests).

Selectivity was calculated by using the corrected concentration of water by using the following formula:

$$[H_2O_2] = \frac{[H_2O_2]}{[H_2O_2] + [H_2O]}$$

The methanol solution after catalytic testing was analysed by atomic absorption spectroscopy (AAS) for palladium leaching by using a Perkin-Elmer Analyst 200.

2.3 Characterization

TEM (transmission electron microscopy) micrographs were acquired by a Philips CM12 Microscope (point-to-point resolution, 3 Å) operating at 200 kV. Samples were prepared by gently scraping the inner part of the tube and dispersing the resulting powder in isopropanol by sonication. The suspension was finally deposited on a holey carbon film supported on a Cu grid. The particle size distributions were evaluated by analysing more than 300 particles.

Temperature-programmed reduction (TPR) measurements were run using a Micromeritics ® Autochem II apparatus. Typically, the catalytic membranes, after calcination or in the reduced state, were machined and then introduced in a U-shaped reactor. The samples were treated at 150°C in helium, cooled to room temperature (20 °C), and then the analysis was started. In a typical analysis, the temperature was raised to 400°C with a ramp (β) of 10°C/min in a 5% H_2/Ar flow.

FT-IR measurements were performed by using a Bruker Equinox 55 instrument, equipped with an MCT detector and a Globar source. All the spectra were registered at room temperature in the range 3000-1400 cm^{-1} (MIR) by using a DRIFT (diffuse reflectance infrared Fourier transform) configuration. Before each experiment, the catalysts were treated at 270°C in He flow with a ramp of 5°C/min, in order to clean the surface of the catalysts form CO_2 and H_2O. The catalysts were then reduced in situ at the final temperature with a constant flow of a 2% H_2/He mixture. At the end of the reduction procedure, the samples were cooled at room temperature in He environment, and a background spectrum was registered. Afterwards, the catalysts were treated with 5% carbon monoxide (CO)/He. In order to eliminate

physisorbed CO, the samples were degased several times, registering several spectra in parallel. At the end of the procedure, to evidence only the Pd-CO interactions, the final spectra were post-processed by subtracting the background coming from the samples.

3. Results and Discussion

3.1 Characterization of the samples

3.1.1 TEM results for the SI samples

TEM micrographs of the SI samples studied in this work are reported in Figure 8, together with the relative particle size distributions (PSD). To further analyse the different activities of the studied catalysts and the observed trends, Pd metallic surface area (MSA) was calculated from TEM data analysis by modelling palladium particles as spheres. This assumption, however, as evidenced in the following discussion, is strictly applicable for the particles obtained by SI technique, given their spherical homogeneity. Likewise, to take into account the contribution of the tinier particles to the selectivity of the direct synthesis, which as reported in the literature is a structure-sensitive reaction [53] the cumulative size distribution (CSD) (Figure 9) and the cumulative surface area distribution CSAD was further analysed (see Figure 10).

The SI-fresh sample, with respect to other reported procedures like NR and ID [31], shows spherical particles and an almost Gaussian distribution with narrow statistical dispersion (σ), in line with the literature [60,61,63,79,80] (see Figure 8 and Table 3). Nonetheless, the prepared samples show large domains of support free of palladium particles and domains with a high density of particles close to each other (see Figure 8). This last peculiarity was related to the colloidal nature of PVA used for the preparation and to the low porosity of the α-alumina surface, giving the formation of large clots because of the low interaction with the support [60]. In the case of sol immobilisation, indeed, as reported by [74], in order to obtain Pd NPs homogeneously dispersed on the surface of a support and both avoiding agglomeration and particle to particle interaction, maximising the sol–support interaction during the immobilisation stage is of paramount importance.

The SI-used(2) and SI-used(12) samples (Figure 8b and c), with respect to the parent sample (SI-fresh), present a wider and asymmetric distribution, shifted towards bigger diameters. With respect to the parent sample, after 12 tests, both the mean diameter and the standard deviation increased respectively to about 9nm and 4 nm (see Table 3), while the metallic surface area showed a large decrease. This phenomenon, justify, in part, the decrease in the activity and the selectivity trends observed during the recyclability study of the catalyst, as will be discussed. In Figure 8c it is also evidenced the presence of some agglomeration. The increase in particle size for the used catalyst is probably favoured by the partial solubilization of PVA, and the increased mobility of the palladium particles on the surface, as already observed in other Pd based catalysts supported on carbon nanotubes and tested in stirred semi-batch reactor [60,61,64]. Furthermore, as reported in Figure 9 by the cumulative PSD, the bigger particles increased their size at the expense of the tinier particles, indicating the presence of an Ostwald ripening process. This was probably favored by 1) the intrinsic instability of exposed nanoparticles, especially for particles below their critical thermodynamic diameter in such a harsh environment; 2) absence of interactions with the support; 3) loss of PVA, which even though presents a very low solubility in organic solvents this could be reasonable

in methanol which presents a very high dipole moment, and 4) by the high metallic surface areas (MSA) of the catalysts prepared by the SI technique (see Table 3) with respect to other reported procedures [31]. This phenomenon was further confirmed by Pd leaching observed for these catalysts, which, even below the quantification limits, appear to be slightly higher with respect to the other catalysts.

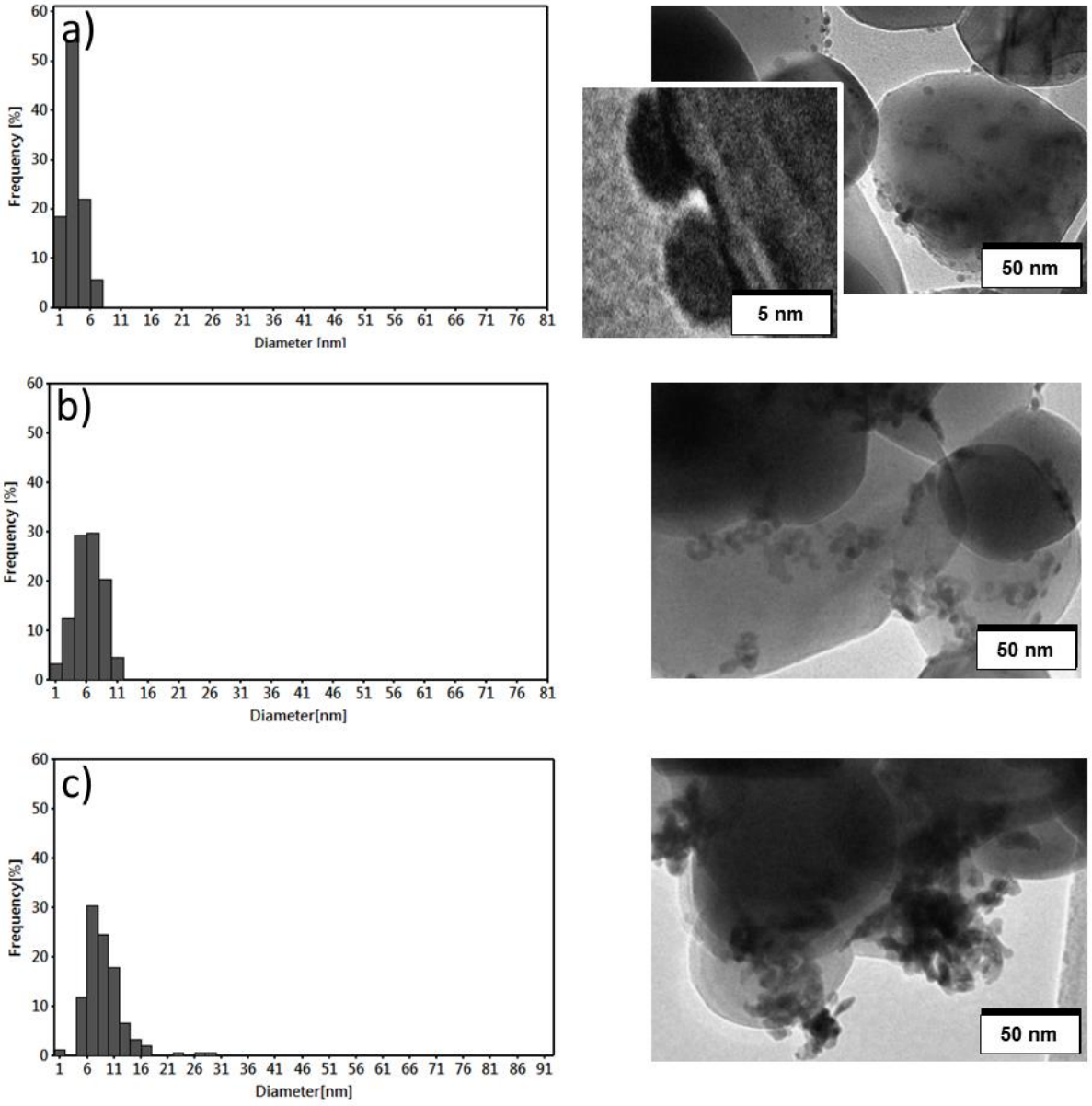

Figure 8. TEM micrographs and PSD for (a) SI-Fresh, (b) SI-used (2 tests) and (c) SI-used (12 tests)

Table 3 – TEM Results (dm, average diameter, dvs Vol.-Surface [nm] used for fitting the Ostwald ripening model)

Sample	Pd [mg]	d_m [nm] (σ [nm])	Dvs	MSA [m²]	MSA [m² / g Pd]
SI-fresh		**3.27 (1.4)**	**4.48**	**0.471**	**112**
SI-(2) after the 2nd test	**4.2**	**5.2 (2.4)**	**7.15**	**0.293**	**69.8**
SI-(12) after the 12th test		**9.15 (3.7)**	**13.2**	**0.159**	**37.9**

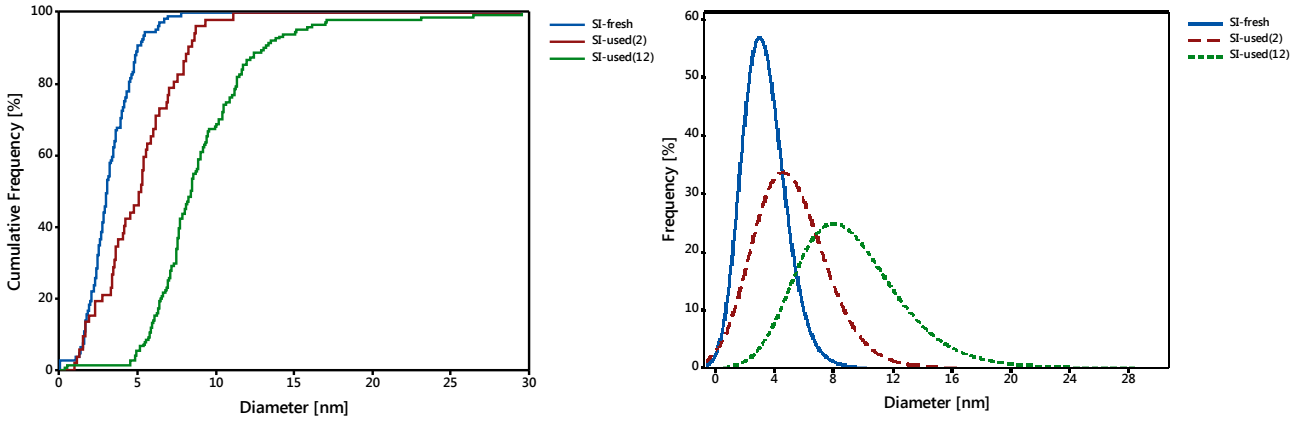

Figure 9 – a) Cumulative PSD for SI-fresh, SI-used(3) and SI-used(12) samples and relative b) fitted 3-parameter log-normal distributions for the SI-fresh, SI-used(3) and SI-used(12) samples

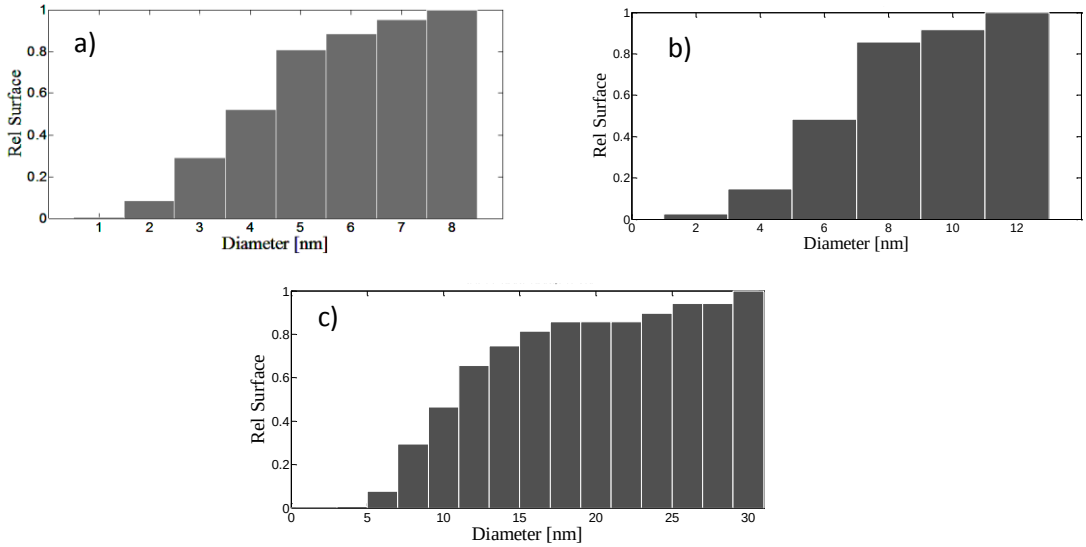

Figure 10 – Cumulative apparent MSA (CSD) distribution with respect to particle diameter calculated by modelling palladium particles as spheres for a)SI-fresh, b) SI-used(2) and c) SI-used(12).

3.1.2 TEM results for the NR and ID samples

The TEM micrographs of the samples prepared by NR and ID techniques are reported in Figure 11 along with their respective particle size distributions. The average diameters and MSAs resulting from micrograph analysis are reported in Table 4. For these samples, by modelling palladium particles as spheres, we also calculated the cumulative distribution of Pd surface area with respect to the particle diameters.

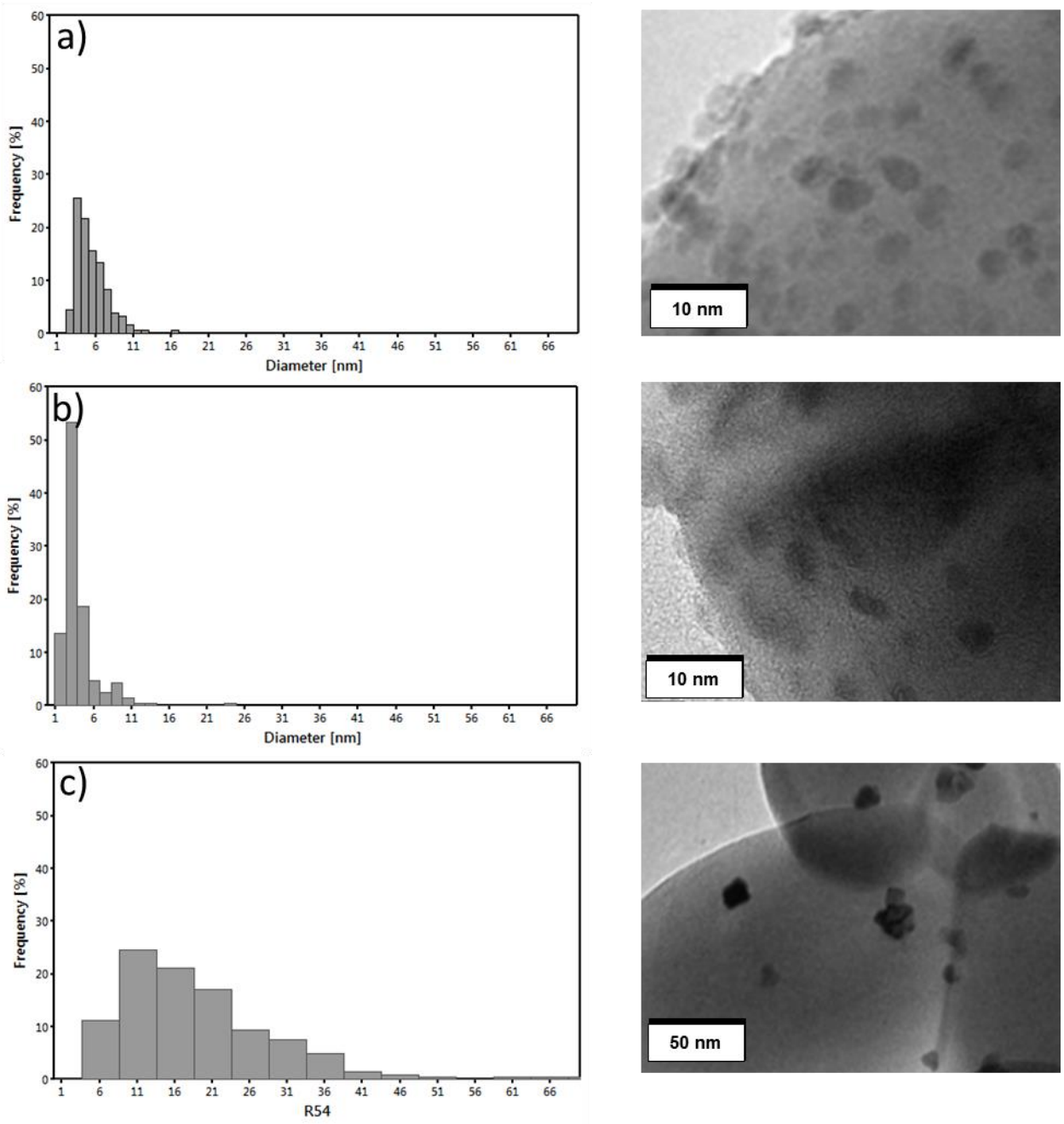

Figure 11 – Particles size distribution and related TEM micrographs for a) ID b) IDC and c) NR catalysts

Table 4 – Metal Surface Area (MSA) calculation: * based on the Pd NPs average TEM diameter, ** based on the TEM particle size distribution (Fig. 2)

Catalyst family	Pd amount [mg]	average diameter (s) [nm]	Pd MSA*[m^2]	Pd MSA**[m^2]	
Sample	Pd [mg]	d_m [nm] (σ [nm])	Dvs	MSA [m^2]	MSA [m^2 / g Pd]
NR	3.5	12 (6.8)	0.092	0.082	23.42
NRC					
ID	4	5.4 (2.1)	0.388	0.289	72.25
IDC		3.8 (2.8)	0.551	0.295	73.75

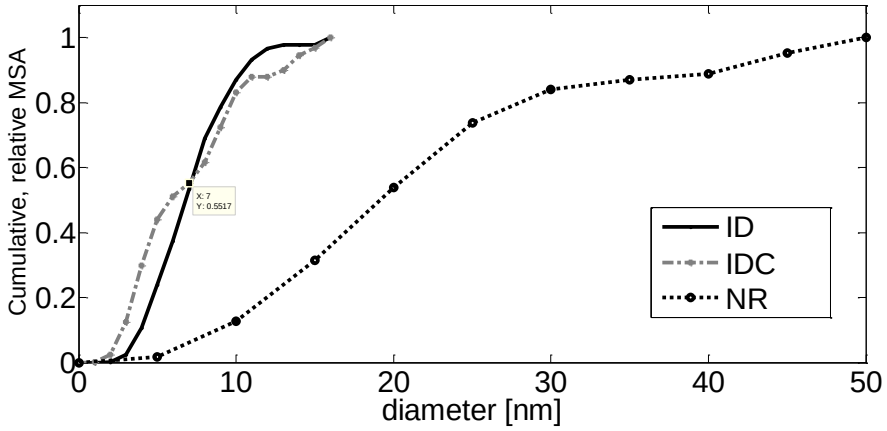

Figure 12 – Cumulative apparent MSA distribution with respect to particle diameter calculated by modelling palladium particles as spheres.

As shown by the reported micrographs, the ID and IDC samples, (Figure 11 a and b), appears quite homogeneous, presenting regular hemispherical shaped particles. The particle size distributions for both samples is asymmetric with diameter modes of about 4 nm and 3 nm, respectively for the ID and IDC samples. For the ID sample, the average diameter is 5.4nm with a standard deviation (s) of 2.1nm, while, after thermal treatments (IDC), presents slightly different features. Specifically, after thermal treatments, in line with the literature [81–84], IDC samples presents regular, round and, apparently, flatter shaped particles, because of the better wettability of PdO on alumina surfaces. The mean diameter (d_m) decreased from 5.4 to 3.8nm while its standard deviation increased (s) to 2.8nm. Furthermore, as evidenced in Figure 12, after thermal treatment the IDC sample, with respect to its parent sample (ID), we observed an increase in the apparent metallic surface area for particles below 7 nm, which decreased for particles above 7-8 nm.

Conversely, the NR sample, as evidenced by the reported micrographs was not homogeneous, exposing large areas of support without Pd particles. Furthermore, with respect to the ID samples, Pd particles show round, irregular shapes, with the presence of macro-aggregates in the range 60-66nm. The particle size distribution was asymmetric, and the average particle diameter (d_m) is about 12 nm with a

standard deviation of about 6.8 nm. After thermal treatments, for the NR sample, no major differences were observed.

3.1.3 Diffuse reflectance infrared Fourier transform spectroscopy for the NR and ID samples

In this section, we report the results of the DRIFT characterization for the ID and IDC samples. For the sample prepared by the NR procedure, we did not observe any significant difference between NR and NRC samples in the DRIFT spectra. Therefore, the results obtained will not be reported for conciseness. In Table 1 we reported a summary for the identified bands assignments. The background subtracted spectra for the ID and IDC samples after reduction are reported in Figure 13, along with the main band ranges. The comparison of the DRIFT spectra for the fresh and calcined samples indicate that the surface of Pd after the calcination treatment reorganises, and these changes are reflected in the distribution of active sites. Moreover, even after reduction, there is the presence of a small peak attributed to oxidised palladium in interaction with the support. The absence of any major differences in the NR a NRC sample in comparison with the present one was correlated with the different particle size obtained by NR and ID procedures and, therefore, to the different interaction with the support created by the calcination treatment, in line with the different features of the particles observed in the TEM micrographs.

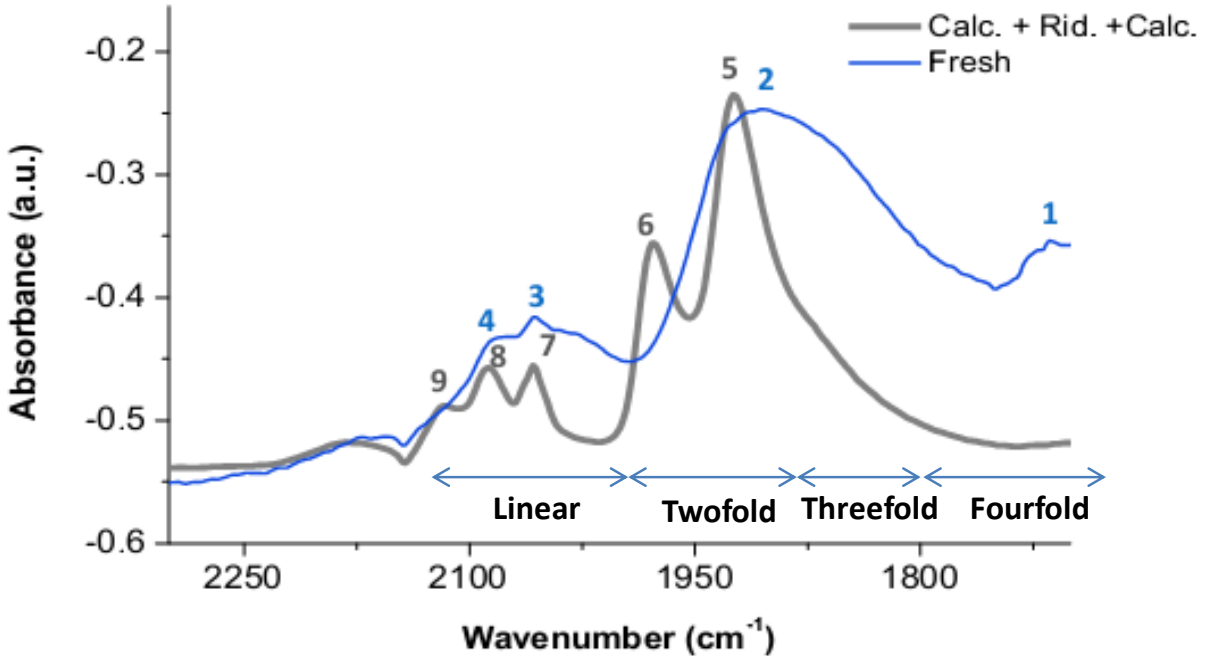

Figure 13 – DRIFT Spectra for the ID and IDC samples after reduction

3.1.4 TPR Results for the NR and ID samples

In order to get more insights about the interaction of Pd with the support, TPR measurements were performed on the ID and IDC samples in the range 25-450°C. With the ID sample (TPR profile not shown) as expected, we did not find any peak, confirming that Pd was fully reduced after the decomposition procedure (see preparation of the catalysts section). The obtained TPR profile for the IDC sample is reported in Figure 14. In this case, two main peaks were identified. The first one (centred at 73°C), attributed to PdO reduction [43], and the second one (centred at 305°C), attributed to nonstoichiometric

palladium aluminates decorating Pd islands [89] or bi-dimensional surface structure of oxidised palladium $[PdO]_{sc}$ [84]. Moreover, the reduction of the palladium took place over the whole temperature range and presumably continues after 450°C as also reported by Ivanova et. al. [89].

Table 5 – DRIFT peak assignment summary along with their reference in square brackets (number in the left side identify the main position on the spectra in Figure 13)

Bands [85]		ID sample	IDC sample
<1800 Fourfold	cm^{-1}	1. 1712 cm^{-1} CO fourfold [85]on (100) planes, associated with big particles	-
1800-1880 Threefold	cm^{-1}	2. 1910 cm^{-1} Composite CO adsorption band assigned to a combination of bridged (2000–1895 cm^{-1}) and threefold species (1920–1830 cm^{-1}) [86]	-
1880-2000 Twofold, Bridge	cm^{-1}		5. 1925 cm^{-1} CO threefold hollow, and bridge on Pd(111) [87] 6. 1978 cm^{-1} CO bridge on Pd(100) and edges and steps [87]
2000-2130 linear	cm^{-1}	3. 2057 cm^{-1} CO bound on (111)/(111) and (111)/(100) edge sites [87] 4. 2082 cm^{-1} CO bound on particle corners [86,87]	7. 2057 cm^{-1} Linear CO bound on (111)/ (111) and (111)/ (100) edge sites [87] 8. 2079 cm^{-1} Linear CO bound on particle corners [87] 9. 2118 cm^{-1} CO bound to Pd particles not totally reduced [88]

3.2 Catalytic Performances

The prepared catalysts were tested for the direct synthesis of H_2O_2 in the semi-batch recirculation reactor apparatus by using the contactor concept described in the experimental part (configuration A).

3.2.1 Testing Results for the SI-used Samples – Recyclability study

Catalysts prepared by sol immobilisation have often been reported in the literature as promising catalysts for the direct synthesis, but a crucial issue is given by the deactivation of the catalysts. The major difference with respect to other catalysts is the presence of PVA. Therefore, to study the effect of PVA on the catalysts prepared by SI technique and their deactivation, a recyclability test was performed. In this case, a total of 12 tests were run, for a total time on stream of 48h. Other tests varying $p_{H_2}^{ext}$ in the 0.3-4 barg

range and studying different ways of introducing O_2 and H_2 (configuration B) were studied but not reported. Here we reported the results for test 1-4, 6 and 12 performed in the same experimental conditions (configuration A, H_2 on the external side of the catalytic membrane at 2 barg, methanol solution containing only H_2SO_4 as a promoter). For conciseness, the results obtained were reported in *appendix I* of this chapter (see Figure 37-Figure 42). During the recyclability study it was observed that activity, productivity and selectivity at the end of each test as a function of time-on stream changed in a peculiar way (see Figure 15). Specifically, while the activity (expressed as hydrogen conversion rate, calculated by $\frac{[H_2O_2]_{4h}+[H_2O]_{4h}}{240min}$) presents a decreasing trend, both the H_2O_2 productivity (expressed as $\frac{[H_2O_2]_{4h}}{240\ min}$) and selectivity passes through a maximum. Another peculiarity is the higher reported selectivity with respect to other reduced catalytic membrane reported in this study which, as will be discussed, could only be explained by a promoting effect of PVA [64]. Conversely, the observed maximum in selectivity could be related to a partial dissolution of PVA and catalyst deactivation, as already reported in previous papers [32,60,64].

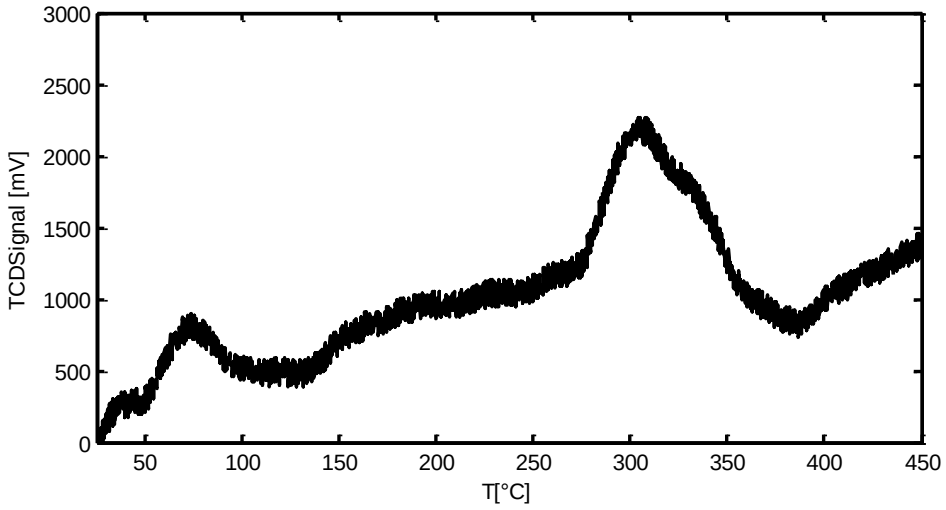

Figure 14 - TPR profile of IDC sample (β=10°C/min, 5% H_2/Ar flow)

More specifically, the low selectivity in the early tests could be related to a limited transport of H_2O_2 in the PVA layer, increasing the contact time of the produced H_2O_2 with the surface of Pd particles. The loss of PVA, then, progressively make the transport of H_2O_2 faster, justifying the observed increase in selectivity between the 2nd-4th test. After the 4th test, however, the further loss of PVA decrease its promotional effect. The decrease in activity with time-on-stream, conversely, can be related to the loss in MSA, as reported in the characterization section. Therefore, the reported trend could be explained by a progressive removal of PVA, together with a partial deactivation of the catalyst. PVA, indeed, is used in this case as a diffusional barrier for Pd in order to get nanoparticles and for preventing their agglomeration, therefore, a diffusional effect on the transport of H_2O_2 from the surface of the catalyst could be expected, especially in the early tests. Furthermore, although PVA shows a very tiny solubility in organic solvents, this could be reasonable in methanol, because of its high polarity. Moreover, as observed in the characterization section, the catalyst progressively deactivated by an Ostwald ripening mechanism. Another interesting

question is related to the routes promoted by PVA. Therefore, to answer all these questions and explain the obtained results, kinetics, transport phenomena and Ostwald ripening process were modelled and discussed.

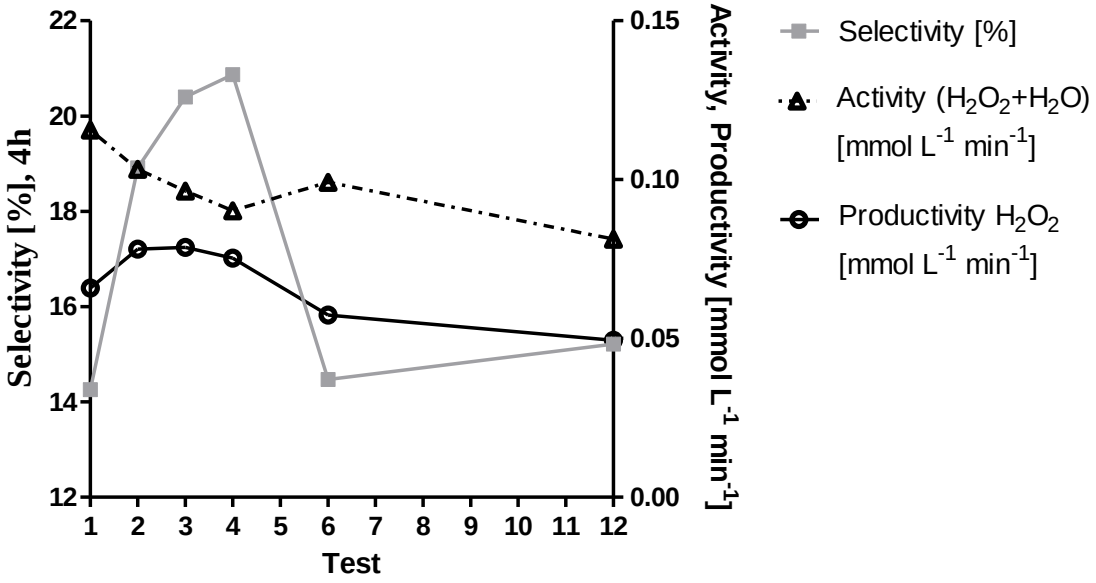

Figure 15 – Trend of Practical Activity, Productivity and Selectivity obtained at the end of each test (tests run only using H_2SO_4 as a promoter)

3.2.2 Testing Results for the NR, ID and SI samples – Effect of the calcination

The main results obtained with the ID catalysts before and after thermal treatments are reported in Figure 16, while the experimental data obtained for the NR catalysts are reported in Figure 16 and Figure 17. As reported in Figure 16 and Figure 17, the trends in the rate of production of H_2O_2 and selectivity before after thermal treatments present some differences. In line with the literature, selectivity to H_2O_2 decreases with time-on-stream for all the reported samples. Additionally, the selectivity for ID catalysts is lower, even though for the ID catalysts all the tests were performed in the presence of KBr, while, in the case of NR/NRC catalysts only H_2SO_4 was used as a promoter, in agreement with the reported structure sensitivity for the reaction [50,51,53]. The selectivity showed by as prepared samples is slightly lower for the ID/IDCR catalysts with respect to the NR samples. Consistently with the apparent increase in MSA, as underlined in the characterization section, after calcination and reduction at 100°C in pure H_2 (see experimental section), the IDCR catalyst shows a slight increase in activity and productivity, but the selectivity is comparable with the fresh ID catalyst. After calcination treatment, both catalyst families have shown an increase in the selectivity and productivity. Further, with both catalysts, after calcination treatment, we observed a slightly lower activity at the beginning of the reaction, which was correlated to the inactivity of PdO.

In the case of the calcination of the SI sample (see Figure 18), the behaviour was quite different. As with previous samples, after calcination, the presence of a slight induction time was noticed, but in this case, both the production rate of H_2O_2 and H_2O presented a decline during the reaction, while the selectivity was constant. Similar decreasing trend in the rate of production of both H_2O_2 and H_2O and

almost constant selectivity with time-on-stream were also evidenced by successive tests, even though there was a decline in selectivity (see Figure 18 for a comparison with the 8th test). All these phenomena were also correlated in this case to the redox dynamicity of the palladium surface. In addition, the observed decreasing rate of formation of both H_2O_2 and H_2O is a typical trend observed in cases of reaction inhibited by the product. A possible hypothesis, in this case, in addition to the observation made on the NRC and IDC samples, is that the reaction was progressively poisoned by the produced H_2O_2, as a consequence of the dynamic change of the $H_2/H_2O_2/O_2$ ratio during the reaction, and, as will be discussed, was correlated to the peculiarity of the particles generated by SI.

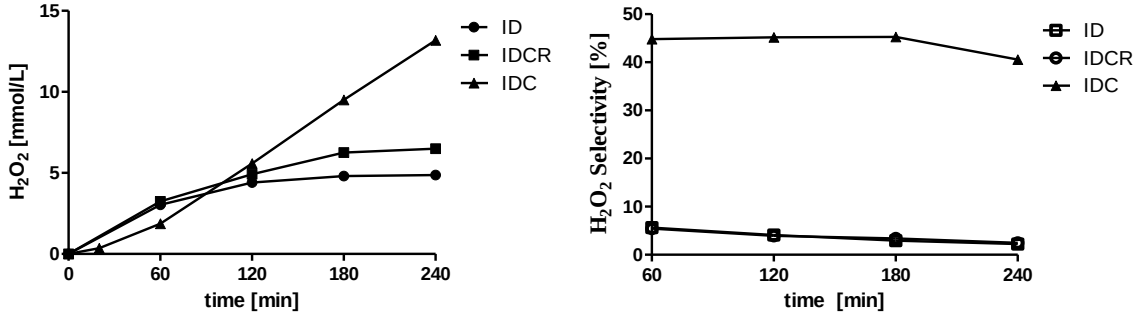

Figure 16 - Formation of H_2O_2 and selectivity as a function of time on stream for ID catalysts before and after thermal treatments (1. Calcination (not tested), 2. Calcination and reduction, 3. Calcination, tests in the presence of KBr and H_2SO_4 as promoters)

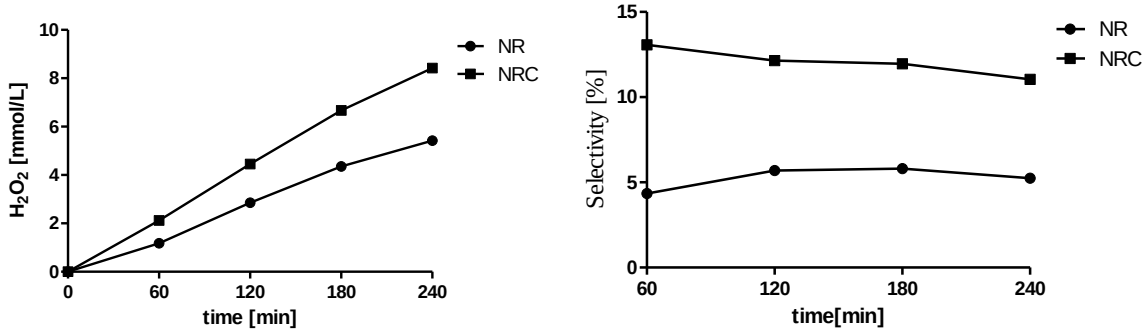

Figure 17 - Formation of H_2O_2 and selectivity as a function of time on stream for NR catalysts before and after thermal treatments (tests in the presence of H_2SO_4 as promoter)

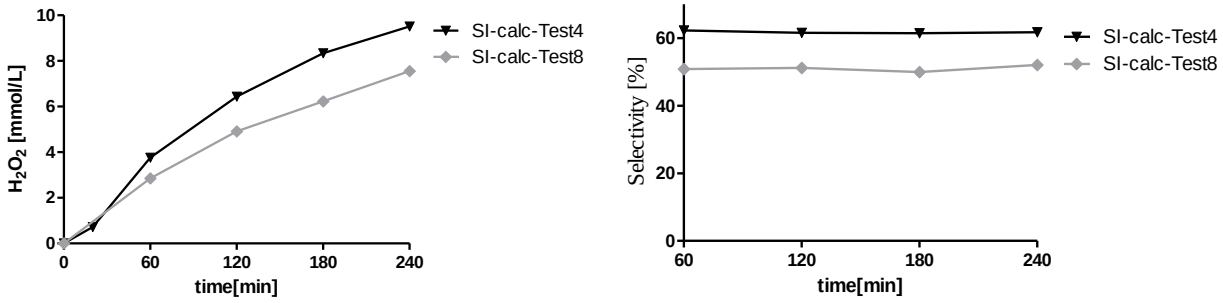

Figure 18 — Formation of H_2O_2 and selectivity as a function of time on stream for SIC-KBr catalysts after thermal treatments (tests in the presence of H_2SO_4 and KBr as promoters)

Therefore, given the results obtained for the NRC, IDC and SIC catalysts, to get further insights on the dynamic nature of the active sites and on the main effect of the applied thermal treatments on the kinetics of the reaction, two kinetic models were developed.

3.2.3 Performance Comparison

A comparison of the performances obtained by the catalytic membranes used in this work for the direct synthesis is reported in Figure 19. Here we reported the productivity of H_2O_2 expressed as $\frac{mmol_{H_2O_2}}{(g_{Pd} \cdot h)}$ and the selectivity, both measured at the end of each test (240 min).

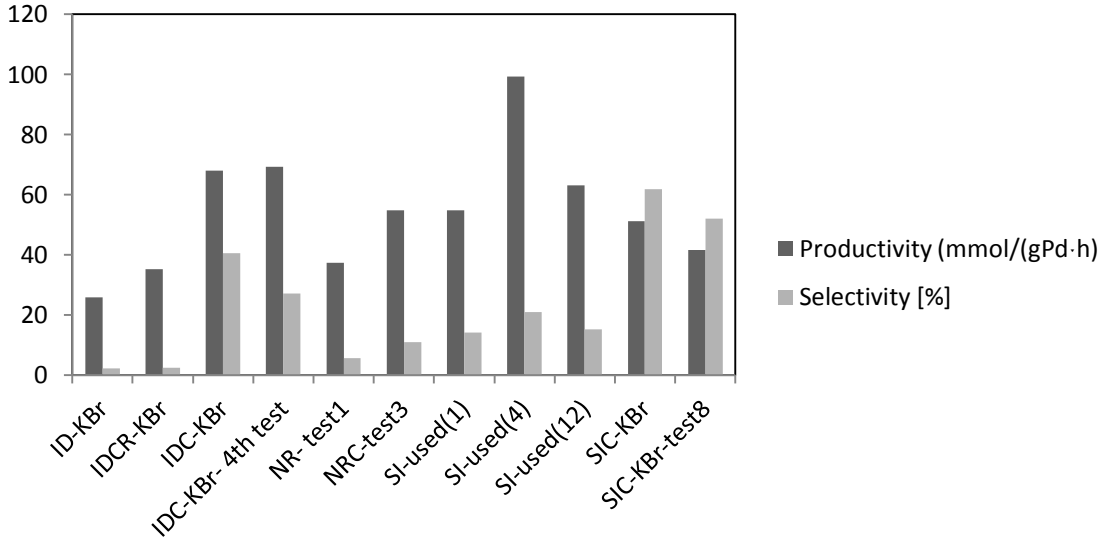

Figure 19 – Productivity and selectivity Comparison for each catalyst at the end of each test (240 min)

The best productivity was reported for the SI-used(4) sample, at the 4th test, although the selectivity is low. In this case, only H_2SO_4 was used as promoter. Conversely, the best selectivity was observed for calcined catalysts, namely, SIC, SiC-test8, IDC and NRC, in decreasing order, while the productivity was comparable. Therefore, comparing all the tested catalysts, the best trade-off between productivity and selectivity was obtained by the SIC catalysts.

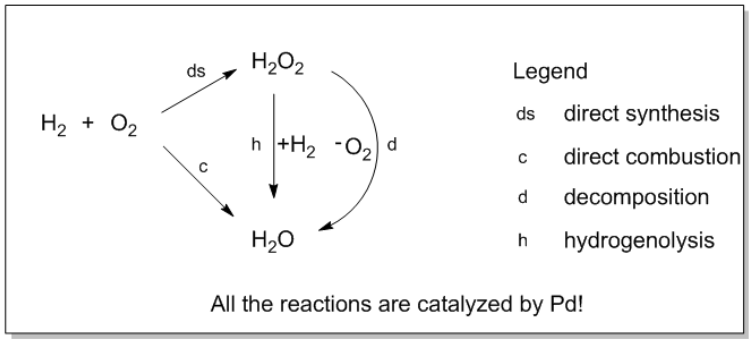

Scheme 3 - Kinetic reaction network in the direct synthesis of H_2O_2 on Pd catalysts

3.3 Kinetic Modelling

The direct synthesis of H_2O_2 on Pd-based catalysts, as previously reported [31,47,90], presents a complex network of reaction (see Scheme 3).

The most important reactions are the direct synthesis (ds) the direct combustion (c), parallel to each other, and the H_2O_2 hydrogenolysis in series to the ds reaction, while, as previously reported in [31,47,91], for Pd supported on ceramic membranes, the decomposition route (d) is much slower than the hydrogenolysis route (h) and, to simplify the kinetic model, can be neglected.

3.3.1 Model 1 - reduced catalysts

Model 1 was originally proposed in [31,47,78]. The main assumptions behind this model are: 1) a constant number of active sites during the tests; 2) a constant concentration of oxygen and hydrogen. The constant concentration of oxygen is ensured by pre-saturation stage (20 minutes) before the starting of the reaction, as described in the experimental section, and for hydrogen by the proximity of the H_2/methanol interface to the catalytic zone of the membrane.

After simplification of the model, the following rate equations may be written (more detail are reported in [31,47,91]) (*model 1*):

$$\frac{d[H_2O_2](t)}{dt} = k_{ds}' - k_h'[H_2O_2](t)$$

$$\frac{d[H_2O](t)}{dt} = k_c' + 2k_h'[H_2O_2](t)$$

$$[H_2O_2](0) = 0$$

$$[H_2O](0) = 0$$

Where k_{ds}', k_d' and k_c' are respectively the pseudo-kinetic constants for the direct synthesis, direct combustion and hydrogenolysis reactions. This set of ODE can be easily reduced to:

$$[H_2O_2](t) = \frac{k_{ds}' - k_{ds}'e^{-k_h't}}{k_h'}$$

$$[H_2O](t) = k_c't + 2k_{ds}'\left(\frac{e^{-k_h't} - 1}{k_h'} + t\right)$$

3.3.2 Model 1d - diffusion of H_2O_2 inside the PVA layer and selectivity (diffusion, non-calcined catalysts)

The catalytic membranes prepared by SI differ with respect to other catalytic membranes prepared by other techniques by the presence of PVA, used as a capping agent. As reported in section 3.2.3, for SI-used(n), selectivities were always higher with respect to other reported catalytic membranes. Therefore a promotion effect by PVA is expected. However, during the recyclability tests (see section 3.2.1), a maximum of selectivity was observed in correspondence of 3rd-4th test. In addition, a decrease in the dispersion of the catalyst was also noted. A possible explanation is that the presence of PVA could limit the transport of the produced H_2O_2 in the early tests, increasing its local concentration in the proximity of the Pd surface and its consumption by hydrogenolysis. This, of course, might explain the low selectivity in

the early tests. The decrease in PVA amount because of its solubilization might explain the observed maximum in selectivity. A further decrease in the PVA amount, in line with the expected promotional effect, conversely, might explain the loss of selectivity in the final tests. Further, the observed decrease in activity during the time-on-stream could be correlated with the Ostwald ripening process, also related to the gradual loss of PVA. Therefore, to get more insight on these phenomena, kinetic modelling could be useful. However, the previously developed model (Model 1) does not take into account transport phenomena nor the Oswald ripening processes. Therefore, in order to take into account the possible presence of transport phenomena in the early tests and the Ostwald ripening processes a different strategy is necessary.

The catalytic contactor concept [75] for the H_2O_2 direct synthesis presents a very tiny static zone inside the mesoporous layer were the reaction take place, and depending on the production rate of H_2O_2 there could be a considerable gradient of H_2O_2 or by the reactants, between the inner part of the catalytic zone and the outer part in contact with the solvent. However, considering 1) the mild operating conditions used in these tests, 2) the large macropores (70nm in diameter) and 3) the very tiny layer of catalyst (almost 10μm) in proximity of the solvent (catalytic membranes prepared as eggshell catalysts), we can exclude internal diffusion phenomena. Nonetheless, PVA forms a static zone on the surface of the Pd NPs. Therefore, assuming the reaction as limited by the mass transfer of the product, the transport of H_2O_2 and H_2O between the Pd particles and the surrounding PVA-environment could be modelled in the same way as the external diffusion:

$$r_{H_2O_2,apparent} = km_{H_2O_2}\,([H_2O_2]_s - [H_2O_2]_b)$$

$$r_{H_2O,apparent} = km_{H_2O}\,([H_2O]_s - [H_2O]_b)$$

where $r_{H_2O_2,apparent}$ and $r_{H_2O,apparent}$ $\left[\frac{\text{mmol}}{\text{L min}}\right]$ are the apparent rate of formation of H_2O_2 and H_2O at the surface of the Pd particle; $[H_2O_2]_s$, $[H_2O_2]_b$, $[H_2O]_s$ and $[H_2O]_b$ $\left[\frac{\text{mmol}}{L}\right]$ are, respectively, the concentration of H_2O_2 and H_2O at the surface of the Pd particles (idendified by the s subscript) and in bulk of the solution (identified by the b subscript); $km_{H_2O_2}$ and km_{H_2O} $\left[\frac{1}{min}\right]$ are the mass transfer coefficient for H_2O_2 through the PVA layer multiplied by the interfacial area PVA/Methanol. Given the kinetics described by *model 1*, the following equations may be written:

$$k_{ds}{}' - k_h{}'[H_2O_2]_s = km_{H_2O_2}\,([H_2O_2]_s - [H_2O_2]_b)$$

$$k_c{}' + 2k_h{}'[H_2O_2]_s = km_{H_2O}\,([H_2O]_s - [H_2O]_b)$$

Because we cannot measure $[H_2O_2]_s$ nor $[H_2O]_s$ we eliminate this term to obtain:

$$[H_2O_2]_s = \frac{k_{ds}{}' + km_{H_2O_2}[H_2O_2]_b}{km_{H_2O_2} + k_h{}'}$$

$$[H_2O]_s = \frac{-k_c{}' - km_{H_2O}[H_2O]_b}{2k_h{}' - km_{H_2O}}$$

Plugging in *model 1* the calculated $[H_2O_2]_s$, the model describing the semi-batch reactor in presence of diffusional limitation on the PVA layer, indicated briefly as *model 1d,* becomes:

$$\frac{d[H_2O_2]_b(t)}{dt} = k_{ds}{}' - k_h{}'\left(\frac{k_{ds}{}' + km_{H_2O_2}[H_2O_2]_b(t)}{km_{H_2O_2} + k_h{}'}\right)$$
$$\frac{d[H_2O]_b(t)}{dt} = k_c{}' + 2k_h{}'\left(\frac{k_{ds}{}' + km_{H_2O_2}[H_2O_2]_b(t)}{km_{H_2O_2} + k_h{}'}\right)$$

$$[H_2O_2]_b(0) = 0$$

$$[H_2O]_b(0) = 0$$

However, a complication, as already discussed in the characterization section, is the changing MSA because of the Ostwald ripening process affect the Pd nanoparticles. These phenomena, in turn, could be related to several factors: 1) the absence of interaction between the Pd NPs and the support, 2) loss of PVA during the reaction and 3) thermodynamic instability of Pd particles below a critical thermodynamic diameter.

To take into account the changing MSA, knowing the dependence of the pseudo-kinetic constants by the Pd MSA, we need to introduce in the above equations the *S* parameter, defined as the integral average MSA for the actual test. Substituting the S parameter in the previous model, we obtained:

$$\frac{d[H_2O_2]_b(t)}{dt} = S\,k_{ds}{}' - S\,k_h{}'\frac{S\,k_{ds}{}' + km_{H_2O_2}[H_2O_2]_b(t)}{km_{H_2O_2} + S\,k_h{}'}$$
$$\frac{d[H_2O]_b(t)}{dt} = k_c{}' + 2k_h{}'\frac{S\,k_{ds}{}' + km_{H_2O_2}[H_2O_2]_b(t)}{km_{H_2O_2} + S\,k_h{}'}$$

$$[H_2O_2]_b(0) = 0$$

$$[H_2O]_b(0) = 0$$

This ODE system was solved symbolically yielding the following expressions:

$$[H_2O_2]_b(t) = \frac{e^{-\frac{k_h{}' km_{H_2O_2} S\,t}{km_{H_2O_2} + k_h{}' S}}\left(-1 + e^{\frac{k_h{}'\,km_{H_2O_2} S\,t}{km_{H_2O_2} + kh{}' S}}\right)k_{ds}}{k_h{}'}$$

$$[H_2O]_b(t) = \frac{e^{-\frac{k_h{}' km_{H_2O_2} S\,t}{km_{H_2O_2} + k_h{}' S}}\left(2k_{ds}{}' - 2e^{-\frac{k_h{}' km_{H_2O_2} S\,t}{km_{H_2O_2} + k_h{}' S}}k_{ds} + e^{-\frac{k_h{}' km_{H_2O_2} S\,t}{km_{H_2O_2} + k_h{}' S}}k_c{}' k_h{}' S\,t + 2e^{-\frac{k_h{}' km_{H_2O_2} S\,t}{km_{H_2O_2} + k_h{}' S}}k_{ds}{}' k_h{}' S\,t\right)}{k_h{}'}$$

For describing the evolution of the average MSA for the case of Ostwald ripening process, a simple model can by derived by the LSW theory, which describes the evolution of the average radius with time[92] by the following equation:

$$r_f^3 - r_o^3 = K\,t$$

Where r_o and r_f are initial and final particle radius and K is a constant an t is the time (see [92] for further details). By taking several measurement and regressing the right hand side of this model, in presence of Ostwald ripening processes, a straight line should be obtained. Then, by the obtained fitting, assuming a negligible loss of Pd by leaching, an approximation of the dynamic change of the average MSA can be calculated.

This kind of modelling strategy is only possible by assuming an almost constant concentration of PVA on the surface of the particles during each test. The first assumption is justified by experimental conditions used for each test. The PVA, indeed, with respect to water, presents a very tiny solubility in organic solvents and in alcohols, therefore, we can assume that PVA reaches its equilibrium concentration in Methanol and a steady layer on the surface of Pd particles in the first 20 minutes of the test, during the O_2 pre-saturation stage (see experimental part).

Further complications in the case of SI are: 1) the unknown thickness of the PVA surrounding the Pd particles; 2) the unknown diffusion coefficient for H_2O_2 in the PVA layer; 3) the intrinsic kinetics for the early tests are unknown; 4) PVA present a promotion effect, probably decreasing the dissociative chemisorption of O_2, and therefore decreasing the relative importance of the direct combustion reaction (k_c'). Therefore, to test these hypotheses, some assumptions need to be made. A rough estimate of the transport coefficient for H_2O_2 for the 1st and 2nd tests can be calculated by assuming the absence of transport limitation (kinetic regime) e.g. for the 3rd and 4th tests and a negligible influence of PVA, in the given range of concentrations, on the direct synthesis and hydrogenolysis kinetics. This assumption is justified by the obtained maximum on selectivity (see Figure 20) and by the negligible difference in selectivity/productivity in both tests. Assuming the 3rd and 4th tests in kinetic regime, we could use *model 1* for calculating the k'_{ds} and $k_h{}'$ for the 4th test, plugging in these values together with the average MSA calculated by the Ostwald ripening model in *model 1 d* and fitting model 1 with the experimental data for the 1st and 2nd tests by nonlinear regression. In this way we can estimate both $km_{H_2O_2}$ and $k_c{}'$ (later indicated as $k_c{}''$ for indicating that this is a fitted value from *model 1d*). The k_c'' value for the fourth test was not plugged in the *model 1d* because of the probable effect of PVA on the direct combustion, as previously discussed. This parameter, further, was used for testing the reliability of the model by comparing k_c'' obtained for the 1st and 2nd tests (fitted parameter in *model 1d*) with the value of k_c' obtained for reference test (4th test) by using *model 1* (4th test, $k_c{}'_{4^{th}Test}$). In this case, a higher k_c'' with respect to the reference $k_c{}'_{4^{th}Test}$ could be interpreted as failure of the previous assumptions while a lower value could be interpreted, as the effect of PVA blocking some of the most active sites for the direct combustion. Therefore, 1) the Ostwald ripening model was used for calculating the average MSA for each test; 2) model 1 was used for fitting all the tests for the SI-used(n) membrane for calculating both the apparent and pseudo-kinetic rate constants; 3) The 1_{st} and 2_{nd} tests were assumed in diffusional regime and were modeled by using model 1d for calculating the transport coefficient and k_c''; 4) all the results were evaluated considering all the pseudo kinetic constants normalized by the respective MSA for each test.

3.3.3 Model 2 - calcined catalysts

In calcined samples, we observed the presence of tiny induction time in the evolution of both H_2O_2 and H_2O. This phenomenon, of course, could be the result of the dynamicity of the oxidation state of the surface the catalysts. Further, it is known that the reduction of PdO begins at a lower temperature than room temperature. A possible hypothesis, as reported in a previous paper [31], could be that PdO, assumed as inactive, could get reduced during the synthesis, modifying the nature of the surface and therefore the activity of the catalyst. Consequently, the number of active sites is not constant during the reaction, adapting their number to the redox environment of the reaction. Assuming that 1) the in-situ dynamic change of the catalyst surface influences only the number of active sites, and 2) PdO is inactive, then, model 1 could then be modified as follows:

$$\frac{d[H_2O_2](t)}{dt} = S_r(t)(k_{ds}{}' - k_h{}'[H_2O_2](t))$$

$$\frac{d[H_2O](t)}{dt} = S_r(t)(k_c{}' + 2k_h{}'[H_2O_2](t))$$

Where the $S_r(t)$ parameter ($0< S_r(t)<1$), proportional to the number of active sites, describes the fraction of reduced Pd on the surface of de catalyst on our conditions of reaction as a function of time-on-stream t for the given test.

As reported for Pd catalysts, the reduction of PdO by using H_2, take place with a *shrinking core mechanism* [93], which, in turn, can be modelled by Kissinger method [94,95]. Therefore, assuming a constant concentration of hydrogen and the surface reduction kinetics proportional to the oxidised surface fraction S_{Ox} ($0<S_{Ox}<1$, $Sr = 1-S_{Ox}$):

$$\frac{dS_r(t)}{dt} = k_{Pd,r}(1 - S_r(t))$$

For the calcined membranes we assumed that the Pd (surface and bulk) is completely oxidised to PdO, so the initial condition was set to:

$$S_r(0) = 0$$

The ODE system was then solved analytically, yielding the following expressions:

$$[H_2O_2] = \frac{k_{ds}{}' - k_{ds}{}' e^{-\frac{k_h'(k_{Pd,r}\,t + e^{-k_{Pd,r}\,t} - 1)}{k_{Pd,r}}}}{k_h{}'}$$

$$[H_2O_2] = -\frac{2\,k_{ds}'\left(k_h'(-e^{-k_{Pd,r}\,t}) - k_h{}'^{k_{Pd,r}}t - k_{Pd,r}\,e^{-\frac{k_h'(k_{Pd,r}t + e^{-k_{Pd,r}\,t} - 1)}{\mathrm{kPd}}} + k_h' + k_{Pd,r}\right) + k_c{}'^{k_h'}\left(-k_{Pd,r}t - e^{-k_{Pd,r}\,t} + 1\right)}{k_h'\,k_{Pd,r}}$$

3.3.3 Model 3 - calcined catalysts

With respect to previously reported membranes prepared both by NR or ID [31], SIC membranes present some peculiar characteristics. Moreover, during the tests we observed: 1) a decreasing trend in both H_2O_2 and H_2O rate of formation and 2) an almost constant selectivity during time-on-stream. The first observation could indicate a sort of inhibition phenomena by the formed products, which was correlated to Pd oxidation by the formed H_2O_2, as already reported in the literature [67–69]. The second observation, instead, indicates a negligible contribution from the hydrogenolysis route during the test in the studied range of experimental values. Therefore, to test these hypotheses *model 2-calc* was modified to consider the increasing concentration of H_2O_2 with time and its oxidative effect on Pd (*model 3-calc*). In this case, we assumed that the rate of oxidation of the surface is proportional to both the available reduced surface and the concentration of hydrogen peroxide:

$$\frac{dS_r(t)}{dt} = k_{Pd,r}\big(1 - S_r(t)\big) - k_{PdOx}\, S_r(t)[H_2O_2](t)$$

$$S_r(0) = 0$$

Moreover, as previously discussed, the hydrogenolysis reaction is probably negligible after the calcination treatment. Therefore, to simplify the model, we discarded the hydrogenolysis kinetics, so the model reduces to:

$$\frac{d[H_2O_2](t)}{dt} = S_r(t)\; k_{ds}'$$

$$\frac{d[H_2O](t)}{dt} = S_r(t)\; k_c'$$

3.4 Kinetic Analysis

The kinetic analysis is divided into two parts. In the first part the results of the kinetic analysis for SI catalysts, regarding a recyclability study will be presented in order to study the effect of PVA on reduced catalysts. The experimental results will be analysed by using both *model 1* and *model 1d*. In this case, *Model 1,* originally developed for analysing reduced catalysts will be used as a reference model, while *Model 1d* will be used for describing the results obtained in the early tests with SI-used(n) catalysts were we expected the presence of transport limitations for H_2O_2.

In the second part, the results of NR, ID, SI and the related calcined tests will be analysed by using *model 1* for reduced catalysts and by using *model 2-calc* and *model 3-calc* for analysing the results obtained for calcined catalysts. Specifically, *model 2-calc* will be used for analysing the results obtained with the IDC catalyst and *model 3-calc* for analysing the results obtained with the SIC catalytic membrane.

The reported kinetic models were fitted by nonlinear regression algorithm with the Matlab 2014 Trust-Region-Reflective optimisation or with Wolfram Mathematica by using the Levenberg-Marquardt algorithm. In the case of *model 3-calc,* the resulting ODE system was too complicated to be solved symbolically. So to fit the kinetic constants of the reaction, we fitted the ODE model by nonlinear regression of the numerical solution of the parameterized ODEs by using Wolfram Mathematica 10, using the LSODA algorithm for the numerical solution of the ODE set.

3.4.1 Recyclability tests on SI catalysts

In the first part of this kinetic analysis, we fitted the experimental data for H_2O_2 and H_2O production to *model 1*, used as a reference to calculate the assumed true and apparent pseudo-kinetic rate constants. The resulting *true and apparent pseudo-rate constants* are reported in Table 6 and Figure 20.

. From the visual analysis of the reported results in Figure 20, we can observe a change in trends for all the apparent pseudo-kinetic constants. Further, k_c' and k_h' for test 1-3 present an opposite trend, with k_c' decreasing from the first through the fourth test, while k_h' and k_{ds}' increase, to reach a plateau between the third and fourth test, which, to the knowledge of the author, is quite atypical for the catalysts used for this reaction. Usually, as observed in the previously reported paper, the selectivity to H_2O_2 and productivity decreases with time-on-stream [32,60,64,80], as often reported in the literature for other catalysts also because of catalysts deactivation. Nonetheless, this kinetic behaviour might hide some features, which, in the present case, by using milder reaction conditions with respect to the previously cited paper, might be revealed. Of course, analysing these results without taking into account the deactivation of the catalyst by the loss of PVA is of little value. The results obtained by nonlinear regression of the *Ostwald ripening model* are reported in Figure 21. In this case, the average TEM diameter data obtained by the three membranes reported in Table 3, used for a different time on stream, were used for the underlined fitting. The results of the regression analysis for the Ostwald ripening model were quite satisfactory, even though only three data points were used (see Figure 21). This simple model allows us to calculate a rough estimate of the average MSA (S) for each test. The leaching was considered negligible with respect to the Pd loading, therefore was not taken into account to calculate the effective loss of Pd (see characterization section). For modelling the reaction, in this case, only the integral averages of the MSA calculated for each test were used, because, with respect to the calcination case study discussed in *model 2,* the variation of active sites during each test can be considered negligible.

Therefore, the obtained parameters should be considered as averaged for each test. A plot of the relative MSA, with respect to the fourth test, was obtained by modelling Pd nanoparticles as mono-dispersed particles of radius *r* is reported in Figure 22, while the integral average of the relative MSA is reported in Table 6.

Using the normalised MSA, with respect to the 4th test, it is possible to follow the activity for the reaction as deactivation proceeds. A comparison of the normalised MSA with respect to the 4th test with the *apparent activities* (obtained by using *model 1*), all normalised with respect to the 4th test, is reported in Figure 23 (see definitions reported in the same figure). By Figure 23, it is possible to notice the almost perfect matching between the activity for hydrogen consumption with the normalised MSA in correspondence of the 2nd -4th tests and the hydrogenolysis activity in correspondence of the 3rd -6th tests. This, of course, give value to the hypothesis of using the 4th test as a reference for the diffusional treatment, as in correspondence of these tests we have a trade-off concentration of PVA.

Table 6 – Apparent pseudo-kinetic constants calculated the R52-SI catalyst for several tests (as obtained by model 1 not normalised by MSA)

Catalyst family	Test Number (n)	Model	k_{ds}', [mmol $L^{-1}min^{-1}$]	k_h' [min^{-1}]	k_c' [mmol $L^{-1}min^{-1}$]	Integral average of MSA relative to the 4th test (S)	Regime (inferred)
	1	1	0.0664±0.0031	0	0.403±0.031	1.61	External diffusion
	2	1	0.0868±0.0080	0	0.347±0.080	1.26	External diffusion
SI-used(n)	3	1	0.1158±0.0107	0.00341±0.0011	0.234±0.029	1.10	Kinetic
	4	1	0.1090±0.012	0.0033±0.0012	0.224±0.032	1.00	Kinetic
	6	1	0.0802±0.0067	0.0029±0.0009	0.291±0.018	0.87	Kinetic
	12	1	0.0789±0.0054	0.0042±0.0008	0.214±0.014	0.69	Kinetic

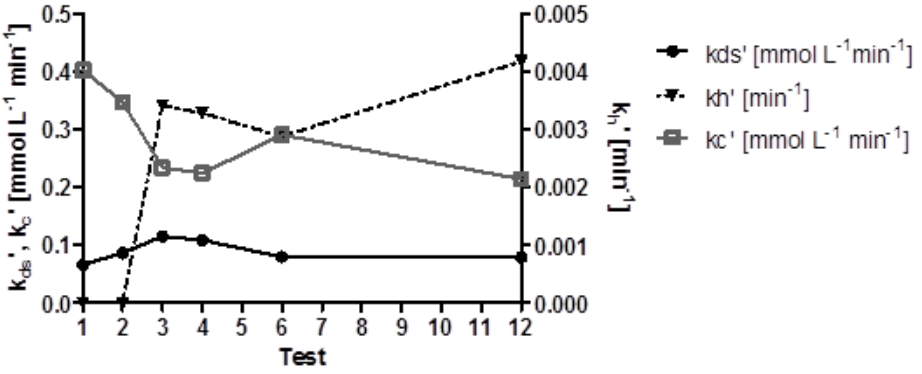

Figure 20 – Apparent pseudo-kinetic rate constants for the SI-used(n) sample in each test as obtained by model 1, not normalised by MSA

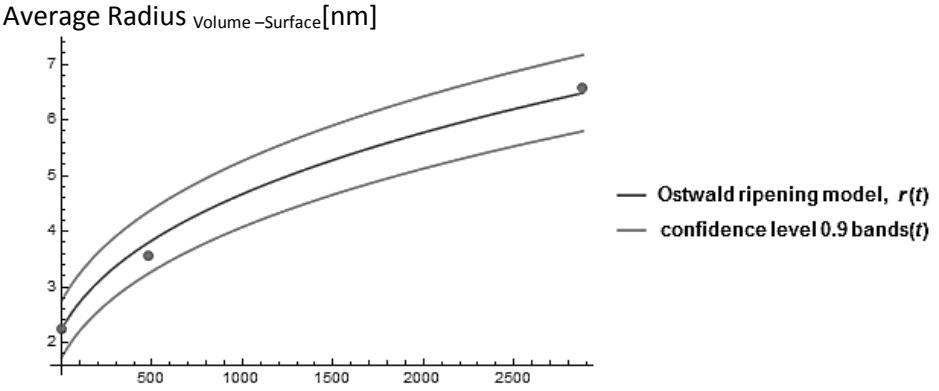

Figure 21 – Ostwald ripening model fitted by nonlinear regression

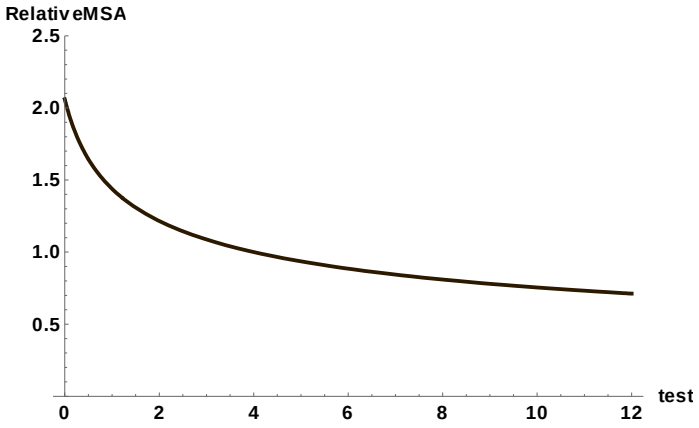

Figure 22 – Evolution of the MSA normalised with respect to the 4th test, with respect to time, calculated by the LSW theory for the SI-fresh and Si-used(n) catalytic membranes

Therefore, to test the assumption about transport limitation of H_2O_2 given by PVA, limiting the selectivity during 1st and 2nd tests, *model 1d* was used. k_{ds}' and k_h' obtained for the 4th test, together with the relative MSA with respect to the 4th test (S) were plugged into *model 1d* while $K_{mH_2O_2}$ and k_c'' (which correspond to the actual k_c' value for each test divided MSA relative to the 4th test), were fitted. The results of the diffusional analysis (*model 1 d*) for the first and second tests are reported in Table 7. Both, H_2O_2 surface concentration and bulk concentration of H_2O_2 predicted by *model 1 d* are reported in Figure 24 for the 1st and 2nd test. The overall quality of the fittings is good, with only an increasing trends in the residuals calculated in the case of the 1st test (the model slightly overestimate the rate of H_2O_2 at the beginning of the test) (see Figure 24). We tried also to repeat on the data relative to the 3rd test the same procedure used for the 1st and 2nd tests with *model 1 d*, but the model predict an infinite transport coefficient and a k_c'' of the same order of magnitude with respect to the 4th test, confirming the hypothesis that the 3rd test is not in diffusional regime.

A plot of the actual pseudo-kinetic constants normalised by the relative MSA is reported in Figure 25. In this plot, we reported the value of the pseudo-kinetic constants obtained by *model 1* divided by the relative surface area for 3rd – 12th tests. For the 1st and 2nd test, we reported the value k_c'' and the value of k_{ds}' and k_h' for 4th test respectively obtained by and plugged in *model 1 d*, which, by the given definitions, represent the equivalent quantity. From Figure 25 it is possible to see that the pseudo-kinetic constant for the direct synthesis is almost constant for each test, while we have a continuous increase in the direct combustion, which is even more marked in correspondence of the 6th test. For this constant, a slight decrease was observed in correspondence of the 12th test. The trend for the hydrogenolysis constant is almost steady till the 6th test and then increases in correspondence of the 12th test.

3.4.2 Calcination Effect on NR and ID samples

The main results obtained after fitting *model 1* and *model 2-calc* for the ID and NR catalysts are reported in Table 8. Figure 26 reports the trend in the pseudo-kinetic constants after each treatment for the ID catalysts family. From the analysis of Figure 26 it is evident that the main effect of the calcination treatments is a decrease in the k_c' and a slight reduction of the k_h' constant. The effect on the k_h' constant is also evidenced by the 2nd test, after calcination and reduction at 100°C. However, in that case, the k_c' constant appears to increase with respect to the same treatment, probably because of the increase in the

number of defects upon reduction at low temperature, correlated to the reduction of the average particle diameter reported in the characterization section.

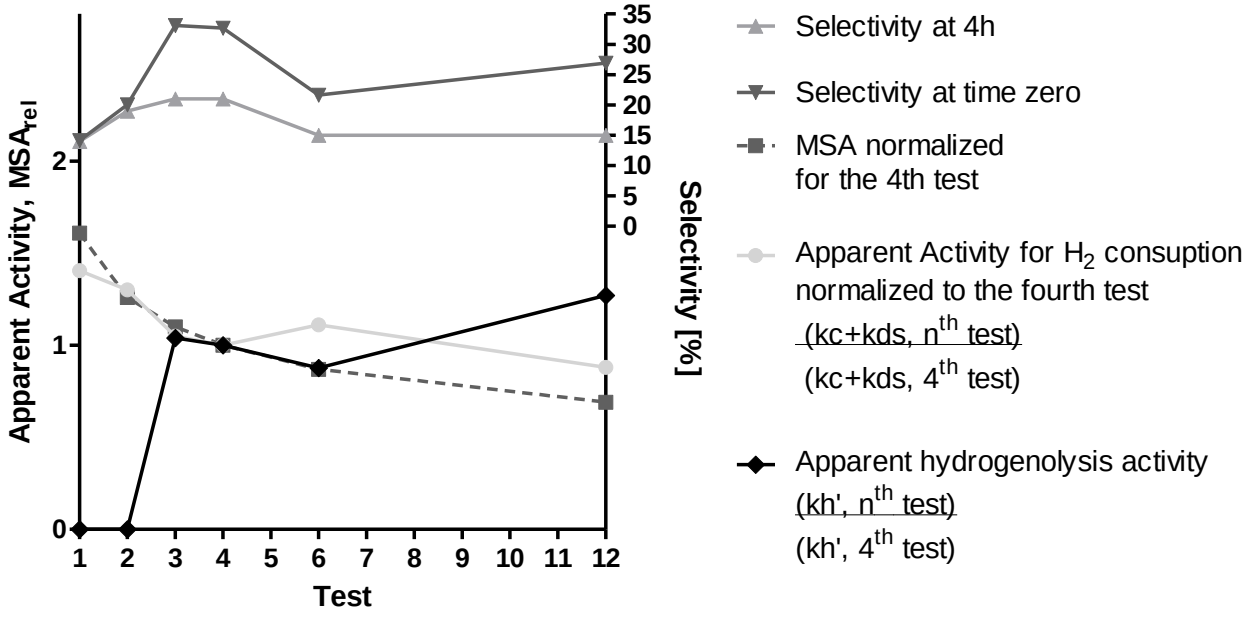

Figure 23 – Apparent activity (expressed as hydrogen consumption at time zero kc'+kds' or kh' relative to the fourth test), MSA (normalised with respect to the fourth test) and Selectivity trends for the SI-used(n) sample

Further, *model 2-calc* predict for IDC catalyst at the end of the test that the reducible surface of Pd in the given conditions is fully reduced at the end of the test (see Figure 27). The results obtained in the 4th test by fitting *model 1*, without any additional treatments further support the modelling results obtained with *model 2-calc* and prove that even if the reducible fraction of Pd (S_r) is completely reduced on the surface, there is no significant variation in the fitted pseudo-kinetic constants. A similar behaviour for the calcined catalyst was observed with the NR catalysts (see Table 8). This data is further supported by the observed conversion trends, reported in Figure 28. it is possible to note that the conversion increases with time on stream for the IDC sample while it is almost steady for the IDC reused.

Table 7 – Results for the diffusion limited kinetics (model 1d), for the 1st and 2nd tests

Catalyst family	Test (n)	Model	Km_{H2O2} [min^{-1}]	k_c'' fitted (normalised with respect to the 4th test) [mmol L^{-1}min^{-1}]	$\frac{k_c'' - k_c'_{4^{th}\,test}}{k_c'_{4^{th}\,test}}$	$k_c' = k_c'' \cdot S$ [mmol L^{-1}min^{-1}]	kds' calculated [mmol L^{-1}min^{-1}]
SI-used(n)	1	1d	0.00481±0.00093	0.1137±0.033	-49.34%	0.183	0.175574
	2	1d	0.03207±0.03010	0.1942±0.053	-13.49%	0.245	0.137639

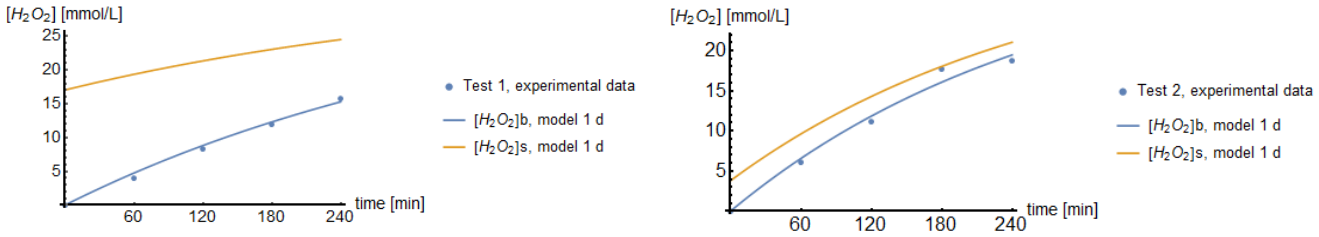

Figure 24 – concentration of H_2O_2 on the surface of the particles and in the solution from the fitting of model 1d for the 1st and 2nd tests

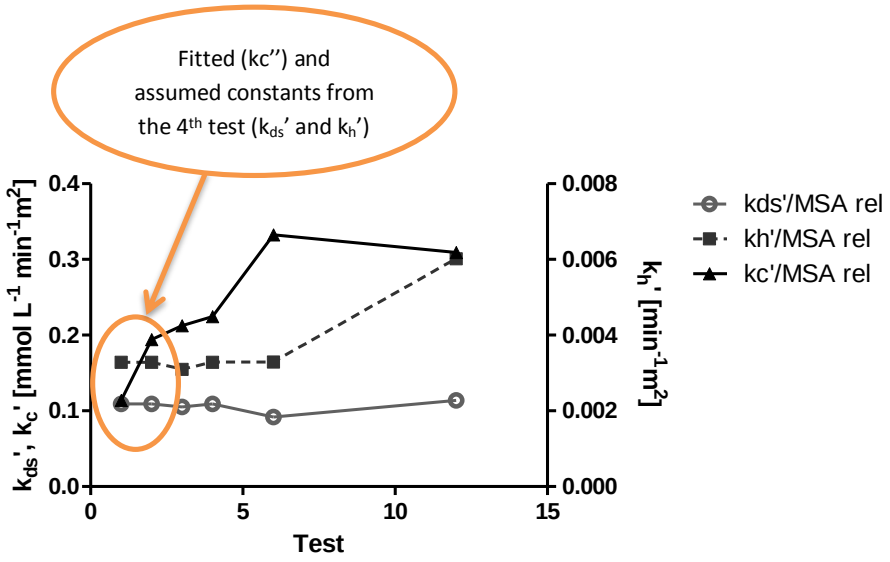

Figure 25 - Pseudo-kinetic rate constants normalised by the relative MSA for the SI-used(n) sample (the marked values are the ones obtained after application of the diffusion treatment).

Table 8 - Pseudo-rate constants (and relative 95% confidence limit) summary for ID and NR catalysts before and after thermal treatments

Catalyst Family	Test	Pre-treatment	KBr [mg/L]	Fitted Model	k_{ds}', [mmol L^{-1} min^{-1}]	k_h' [min^{-1}]	k_c' [mmol L^{-1} min^{-1}]	$k_{Pd,r}$
ID	1	None	60	1	0.08038±0.012	0.0159±0.003	0.7747±0.004	-
	2	Calcination and Reduction	60	1	0.07132±0.013	0.009765±0.002	0.9481±0.035	-
	3	Calcination	60	2	0.09298±0.013	0.00257±0.0017	0.0742±0.008	0.0153±0.004
	4	None	60	1	0.0842±0.010	0.003972±0.001	0.09182±0.012	-
NR	1a	None	0	1	0.03148±0.009	0.002471±0.003	0.3851±0.004	-
	3a	Calcination	0	2	0.04814±0.025	0.002337±0.004	0.2817±0.015	0.07013±0.080

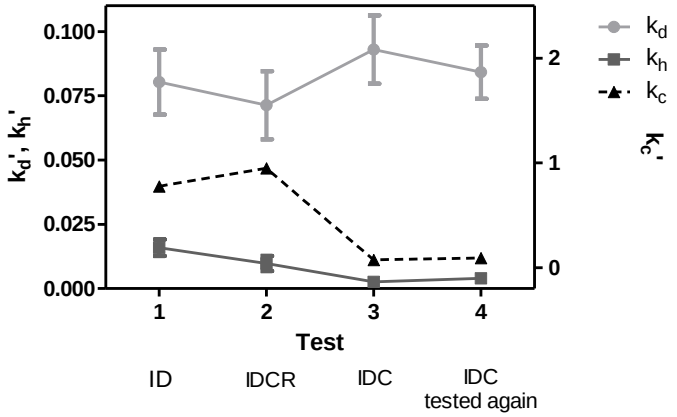

Figure 26 - Pseudo-rate constants determined for ID family of samples as a function of the catalyst pre-treatment, together with the 95% confidence interval as determined by the above reported fitting procedure.

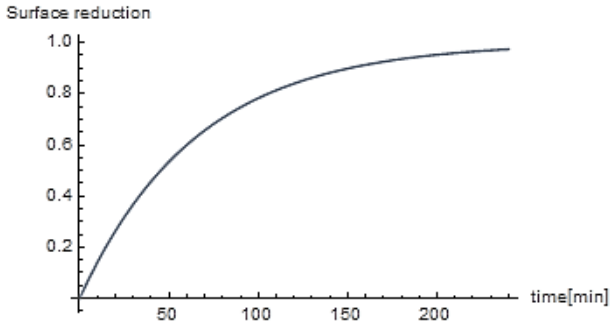

Figure 27 - Surface reduction dynamics for the IDC catalyst predicted by *model 2 calc (3rd test)*

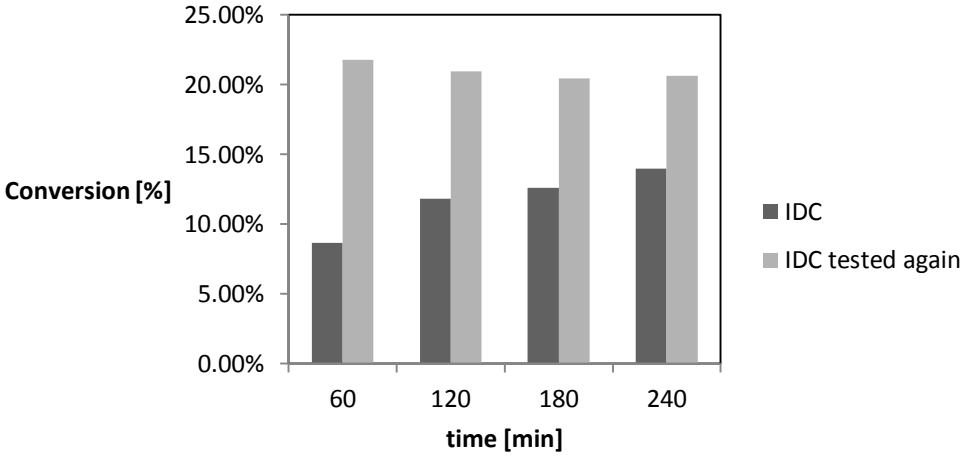

Figure 28 – Conversion of Hydrogen per hour, obtained by integration of the data obtained by a thermal mass flow meter positioned in the hydrogen feeding line for the IDC catalyst and the data for H_2O_2 and H_2O

3.4.3 Calcination Effect on kinetics for SI Samples

The effect of the calcination is even more evident in the reported SI membrane. In this case, because of the specific peculiarity of this sample, to study the effect of calcination on the kinetics for the direct synthesis *model 3 calc* was chosen as the best fitting model. The fitting results by using model 3-calc are reported in Table 9. We also tried to fit *model 1* and *model 2*, but because of the specific features of this catalyst, there was a lack of fit. This peculiar behaviour was correlated with the lower diameter of the Pd NPs prepared by sol immobilisation. More specifically: 1) the trend in selectivity with time is not decreasing with the time-on-stream, therefore, the hydrogenolysis / decomposition routes can be considered as not active; 2) the rate of production of both H_2O_2 and H_2O is decreasing with time, a trend never observed for the direct synthesis in semi-batch conditions; 3) the conversion of H_2 is decreasing with the time-on-stream (see Figure 30). The latter observations can only be explained by an inhibition effect by one of the products (H_2O or H_2O_2) or by a re-oxidation of the surface of the catalyst by the produced H_2O_2. Considering that both the hydrogenolysis rate and the decomposition appear to be inhibited, the second hypothesis seems more reasonable. The hypothesis of a negligible contribution from the hydrogenolysis route appears in line previously reported results for the ID catalysts which indicated a progressive reduction of the hydrogenolysis route upon thermal treatments [31]. The fitted model, further, predicts the state of the Pd surface with respect to the reducible surface, which is first reduced by the fed hydrogen and then re-oxidized by the produced H_2O_2 (see Figure 29) as a consequence of the decreasing reduction potential with the time-on-stream, given by $H_2/H_2O_2/O_2$ ratio. Therefore, re-oxidation of the catalytic particles by the produced H_2O_2 makes the catalyst progressively less active, determining both a decreasing trend in hydrogen conversion and in H_2O_2 and H_2O production rates (see Figure 29). These results are confirmed by successive tests in which we observed a decreasing rate of H_2O and H_2O_2 production, constant selectivity and reduction of H_2 conversion per hour. With respect to the previously reported case with the IDC samples, further tests were not fitted by *model 1*, nor by *model 2-3 calc*, because of the uncertainty on the initial state of the Pd Surface. This is related to the necessity of estimation of Sr(0) in *model 2 calc and model 3 calc*, which given the low number of data points in the first minutes of reaction and present noise would result in a poor estimation of fitted parameters.

Table 9 – Pseudo-rate constants (and relative 95% confidence limit) for the SIC catalyst

Catalyst family	Test	Model	kds', [mmol $L^{-1}min^{-1}$]	kh [min^{-1}]	kc' [mmol $L^{-1}min^{-1}$]	$k_{Pd,r}$	$k_{Pd,ox}$	Regime
SIC	4	3	0.2198± 0.0887	-	0.1594±0.005	0.0189 ± 0.0088	0.0160± 0.0015	Transient

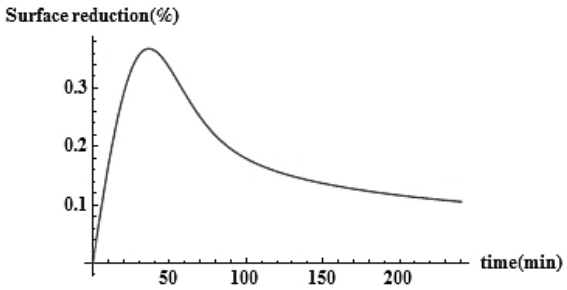

Figure 29 – Surface reduction dynamics for the SIC catalyst predicted by *model 3 calc*

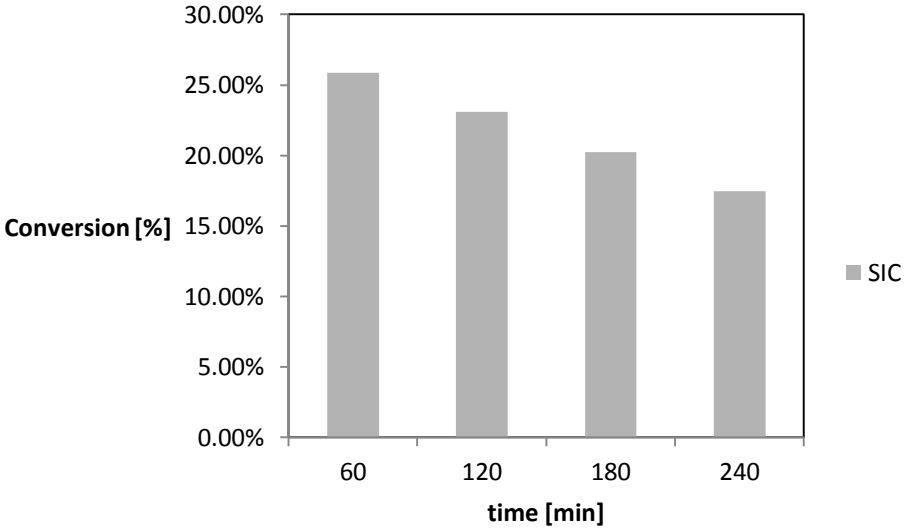

Figure 30 – Conversion of Hydrogen per hour, obtained by integration of the data obtained by a thermal mass flow meter positioned in the hydrogen feeding line

3.4.4 Kinetic Comparison

A comparison of the results obtained by the NR, ID and SI-used(n) catalysts is reported in Figure 31, Figure 32 and Figure 33, where the respective pseudo-kinetic rate constants were normalised by the apparent MSA. From the analysis of this plot it is evident that the SI samples, tested in the absence of KBr as a promoter, has always shown the highest k_{ds}'/MSA and the lowest k_h'/MSA and k_c'/MSA, in line with its superior productivity and selectivity and the promotion effect expected by PVA. It is further evident, that the k_h'/MSA for the ID sample is higher with respect to the NR sample, even though in the first case KBr was used as promoter. The NR catalyst, conversely, has shown the highest k_c'/MSA, in line with the absence of KBr as a promoter.

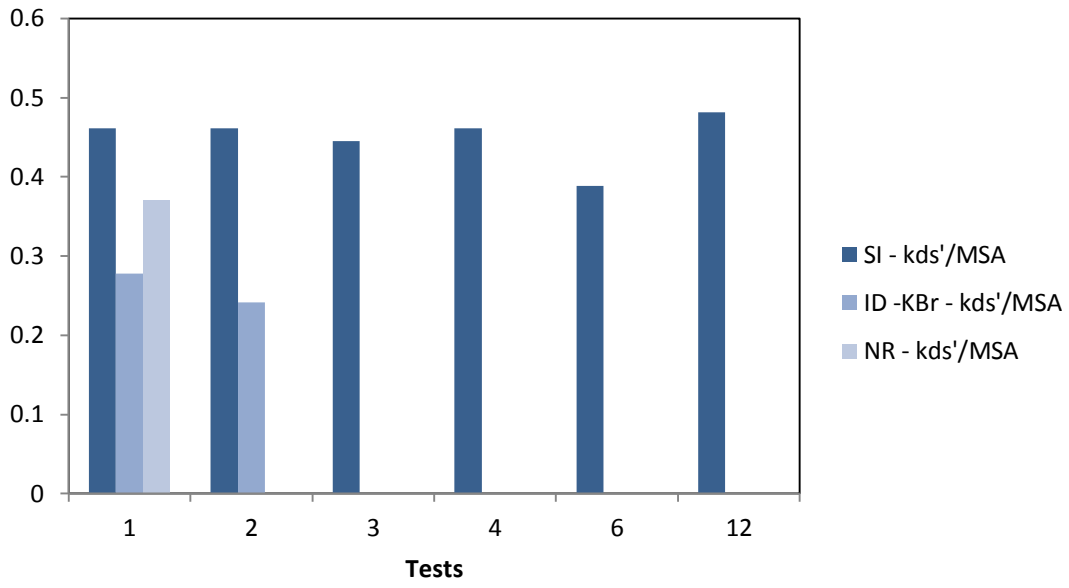

Figure 31 – Comparison of the k_{ds}' normalised by the apparent MSA for the ID and NR and SI catalysts

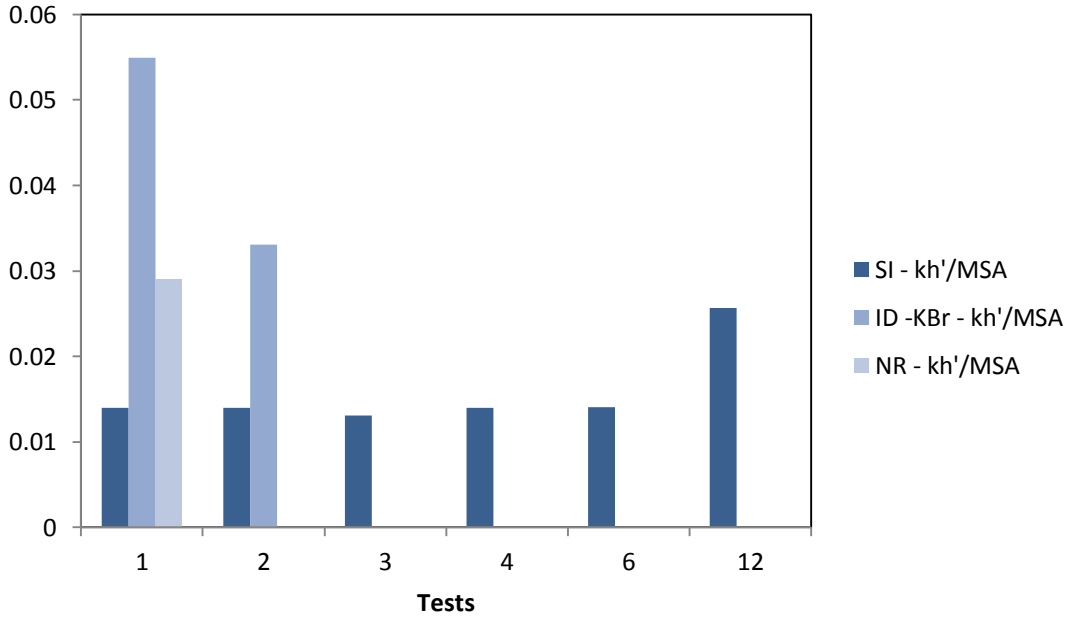

Figure 32 – Comparison of the k_h' normalised by the apparent MSA for the ID and NR and SI catalysts

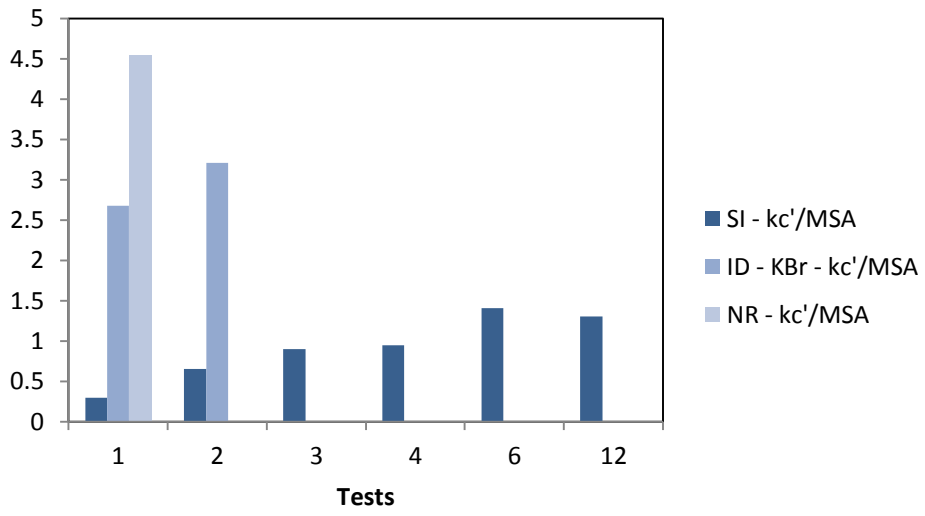

Figure 33 – Comparison of the k_c' normalised by the apparent MSA for the ID and NR and SI catalysts

A comparison of the results obtained by the NRC, IDC and SIC catalysts is reported in Figure 34, where the respective pseudo-kinetic rate constants were normalised by the apparent MSA and reported in order of decreasing average diameter for the Pd NPs. To show all the constants on the same scale, kh'/MSA was multiplied by a factor of 20, while $k_{Pd,r}$/MSA and $k_{Pd,ox}$/MSA by a factor of 2. From the analysis of this plot, it is evident that the ID and SI samples, showing the largest dispersion, presents similar pseudo-rate constant for the direct synthesis and strongly lower pseudo-rate constants for hydrogenolysis and a markedly lower pseudo rate constant for the direct combustion. Finally, the reduction constant normalised by surface area in the case of the IDC and SIC catalysts is largely lower, probably because of the effect of interaction with the support or enhanced by the presence of KBr during the tests.

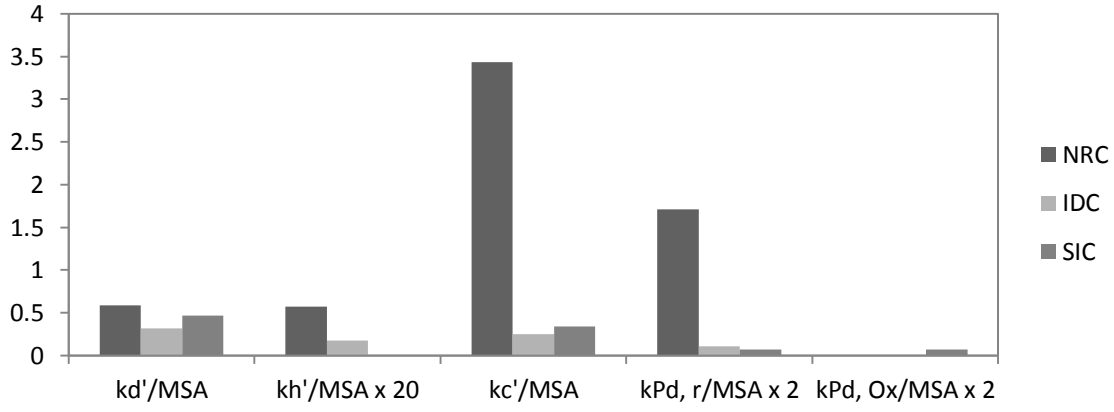

Figure 34 – Comparison of the pseudo-kinetic rate constants normalised by the apparent MSA for the SIC-KBr, IDC-KBr and NRC catalysts, (catalysts ordered by decreasing average diameter)

3.5. Discussion

3.5.1 SI recyclability tests, beneficial and side effect of PVA

During the recyclability tests, a maximum in selectivity to H_2O_2 has been observed and correlated to the gradual loss of PVA. Similar trends, correlated with the concentration of PVA on the surface of NPs were also reported for glycerol oxidation on Au catalysts prepared by SI technique [79]. In this last case, as already reported [79], increasing the ratio of PVA/active metal during the preparation stage, a volcano trend in the activity was observed, and also the selectivity was affected, indicating a sort of promotion effect at low concentration and lower activity at high concentration of PVA, while, with no PVA the catalysts presented a very poor selectivity. The SI technique was successfully applied for the preparation of Pd and Pd/Au nanoparticles for the direct synthesis of H_2O_2 [32,51,60,61,63,80,96–101] and was indicated as a promising technique for achieving high productivities and selectivities. Unfortunately, as reported in a previous work [60], the washing of PVA during the test give rise to a decrease in selectivity and sintering. This effect has been already documented for the direct synthesis [61,64] and also for other reactions during recyclability tests, documenting the washing of PVA by FTIR measurements [79]. The observed Ostwald ripening process is related to 1) the absence of Pd-support interaction 2) the low NPs size, probably below the critical thermodynamic diameter 3) loss of PVA. Further, PVA has been reported as a possible promoter for this synthesis [32,64] and as an active ingredient of the catalyst for other reactions [79]. Nonetheless, to the knowledge of the author, despite the number of publications in this area, the role of PVA on both activity and selectivity was never considered in the literature, except from [32,60,64]. By the obtained kinetic results, comparing SI membranes with respect to the fresh ID and NR membranes, the selectivity reported for SI membranes was higher. This result was correlated with a promotion effect by PVA as will be discussed [60]. However, as observed, in the recyclability study a high concentration of PVA can give rise to low selectivities, an increase in the apparent direct combustion rates and a decrease in the apparent hydrogenolysis rate (see Table 6 and Figure 15). This phenomenon was correlated to the presence of transport phenomena for the produced H_2O_2 and therefore to an increase in its local concentration on the Pd NPs surface and therefore enhancing its hydrogenolysis.

These phenomena, modelled by using model 1, give rise to a high apparent direct combustion rate and a low apparent direct synthesis rate. Therefore, to test the hypothesis of transport phenomena model 1 d was used on the 1st and 2nd tests. The reported modelling approach for taking into account transport phenomena and the Ostwald ripening process is quite unconventional and to the knowledge of the author such a treatment was never attempted for this reaction. There is only one paper addressing similar phenomena for glycerol oxidation on Au NPs prepared by sol immobilisation technique [79], but without following the underlined mathematical treatment. Therefore, even though the results appear to be in line with the proposed explanation, further studies are necessary in order to clarify this effect. However, the results obtained by *model 1d*, for the early tests are compatible, with the hypothesis of transport limitations of H_2O_2 by PVA. As expected, the values of the coefficient of transport for H_2O_2 in the PVA layer increased from the 1st to the 2nd test (see Table 7), providing some indications for the influence of the loss of PVA on transport phenomena. The increasing trends in the residuals observed for H_2O_2 trend for the 1st test Figure 24), even though very tiny, could be explained as the results of the dynamic modification of the structure of PVA in methanol during the first test, getting, probably, more jelly and porous in contact with the methanol solution. The increasing values of k_c'/MSA for the 1st and 2nd tests obtained by fitting *model*

1 d, are in line with the observed increase in the k_c'/MSA observed for successive tests (3^{rd}-12^{th} tests) calculated by using model 1 and related to the loss of PVA. This was correlated with the promotional effect of PVA, limiting the dissociative chemisorption of O_2. For the direct synthesis of H_2O_2, the presence of chemisorbed O_2 in non-dissociated form has been demonstrated by Raman measurements to be determinant in order to synthesise H_2O_2 selectively and avoiding the formation of H_2O, which, conversely, is formed by dissociative chemisorption of O_2 [102]. The lower value for the combustion reaction observed for SI-used(n) membranes with respect to other procedures, and its increasing value after the removal of PVA are in agreement with previously reported results reported by Arrigo et. al. [74], in which by microcalorimetry and XRD demonstrated that PVA was acting in some way as negative promoter for the dissociative adsorption of O_2 without hindering hydrogen adsorption [74]. Further, the value of the k_{ds}'/MSA and k_h'/MSA, to some extent, were constant for the entire time span of the recyclability tests, therefore, the assumption behind model 1 d of taking these values from the 4_{th} test could be considered reasonable. The promotion effect of PVA for the direct synthesis was also proved by washing a catalytic membrane prepared by SI with deionized water at 353 K by the procedure reported by Villa et. al. [74]. By fitting the testing results by using model 1 (results not reported), in this case, an increase in pseudo-kinetic constant for the direct combustion was observed. Further, because of the considerable washing of Pd, the corresponding constant for the direct synthesis was very low, and the contribution for the hydrogenolysis constant was negligible. Therefore, the increase in k_c''/MSA in Figure 25 from the 3^{rd} -12^{th} tests indicate the liberation of the most energetic active site by the progressive solubilization PVA, revealing also the structure sensitivity of the reaction for the formation of water, and confirming the role of PVA in inhibiting the dissociative adsorption of O_2. The sudden increase in the k_h'/MSA (see Figure 25), and the corresponding slight decrease of k_c'/MSA observed for the 12^{th} test, even though tiny, could be explained by the loss of the stabilization effect of PVA, giving rise to the surface modification of Pd, increasing its activity toward H_2O_2 hydrogenolysis. Capping agent and the environment, usually modify the stability of the exposed faces. This was confirmed by the loss of selectivity and by morphological changes on the surface of the exposed Pd documented by Arrigo et. al. [60], both correlated to the loss of PVA. Therefore, PVA present probably also a stabilisation effect on the exposed faces. Further, the constant trend in the k_{ds}'/MSA and the increasing trend in the k_c'/MSA reported in Figure 25, indicate that the direct synthesis is structure-insensitive while the direct combustion is structure-sensitive, in agreement with the literature indicating the most unsaturated sites (corners and edges) as responsible for the direct combustion and terraces as active sites for the direct synthesis (see Scheme 3) [54,55,103,104], but in contradiction with the conclusions reported by Gemo et. al. [53]. The promotional effect of PVA, hindering O_2 dissociative chemisorption and its influence on selectivity, were further demonstrated for partial oxidation reactions [74] Also in this case, the greater selectivity observed with by using SI catalysts with respect to other procedures was attributed to the presence of PVA, inhibiting O_2 dissociative chemisorption. The interaction between PVA and Pd is, further, confirmed by XPS data indicating the electronic influence of PVA on Pd [64,74]. Therefore, the effect of PVA, specifically, could be the poisoning of defective sites (corner and edges), which are also the most unsaturated ones, by its –OH groups, while on terraces, being less unsaturated, the direct synthesis is probably less affected. Another effect of the Ostwald ripening process, in this case, should be a decrease in the relative importance of the most defective sites. However, the increase in the k_c'/MSA indicates that the loss of PVA during time-on-stream is probably making available more defective sites than those lost by the Ostwald ripening mechanism. A schematic representation of

the suggested effects is reported in Figure 35. Further, comparing the results obtained by the SI-used(n) catalysts with NR and ID catalysts in reduced state (as prepared, as calcined and then reduced), as can be noted from Figure 31, Figure 32 and Figure 33, it is evident that the SI sample has shown the lowest k_c'/MSA, in line with the previous discussion about the hindering of O_2 dissociative chemisorption. Nonetheless, it might also be noted that for the SI-used(n), the k_{ds}'/MSA is higher and k_h'/MSA is lower with respect to other catalytic membranes. This, of course, could also be the effect of some small errors in calculating the surface area, but could also be the result of a further promotion effect mediated by the –OH groups on the structure of PVA. As evidenced by Wilson and coworkers [104], the direct synthesis is favoured by the presence of protic solvents, like methanol and water, while its performances are much lower in aprotic solvents. Therefore, it might be reasonable that the high density of –OH groups, close to the surface of Pd might mediate the reaction, increasing the k_{ds}'/MSA and decreasing k_h'/MSA. The higher concentration of –OH on the surface could increase the local protonic concentration by coordinating with the acid present in solution by electrostatic interaction, in line with the observation of Ntainjua and coworkers [105], stating the importance of using supports with a low isoelectric point, and therefore, decreasing the kinetics of hydrogenolysis and decomposition of H_2O_2 [23], or as proposed by Abate et. al. [47], increasing the production rate of H_2O_2 by interacting directly with O_2* adsorbed on the surface of the catalyst.

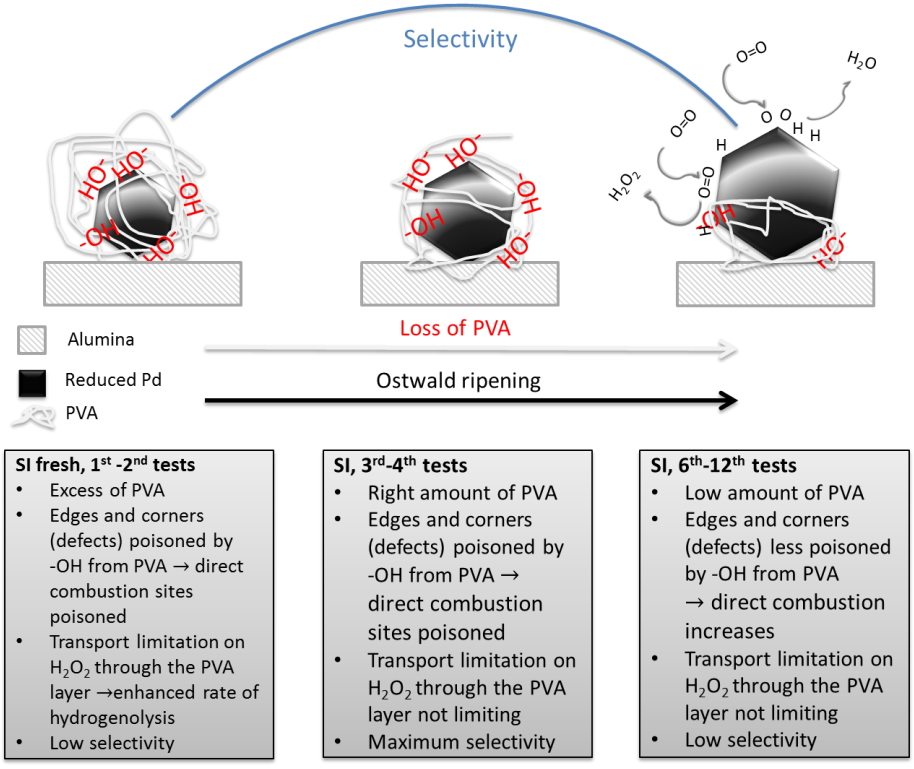

Figure 35 – Schematic representation of the processes bringing to deactivation of the SI-used(n) catalyst

Al these effects, as underlined, depend on the amount of PVA and its concentration used for the synthesis, Active Metal/PVA ratio and the support on which the sol is immobilised [79]. Therefore, to optimise the catalyst it is necessary to find a trade-off in the PVA/active metal ratio. Of course, these

results, obtained in such mild conditions confirm that further work is necessary in order to stabilise these catalysts. Possible alternatives to test, in order to take advantage of the role of PVA, could be its use on reduced catalysts prepared by other conventional techniques, as already proposed by Villa et. al. [79]. Nevertheless, even in the presence of deactivating phenomena, this results gives fresh insights and questions on the mechanism and could open the way for new development for improving the performances of the direct synthesis.

3.5.2 Calcination Effects on NR, ID and SI samples

There are still open questions about the nature of active sites. Between these, the structure sensitivity of the reaction, closely related to the dispersion of the catalysts and to the morphology of the particles, and the oxidation state of the active sites. Regarding the second question, about the oxidation state of the active sites, there is still a great debate in the literature as stated previously [56]. The situation is further complicated by the dynamic change of the oxidation state of Pd NPs under the influence of the redox potential of the solution [60], which is probably related also to the nature of Pd NPs. These phenomena make hard giving an exact answer to this question. Nevertheless, these factors have been limitedly considered [32,60–64]. During our testing campaign on calcined catalysts, we observed the presence of an induction time at the beginning of the reaction. The calcination treatment, as demonstrated by TPR and DRIFT data can lead to significant oxidation of the Pd nanoparticles. Therefore, we hypothesized, assuming the inactivity of the PdO phase, that the dynamic reduction of the catalyst in situ by the supplied hydrogen could explain this trend and by using *model 2-calc* and later *model 3-calc*, we tried to answer this question. In agreement with the hypothesized inactivity of PdO, the activity shown by the calcined catalysts was quite low at the beginning of the tests, while the selectivity was higher than the as-prepared catalysts, in line with the literature claiming better selectivity after the peroxidation of the catalyst. The observed induction time was more evident for ID catalysts and less evident for NR catalysts (see Figure 16 and Figure 17). This last observation might be explained by the faster reduction of NRC samples with respect to the ID and SI catalysts. Therefore the corresponding induction time was lower and barely visible in our experiments (see Figure 16 and Figure 17). The assumption behind *model 2-3 calc*, about the inactivity of PdO and further reduction, is in agreement with the small induction period was observed by Choudhary et. al. during the reduction of H_2O_2 on PdO particles [106,107] and with the observation made by Melada et al. reporting that reddish brown PdO catalysts turned into grey or black during the direct synthesis, evidencing the reduction of PdO to metallic Pd [78]. Further, Lunsford and coworkers [108], working with an O_2/H_2=15 at atmospheric pressure, the PdO, prepared by calcination in a flux of pure oxygen at 550°C, is inactive for the direct synthesis. By using *model 2-calc* and *model 3-calc,* the kinetics of the reaction and the reduction degree of the reducible Pd NPs surface during the synthesis was predicted. By the assumed mechanism, the in-situ reduction of Pd, by the H_2 present in the reaction environment can restore the active sites for the synthesis while simultaneously, in our experimental conditions, creating a less defective surface and therefore a more selective catalyst. This might be a consequence of the increased wettability of the support by PdO, leading to flatter particles in close interaction with the support [81,82,109] and therefore to less defective metallic surfaces upon in-situ reduction. This hypothesis is in agreement with the lower values reported for the pseudo-kinetic constants for direct combustion pathway with respect to as prepared and reduced catalysts, which was also verified by successive tests for the IDC catalytic membrane (see Figure 26 and Table 8). Further support for this hypothesis could be funded by the reported TEM results, evidencing the formation of elongated particles upon calcination, even though not very significant. This hypothesis is also

supported by DRIFT analysis on the NRC and IDC catalysts, which after reduction have shown a different pattern in the CO-FTIR spectra. Specifically, by DRIFT analysis, in the case of NR/NRC samples, negligible differences between the as-prepared catalyst and the calcined was observed, while, in the case of ID/IDC, presenting higher dispersion, the difference between the two spectra was quite significant. This phenomenon can be correlated as an effect of the interaction with the support leading to a reorganised surface upon in-situ reduction, in this case, more selective for the direct synthesis. In addition, the results obtained by *model 3-calc* on the SIC sample, about the further oxidation of the catalyst by the formed H_2O_2, are quite in agreement with the results obtained by Gemo et. al. [53] observing an increased oxidation at the end of each test, which was more evident with the most dispersed catalysts and with other authors [67–69], reporting catalyst deactivation attributed to the formation of H_2O_2 oxidizing the surface of catalyst, even though in these cases reduced catalysts were used. As observed from the analysis of the kinetic results it is apparent that an oxidation pretreatment leads to significantly better selectivity for the direct synthesis, because of the significant reduction of the direct combustion and hydrogenolysis pathways. Further, by comparing the results obtained by the NRC, IDC and SIC, respectively ordered by decreasing average NPs average diameter, it is evident that this effect is even stronger with decreasing particle diameter (see Table 8, Table 9 and Figure 34). In addition, the induced effect of the thermal treatment (calcination), persisted even after the in-situ reduction of the catalyst (see results for the 4th test with IDC catalyst in Figure 26), confirming the goodness of model 2-calc, predicting a fully reduced surface at the end of the test. Therefore, the observed increase in selectivity after calcination cannot be simply related to the presence on the surface of palladium oxide (see Figure 26). The observed reduction in k_c' for the calcined catalysts and almost constant k_{ds}' (see Figure 26) can be interpreted in light of the structure sensitivity for the direct combustion, while the direct synthesis, is not, as also observed in the previous section, even though also electronic effects might be important [110]. Therefore, it is reasonable to assume that the in-situ reduction, as confirmed by the trend of the reported k_{ds}' (see Figure 26), lead essentially to similar reduced MSA with respect to the as-prepared catalyst, while the lower presence of defects (corners, edges) lead to a switch-off of the direct combustion kinetics.

However, the results obtained by the SIC sample by using *model 3-calc*, predicting also the further oxidation of the catalyst by the formed H_2O_2, and the observed differences in the kinetics of surface reduction (see kPd,r/MSA, Figure 34), highlight also a possible effect of the redox properties of oxidized Pd, correlated to the greater interaction with the support. In this case, indeed, as reported in the characterization section the catalyst present a smaller average diameter and a very narrow distribution with respect to the NRC and IDC membranes. Therefore, by calcination, it is likely to have a greater interaction with the support, inducing the stabilisation of the oxidised structure and electronic effects, as verified by Kacprzak and coworkers [110] by DFT calculations of Pd_9 clusters on alumina. Further, the interaction with the support upon calcination can give rise to flatter particles [81,82,109], probably forming less unsaturated sites when reduced by H_2 on the surface in the reaction environment. This might be a consequence of the hindrance of the structure in interaction with the support, the low temperature during the tests and low H_2 concentration in the solvent. Therefore, the final reduced surface is probably not the equilibrium structure. This observation is agreement with the reported $k_{Pd,r}$/MSA (see Figure 34) and with the result reported by *model 3-calc* about the further oxidation of the catalyst by the produced H_2O_2. A non-equilibrium surface indeed is easier to oxidise with respect to an equilibrated surface, because of the lower contribution of the stabilisation by its reticular energy. In this case, this is expected because of the

higher interaction with the support expected for the SIC sample. Further support for this hypothesis can also be found by the results obtained by the IDCR catalyst where we observed that the structure was apparently more defective with respect to the fresh sample. The reduction by pure hydrogen in that range of temperature (100 °C), indeed, could give rise to the beta phase formation, with consequent expansion of the lattice, destroying in part, the interaction with the support created by the calcination treatment, leading therefore to the reorganization of the surface in a more equilibrated way, similar to what obtained with the fresh samples. Conversely, the reduction at a lower temperature in the reaction environment determine a lower reduction potential and therefore, does not have the driving force for reducing completely the Pd NPs and fully reorganising the structure to reach the equilibrium obtainable at a higher temperature, an effect which is even more marked in the presence of interaction with the support. Of course, this is a function of the reducing potential for the solution in contact with the Pd NPs, which, in turn, can be expressed as $H_2/O_2/H_2O_2$ ratio, and probably, as also hypothesized by the energetic status of the created surface, which could be more or less oxidizable/reducible. The difference in the $k_{Pd,\ r/MSA}$, as reported in Figure 34, indeed give a dynamic view of this phenomena, as the reduction kinetics for the surface for the IDC sample, presenting tiny particles is lower than the one shown by the NRC catalyst. Even though in this case, the presence of KBr as a promoter for the tests with the IDC sample could have decreased the kinetics of surface reduction ($k_{Pd,\ r/MSA}$). However, the oxidation kinetics shown by the SIC catalyst, which presents the lower average Pd NPs diameter with respect to the other reported preparation techniques, confirm the hypothesis of a greater interaction with the support favouring the formation of less stable reduced surfaces. A schematic representation of the previously described phenomena is reported in Figure 36.

The continuous decrease of the k_h'/MSA seems to be in line with these results (Figure 34). Further, as reported by Voloshin et. al. [111], one of the most probable mechanisms for H_2O_2 decomposition proceeds in two steps:

1) $H_2O_2 + Pd \rightarrow H_2O + PdO$

2) $H_2O_2 + PdO \rightarrow H_2O + O_2 + Pd\ (slow)$

Therefore, it might be possible that, in the case of the SIC sample, the reaction is limited by step (2) of the above-reported network, increasing the oxidation of the surface by the produced H_2O_2. This assumption also explains the trends observed in the case of the SIC catalytic membrane for the rate of production of both H_2O and H_2O_2, both decreasing with time, and the observed reduction in the hydrogen consumption per hour measured by a thermal mass flow meter as reported in Figure 28. Similar trends were also observed for successive tests without further treatment of the catalyst (see Figure 18). Furthermore, at the end of the test, it was noted that the colour of the catalyst was still reddish, similarly to the same sample after calcination procedure, and not black as in the case of the NRC or IDC samples, indicating its partial oxidation on the surface.

4. Conclusions

The kinetic analysis of the recyclability on the SI-used(n) sample coupled with TEM characterization has provided some insight into the mechanism of the reaction and deactivation of the catalyst. Further insights on the mechanism were obtained by comparison of the obtained kinetic results with ID and NR.

PVA has a role of capping agent, but also present a strong influence on the mechanism and probably, also transport phenomena, although this needs further confirms. The main effect of PVA on the reaction is the poisoning of active sites for the direct combustion pathway. Although further proofs are needed, the promoting effect of PVA was also correlated to the promotion of the direct synthesis and inhibition of the hydrogenolysis pathway, probably enhanced by the higher local concentration of protons.

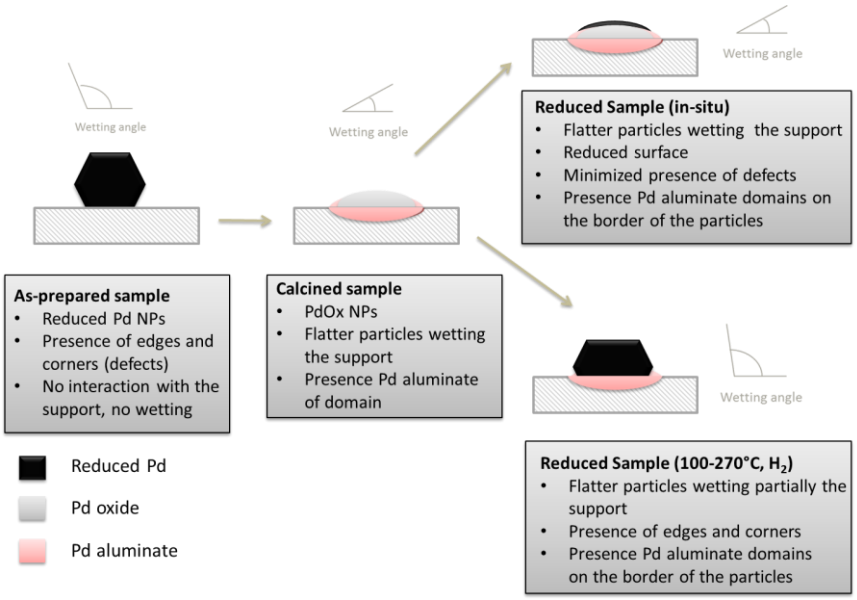

Figure 36 – Schematization of the effect of thermal treatment and reduction on the morphology of Pd NPs

Conversely, the kinetic analysis on the calcined catalysts with different average particle size has provided some insight on the nature of the active sites. By the reported results we concluded that the active phase for the direct synthesis is metallic palladium, while PdO is inactive. This, as reported, is the result of a dynamic change in the oxidation state of Pd during the test in the reported working conditions. In this case, an O_2/H_2 ratio of 0.9 was used, which is quite low with respect to other reports. Therefore, the reduction of the surface of the catalyst during the synthesis might be expected. The effect of the calcination treatment has been correlated with the interaction with the support, giving, after in-situ reduction, more selective surfaces. This was correlated to the creation of less defective surfaces with a decreased presence of corners and edges. In this case, we used alumina supports, but with other supports, the results might be different. Anyway, we believe that the reported results, in a certain sense, might be viewed as a bridge between papers reporting PdO and other reporting Pd as active phase.

By the analysis of the kinetics for both reduced and calcined catalysts, the structure sensitivity of the reaction was further analysed and discussed. Edges and corners were correlated to dissociative adsorption of O_2, in agreement with other reports. These sites, as widely reported, are present in a larger amount when smaller particles of Pd are present.

Considering the potential of the given results, a more severe oxidation pretreatment might be beneficial. In this case, although, the maximum temperature for the pretreatment was constrained by the reported ceramic supports. Further, pretreating at high temperature could result in a considerable sintering. Anyway, a treatment in pure oxygen might be considered. In addition, the potential of DRIFT

analysis might be exploited for accessing reduced surfaces for further insights. Furthermore, the effect of the O_2/H_2 ratio might be accessed in the future. In the present case, this was not done because of specific constraints in the solubility of both O_2 and H_2 and related to the membrane features used for this work. Nonetheless, the reported results give some fresh understanding about this old but still unknown reaction.

Appendix 1

Fitting results for the Si-used(n) sample – recyclability study

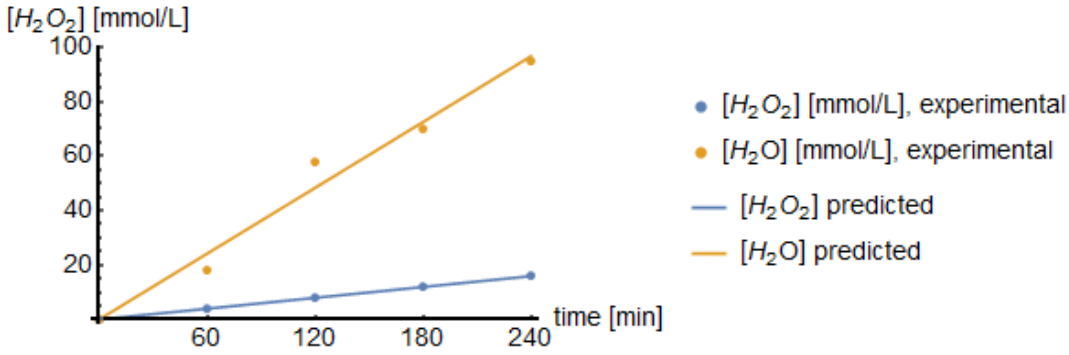

Figure 37 – Si-used(1) data and fitting, *model 1*

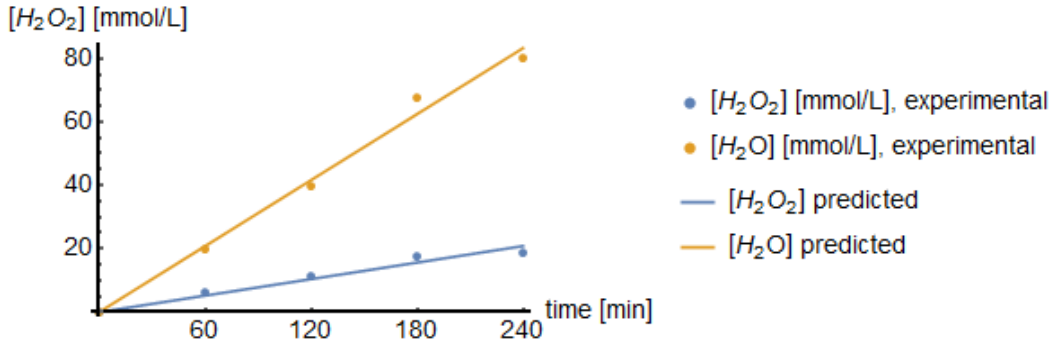

Figure 38 – Si-used(2) data and fitting, *model 1*

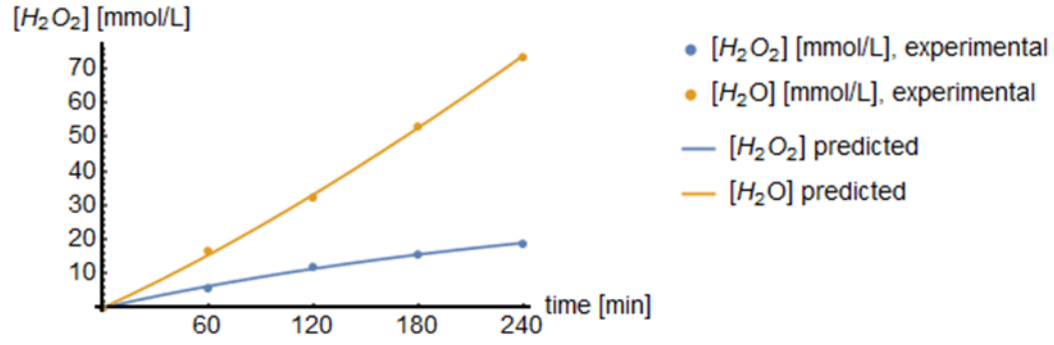

Figure 39 – Si-used(3) data and fitting, *model 1*

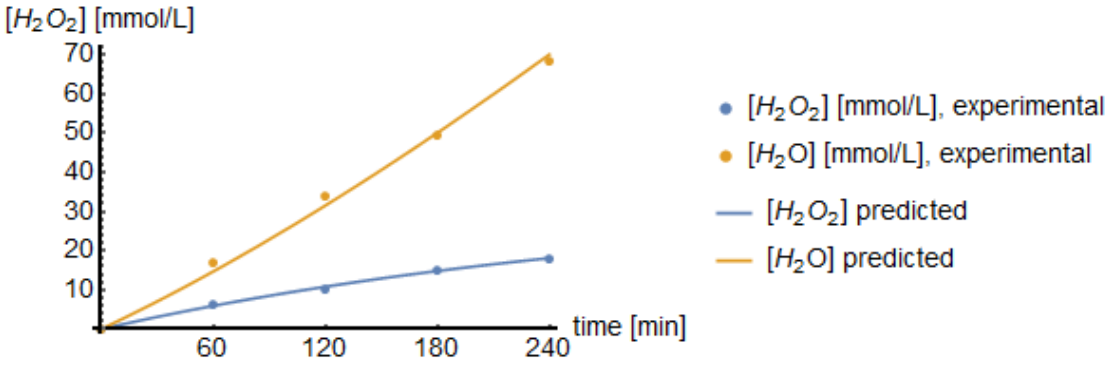

Figure 40 – Si-used(4) , *model 1*

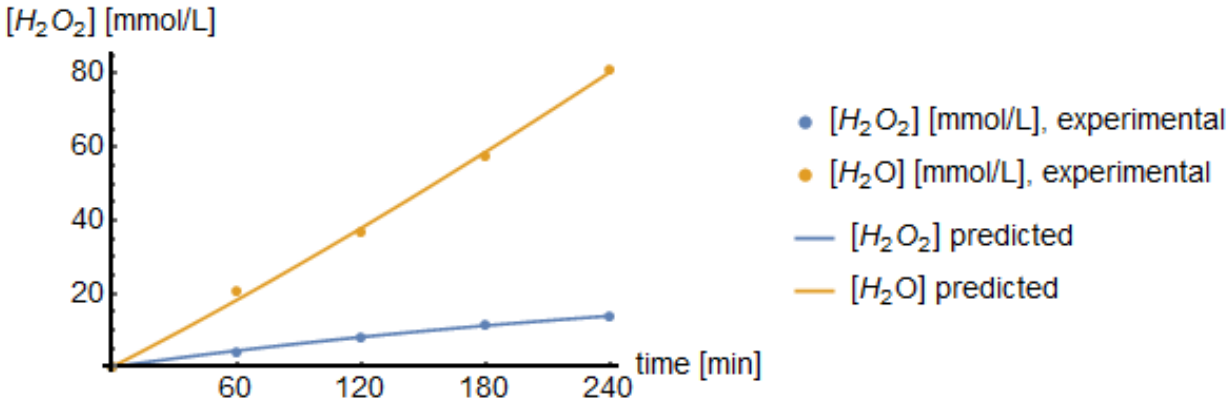

Figure 41 – Si-used(6) data and fitting, *model 1*

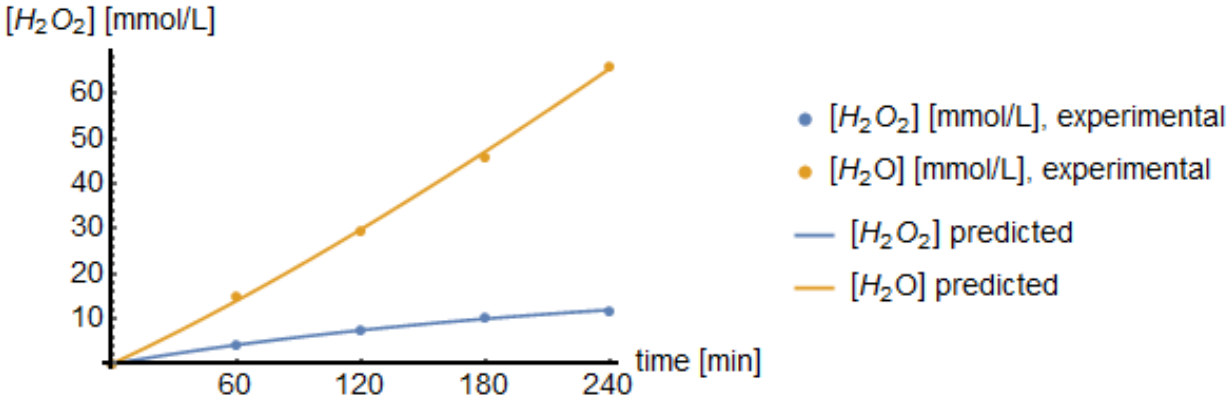

Figure 42 – Si-used(12) data and fitting, *model 1*

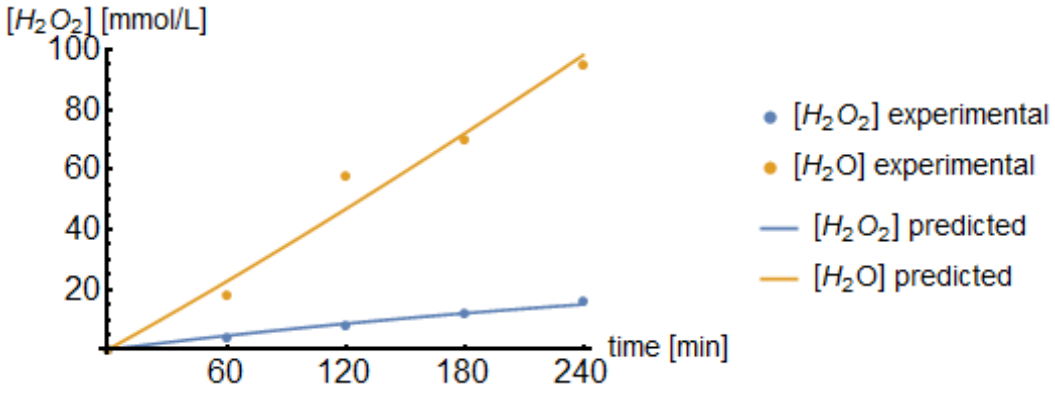

Figure 43 – SI-used(1), *model 1d*

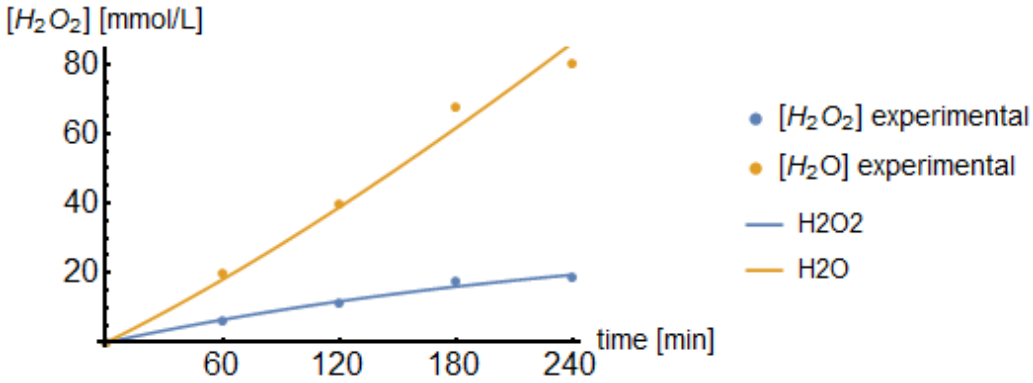

Figure 44 – SI-used(2), *model 1d*

Fitting results for the NR/NRC sample

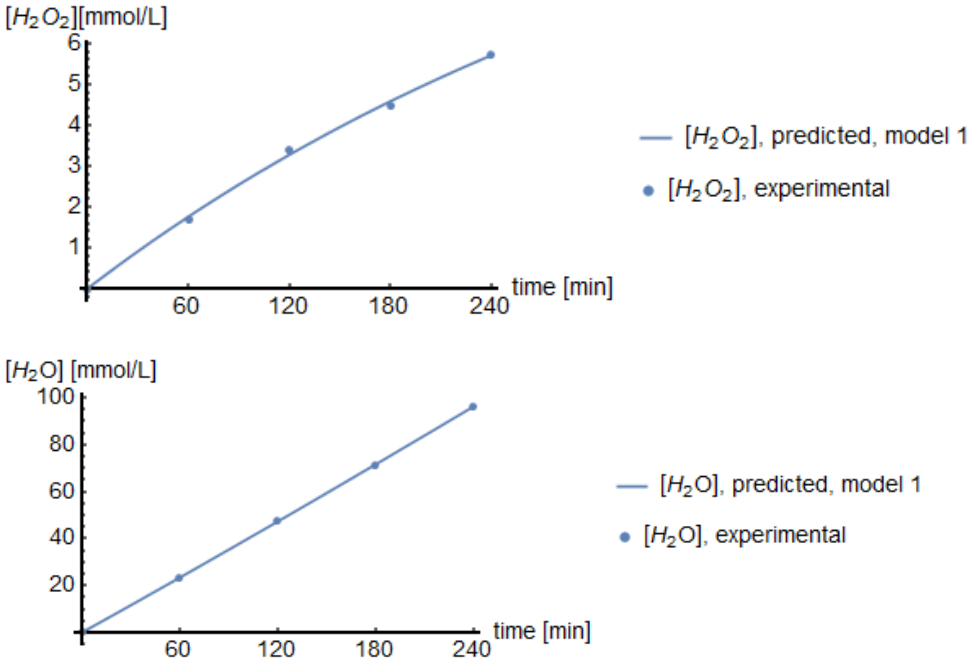

Figure 45 – NR, test 1, *model 1*

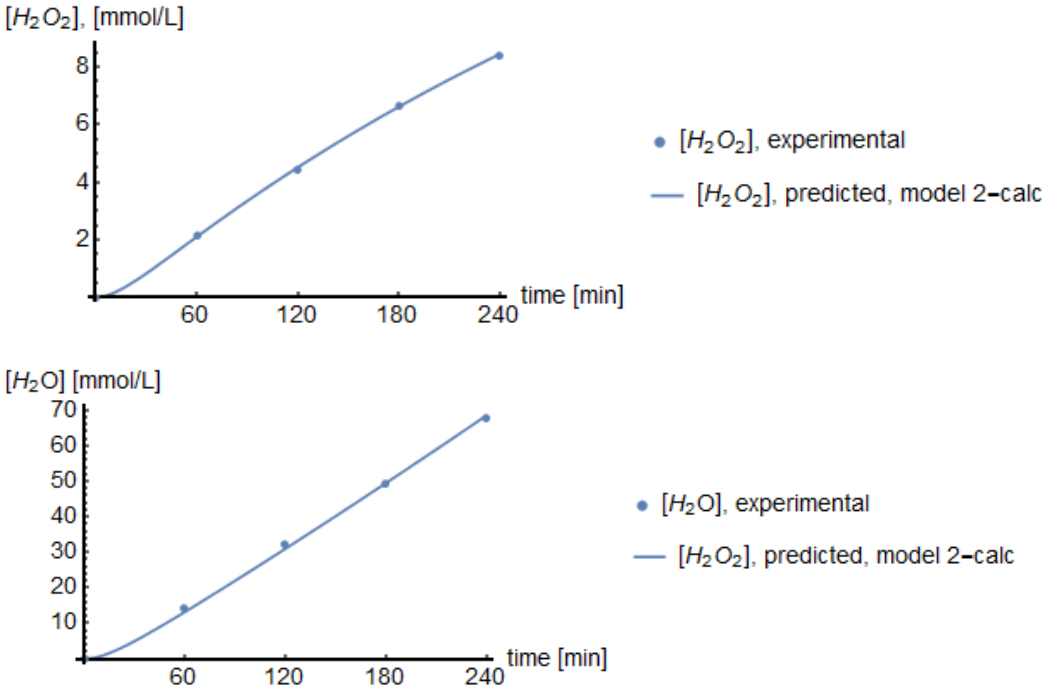

Figure 46 – NRC, test 3, *model-2 calc*

Fitting results for the ID/IDC/IDCR sample

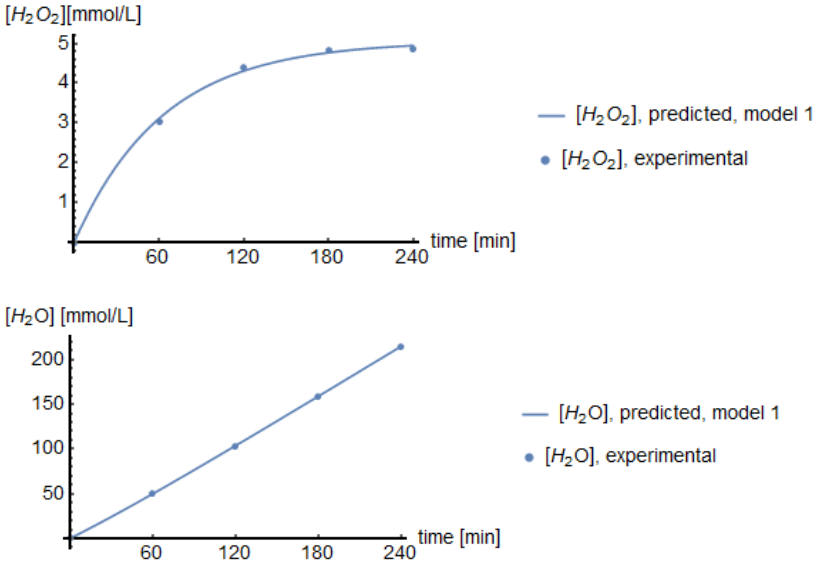

Figure 47 - ID test 1, *model 1*

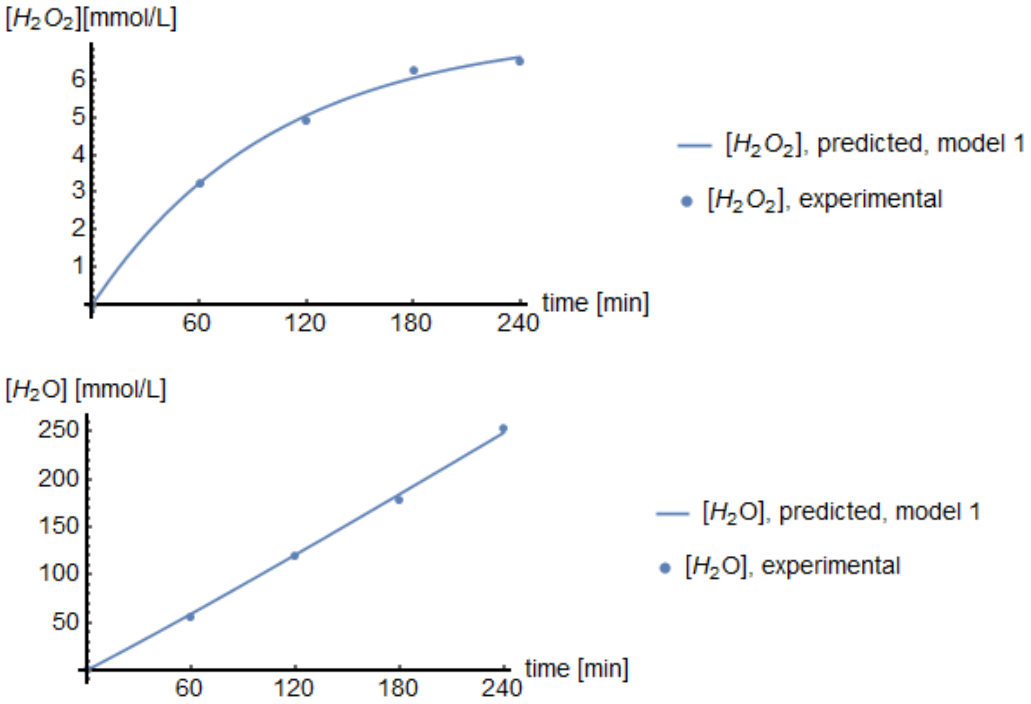

Figure 48 – IDCR, test 2, *model 1*

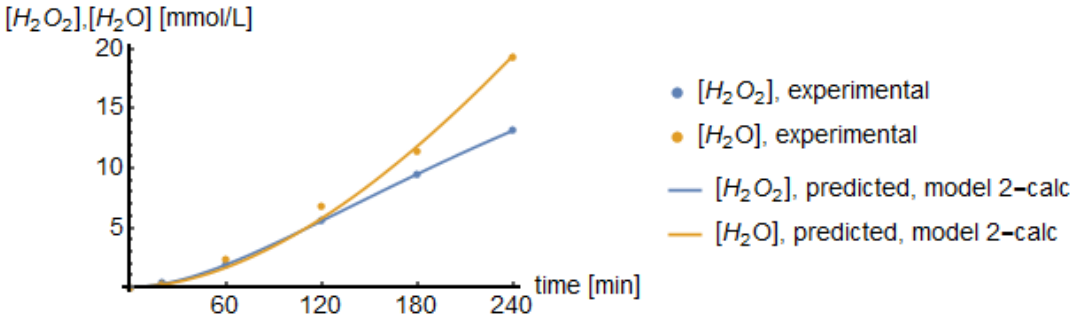

Figure 49 - IDC, test 3, *model 2-calc*

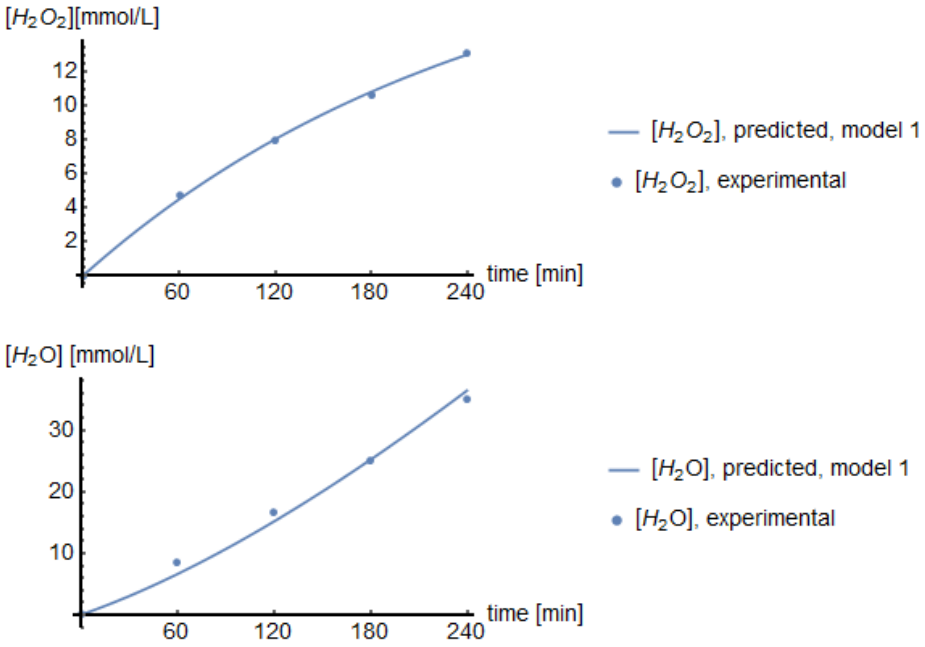

Figure 50 – IDC, test 4, *model 1*

Fitting results for the SiC sample

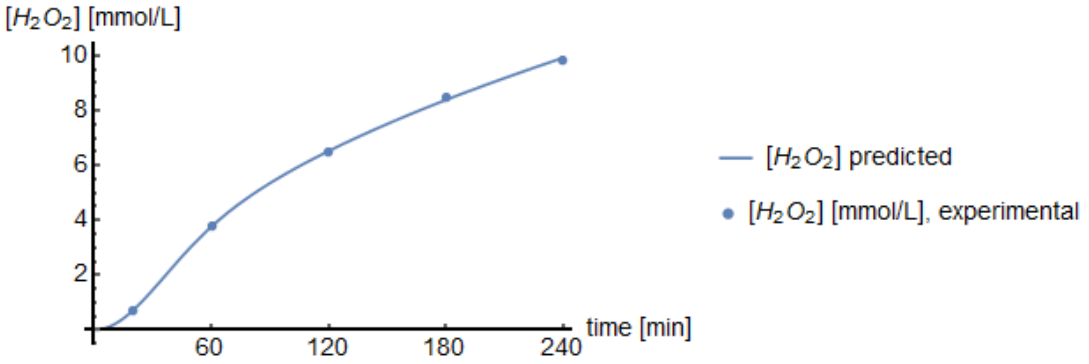

Figure 51 – SIC, H_2O_2 data and fitting, *model 3 - calc*

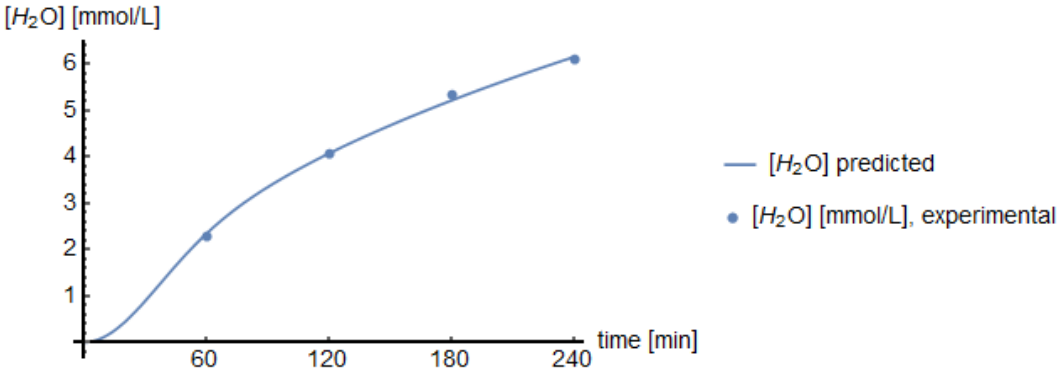

Figure 52 – SIC, H_2O data and fitting, *model 3 - calc*

References

1. F. Cavani, G. Centi, and S. Perathoner, *Sustainable Industrial Processes*, 2009.

2. G. Centi, F. Cavani, and F. Trifirò, *Selective Oxidation by Heterogeneous Catalysis*, Springer US, Boston, MA, 2001.

3. G. Centi and S. Perathoner, *Catal. Today*, 2009, **143**, 145–150.

4. D. Hâncu, J. Green, and E. J. Beckman, *Acc. Chem. Res.*, 2002, **35**, 757–764.

5. J. M. Campos-Martin, G. Blanco-Brieva, and J. L. G. Fierro, *Angew. Chem. Int. Ed. Engl.*, 2006, **45**, 6962–84.

6. Y. Yi, L. Wang, G. Li, and H. Guo, *Catal. Sci. Technol.*, 2016, **6**, 1593–1610.

7. F. Cavani and G. Centi, *Kirk-Othmer Encycl. Chem. Technol.*, 2011, 1–61.

8. R. Noyori, M. Aoki, and K. Sato, *Chem. Commun.*, 2003, 1977.

9. G. Blanco-Brieva, M. C. Capel-Sanchez, M. P. de Frutos, A. Padilla-Polo, J. M. Campos-Martin, and J. L. G. Fierro, *Ind. Eng. Chem. Res.*, 2008, **47**, 8011–8015.

10. K. Kamata, *Science (80-.).*, 2003, **300**, 964–966.

11. P. Tundo, *Green Chemical Reactions*, Springer Netherlands, Dordrecht, 2008.

12. W. Eul, A. Moeller, and N. Steiner, *Kirk-Othmer Encycl. Chem. Technol.*, 2001.

13. G. Goor, D. Ag, and G. Chap, *Ullmann's Encycl. Ind. Chem.*, 2007.

14. G. Centi, S. Perathoner, and S. Abate, *Mod. Heterog. …*, 2009, 1–33.

15. Q. Chen, University of Pittsburgh, 2007.

16. C. Samanta, *Appl. Catal. A Gen.*, 2008, **350**, 133–149.

17. D. Hâncu and E. J. Beckman, *Green Chem.*, 2001, **3**, 80–86.

18. D. Hâncu, J. Green, and E. J. Beckman, *Ind. Eng. Chem. Res.*, 2002, **41**, 4466–4474.

19. I. Yamanaka, *Catal. Surv. from Asia*, 2008, **12**, 78–87.

20. R. Dittmeyer, J. D. Grunwaldt, and A. Pashkova, *Catal. Today*, 2015, **248**, 149–159.

21. I. Yamanaka, *J. Japan Pet. Inst.*, 2014, **57**, 237–250.

22. B. R. Locke and K.-Y. Shih, *Plasma Sources Sci. Technol.*, 2011, **20**, 34006.

23. J. García-Serna, T. Moreno, P. Biasi, M. J. Cocero, J.-P. Mikkola, and T. O. Salmi, *Green Chem.*, 2014, **16**, 2320–2343.

24. B. Zhou, 2007, 1–16.

25. B. Zhou, M. Rueter, and S. Parasher, *US Pat. 7,011,807*, 2006.

26. B. Zhou and M. Rueter, *US Pat. 7,045,479*, 2006.

27. M. Rueter, B. Zhou, and S. Parasher, *US Pat. 7,144,565*, 2006.

28. S. Parasher, M. Rueter, and B. Zhou, *US Pat. 7,045,481*, 2006.

29. M. Rueter, *US Pat. 7,067,103*, 2006.

30. B. Zhou and L. Lee, *US Pat. 6,168,775*, 2001.

31. S. Abate, K. Barbera, G. Centi, G. Giorgianni, and S. Perathoner, *J. Energy Chem.*, 2016, **25**, 297–305.

32. S. Abate, R. Arrigo, S. Perathoner, and G. Centi, *Top. Catal.*, 2014, **57**, 1208–1217.

33. J. F. Ng, Y. Nie, G. K. Chuah, and S. Jaenicke, *J. Catal.*, 2010, **269**, 302–308.

34. Y. Voloshin and A. Lawal, *Appl. Catal. A Gen.*, 2009, **353**, 9–16.

35. T. Inoue, K. Ohtaki, S. Murakami, and S. Matsumoto, *Fuel Process. Technol.*, 2012, 1–4.

36. T. Inoue, M. A. Schmidt, and K. F. Jensen, *Ind. Eng. Chem. Res.*, 2007, **46**, 1153–1160.

37. S. Maehara, M. Taneda, and K. Kusakabe, *Chem. Eng. Res. Des.*, 2008, **86**, 410–415.

38. Y. Voloshin, R. Halder, and A. Lawal, *Catal. Today*, 2007, **125**, 40–47.

39. T. Inoue, Y. Kikutani, S. Hamakawa, K. Mawatari, F. Mizukami, and T. Kitamori, *Chem. Eng. J.*, 2010, **160**, 909–914.

40. Y. Voloshin and A. Lawal, *Chem. Eng. Sci.*, 2010, **65**, 1028–1036.

41. V. R. Choudhary, A. G. Gaikwad, and S. D. Sansare, *Angew. Chem. Int. Ed. Engl.*, 2001, **40**, 1776–1779.

42. S. Abate, S. Melada, G. Centi, S. Perathoner, F. Pinna, and G. Strukul, *Catal. Today*, 2006, **117**, 193–198.

43. S. Abate, G. Centi, S. Perathoner, and F. Frusteri, *Catal. Today*, 2006, **118**, 189–197.

44. M. Selinsek, M. Bohrer, B. K. Vankayala, K. Haas-Santo, M. Kraut, and R. Dittmeyer, *Catal. Today*, 2016.

45. M. Janicke, *J. Catal.*, 2000, **191**, 282–293.

46. S. Abate, G. Centi, S. Melada, S. Perathoner, F. Pinna, and G. Strukul, *Catal. Today*, 2005, **104**, 323–328.

47. S. Abate, G. Centi, S. Perathoner, S. Melada, F. Pinna, and G. Strukul, *Top. Catal.*, 2006, **38**, 181–193.

48. G. Centi, R. Dittmeyer, S. Perathoner, and M. Reif, *Catal. Today*, 2003, **79–80**, 139–149.

49. M. Reif and R. Dittmeyer, *Catal. Today*, 2003, **82**, 3–14.

50. V. R. Choudhary and P. Jana, *Catal. Commun.*, 2008, **9**, 2371–2375.

51. J. Pritchard, M. Piccinini, R. Tiruvalam, Q. He, N. Dimitratos, J. a. Lopez-Sanchez, D. J. Morgan, A. F. Carley, J. K. Edwards, C. J. Kiely, and G. J. Hutchings, *Catal. Sci. Technol.*, 2013, **3**, 308–317.

52. S. Zancanella, U. Rossi, L. Artiglia, G. Granozzi, and P. Canu, in *International Symposium on Chemical Reaction Engineering*, 2012, pp. 2–3.

53. N. Gemo, S. Sterchele, P. Biasi, P. Centomo, P. Canu, M. Zecca, A. Shchukarev, K. Kordás, T. O. Salmi, and J.-P. Mikkola, *Catal. Sci. Technol.*, 2015, **5**, 3545–3555.

54. T. Deguchi, H. Yamano, and M. Iwamoto, *Catal. Today*, 2015, **248**, 80–90.

55. T. Deguchi and M. Iwamoto, *J. Phys. Chem. C*, 2013, **117**, 18540–18548.

56. J. K. Edwards and G. J. Hutchings, *Angew. Chem. Int. Ed. Engl.*, 2008, **47**, 9192–8.

57. S. J. Freakley, Q. He, J. H. Harrhy, L. Lu, D. A. Crole, D. J. Morgan, E. N. Ntainjua, J. K. Edwards, A. F. Carley, A. Y. Borisevich, C. J. Kiely, and G. J. Hutchings, *Science (80-.).*, 2016, **351**, 965–968.

58. J. Li and K. Yoshizawa, *Catal. Today*, 2015, **248**, 142–148.

59. G. J. Hutchings, *Catal. Today*, 2008, **138**, 9–14.

60. R. Arrigo, M. E. Schuster, S. Abate, S. Wrabetz, K. Amakawa, D. Teschner, M. Freni, G. Centi, S. Perathoner, M. Havecker, and R. Schlögl, *ChemSusChem*, 2014, **7**, 179–194.

61. S. Abate, M. Freni, R. Arrigo, M. E. Schuster, S. Perathoner, and G. Centi, *ChemCatChem*, 2013, **200**, 1–8.

62. S. Abate, S. Perathoner, and G. Centi, *Catal. Today*, 2012, **179**, 170–177.

63. S. Abate, S. Perathoner, and G. Centi, *Top. Catal.*, 2011, **54**, 718–728.

64. R. Arrigo, M. E. Schuster, S. Abate, G. Giorgianni, G. Centi, S. Perathoner, S. Wrabetz, V. Pfeifer, M. Antonietti, and R. Schlögl, *ACS Catal.*, 2016, **6**, 6959–6966.

65. T. Kilpiö, P. Biasi, A. Bittante, T. Salmi, and J. Wärnå, *Ind. Eng. Chem. Res.*, 2012, **51**, 13366–13378.

66. A. Pashkova, R. Dittmeyer, N. Kaltenborn, and H. Richter, *Chem. Eng. J.*, 2010, **165**, 924–933.

67. O. Osegueda, A. Dafinov, J. Llorca, F. Medina, and J. Suerias, *Catal. Today*, 2012, **193**, 1–9.

68. V. R. Choudhary and P. Jana, *Appl. Catal. A Gen.*, 2009, **352**, 35–42.

69. T. Deguchi and M. Iwamoto, *J. Catal.*, 2011, **280**, 239–246.

70. J. K. Edwards, B. Solsona, P. Landon, A. Carley, A. Herzing, C. Kiely, and G. J. Hutchings, *J. Catal.*, 2005, **236**, 69–79.

71. V. R. Choudhary and C. Samanta, *J. Catal.*, 2006, **238**, 28–38.

72. V. R. Choudhary, C. Samanta, and P. Jana, *Appl. Catal. A Gen.*, 2007, **317**, 234–243.

73. C. Samanta and V. R. Choudhary, *Appl. Catal. A Gen.*, 2007, **326**, 28–36.

74. R. Arrigo, S. Wrabetz, M. E. Schuster, D. Wang, A. Villa, D. Rosenthal, F. Girsgdies, G. Weinberg, L. Prati, R. Schlögl, and D. S. Su, *Phys. Chem. Chem. Phys.*, 2012, **14**, 10523–32.

75. A. Pashkova, K. SVAJDA, and R. Dittmeyer, *Chem. Eng. J.*, 2008, **139**, 165–171.

76. S. Biella, F. Porta, L. Prati, and M. Rossi, *Catal. Letters*, 2003, **90**.

77. N. Dimitratos, A. Villa, D. Wang, F. Porta, D. Su, and L. Prati, *J. Catal.*, 2006, **244**, 113–121.

78. S. Melada, R. RIODA, F. MENEGAZZO, F. Pinna, and G. STRUKUL, *J. Catal.*, 2006, **239**, 422–430.

79. A. Villa, D. Wang, G. M. Veith, F. Vindigni, and L. Prati, *Catal. Sci. Technol.*, 2013, **3**, 3036.

80. S. Abate, R. Arrigo, M. E. Schuster, S. Perathoner, G. Centi, A. Villa, D. Su, and R. Schlögl, *Catal. Today*, 2010, **157**, 280–285.

81. J. J. Chen and E. Ruckenstein, *J. Phys. Chem.*, 1981, **85**, 1606–1612.

82. E. Ruckenstein, *J. Catal.*, 1981, **70**, 233–236.

83. E. Ruckenstein and J. . Chen, *J. Colloid Interface Sci.*, 1982, **86**, 1–11.

84. H. Lieske and J. Voelter, *J. Phys. Chem.*, 1985, **89**, 1841–1842.

85. J. W. Niemantsverdriet, *Spectroscopy in Catalysis: an introduction*, Wiley-VCH Verlag GmbH & Co. KGaA, Weinheim, Germany, 2007.

86. B. Zhu, G. Thrimurthulu, L. Delannoy, C. Louis, C. Mottet, J. Creuze, B. Legrand, and H. Guesmi, *J. Catal.*, 2013, **308**, 272–281.

87. T. Lear, R. Marshall, J. A. Lopez-Sanchez, S. D. Jackson, T. M. Klapötke, M. Bäumer, G. Rupprechter, H.-J. Freund, and D. Lennon, *J. Chem. Phys.*, 2005, **123**, 174706.

88. D. Tessier, A. Rakai, and F. Bozon-Verduraz, *J. Chem. Soc. Faraday Trans.*, 1992, **88**, 741.

89. a. S. Ivanova, E. M. Slavinskaya, R. V. Gulyaev, V. I. Zaikovskii, O. a. Stonkus, I. G. Danilova, L. M. Plyasova, I. a. Polukhina, and a. I. Boronin, *Appl. Catal. B Environ.*, 2010, **97**, 57–71.

90. S. Melada, F. Pinna, G. Strukul, S. Perathoner, and G. Centi, *J. Catal.*, 2006, **237**, 213–219.

91. S. Melada, R. Rioda, F. Menegazzo, F. Pinna, and G. Strukul, *J. Catal.*, 2006, **239**, 422–430.

92. E. M. Wong, J. E. Bonevich, and P. C. Searson, *J. Phys. Chem. B*, 1998, **102**, 7770–7775.

93. S. C. Su, J. N. Carstens, and A. T. Bell, *Sci. York*, 1998, **135**, 125–135.

94. R. A. Santen and J. A. Moulijn, *Catalysis: An Integrated Approach*, Elsevier, 2000.

95. M. Schmal, in *Heterogeneous Catalysis and its Industrial Applications*, Springer International Publishing, Cham, 2016, pp. 99–160.

96. J. A. Lopez-Sanchez, N. Dimitratos, N. Glanville, L. Kesavan, C. Hammond, J. K. Edwards, A. F. Carley, C. J. Kiely, and G. J. Hutchings, *Appl. Catal. A Gen.*, 2011, **391**, 400–406.

97. J. A. Lopez-Sanchez, N. Dimitratos, P. Miedziak, E. Ntainjua, J. K. Edwards, D. Morgan, A. F. Carley, R. Tiruvalam, C. J. Kiely, and G. J. Hutchings, *Phys. Chem. Chem. Phys.*, 2008, **10**, 1921–30.

98. J. C. Pritchard, L. Kesavan, M. Piccinini, Q. He, R. Tiruvalam, N. Dimitratos, J. A. Lopez-Sanchez, A. F. Carley, J. K. Edwards, C. J. Kiely, and G. J. Hutchings, *Langmuir*, 2010, **26**, 16568–77.

99. J. K. Edwards, S. J. Freakley, A. F. Carley, C. J. Kiely, and G. J. Hutchings, *Acc. Chem. Res.*, 2013, 845–854.

100. R. Tiruvalam, J. Pritchard, N. Dimitratos, J. Lopez-Sanchez, J. Edwards, A. Carley, G. Hutchings, and C. Kiely, *Faraday Discuss*, 2011, **152**, 63–86.

101. A. Villa, S. Freakley, M. Schiavoni, J. Edwards, C. Hammond, G. M. Veith, W. Wang, D. Wang, L. Prati, N. Dimitratos, and G. Hutchings, *Catal. Sci. Technol.*, 2015.

102. D. Dissanayake, *J. Catal.*, 2003, **214**, 113–120.

103. S. Abate, G. Centi, S. Melada, S. Perathoner, F. Pinna, and G. Strukul, *Catal. Today*, 2005, **104**, 323–328.

104. N. M. Wilson and D. W. Flaherty, *J. Am. Chem. Soc.*, 2016, **138**, 574–586.

105. E. Ntainjua N., J. K. Edwards, A. F. Carley, J. A. Lopez-Sanchez, J. a. Moulijn, A. a. Herzing, C. J. Kiely, and G. J. Hutchings, *Green Chem.*, 2008, **10**, 1162.

106. V. R. Choudhary and P. Jana, *Catal. Commun.*, 2008, **9**, 1624–1629.

107. V. R. Choudhary, C. Samanta, and T. V. Choudhary, *Catal. Commun.*, 2007, **8**, 1310–1316.

108. Q. Liu, K. K. Gath, J. C. Bauer, R. E. Schaak, and J. H. Lunsford, *Catal. Letters*, 2009, **132**, 342–348.

109. H. Knozinger and E. Taglauer, in *Handbook of Heterogeneous Catalysis*, Wiley-VCH Verlag GmbH & Co. KGaA, Weinheim, Germany, 2008, pp. 29–37.

110. K. a Kacprzak, I. Czekaj, and J. Mantzaras, *Phys. Chem. Chem. Phys.*, 2012, **14**, 10243.

111. Y. Voloshin, J. Manganaro, and A. Lawal, *Ind. Eng. Chem. Res.*, 2008, **47**, 8119–8125.

Chapter 3
Jet Fuel from Microalgae Oils by using Ni supported on Hierarchical Zeolites in one-step

Abstract

Four catalysts were prepared by using two commercial Bea zeolites supplied by Zeolyst (CP811E-75, CP814E) and a homemade SBA-15. The deposition of 8%wt of the Ni active metal was performed by incipient wetness. To minimise diffusional problems inside the pore of zeolites, the desilication treatment was performed on the commercial BETA zeolite CP811E-75 determining an increase of both, surface area and volume in the mesopore range. The prepared Ni-based catalysts were tested for methyl palmitate conversion in a batch autoclave reactor. Analysis of the results revealed the role of the surface acidity of the catalysts for the hydrogenolysis of methyl palmitate to palmitic acid, further evidencing the role of the greater available surface area and mesoporosity by the desilicated Ni/CP811E-75 in directing the selectivity toward the production of the C_{12} fraction.

1. Introduction

The combustion of fossil fuels over the last hundred years has led to a significant increase in greenhouse gas emissions, which is the main cause of the increase in the global mean temperature and to the depletion of fossil reserves [1]. Consequently, renewable and sustainable fuel sources are receiving increased attention. Till now, much of the efforts for developing new biofuels were addressed to the production of biodiesel [2]. However, the need of methanol often produced starting from fossil resources, the coproduction of glycerol and the not fully compatibility with actual engines make the exploitation of this alternative fuels challenging. Further, this kind of fuel is not exploitable in the aviation industry. UOP/ENI One of the main sectors pushing the demand for renewable fuels is the aviation industry, responsible for 2-6% GHG emissions [3]. Further, forecasts for jet fuel production indicate an increasing demand related to the expansion of the aviation market and increasing prices. The main challenges for replacing conventional jet fuel are: stricter specification compared to other sectors, production costs and availability of feedstocks. Presently, several processes have been proposed for the production of bio jet fuel, and these are both in the development and in commercial stage [3]. One of the most promising route, investigated by petroleum companies (UOP/ENI, Neste Oil, Synfining, Petrobras and Conoco Philips), is the hydrodeoxygenation of triglycerides (HDO) followed by an isomerization/cracking stage [3,4]. These

processes, in principle, could reduce environmental impact and achieve a flexible production of Bio Jet Fuel, Green Diesel and Green Gasoline. These processes can use several vegetable oils and fats as feedstock with high flexibility. However, considering the number of steps required by the current technologies to obtain good quality bio jet fuels as well as other fractions, it is necessary to integrate the process to make it viable economically. Therefore, the intensification of the process in one-step could be interesting to minimise costs and environmental impacts. Typical hydroprocessing catalyst suitable for one-step processes should contain hydrogenation/dehydrogenation sites and acid sites for isomerization and cracking. Recently catalysts based on Ni/zeolite to synthesise green diesel directly from lipid fractions of microalgae have been investigated [5]. Unfortunately this kind of materials, because of the nature of their textural features, usually presents severe diffusion limitations, especially with bulky molecules like triglycerides. Hierarchical zeolites, however, compared to conventional zeolites present high level of mesoporosity with improved accessibility and molecular transport. Based on this approach, encouraging results for the production of jet fuel were recently reported [6,7]. The possibility of producing Jet fuel has been studied by using zeolite with hierarchical porosity by Varma et. al. [6] on Ni-W/ZSM-5 and sulfided Ni-Mo/ZSM-5 and later by Chen et. al. [7] on sulfided Ni-Mo/ZSM-5. However, the results were reported for catalysts working in quite severe reaction conditions. Further, the use of sulfided catalysts contaminate the products by sulphur leaching [8] and catalysts in the absence of a source of sulphur present deactivation problems. In addition, the usage of large pore zeolites like zeolite BEA could in principle minimise deactivation by coking and improving the transport through the micropore network. Consequently, studying the use of non-sulfided, non-noble catalysts, like Ni on hierarchical beta zeolites is quite interesting.

In this work, the results of Ni/BEA catalysts prepared starting from commercial zeolites and upon desilication treatment will be studied. In order to simplify the study of the reaction, Methyl Palmitate was used as a model compound, mimicking the chemistry of microalgae oils. Furthermore, to get further insight on the role of the acidity on the HDO reactions a Ni/SBA-15 catalyst was prepared and tested.

2. Experimental

2.1 Preparation of the Catalysts

Two commercial BEA zeolites were used as supports, namely CP814E and CP811E-75. In order to introduce a controlled mesoporosity, the CP811E-75 was treated by a standard desilication procedure [9] and identified as CP811E-75D and in turn, used as support. Finally, a SBA-15 was prepared according to a previously reported procedure [10]. All the zeolites, as received and treated were converted into their respective acidic form. The CP811E-75D was exchanged by a NH_4NO_3 solution (1 M) for a total of three times, dried at 110°C and calcined (450°C, 6h, 2°C/min).

For this work, a total of 4 catalysts were prepared, tested and characterised, namely Ni/CP814E, Ni/CP811E-75, Ni/CP811E-75D, Ni/SBA-15. All the catalysts were prepared by incipient wetness [5]. A solution of $Ni(NO_3)_2 \cdot 6H_2O$ was prepared and impregnated slowly on each respective support to get a final loading of 8% Ni. After, the impregnation procedure, all the prepared catalysts were dried overnight at room temperature and then at 110 °C for 12 h. Then, the catalysts were calcined at 400 °C with a rate of 2 °C/min for 4 h. Before use, all the catalysts were reduced in a tubular reactor with a flux of 100 ml/min pure H_2 at 500 °C, with a rate of 2 °C/min for 4 h. After the reduction, all the reduced catalysts were cooled

at room temperature in a stream of pure N_2 and quickly transferred into the reactor, by using a catalyst addition device by Parr Inc. An overview of the prepared catalysts is reported in Table 12.

2.2 Characterization

The texture of the prepared catalysts and parent zeolites was characterised by N_2 physisorption at -196.79 °C by using an ASAP2010 instrument (Micromeritics) according to the last IUPAC technical report [11]. BET surface areas were calculated by using the Rouquerol's method [11–13] in the p/p° range 0.006-0.09. Total pore volume was estimated at p/p°=0.95, according to the Gurvich rule [11,14,15]. Micropore volume (V_μ) and external surface areas (S_{meso}) were determined by using the t-plot method in the t range 0.354-0.6nm [11,16–19], while microporous surface area (S_{micro}) was determined by difference between the BET surface area and mesoporous surface area ($S_{BET} - S_{meso}$). The t-plot was calculated by using the t-reference curve reported by Galarneau et. al. [20], developed for hierarchical zeolites. Mesoporous volume was calculated by difference of the microporous volume and the total pore volume [21]. The pore size distribution was calculated by using the BJH method in the desorption branch as it is closer to the thermodynamic equilibrium [22,23]. The Hierarchy Factor [21], defined as $\frac{V_\mu}{V_t} \cdot \frac{S_{meso}}{S_{BET}}$ was used to characterize the hierarchy of the zeolites.

The commercial zeolites as-received, after thermal and post-synthesis treatments and the prepared catalysts, were characterised by PXRD by a Bruker D2 Phaser (Cu kα1 radiation, 5<2θ<50, 30<2θ<70, increment 0.02°, time step 3.6sec, Lynxeye detector 1D). The nickel crystallite size was determined by the Scherrer equation, by using the (111) and the (200) reflection shown at 44.425° and 51.765° (2θ) [24,25]. The Si/Al ratio for the CP811E-75 was determined by the Cohen's method [26] as reported by Millini [27] by least-squares fit of the interplanar spacings associated with the sharp reflections ((004), (300), (302), (304), (008), (306), (600)), indexed according to the tetragonal $P4_122$ space group and associated to the polymorph A by taking the literature value of the Si/Al for the CP814E [28] as a reference. In the case of zeolite BETA, indeed, given the complexity of the structure which is the result of the intergrowth of at least three polymorphs, it is not possible to apply the Rietveld method [27].

The acidity of the parent zeolites and the CP811E-75D was characterised by NH_3 TPD (TPDA) by using the Autochem II apparatus (Micromeritics) equipped with a TCD detector. The zeolite samples, about 100 mg, were treated inside a U-shaped reactor at 500°C in 5%H_2/Ar flow for 4h. Then, the samples were treated in a 10% NH_3/He flow at 150 °C for 1 h. This step was followed by purging in He flow (30ml/min STP) for 90 min at the same temperature for eliminating physisorbed ammonia. The samples were the cooled at room temperature and the analysis performed in the range 150-700 °C. To take into account the dehydroxylation of the support, blank tests in the same conditions were performed on the zeolites skipping the NH_3 adsorption stage [29–31]. The signal obtained for the analysis was then subtracted to the signal obtained for each respective blank test.

Metal surface areas (MSA) were characterised by dynamic pulse chemisorption of CO after reduction of the catalysts, in the same conditions for catalytic tests (see above). The CO chemisorption measurements were conducted by using the same apparatus used for TPDA measurements. For calculating the MSA a stoichiometric factor of 1 (CO/Ni=1) was assumed [32]. The sample was heated in He with a ramp of 10 °C/min to 500°C. Then, the gas feed was switched to a 5 % H_2/Ar (reduction stage). This stage lasted

for 240 min. Afterwards, the catalyst was cooled at 35°C in He. At the same temperature, after the equilibration of the signal and temperature, a series of pulses of a 10 % CO/He mixture were sent over the sample and the signal registered. This low temperature was chosen in order to minimise the formation of Nickel carbonyl, which is favoured above 77-97 °C and CO partial pressures above 1.013 bar [52].

Ni particle size and zeolite surface features were also accessed by TEM microscopy by using a PHILIPS CM12 Microscope (point-to-point resolution 3Å) operating at 200kV. Samples were prepared by suspending freshly reduced catalyst powder in 2-propanol followed by sonication. The suspension was then dispersed on standard copper grids. The samples were analysed by short exposure times to minimise the amorphization of the zeolites [33].

SEM microscopy and EDX technique were used to characterise the zeolites "as received" and after desilication by using Phenom ProX instrument, equipped with BSD and EDX detectors. To obtain a good separation between the particles and a better point-to-point resolution, the samples were prepared by suspending the zeolite powder in isopropanol. The solution was then sonicated and deposited on a clean surface. The deposited powder was dried to eliminate the solvent and finally transferred onto a stab.

2.3 Testing

The performance of the prepared catalysts was tested in 300ml Parr Autoclave in batch mode at 240°C and a final pressure of 40 barg. N-heptane was used as a solvent (100 ml), while methyl palmitate (MP) was used as a model compound (1 g). At the beginning of the testing procedure, the catalyst (0.1 g) was loaded in a pneumatic catalyst addition device (Parr Inst. ®). This was necessary in order to keep the catalyst and substrate separated, minimising any reaction before equilibrating temperature and pressure during the heating procedure. Then, the reactor was sealed and, at room temperature, purged for three times with N_2. After this step, the reactor was purged three times with H_2 and filled up to a final pressure of 18 barg. Then, the heating procedure was started up to the final temperature while stirring at the same time at the final stirring set up (1055 rpm). After this step, the final pressure was set at 40 barg and equilibrated (15'). Finally, the catalyst was pneumatically discharged. This was considered as the time zero of the reaction. A schematic view of the experimental apparatus used for testing is reported in Figure 53. The reaction was, then, run isothermally for 4 h. Liquid samples were withdrawn from the reactor at the beginning of the test (before discharging the catalyst), after 2 h and at the end of the test (4 h).

2.4 Analytical Procedures

The collected liquid samples were diluted in n-heptane and analysed by GC/MS and GC-FID by using a Thermo, Trace GC 2000, Trace MS and GC-FID Thermo, Trace GC 2000 both equipped with a Restek Rxi-5MS column (L=30m, ID=0.25mm, d_f =0.25µm). He was used as carrier gas. The injector was set in split mode at 280°C and a split ratio of 1:10. The GC oven was set at an initial temperature of 60°C. The temperature was then ramped up to 80°C with a rate of 2°C/min and then up to 300°C with a ramp of 10°C/min. The final temperature was held for 15min [5].

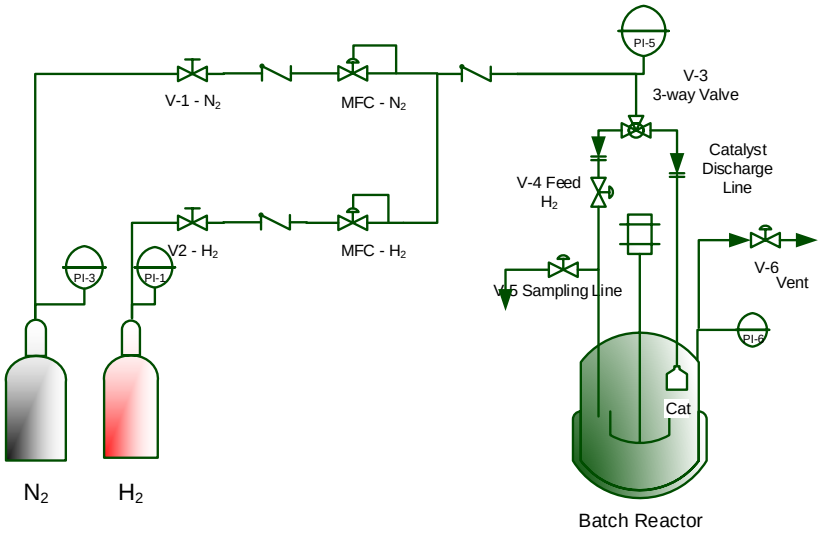

Figure 53 – Schematic view of the experimental apparatus used for testing the catalysts

3. Results and discussion

3.1 Characterization

The main chemical characteristics of the zeolites used in this work are summarised in Table 10 as reported in the literature and from the manufacturer. The extent of the desilication treatment can also be observed in the decrease of the Si/Al in the framework, calculated by the method used by Millini and coworkers [27]. These values, in this case, should be taken as indicative, because of the presence of amorphous debris, decreasing the signal to noise ratio. Nevertheless, the reported values are in agreement with the desilication treatment. The effect of the decrease of the Si/Al ratio is even more evident on the surface. Also in this case, the Si/Al ratio should be taken with care as calculated by using a semi-quantitative method (EDX). Nevertheless, the value reported for the CP814E is in agreement with the literature XPS value. In accordance with the reported values the Si/Al ratio decreased by half the initial value after the desilication treatment. The agreement between the two values confirms a deep desilication even in the bulk of the zeolite crystals. The framework value for the CP811E-75 is in agreement with the value calculated by TPDA as reported by Millini et. al [27]. For the CP811E-75D the framework SI/Al calculated by the methods suggested by Millini et. al. are not in agreement, probably because of the creation of other Brønsted sites during the desilication treatment, as a result of the presence of EFAL species.

Table 10 – Main chemical Characteristics of Zeolites ([a] calculated according to Millini et. al. [27], [b] calculated by NMR, [c] semi-quantitative, estimated by EDX analysis, [d] estimated by XPS analysis, [e] calculated by TPDA)

Zeolites	Si/Al Bulk	Si/Al Framework	N_{EFAL}	Si/Al[c] surface
CP814E	12.5 [34]	33 [28b]	3.1 [28]	10.78 [35d], 9.5
CP811E-75	37.5 [34]	54[a], 58[e]	-	22.1
CP811E-75D	-	25[a], 49.22[e]	-	11.3

The obtained N_2 physisorption isotherms for the parent and desilicated zeolites are reported in Figure 55 while in Table 11 are reported the main textural features. From Figure 55 it is possible to note that all the isotherms are superpositions of type I-IV isotherm, because of the presence of both micro- and mesopores. The CP814E and CP811E-75 zeolites present similar physisorption features. The hysteresis, however, is much more evident for the CP811E-75D, because of its hierarchical structure. The hysteresis loop resembles a H2(b) type, often associated with pore blocking in complex pore networks in the presence of a large distribution of pore widths for ink-bottle pores [11,18,23]. This kind of pore geometry was already reported for desilicated zeolites and was evidenced by physisorption analysis, TEM and SEM micrographs [36]. In Figure 58 the BJH pore size distribution was reported. As evidenced in Figure 58, all the reported samples present a certain degree of mesoporosity. For the non-treated samples, this was related to the roughness of the surface of the crystals, as already reported in the literature [37]. In line with the literature, the mesoporosity in the case of the CP811E-75D is much more pronounced, and the average size is around 6 nm. This value, however, given the reported conclusions on the kind of the hysteresis was related to the neck of the pores. In this case, it is possible, therefore, to exploit the desorption branch of the isotherm to calculate the neck size while from the adsorption isotherm it is possible to calculate the internal size [38]. For the desilicated zeolite CP811E-75D, in line with literature data [21], compared to its parent zeolite, we observed an increase in the apparent BET surface area in the mesopore region at the expense of the micropore surface area (see Figure 58). Further, the volume of the mesopores increased at the expense of the micropore volume.

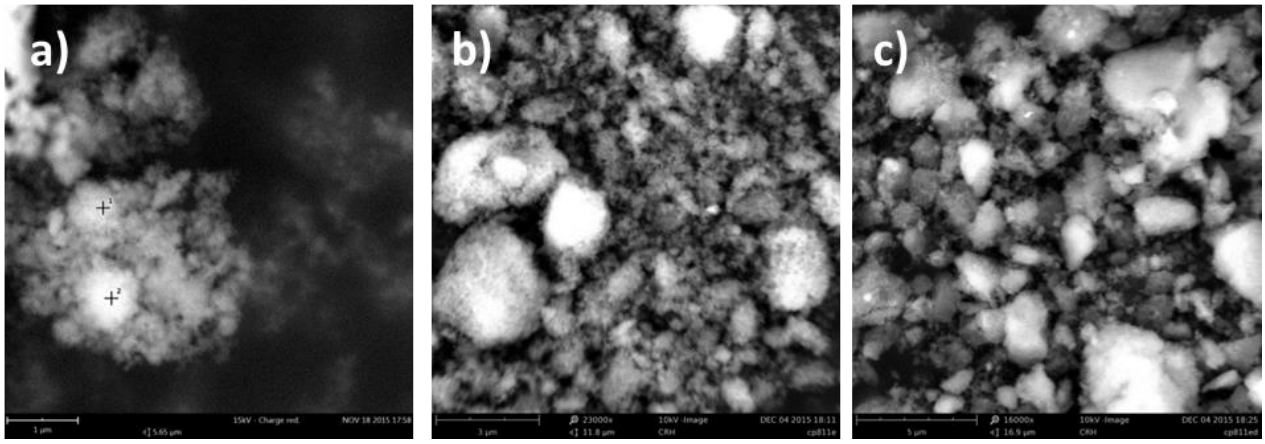

Figure 54 – SEM Micrographs for the a) CP814E, b) CP811E-75, c) CP811E-75D

From the physisorption isotherms reported in Figure 55, it is possible to note an increase in the adsorption volume in the p/p° 0.05-1 range for the CP811E-75D, while a slight decrease is observed in the 0-0.05 range, in line with the decrease of the micropore volume and the corresponding increase in the mesopore volume. According to the data reported in Figure 58, the parent samples present some mesoporosity features. This might be induced by some post treatments applied by the producer (e.g. deallumination). However, after desilication treatment there a huge improvement in the mesopore area in the range 5-50 nm.

The XRD profiles for the supports used in this work are reported in Figure 59 and Figure 60. Figure 59, shows the typical features, for SBA-15, confirming its structure. The parent zeolites present (see Figure 60) the typical reflections reported for BEA zeolites [39]. Conversely, in line with the literature [40], in the case of

the desilicated sample (CP811E-75D), a reasonable decrease in the crystallinity of the sample was observed (see Figure 60).
The prepared catalysts, as observed from TEM micrographs (see Figure 61), for the Ni/CP814E, reveal the presence of small particles, presumably in the mesopores. Conversely, the presence of big particles with irregular shapes was observed for the Ni/CP811E-75, Ni/CP811E-75D and Ni/SBA-15 (see Figure 61). The presence of agglomeration by using $Ni(NO_3)_2 \cdot 6H_2O$ was also observed by Chen et. al. [8], and it is probably the result of the low affinity between the surface of the zeolite and the precursor. This is especially true in the case of high Si/Al ratio, because of the lower hydrophilic character of the surface in this case.

The results of CO pulse chemisorption are reported in Table 12. The higher Ni dispersion in the CP814E is probably related to a better penetration of the impregnating solution inside the micropores, but the values of the mean particle diameter, 9.36 nm, demonstrate that most of the nickel was deposited inside the mesopores originally present in the zeolite. The lower dispersion obtained for the Ni/CP811E-75D is probably due to the particles deposited on the external surface of the zeolites. In the case of Ni/SBA-15 catalyst can be related to the lower contribution of the mesopore volume and to the high loading of Ni (see Table 12).

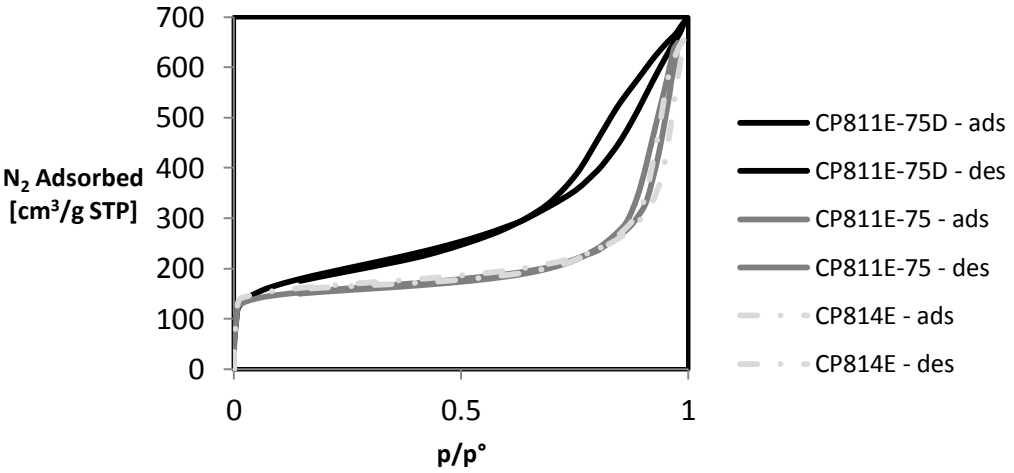

Figure 55 – Nitrogen physisorption isotherm for treated and untreated samples

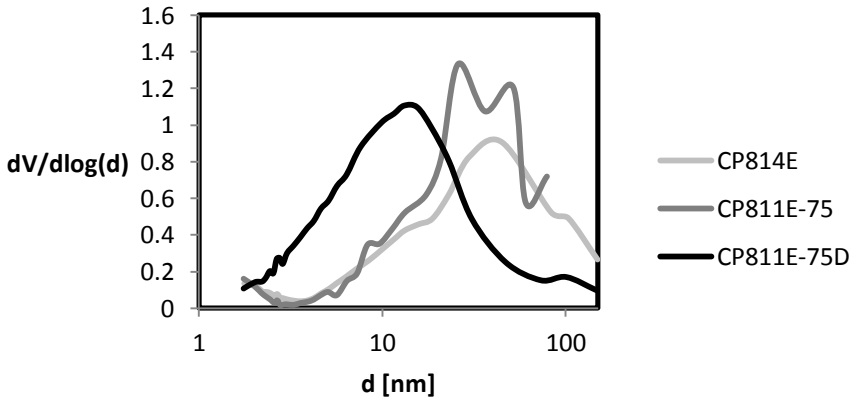

Figure 56 - BJH pore size distribution calculated for the adsorption branch based on the volume of the pores

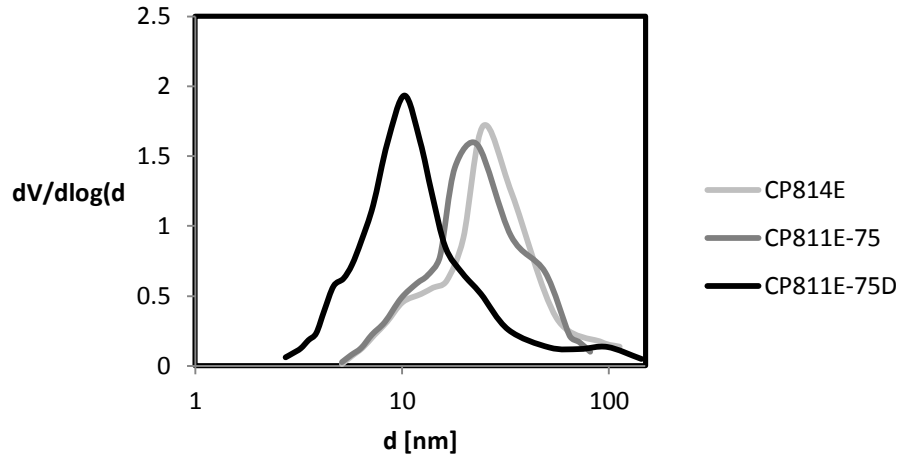

Figure 57 - BJH pore size distribution calculated for the desorption branch based on the volume of the pores

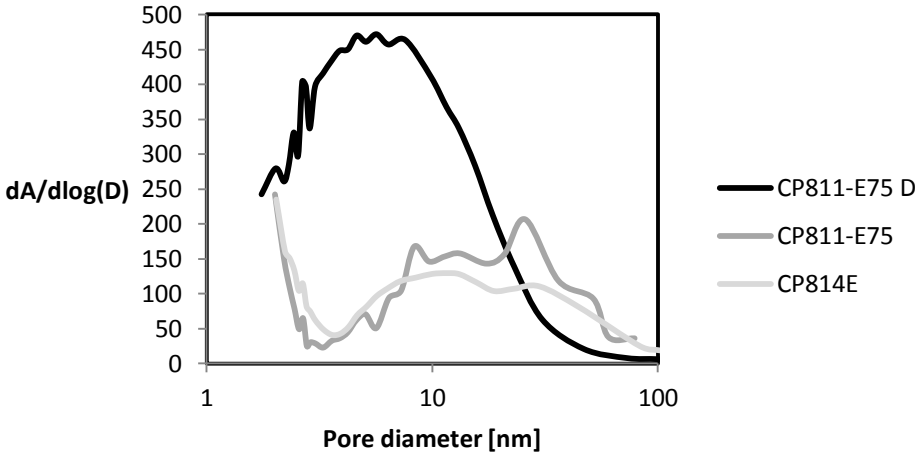

Figure 58 - BJH pore size distribution calculated for the desorption branch based on the surface area of the pores

The crystallite size of Ni, measured by XRD by using Scherrer equation, are reported in Table 12. As clearly evidenced, the Ni crystallite size for the Ni/CP814E is similar to the particle size reported by CO chemisorption, while for the other catalysts is far below. This is in line with the presence of aggregates of Ni as evidenced by TEM micrographs.

The TPDA profiles for the parent and desilicated (see Figure 62) have been deconvoluted in three Gaussian components, respectively at low (LT), medium (MT) and high temperature (HT) [41,42]. The main results from the deconvolution analysis are reported in Table 13. As reported in the literature [43], LT peaks were related to NH_3 weakly chemisorbed or physically adsorbed or on weak Lewis acid sites like Na^+, while MT peaks were related to the number of Al atoms in the framework, and associated to the Brønsted sites [42,44]. Sorting by the area of the MT peaks, the density of acid sites [µmol NH_3/g] decreases with the following order CP814E (Si/Al_{bulk}=12.5) < CP811E-75D (Si/Al_{bulk}<37.5) < CP811E-75 (Si/Al_{bulk}=37.5), following the trend in Si/Al ratio in the framework. The CP811E-75D compared to the parent zeolite has shown a shift to lower temperatures and a higher density of acid sites [43]. This was related to the lower Si/Al ratio and the lower contribution of micropores. The lower volume of the micropores, indeed, in the case of the

desilicated sample, imply a lower contribution from the confinement effect, and therefore a decrease in the strength of the acidic sites [45]. The shift to lower temperatures, further, could also be explained by the improved diffusion of ammonia because of hierarchical structure [42]. Nonetheless, in this case, all these effects are expected.

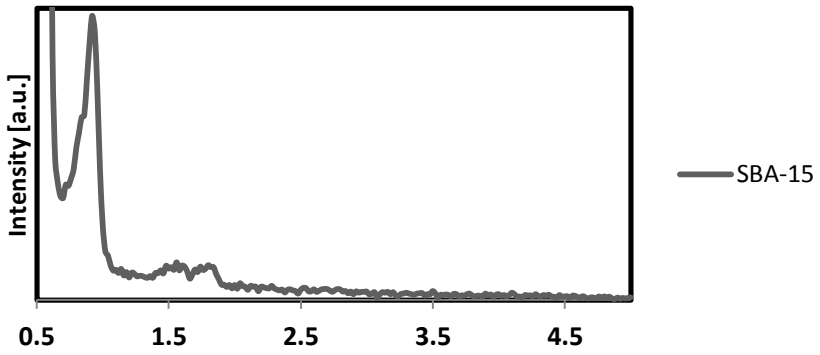

Figure 59 – XRD profiles SBA-15 sample

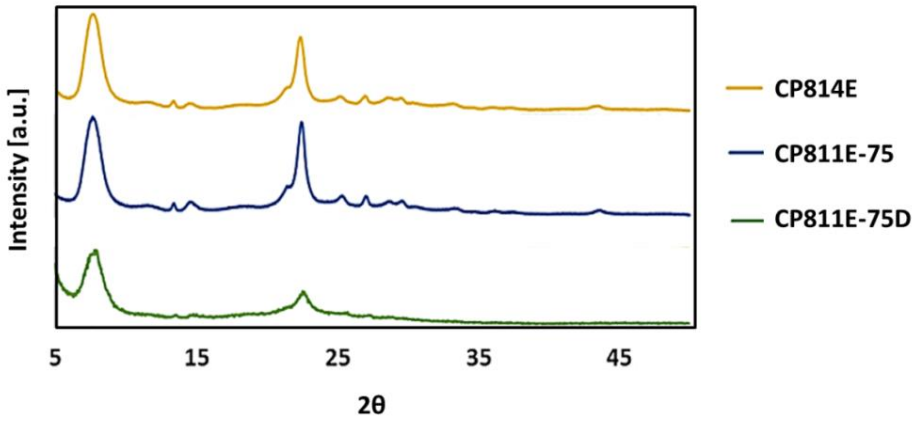

Figure 60 - XRD profiles for the CP814E, CP811E-75 and CP811E-75D

The observed HT peaks were attributed to strong Lewis sites [42]. Their maxima appear at nearly the same temperature for all the samples while the area is dependent on the features of the zeolites. Comparing the desilicated zeolite (CP811E-75D) with the non-desilicated one (CP811E-75), the area of the HT peak in the first case is at almost three times larger in comparison to the parent sample. This is probably due to the realumination process, by the desilication treatment, which could give rise to the increase of Lewis acidity [9].

The effectiveness of the desilication technique is further demonstrated by the values of the surface Si/Al ratio determined by EDX, reported in Table 10. The difference between the bulk Si/Al and surface Si/Al evidences aluminum zoning on the external side of the support already present in the parent zeolites.

The TPR profiles for the calcined catalysts reported in Figure 63. The reported profiles have been deconvoluted in three or four Gaussian components. The deconvolution results are reported in Table 14. As shown by the TPR profiles, depending on the interaction of the precursor with the support, there is a marked effect on the reducibility of NiO species upon calcination. As reported in the literature, bulk NiO

shows only one reduction peak at 300-400°C [47,48]. Therefore, the low-temperature components, below 400°C were attributed to NiO particles weakly anchored to the support or unsupported [47]. These peaks of easily reducible NiO, in agreement with TEM analysis, are more abundant on Ni/CP811E-75, while this contribution is minimal for Ni/CP814E and negligible for Ni/CP811E-75D and Ni-SBA-15. The peaks at 450-550°C were associated with the reduction of Ni phyllosilicate [49]. The peaks at high temperature (520-600°C) were attributed to Ni aluminate or ion-exchanged Ni, which upon calcination can lead to highly dispersed oxides and silicates [47]. For the Ni/CP814E the most abundant peak was found at 600°C, in agreement with the high dispersion observed with this catalyst.

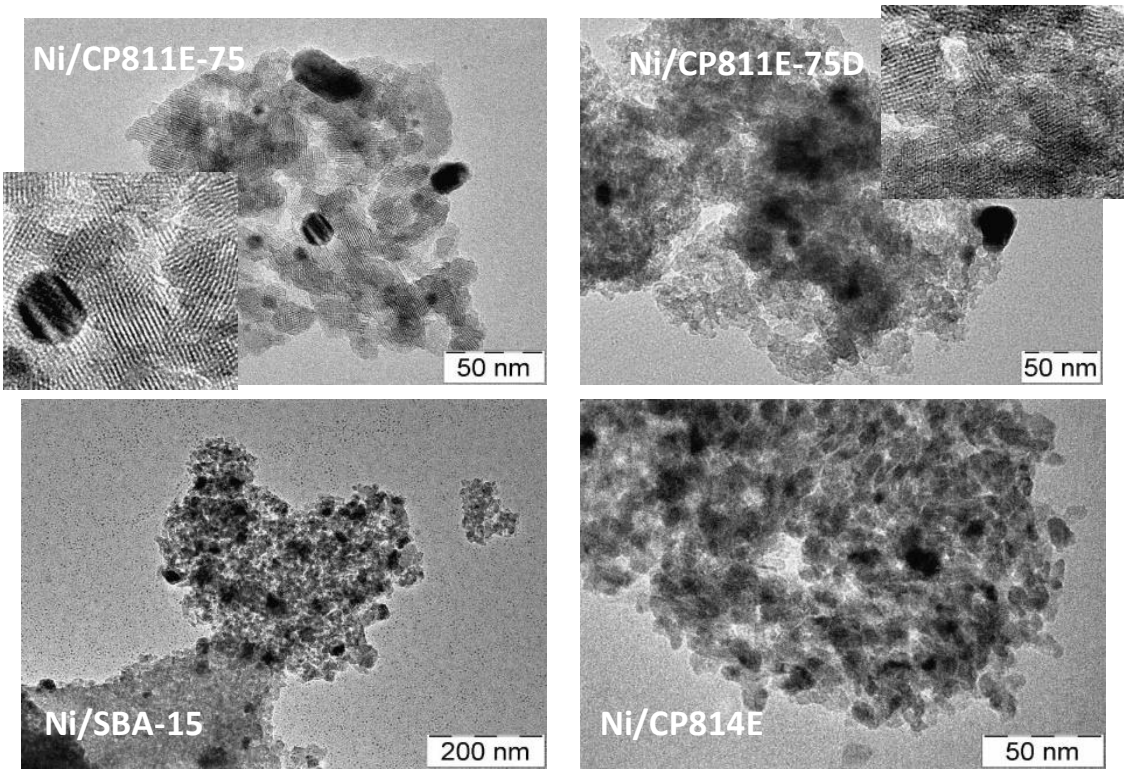

Figure 61 - TEM micrographs for the catalysts

Table 11 – Main textural features of Zeolites and SBA-15 ([a] values from the literature calculated by SEM analysis)

Support	S_A BET [m²/g]	S_{μ}[m²]	S_{meso}[m²/g]	Pore Volume [cm³/g]	V_{μ} [cm³/g]	V_{meso} [cm³/g]	HF	Particle size [µm]
CP814E	624.22±1.66, C=1671.64	426.23	197.99	0.97	0.17	0.80	0.056	0.2[a46]
CP811E-75	590.16±1.36, C=1124.50	388.47	201.67	1.00	0.16	0.85	0.053	0.2[a 46]
CP811E-75 D	677.91±5.75, C=301.4947	140.15	537.75	1.09	0.07	1.03	0.047	n.d.
SBA-15	189.7±0.47 C=93.27	0	189.7	0.29	0	0.29	n.d.	n.d.

Table 12 - Active phase features ([a] determined by AAS; [b] determined by CO chemisorption; [c] Cubic crystal size; [d] determined by XRD on freshly reduced catalysts)

Catalysts	%Ni[a]	Ni Particle size[nm][b,c]	Ni Crystallite size[d]	MSA [m^2/g_{Cat}][b]
Ni/CP814E	7.87	9.4	13	4.72
Ni/CP811E-75	8.31	39	9.1	1.19
Ni/CP811E-75D	7.31	71	16.7	0.57
Ni/SBA-15	7.61	72	9.7	0.70

Table 13 – Ammonia TPD deconvolution results

Zeolite	NH_3 total [µmol/g]	LT [µmol/g, °C]	MT [µmol/g, °C]	HT [µmol/g, °C]	NH_3 [µmol/m^2]	NH_3 [µmol] Micropores	NH_3 [µmol] Mesopores
CP811E-75	404.2	48.4 (216.4)	279.6 (343.3)	40.4 (543.7)	0.47	184.5	95.3
CP811E-75 D	524	78.9 (222.9)	331.5 (316.2)	113.6 (540.4)	0.49	68.5	262.9
CP814E	783.3	221.3 (236.7)	492.1 (330.7)	89.9 (540.7)	0.79	336.1	156.1

Table 14 – TPR deconvolution results

Catalyst	Peak 1 [°C, (%Ni)]	Peak 2 [°C, (%Ni)]	Peak 3 [°C, (%Ni)]	Peak 4 [°C, (%Ni)]
Ni/CP814E	348.2 (14%)	439.5 (19%)	554.6 (21%)	600.3 (46%)
Ni/CP811E-75	332.7 (63%)	357.1 (16%)	520 (21%)	
Ni/CP811E-75D	344.6 (5%)	437.1 (65%)	455.3 (5%)	569.6 (25%)
Ni/SBA-15	326.1 (3%)	370.2 (44%)	425.4 (16%)	576.6 (38%)

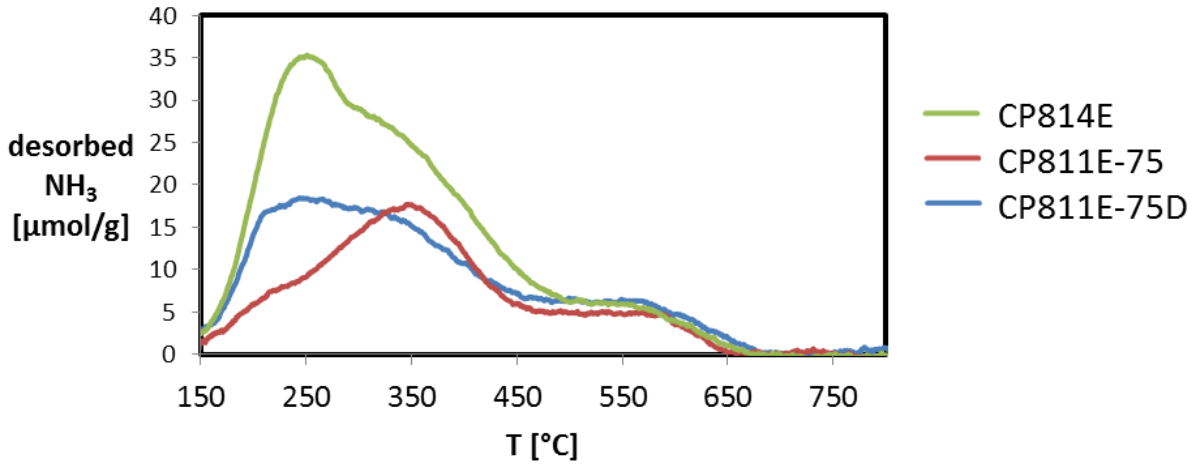

Figure 62 – Blank subtracted TPDA curves for the parent and desilicated zeolites

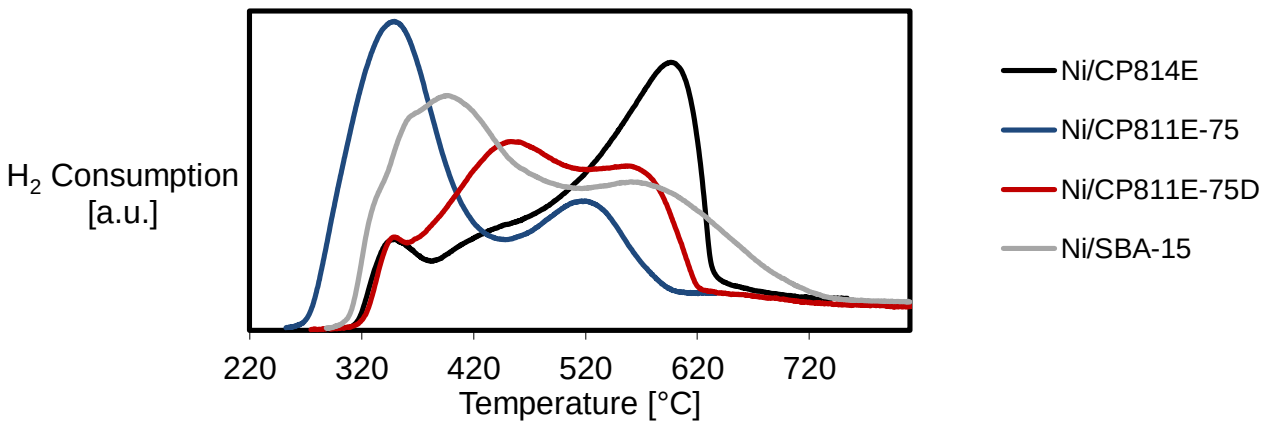

Figure 63 – H_2-TPR profiles for the calcined catalysts

3.2 Testing - Effect of the acidic sites, hydrogenation functionality and hierarchical structure

The analysis of the products of the reaction was split into two parts: in Figure 64 the main results for the hydrodeoxygenation (HDO) and decarbonylation/decarboxylation reactions (DeCOx) were analysed, while in Figure 65 the cracking product distributions were reported. In Figure 64 the conversion and yield of the most important intermediates, namely palmitic acid (PA), n-hexadecane (n-C_{16}) and n-pentadecane (n-C_{15}) were reported. In line with the literature [8], cetyl alcohol and cetyl palmitate were also obtained, but only in trace amounts, therefore the yield of these products was not reported. The used catalysts were ordered by their respective Si/Al ratio. For completeness, Ni surfaces areas, the density of acidic sites ($\mu molNH_3/g$), acidic strength (expressed as the normalised temperature of the MT peak in the TPDA analysis) and the ratio of acidic to hydrogenation sites ($(\mu molNH_3/g)/(m^2Ni)$) were reported. As reported in Figure 64, between the studied catalysts, the highest conversion was achieved by using the Ni/CP811E-75 catalyst. In this case, also a reasonable yield to PA and the highest yields of n-C_{16} and n-C_{15} were obtained. The n-C_{16}/nC_{15} ratio, further, was the highest between the reported catalysts, indicating the relatively higher predominance of HDO reactions over DeCOx reactions with respect to other analysed catalysts. The Ni/SBA-15 catalyst, presenting a very low density of Brønsted sites, conversely, has shown the worst performance, a very low n-C_{15}/n-C_{16} ratio and a negligible yield of PA. All these observations suggest a synergy between the hydrogenation functionality and acidic sites for HDO reactions, as also suggested by Chen et. al. [8]. The high yield to PA obtained for zeolite base catalysts, further, demonstrate that the HDO reaction of PA is a limiting step in the case of zeolite based catalysts. HDO reactions proceed through a series of steps. The first step, in the presence of esters or fatty acids methyl esters (FAME), is the hydrolysis of these compounds to get their respective acids. In this case, MP is converted to PA, methane and water [8]. PA is subsequently hydrogenated to its corresponding aldehyde and alcohol on the surface of the metal. In line with our experimental findings, cetyl alcohol is quickly dehydrated on acidic sites and quickly hydrogenated to n-C16 [8] while only a minor amount is converted to cetyl palmitate on acidic sites. PA can also be decarboxylated to give n-C_{15} and CO_2. n-C_{15} can also be obtained by decarbonylation of palmitaldehyde on the surface of the catalyst, formed upon reduction of PA. Both decarbonylation and decarboxylation reactions, probably do not require the presence of acidic sites. In agreement, for the Ni/SBA-15 sample, because of the negligible density of acidic sites, methyl palmitate

(MP) is slowly converted to n-C15, as confirmed by the low n-C_{16}/n-C_{15} ratio and the low yield to n-C_{15}, n-C_{16} and PA. DeCOx reactions, compared to HDO reactions are much slower and favoured at high temperatures [8], and this is probably the case also for the reaction of methyl palmitate to n-C_{15}. The low reactivity of the ester group, usually employed as a protective group, widely documented in most organic chemistry textbooks, might further explain the low conversion rates observed in the case of Ni/SBA-15 catalyst. Therefore, to achieve high conversion rates and increase the importance of HDO reactions, the presence of strong Brønsted sites together with hydrogenation functionalities is required [8]. In the case of the Ni/CP811E-75D and Ni/CP814E, with respect to the Ni/CP811E-75 catalyst, the conversion is lower, while the PA yield is higher and the yield of n-C_{16} and n-C_{15} are lower, together with the ratio n-C_{16}/n-C_{15}. This, especially for the Ni/CP814E was unexpected, given the high density of acidic sites observed for the parent zeolite and the high MSA shown by the as-prepared catalyst. In this case, as reported in the characterization section, Ni particles are mostly located in the bulk of the zeolite crystals. This, restrict the accessibility of MP and PA to the hydrogenation functionality and therefore its further conversion to n-C_{15} and n-C_{16}, justifying the higher yield of PA. The lower n-C_{16}/n-C_{15} ratio is consistent with the results reported by Chen et. al. which observed that by increasing the Ni loading on HBEA zeolite there was a decrease of the importance of the HDO reactions with respect to decarbonylation/decarboxylation reactions and attributed this phenomenon to the occupation of acidic sites by Ni [8]. For the Ni/CP811E-75, conversely, because of the preferential locations of Ni particles on the surface and agglomeration, the higher availability of acidic sites and the greater accessibility of Ni increases the conversion rate of MP and PA [8]. The high availability strong Brønsted acidic sites, further, explain also the high n-C_{16}/n-C_{15} ratio obtained by using this catalyst [8]. Similarly, also for the Ni/CP811E-75D particles are located preferentially on the surface, and Ni agglomeration was also observed for this catalysts. However, in this case, the availability of strong Brønsted acid sites is probably greatly reduced because of the desilication treatment. This might justify the lower conversion of MP with respect to the conversion obtained for the Ni/CP811E-75. However, the improvement in the mesoporous surface area achieved after the desilication treatment increased the surface accessibility. Further, in line with the greater accessibility of Ni particles and acidic sites, in this case, the obtained n-C_{16}/n-C_{15} ratio was larger compared to the Ni/CP814E and only slightly lower compared to the Ni/CP811E-75 catalyst. In the literature [7], in slightly different conditions, an increase in the prevalence of decarbonylation reactions in respect to HDO reactions was reported after desilication and was related to the induced mesoporosity. Nonetheless, the last observation might be related to the decrease of the accessibility of strong Brønsted sites upon desilication with part of the aluminium migrating in extra-framework position, depositing on the surface and hindering the access to micropores [9]. Therefore, the conversion rate depends on the amount/strength of acidic and hydrogenation functionalities, but also on their accessibility.

As reported in Figure 65, the cracking product distribution was dependent on the texture of the catalysts and probably on the acidic strength of the parent zeolites. The relative amount i-C_{16} and i-C_{15} (not evidenced in Figure 65), increased with the time of reaction. By using the Ni/CP814E catalyst, in line with its low MP conversion activity, we did not observe any significant amount of cracking products in the C_9-C_{12} range. Both the low conversion and low yield in cracking products might be explained by the lower accessibility of acidic/hydrogenation sites, in agreement with the results reported by Chen. Et. al. [8]. Conversely, by using the Ni/CP811E-75D and Ni/CP811E-75 catalysts a reasonable yield of products between the C_9-C_{12} range was observed. The best yields in the C_9-C_{12} range were observed for the

Ni/CP811E-75D, although, as previously evidenced this catalyst was less active for MP conversion. The highest yield was observed for shorter reaction time because of the high reactivity of iso-alkanes in respect to linear alkanes [8,50] (see Figure 65 after 2h and 4h).

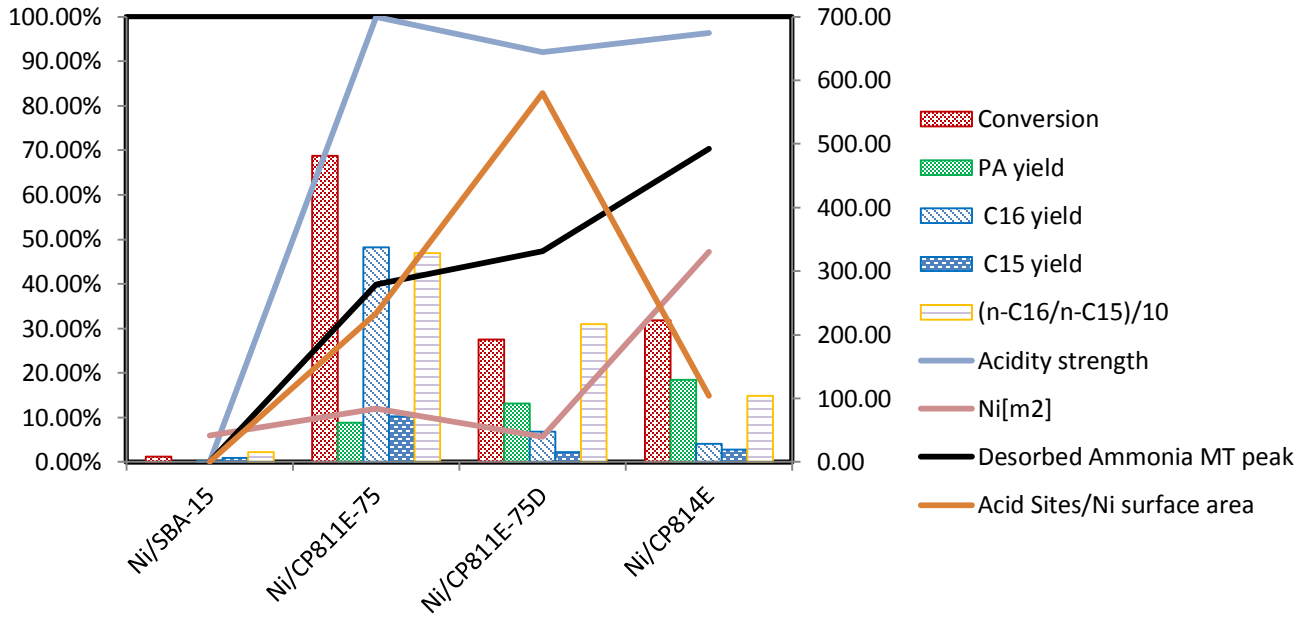

Figure 64 – Conversion and yields of the most abundant intermediates for the catalysts tested (bar); continues lines are concentration of active sites (black line), acidic strength and the ratio ($\mu molNH_3/g)/(m^2Ni$)

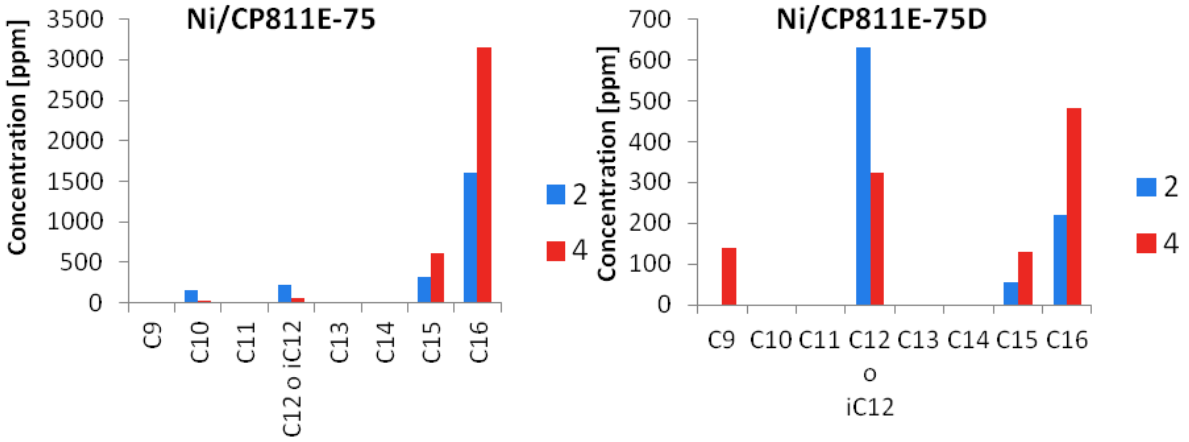

Figure 65 – Product distribution for the catalysts tested, after 2 h (blue) and 4 h (red) of reaction time for the Ni/CP811E-75, Ni/CP811E-75D

In the case of the Ni/CP811E-75D catalyst, the presence nickel on the external surface of the support, close to Lewis acid sites (related to extra-framework Al), and the higher mesoporous surface, together with a reduced contribution from the micropores probably play a major role. To note, also, that a high selectivity to C_{12} hydrocarbons cannot be the result of a statistical cracking. This results might be

interpreted as the result of a selective chemisorption on the surface, in line with the concept of pore mouth catalysis [51]. By this concept, hydrocarbons are only partially chemisorbed at the entrance of the micropores and activated. Therefore, to increase the yield for the C_9-C_{12} fraction, the hydrogenation function should be located on the external surface of a mesoporous zeolite, likely in close vicinity to Lewis acid sites (EFAL), and channels in which the hydrocarbon is partially adsorbed. In agreement with the suggested mechanism, we may note the absence of correlation between the HF factor [21] and the catalytic behaviour.

Conclusions

In this work, the results obtained for the one-step hydrodeoxygenation/hydrocracking of Methyl Palmitate by using Ni/BEA with microporous and hierarchical structure have been compared with a home-made Ni-SBA-15 catalyst. The comparison of the results for Ni/HBEA and Ni/SBA-15 catalysts has shown the role of the Brønsted acidity of the catalyst on HDO/DeCOx reactions. The presence of Brønsted acidic sites together with hydrogenation functionality has been shown to be synergistic for achieving high conversion for HDO reaction [8], while the relative amount of both functionalities has shown a large influence on product distribution. In agreement with the reported results, the location of Ni particles on the external surface of the zeolite has shown the best conversion performances. Furthermore, to improve the kinetics of HDO reactions, Brønsted acidity is necessary and synergic with hydrogenation sites.

Comparing the performances of Ni/HBEA with different Si/Al ratio, before and after desilication has shown some interesting results for obtaining hydrocarbons in the jet fuel range. Considering the cracking reactions, high mesoporous surface areas, together with the presence of extra-framework Al are necessary to tune the cracking product distribution toward the C_9-C_{12} fraction, likely with a selective pore mouth mechanism. Conversely, in the presence of high microporous volumes and low external surface areas, only negligible yields of cracking products were observed. The reported data do not give indications about catalyst deactivation. Furthermore, the use of algal oil with a variable degree of purity could deactivate the catalyst as well. However, although further studies are required, these results provide good indications for developing new catalysts for achieving a selective conversion of microalgae oil in a one-step HDO/Hydrocracking process.

References

1. S. Abate, G. Centi, and S. Perathoner, *Natl. Sci. Rev.*, 2015, **2**, 143–145.
2. J. Y. Park, M. S. Park, Y. C. Lee, and J. W. Yang, *Bioresour. Technol.*, 2015, **184**, 267–275.
3. W.-C. Wang and L. Tao, *Renew. Sustain. Energy Rev.*, 2016, **53**, 801–822.
4. F. Baldiraghi, M. Di Stanislao, G. Faraci, C. Perego, T. Marker, C. Gosling, P. Kokayeff, T. Kalnes, and R. Marinangeli, in *Sustainable Industrial Chemistry*, Wiley-VCH Verlag GmbH & Co. KGaA, Weinheim, Germany, 2009, pp. 427–438.
5. B. Peng, Y. Yao, C. Zhao, and J. a. Lercher, *Angew. Chemie*, 2012, **124**, 2072–5.
6. D. Verma, R. Kumar, B. S. Rana, and A. K. Sinha, *Energy Environ. Sci.*, 2011, **4**, 1667.
7. H. Chen, Q. Wang, X. Zhang, and L. Wang, *Ind. Eng. Chem. Res.*, 2014, **53**, 19916–19924.
8. L. Chen, J. Fu, L. Yang, Z. Chen, Z. Yuan, and P. Lv, *ChemCatChem*, 2014, **410004**, n/a-n/a.
9. D. Verboekend and J. Pérez-Ramírez, *Catal. Sci. Technol.*, 2011, **1**, 879.
10. S. Abate, P. Lanzafame, S. Perathoner, and G. Centi, *Catal. Today*, 2011, **169**, 167–174.
11. M. Thommes, K. Kaneko, A. V. Neimark, J. P. Olivier, F. Rodriguez-Reinoso, J. Rouquerol, and K. S. W. Sing, *Pure Appl. Chem.*, 2015, **0**.
12. J. Rouquerol, P. Llewellyn, and F. Rouquerol, in *Studies in Surface Science and Catalysis Vol 160*, 2007, vol. 160, pp. 49–56.
13. S. Brunauer, P. H. Emmett, and E. Teller, *J. Am. Chem. Soc.*, 1938, **60**, 309–319.
14. F. Rouquerol, J. Rouquerol, K. S. W. Sing, P. Llewellyn, G. Maurin, J. Rouquerol, P. Llewellyn, and K. Sing, *Adsorption by Powders and Porous Solids*, 2014.
15. T. M. Lowell S, Shields JE, Thomas MA, S. Lowell, J. E. Shields, M. A. Thomas, and M. Thommes, *Characterization of Porous Solids and Powders: Surface Area, Pore Size and Density*, Springer Netherlands, 2012.
16. P. Hudec, A. Smiešková, Z. Idek, P. Schneider, and O. Ŝolcová, in *Studies in Surface Science and Catalysis*, 2002, vol. 142, pp. 1587–1594.
17. P. Voogd, J. J. F. Scholten, and H. van Bekkum, *Colloids and Surfaces*, 1991, **55**, 163–171.
18. M. Thommes, R. Guillet-Nicolas, and K. A. Cychosz, in *Mesoporous Zeolites: Preparation, Characterization and Applications*, eds. J. García-Martínez and K. Li, Wiley-VCH Verlag GmbH & Co. KGaA, Weinheim, Germany, 2015, pp. 349–384.
19. B. C. Lippens and J. H. de Boer, *J. Catal.*, 1965, **4**, 319–323.
20. A. Galarneau, F. Villemot, J. Rodriguez, F. Fajula, and B. Coasne, *Langmuir*, 2014, **30**, 13266–74.
21. J. Pérez-Ramì-rez, D. Verboekend, A. Bonilla, and S. Abelló, *Adv. Funct. Mater.*, 2009, **19**, 3972–3979.
22. E. P. Barrett, L. G. Joyner, and P. P. Halenda, *J. Am. Chem. Soc.*, 1951, **73**, 373–380.
23. L. Zhang, A. N. C. van Laak, P. E. de Jongh, and K. P. de Jong, in *Zeolites and Catalysis*, Wiley-VCH Verlag GmbH & Co. KGaA, Weinheim, Germany, 2010, pp. 237–282.

24. S. Gražulis, D. Chateigner, R. T. Downs, A. F. T. Yokochi, M. Quirós, L. Lutterotti, E. Manakova, J. Butkus, P. Moeck, and A. Le Bail, *J. Appl. Crystallogr.*, 2009, **42**, 726–729.

25. S. Gražulis, A. Daškevič, A. Merkys, D. Chateigner, L. Lutterotti, M. Quirós, N. R. Serebryanaya, P. Moeck, R. T. Downs, and A. Le Bail, *Nucleic Acids Res.*, 2012, **40**, D420–D427.

26. M. U. Cohen, *Rev. Sci. Instrum.*, 1935, **6**, 68–74.

27. R. Millini, C. Perego, W. O. Parker, C. Flego, and G. Girotti, in *Recent Advances in the Science and Technology of Zeolites and Related Materials Part B - Studies in Surface Science and Catalysis - Volume 154 - Proceedings of the 14th International Zeolite Conference*, 2004, vol. 154, pp. 1214–1221.

28. J. . Marques, I. Gener, P. Ayrault, J. . Bordado, J. . Lopes, F. Ramôa Ribeiro, and M. Guisnet, *Microporous Mesoporous Mater.*, 2003, **60**, 251–262.

29. A. . Camiloti, S. . Jahn, N. . Velasco, L. . Moura, and D. Cardoso, *Appl. Catal. A Gen.*, 1999, **182**, 107–113.

30. C. Costa, I. . Dzikh, J. M. Lopes, F. Lemos, and F. R. Ribeiro, *J. Mol. Catal. A Chem.*, 2000, **154**, 193–201.

31. C. Costa, J. M. Lopes, F. Lemos, and F. R. Ribeiro, *J. Mol. Catal. A Chem.*, 1999, **144**, 221–231.

32. R. J. Farrauto and C. . Bartholomew, *Fundamentals of Industrial Catalytic Processes*, Blackie Academic & Professional, 2nd edn., 2010.

33. I. Diaz and A. Mayoral, *Micron*, 2011, **42**, 512–527.

34. 2015.

35. F. M. Alotaibi, R. H. Abudawood, H. a. Al-Megren, M. C. Al-Kinany, E. H. Jamea, and A. a. Garforth, *Appl. Petrochemical Res.*, 2014, **4**, 95–136.

36. J. C. Groen, T. Bach, U. Ziese, A. M. Paulaime-van Donk, K. P. de Jong, J. a. Moulijn, and J. Pérez-Ramírez, *J. Am. Chem. Soc.*, 2005, **127**, 10792–10793.

37. F. M. Alotaibi, R. H. Abudawood, H. a. Al-Megren, M. C. Al-Kinany, E. H. Jamea, and A. a. Garforth, *Appl. Petrochemical Res.*, 2014, **4**, 95–136.

38. A. V. Neimark, K. S. W. Sing, and M. Thommes, in *Handbook of Heterogeneous Catalysis*, Wiley-VCH Verlag GmbH & Co. KGaA, Weinheim, Germany, 2008, pp. 721–738.

39. J. B. Higgins, R. B. LaPierre, J. L. Schlenker, A. C. Rohrman, J. D. Wood, G. T. Kerr, and W. J. Rohrbaugh, *Zeolites*, 1988, **8**, 446–452.

40. J. Groen, *Microporous Mesoporous Mater.*, 2004, **69**, 29–34.

41. E. G. Derouane, J. C. Védrine, R. R. Pinto, P. M. Borges, L. Costa, M. A. N. D. A. Lemos, F. Lemos, and F. R. Ribeiro, *Catal. Rev.*, 2013, **55**, 454–515.

42. A. N. C. van laak, L. Zhang, A. N. Parvulescu, P. C. A. Bruijnincx, B. M. Weckhuysen, K. P. de Jong, and P. E. de Jongh, *Catal. Today*, 2011, **168**, 48–56.

43. M. Niwa and N. Katada, *Catal. Surv. from Asia*, 1997, **1**, 215–226.

44. Y. Miyamoto, N. Katada, and M. Niwa, *Microporous Mesoporous Mater.*, 2000, **40**, 271–281.

45. B. Hunger, M. Heuchel, L. a. Clark, and R. Q. Snurr, *J. Phys. Chem. B*, 2002, **106**, 3882–3889.

46. A. Chica, K. G. Strohmaier, and E. Iglesia, *Appl. Catal. B Environ.*, 2005, **60**, 223–232.

47. J. M. Escola, D. P. Serrano, J. Aguado, and L. Briones, *Ind. Eng. Chem. Res.*, 2015, **54**, 6660–6668.

48. B. Mile, D. Stirling, M. A. Zammitt, A. Lovell, and M. Webb, *J. Catal.*, 1988, **114**, 217–229.

49. R. Gómez-Reynoso, J. Ramírez, R. Nares, R. Luna, and F. Murrieta, *Catal. Today*, 2005, **107–108**, 926–932.

50. J. A. Martens, W. Souverijns, W. Verrelst, R. Parton, G. F. Froment, and P. a Jacobs, *Angew. Chemie Int. Ed. English*, 1995, **34**, 2528–2530.

51. W. Souverijns, J. A. Martens, G. F. Froment, and P. A. Jacobs, *J. Catal.*, 1998, **174**, 177–184.

52. Anderson JR, Pratt KC (1985) *Introduction to characterization and testing of catalysts*. Academic Press

Chapter 4
Effect of the solvent and temperature for the Hydrodeoxygenation of Furfural to 2-methyl-furan: a High-Throughput Approach

Abstract

The hydrogenation of furfural is a very versatile reaction which can be used for obtaining a variety of high-value chemicals and potential biofuels. Between these potential biofuels, 2-methylfuran has been recently identified as high-value fuel/octane booster and has triggered an increasing the interest by the scientific community toward this reaction. The hydrogenation of furfural has been studied by many research groups, producing a large number of publications. However, the variation in the conditions used for this synthesis is huge, and a comparison with commercial catalysts is missing. Furthermore, the effect of the solvent has been only scarcely analysed. In this study, a large number of commercially available catalysts, comprising Cu, Ni, Pd, Pt, Ru, Rh dispersed on common supports or used as Raney catalysts were analysed using a high-throughput approach. The effect of the solvent and temperature was further analysed and discussed.

This research was conducted for Avantium Chemicals, a spin-off from Shell, in Amsterdam, The Netherlands. A potentially patentable catalyst has been found. Further, the effect of various promoters has been studied. However, for avoiding patenting issues, these results will not be presented.

1. Introduction

The growing energy demand, connected with the use of fossil resources, and the consequent production of greenhouse gases (GHG) and depletion of fossil reserves has led to an increased interest in biomass for the production of biofuels. In this framework, the use of lignocellulose derived chemicals, like furfural and hydroxymethylfurfural obtained by hydrolysis and dehydration of sugars, represents two high potential chemical platforms for making high-quality biofuels by Hydrogenation and hydrodeoxygenation (HDO) reactions [1–3]. In particular, the main products from HDO of furfural and hydroxymethylfurfural, 2-methylfuran and 2,5-dimethylfuran, show very promising properties. More specifically, they have a vapour pressure similar to gasoline as well as a very high research octane number of, respectively, 131 and 119, low solubility in water and energy densities (30 kJ/cm^3), about 40% higher than ethanol [3,4]. Furthermore, several tests on internal combustion engines confirm an increase of 18% increase in efficiency full load by using 2-MF [5]. Thus, 2-MF and DMF represent an alternative way of producing new renewable surrogated gasolines or in mixture as octane booster [2]. Further, these compounds are considered as the compounds which will substitute 2nd generation bioethanol from lignocellulose [6].

The hydrogenation/hydrodeoxygenation (HDO) of furfural has been the object of a number of reviews and specialised articles [2,7–13]. Generally speaking, hydrogenation of furfural is a very flexible reaction, which depending on the catalyst and reaction conditions, can lead to several high value products [11], e.g.: furfuryl alcohol (2-FM), 2-methylfuran (2-MF), furan, tetrahydrofurfuryl alcohol (THFA), 2-methyltetrahydrofuran (2-MTHF), tetrahydrofuran (THF), 1,2- and 1,5-pentanediol and butanol. The potential uses of these products span from the production of solvents, resins, fuels, speciality chemicals and perfume intermediates.

Currently, 2-methylfuran (2-MF) is produced by HDO of furfural by a multistep reaction with a complex kinetics, even though a direct route has been proposed [12]. A key intermediate in this reaction is furfuryl alcohol (2-FM) [11], which, depending on the reaction conditions, catalysts, solvents and presence of promoters can also be prone to unwanted side-reactions, like ring opening reactions by hydrolytic cleavage, resinification, etc. [2,14]. For a schematic network of the hydrogenation of furfural see Scheme 4. A simplified network is reported in Scheme 5. Furfural, conversely, because of the withdrawing and steric effect of the aldehyde group, is less affected by ring opening reactions [11]. Other important parasitic reactions are decarbonylation to produce furan and ring hydrogenations [2,14]. From the thermodynamic point of view, all the reported reactions can be considered irreversible, except furfural hydrogenation to 2-FM [15].

For this reaction, several catalysts have been reported [11]: Cu [16–19], Ni [11,18], Pt [20,21], Pd [11,15,18,20,22], Ru [11,20], Rh [23], Re [20]. Also bimetallics have been used: Mo-Co-B[24]. Ni-P, Ni-B, Ni-P-B [25], Ni-B-Fe [26], Ni/Fe[19], Cu/Fe [27], Pd/Ru [22]. Copper catalysts are very selective to 2-FM and to 2-MF while the kinetics of decarbonylation reactions and ring hydrogenation is negligible, and up to now represent the best reported catalysts for the production of 2-MF [16,17,28].

Currently, 2-methylfuran is produced industrially as a by-product of furfuryl alcohol production by using a gas phase process, operating at 130-160°C with Cu/chromite catalyst [10]. The best reported system for 2-MF is manganese promoted copper chromite, operating in gas phase between 200-240°C, with selectivity up to 96% to 2-MF and the possibility of switching the production to furfuryl alcohol by changing only on the temperature [29]. However, because of the toxicity of the support and deactivation issues [11,12,30], research has been recently focused on other support and catalytic systems [17,31]. Conversely, Ni catalysts are mildly active for ring hydrogenation reactions and present potential applications in the synthesis of THF [11,30], but this reaction leads to coke, which deactivates the catalyst [11]. Pd catalysts are very active for decarbonylation reactions. Furan is produced commercially by decarbonylation using Pd/C catalysts promoted with K_2CO_3 as a cocatalyst with yields around 98%, the same catalyst can also be used to make THF, but this reaction leads to coke[11]. Pt was more selective to carbonyl hydrogenation than Pd which showed preferred ring hydrogenation activity [21], the difference in selectivity was explained by the d- band width between Pd (shorted d band width) and Pt (larger d band width)[21]. Furthermore, Pt was found to activate also ring opening reactions [14]. Ir has shown very good selectivity to 2-FM [32,33]. Ru, together with Rh and Re has shown a high ring hydrogenation activity [11,20,30 13]. Mo-Co-B[24], Ni-P, Ni-B, Ni-P-B [25], Ni-B-Fe [26] have shown good selectivity to 2-FM while good selectivity to 2-MF was reported for Ni/Fe[19], Cu/Fe [27] and Pd/Ru [22]. Besides, several promoters have been proposed, like self-assembled monolayers of organic thiolates [15,34] and acids [35]. Unfortunately, because of the variety of experimental conditions reported in the literature, it is difficult to make a comparison between the different reported systems. Furthermore, most of the papers reported homemade catalysts, while a systematic comparison with industrial catalysts already on the market is completely missing, except the paper reported by Garcia-Olmo et. al. [36], which, however, limited the study to only one temperature and one solvent. In addition, most of the studies reported in the literature for the synthesis of 2-MF are conducted in the vapour phase, in excess of

hydrogen. Good results were obtained also using methanol as a hydrogen donor in the vapour phase, with yields up to 83% [37].

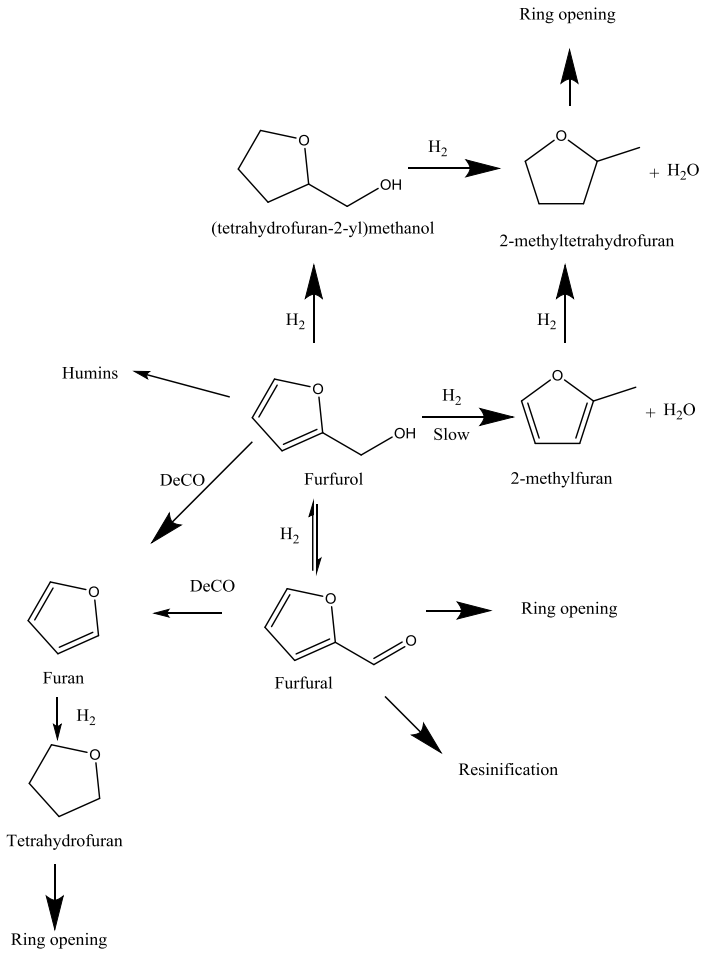

Scheme 4 – Furfural hydrogenation network

Nonetheless, one of the most important problems for processes operating in the vapour phase, at high temperature, is the rapid deactivation of catalysts. This has triggered the question about the feasibility of the reaction at lower temperature [13]. The hydrogenation of furfural in liquid phase could be a reasonable alternative. Indeed, using a solvent could potentially: 1) increase the selectivity; 2) improve the rate of the reaction e.g. by the stabilisation of the key transition states or products; 3) reduce the effect of hot spots; 4) minimise deactivation rates. Of course, to exploit the possible beneficial effect of a solvent, it is necessary to develop and/or find a catalyst that is selective and productive at a lower temperature with respect to the actual catalysts used for the gas phase reaction. This, of course, could also improve the economics of the process and reduce its environmental impact. Nonetheless, choosing the optimal solvent for hydrogenation reaction is not an easy task. The most important solvent parameters for hydrogenation reactions are: 1) hydrogen solubility and its respective activity; 2) stability and activity of reactants and transition states; 3) transport properties; 4) catalyst stability; 5) solvent polarity, availability of active hydrogen, basicity [38]. Solvent polarity, specifically, together with basicity/acidity of the solvent, have often been reported to influence the kinetics of many reactions and also in the case of hydrogenation reactions play a determining role [38–40], and also for the hydrogenation of furfural have been reported to have a

significant influence [3,18,21,22,32,33,41–45]. Till now the hydrogenation of furfural in liquid phase has been investigated by using H_2 and other hydrogen active molecules as hydrogen donors [12] or both at the same time. The last approach is useful for achieving at the same time the production of additional high-value chemicals and avoiding the use of pure hydrogen. Using alcohols as hydrogen donor, the selectivity to 2-MF increases with decreasing solvent polarity and increasing alcohol-dehydrogenation activity [42,44,45], while the selectivity to 2-FM and THFA was higher in methanol. Nonetheless, using alcoholic solvents and, in particular, methanol, a larger amount of side products were detected [22], as a consequence of the formation of acetals [22,31] and reductive etherification [31]. Using water as a solvent could be the best option from the environmental point of view, but in this case ring opening reactions are a big issue, as observed for HMF. Even using a biphasic mixture did not solve this problem [46]. Conversely, using non-reactive solvents minimised the presence of by-products [22].

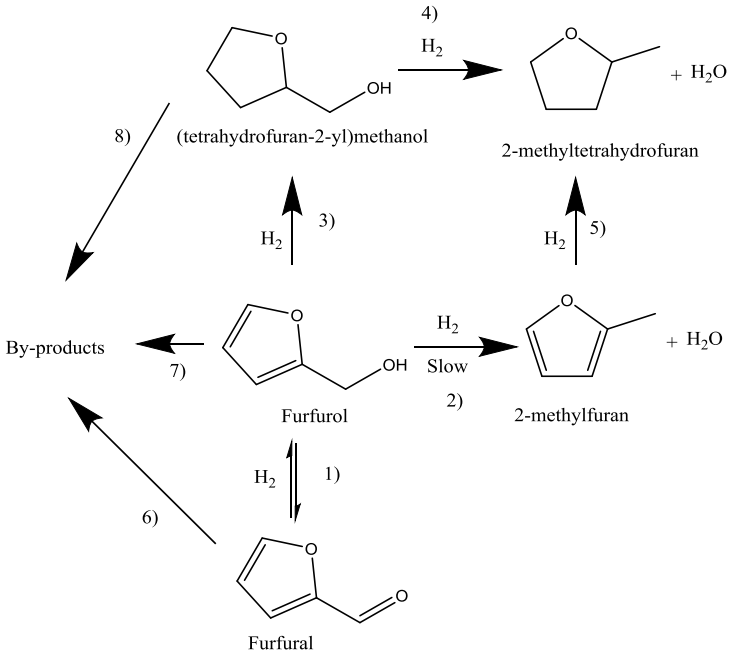

Scheme 5 - Furfural hydrogenation simplified network

In this framework, understanding the features of the solvent and having catalytic data reported in the same conditions is of paramount importance. Furthermore, for reducing the time to market of this new route to 2-MF, using reliable and tested catalysts is almost imperative. A solution is given by high-throughput catalysis, which, combined with data mining techniques, could improve the knowledge of this reaction in relation to different catalytic systems and solvents [47]. For achieving these objectives, the results of a high-throughput screening of 35 commercial catalysts tested at three temperature and three different solvents will be presented. Specifically, the hydrogenation of furfural was conducted at 60, 120 and 180 °C. All the tests were run for 1h in batch mode (experimental conditions summarised in Table 17). In order to access the influence of the metal and supports in the screening campaign, the commercial catalysts were chosen in order to span across several supports, active metal and loadings, all active for hydrogenation/hydrodeoxygenation reactions. A summary for all the used catalysts is reported in Table 15, while the experimental composition matrix for all the used catalysts, reporting active phases and supports is reported in Table 16. Furthermore, in order to simplify the study, only solvents not containing

active hydrogen were used. For comparison, the results obtained in methanol from a previous paper will also be included [31].

Table 15 - Commercial Catalysts used in this work and related applications and specifications issued by the supplier (*Patent pending)

Catalyst Id #	Catalyst Name	Application	M1	M1 loading wt%	M2	M2 loading Wt%
1	Cu / Cr / Ba catalyst	Hydrogenolysis	Cu	35	Cr, Ba	29% Cr 5% Ba
2	Ni (65%) on silica	Hydrogenation	Ni	65		
3	Ni (69%) on alumina	Hydrogenation	Ni	69		
4	Ni (24%) on alumina	Hydrogenation	Ni	24		
5	Ni (66%) on silica	Hydrogenation	Ni	66		
6	5% Pd / Al2O3		Pd	5		
7	Pd (0.03%) + Cu (0.02%) on alumina	Hydrogenation	Pd	0.03	Cu	0.02
8	Pd (5%) on activated carbon	Hydrogenation	Pd	5		
10	Pd (10%) on BaSO4		Pd	10		
11	Platinum on activated carbon	Hydrogenation	Pt	5		
12	Pt (4%) on titania		Pt	4.2		
13	Nysofact 120 catalyst	Hydrogenation	Ni			
14	Cu-Zn catalyst	Hydrogenolysis	Cu		Zn	
15	Cu chromite catalyst	Hydrogenolysis	Cu		Cr	
16	Nickel catalyst	Hydrogenation	Ni			
17	Pd (5%) on alumina	Hydrogenation	Pd	5.07		
18	Pd (5%) on graphite	Hydrogenation	Pd	4.63		
20	Pd (5%) on carbon		Pd	4.95		
21	Cu-Zn-alumina	MeOH synthesis	Cu	>65 (CuO)	ZnO	>25
22	Ni catalyst		Ni	55		
23	Cu catalyst		Cu	41	Zn	26
24	Ni catalyst	Hydrogenation catalyst	Ni	55		
25	Cu catalyst	Hydrogenation catalyst	Cu	62		
26	Pt on alumina	Hydrogenation	Pt	5		
27	Pt on activated carbon	Hydrogenation	Pt	5		
28	Pt (1%) on graphite		Pt	1.01		

Table 16 – Experimental Composition Matrix (modifiers, promoters, and other metals as promoters were reported under brackets)

Supports	None	C	silica	alumina	titania	chromite	$BaSO_4$	?	Sum
Cu	1 (Zn)		1; 1 (Cr Ba)	1 (Zn)		1		1	6
Ni			3; 2 (Mg)	3				1	9
Pd	1	4		2; 1 (Cu)			1		9
Pt	1	3; 1 (S)		1	1				7
Ru		1							1
Rh		1							1
Sum	3	10	7	8	1	1	1	2	33

3. Experimental section

2.1. Chemicals

Furfural (99%) and 1,4-Dioxane and all the used solvents were purchased from Sigma-Aldrich Chemie BV (Zwijndrecht, The Netherlands). All the chemicals were used as received without further purification.

2.2. Catalysts

In this study, a selection of 35 commercially available industrial catalysts currently used for hydrogenation reactions was used (see Table 15). The choice of industrial catalysts was dictated by the availability of a large amount of catalysts ready for commercialization or already commercialised to speed up the industrial development of the process and make it economically appealing. All the catalysts were also chosen as a function of the composition in order to maximise its span, within the available library of catalysts (see experimental composition matrix Table 16).

2.2.1 Catalyst reduction

Some of the catalysts were already reduced by the supplier and tested without further treatment.

Before the experimental campaign, all the non-reduced catalysts were divided into two subgroups and reduced in a tubular oven with a 7%H_2/N_2 mixture with a flux of 100ml/min after purging with N_2. The first subgroup, comprising Pt, Pd and Cu was reduced at 200°C, with a heating rate of 2°C/min and a holding time of 4h. The second subgroup, comprising Ni and Co catalysts was reduced using a two segment heating program; the oven was heated to 350°C with a heating rate of 2°C/min and then at 450°C with a heating rate of 5°C/min, with a holding time of 4h. After the reduction procedure, the tubular oven was purged with nitrogen at room temperature and opened. All the catalysts were quickly stored under a N_2 atmosphere in a glove box.

Especially for the non-noble metal catalysts, this procedure could lead to a slight oxidation of the catalysts on the surface. To minimise this effect on the bulk, the catalysts were stored in a N_2 atmosphere and exposed to air only for short periods. The effect of oxidation on the performance of the catalysts was investigated by repeating some tests in random order without observing any difference in activity and/or selectivity, so we concluded that this phenomenon was not significant for this study. Furthermore, a slight oxidation is even desirable in this context, in order to passivate base metal, like nickel, for safety reason.

Because of non-analysis agreement, the catalysts were not further characterised, and all the data supplied by the suppliers is provided in Table 15.

2.3. Testing

The activity of the catalysts with respect to the hydrogenation of furfural was tested by using the *Avantium Quick Catalyst Screening (QCS) apparatus* (Avantium, Amsterdam, The Netherlands). The QCS is a high-throughput system equipped with a heating mantle capable of running 72 independent stainless steel batch reactors simultaneously. All the reactors are subdivided into blocks of twelve reactors with a volume of around 7.5 mL each, with an effective reaction volume of 1 mL. Each reactor is equipped with a PTFE internal liner and septa to avoid the contact of the internal solutions with the walls of the reactors. Each reactor is sequentially loaded with 15±1 mg of catalysts, 1.00 mL of a stock solution containing 71.5 $g \cdot L^{-1}$ of furfural and a stirring bar. In the case of heptane, given the low solubility of furfural at room temperature, furfural and heptane were introduced separately by the same procedure and weighted after each step. The concentration of furfural was set at 0.740 $mol \cdot L^{-1}$. For this campaign of experiments the investigated solvents were: ethyl acetate, isopropyl ether and n-heptane (see Table 17 for the complete matrix of experiments). Each reactor was sequentially weighed after each step. Each block was sealed and purged with 10 barg N_2 three times and pressurised at room temperature at 50 barg with H_2 before insertion in the QCS. The high surface to volume ratio and the stirring rate of each reactor allow reaching the final temperature within 5 min, allowing to study the reaction in pseudo-isothermal conditions. The activity of each catalyst was studied at three different temperatures: 60, 120 and 180 °C (see the matrix of experiments in Table 17). The reaction time was set to 60 min. Thereafter, each block was removed from the heating mantle, quenched in an ice bath, and depressurized.

2.4 Analytical Procedures

After opening each block, the solutions contained in each reactor were diluted 5 times with a 4.00 ml solution of 1,4-dioxane (internal standard) in acetonitrile or n-heptane. The use of the two solvents is justified by the low miscibility of n-heptane in acetonitrile. The reactors were weighted after each step to increase the accuracy of the final results. Finally, each solution was filtered by using standard PTFE syringe filters (0.2 µm), collected in sample vials and analyzed by gas chromatography, by using a Trace 1310 GC-FID system equipped with a TriPlus RSH autosampler (Thermo Scientific, Bremen, Germany), and a DB-624UI column (30 m × 0.25 mm × 1.4 µm, Agilent Technologies, Palo Alto, CA, USA). The injector was set in split mode (Split ratio 1:100) at a temperature of 250 °C. He was used as carrier gas. The GC oven was held at 50 °C for 1 min, then ramped to 250 °C at 40 °C/min and finally at 250 °C for 1 min.

Table 17 - Matrix of Experiments

Temperatures		60°C	120 °C	180 °C	Number of experiments for each solvent
Ethyl acetate		+	+	+	99
Diisopropyl ether		+	+	+	99
n-heptane		+	+	+	99
Total Number of experiments		297 + 9 blank reactions			
Number of catalysts		33			
Number of blanks on three blocks, for each temperature		1			
Number of test for each catalysts		9			
Total number of repeated tests at a given temperature		3			
Fixed Parameters	Stirring rate	1000 rpm			
	H_2 Pressure at r.t.	50 barg			
	Reaction time	60 min			
	Furfural Initial concentration	0.740 mol/L			
	Catalyst/Solvent ratio	15 g/L			

Furfural conversion, product selectivities and selectivities to unidentified products are calculated by the following relationships:

$$Furfural\ Conversion, \qquad \varepsilon = \frac{n^0_{Furfural} - n^t_{Furfural}}{n^0_{Furfural}}$$

$$Product\ selectivity, \qquad s_{P_i} = \frac{n^t_{Product_i}}{n^0_{Furfural} - n^t_{Furfural}}$$

$$Selectivity\ to\ unidentified\ products, \qquad s_{UP} = 1 - \sum_i^n s_{P_i}$$

$$Ring\ hydrogenation\ selectivity, \qquad S_{RI} = \frac{n^t_{THFA} + n^t_{2-MTHF}}{n^0_{Furfural} - n^t_{Furfural}}$$

$$Carbonyl\ hydrogenation\ selectivity, \qquad S_{RI} = \frac{n^t_{2-FM} + n^t_{2-MF}}{n^0_{Furfural} - n^t_{Furfural}}$$

3. Results and discussion

3.1 General overview and temperature effects

Generally speaking, the temperature has a huge effect on the selectivity to 2-MF and is one of the most important parameters in this reaction. The main results are reported in Figure 67 where it is shown that increasing the temperature in the range 60-180 °C, increases not only the conversion but also the selectivity to 2-MF. This effect of the temperature was expected, as the reaction of hydrodeoxygenation of furfuryl alcohol (2-FM) has often been reported to have a higher activation barrier and the substrate presents a weak chemisorption compared to furfural [19,48,49]. In addition, when the conversion is low, also the selectivity is low, as also observed for a similar reaction network [50]. The last observation is in line with the kinetics of the reaction and was attributed to the activity of the catalysts. This is because 2-MF is produced by a consecutive reaction by 2-FM, even though a direct route from furfural was reported to be active. Therefore, in the case, the catalyst was not sufficiently active, or the metal surface area is not high enough, we observed both a decrease in the conversion and in the selectivity in the considered reaction time. Pt catalysts have shown the best selectivities, while interesting results were also shown by Rh, Ni and Cu at 180 °C. With Pd and Ni, in accordance with the literature [2,51] high selectivities to 2-MTHF and THFA and other products were observed, highlighting the remarkable activity of these metals to ring hydrogenation reactions often reported as a consequence of the adsorption with the furanic ring parallel to the surface, while this is not the case for Cu [2,18].

Activation energy reported in the literature for the reaction of furfural to 2-FM are generally higher for Cu than Pt, probably because of the different way of adsorption of furfural on the surface of these metals which also brings to a different product distribution in the second case increasing the rate of decarbonylation reaction and ring hydrogenation[2].

3.2 General trends

Data mining and visualisation techniques associated with data reduction are of paramount importance for high throughput experimentation. By using these techniques, it is possible to obtain a schematic picture of the chemistry behind a certain reaction and with a good database, highlighting general trends. Without a complete full factorial design of experiments, though, there is a limit to the conclusions that can be drawn. Here the results obtained by dividing the catalysts into classes of the main

metal and averaging all the selectivities obtained at 180 °C and conversions over 90%, the chemistry of each metal is evidenced (see Figure 67). The results show an apparent increasing selectivity to 2-MF by the following order Ru<Pd<Ni<Pt<Cu<Rh, while the selectivity to 2-FM increases in the following order Pd<Ni<Rh<Cu<Pt. Conversely the selectivity to other products increases by the following order Ni<Cu<Ru<Pd<Pt<Rh. Additionally, the high ring hydrogenation activity of Ru, Pd, and Ni is evident from the high yields of THFA and 2-MTHF when using these metals. Specifically, the selectivity to 2-MTHF decreases with the following order Ru>Pd>Ni, while the selectivity to THFA follows the opposite trend. This, of course, could be correlated to the intrinsic activity of these metals and with metal loadings. Ni indeed presents the lowest hydrogenation activity in this series even considering its loading (the highest of the series) (see Table 15), while the data for Pd, which presents the highest activity. As evidenced by the data for maxima and minima in Figure 67, the effect of loading, support and solvent are enormous. Consequently, these conclusions should be taken with care. Therefore, to better compare the results, the data in the conditions with the best selectivities to 2-MF were selected and presented in Figure 68.

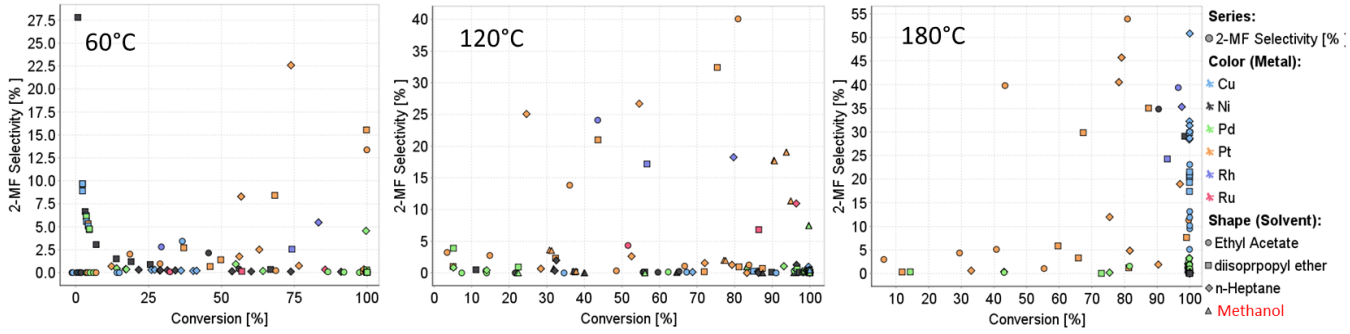

Figure 66 – Temperature effect on conversion and selectivity

The data for heptane at 180 °C were specifically kept in, and the data were grouped by active metal with a loading range between 4-6% of carbon as support (see Figure 68).

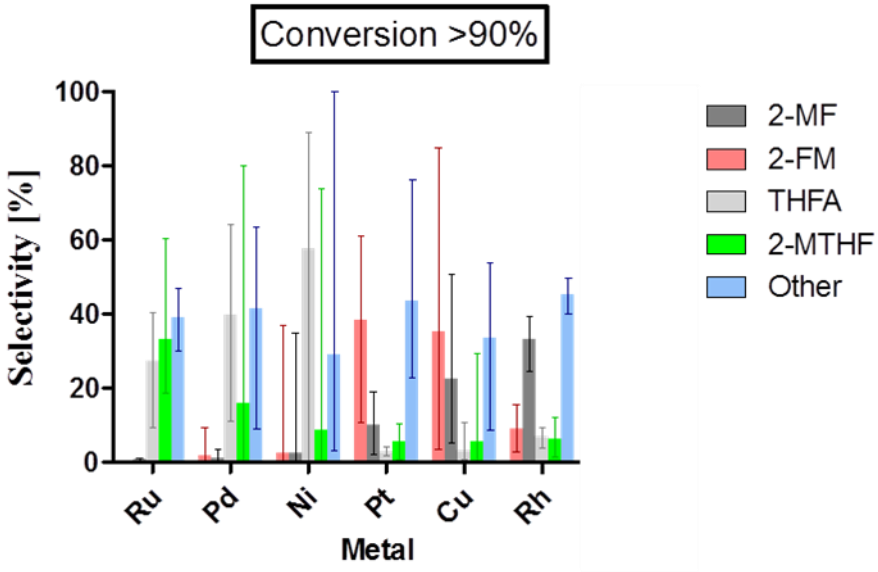

Figure 67 - Selectivity trends for each metal by averaging all the results obtained at 180 °C with all the solvents, obtained with a conversion greater than 90% and error bars displaying maximum and minimum selectivities in all the solvents analysed, ordered by 2-MF selectivity

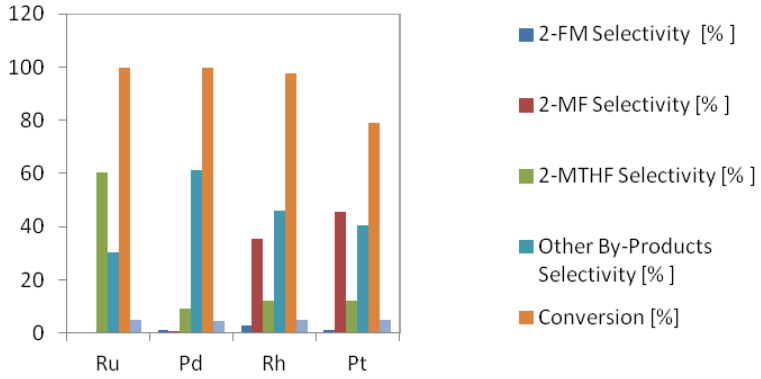

Figure 68 - Filtered data (Solvent: n-heptane, Temperature: 180 °C, Maximum selectivity to 2-MF, Loading: 4-6 %, support: carbon)

From the data in Figure 68, Pt shows the lowest conversion. This, in agreement with the data in Figure 66, indicates a lower activity for this reaction. Considering the high selectivity to other by-products, this might be related to the deactivation of the catalysts.

3.3 Support Effects

3.3.1 Pd catalysts

Five Pd catalysts with a similar loading (4.6-5.1%) were analysed in this study: three with carbon as support and two with alumina as support. In the case of Pd, a very low selectivity to 2-MF was observed, while the main products were 2-MTHF and THFA. Pd/C-8-5% has shown the highest selectivity to 2-MTHF and the lowest to THFA. This, combined with complete conversion for all the catalysts, indicates a strong hydrogenation activity, probably related to the presence of acidic sites. Conversely, by using Pd/C-18-5%, with graphite as support, the formation of only a small amount of 2-MTHF was observed combined with a large amount of THFA and the highest selectivity to other by-products. In this case, the support does not seem to have a great influence on product distribution, except for the Pd/C-8-5% and Pd/C-20-4.950% which present the highest 2-MTHF and the lowest THFA selectivity. This might be related to the presence of strong and abundant acidic sites on the surface of the support. Pd/C-8-5% shows the highest ring hydrogenation activity, which could be caused by higher metal dispersions [52].

3.3.2 Pt catalysts

With Pt catalysts, the best results were reported at 180 °C, even though the results at 60°C and 120 °C were also remarkable. Therefore a comparison between some of the Pt catalysts with similar loading at 180 °C is presented. The results with heptane as the solvent are shown, as this gave the best performance (see Figure 70). In the present study the activity of five Pt catalysts with similar loading (4.2-5%), of which one was partially sulphided (not reported in Figure 70), were tested. From the results reported in Figure 70, it is apparent that carbon supports possess better selectivity to 2-MF than metal oxide supports. Pt/titania performed slightly better compared to Pt/alumina. In literature, this has been attributed to the strong metal support interaction (SMSI) effect [53], which should not be highly pronounced in this case, because of the mild temperature used for reducing the Pt catalysts (200°C).

Considering the ring hydrogenation activity, Pt/C catalysts gave lower selectivity to THFA, while the selectivity to 2-MTHF was similar for all the reported catalysts. This together with the previous observation on Pd catalysts, suggests a role of carbon in enhancing the selectivity to 2-MTHF at the expenses of THFA, in line with the reported highest selectivity to 2-MF. Therefore, the high selectivity to 2-MF and 2-MTHF on Pd/C catalysts could be explained by the higher surface area of the supports, influencing metal

dispersion, abundance of acidic sites and interaction with the support. Acidic sites, specifically, are reported to increase the rate of alcohol hydrodeoxygenation [54], increasing the rate of conversion of 2-FM to 2-MF and THFA to 2-MTHF. Furthermore, carbon supports are often reported to have an electron donating effect, which, as reported by Gallezot [55], could cause a weaker adsorption for alpha-beta unsaturated molecules, with a weak repulsion from the surface with respect to the double bond, while at the same time enhancing the back-bonding to the π*CO and therefore increasing the adsorption from the carbonyl and enhancing its hydrogenation with respect to the double bond. This is also in agreement for the case for furfural. The adsorption geometry of furfural, indeed, has often been reported as the main parameter influencing the selectivity of the reaction toward carbonyl hydrogenation and/or ring hydrogenation/decarbonylation [2]. This effect could also be present in the Pt/TiO_2 catalyst. In this case, the SMSI (strong metal support interaction) effect has been reported to increase the electron density of Pt and to create Lewis acid sites for the activation of the carbonyl group [56,57], as already demonstrated for the hydrogenation of crotonaldehyde [53]. Therefore, the lower selectivity to other products could also be the result of the electron donation by the support, which as reported for alpha-beta unsaturated aldehydes, promotes the selectivity to the unsaturated alcohol. Results for Pt/TiO_2, furthermore, confirm an increase in selectivity to 2-FM and a decrease in the selectivity to furan [52], indicating a different geometry of adsorption for furfural and 2-FM.

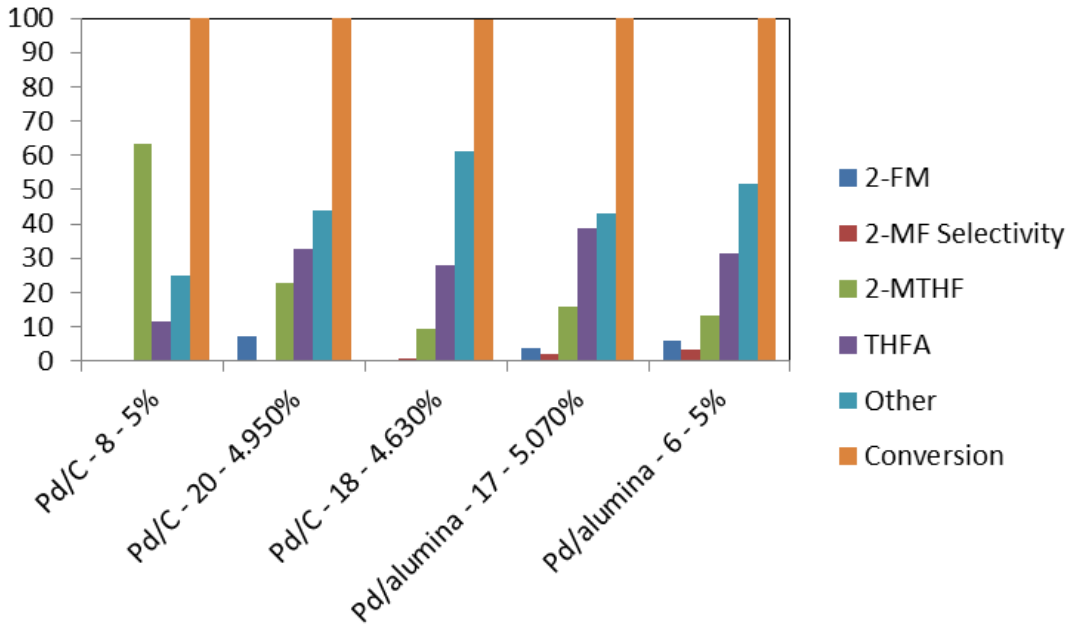

Figure 69 – Support Effects for Pd catalysts (data filtered for Solvent: n-heptane, temperature: 180 °C, loading: 4-6%)

Another factor influencing the selectivity to 2-MF is the dispersion of the catalysts. These catalysts were prepared in different ways by different producers. Because of the non-analysis agreement, it was not possible to measure the dispersion in each catalyst. In the literature, the reduction of furfural to 2-FM and 2-MF is reported to be a structure-sensitive reaction on Pt [58,59] and higher selectivities has been reported at lower dispersions. The degree of dispersion is probably the difference between Pt/C-11-5% and Pt/C-27-5-%, which were prepared by the same producer on active carbon.

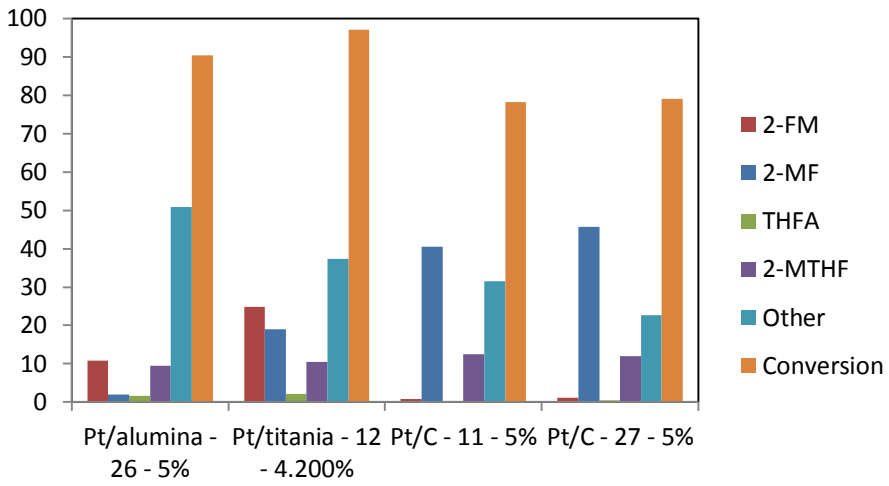

Figure 70 - Support Effects for Pt catalysts (data filtered for Solvent: n-heptane, temperature: 180 °C, loading: 4-6%)

3.4 Solvent Effects

The most interesting results for the production of 2-MF, as outlined in the previous sections, were obtained at 120 °C and 180 °C. Therefore, for conciseness, in this section, only these results will be discussed. At lower temperatures, it was observed that other effects, like the basicity of the solvent, played a major role. Especially copper catalysts at 60°C showed negligible conversions (result not shown).

The results obtained in each solvent for each catalyst at 120 °C are shown in Figure 72-Figure 77. In this case, a comparison with methanol by using the results of Pizzi et. al.[31], was reported. The results obtained at 180 °C are reported in Figure 78- Figure 85.

At 120 °C, as reported in Figure 72, the effect of the solvent on the conversion was a function of the active metal/support and solvent. This might be the effect of some deactivation phenomena, enhanced in one case or another. In the case of methanol, additionally, the higher conversion observed in some cases with respect to other solvents might be related to the presence of active hydrogen and the presence of the reductive etherification pathway. Further experiments are probably necessary to explain these trends. At 180 °C (see Figure 78), conversely, the conversion was almost always decreasing in the following order n-heptane > diisopropyl ether > ethyl acetate, which corresponds to an increasing order of polarity (see Table 20). The selectivity to 2-FM was also almost always decreasing with decreasing polarity of the solvent (see Figure 73 and Figure 79). At 120 °C some exceptions to this trend were observed by using methanol, especially in the case of Pd and Pt (see Figure 73). These catalysts correspond, in effect, to the ones which have shown the best productivity to 2-methoxytetrahydrofuran (etherification pathway, not reported in Scheme 4 and Scheme 5). Therefore, the lower selectivity might be ascribed to the faster consumption of 2-FM by the additional reductive etherification pathway active in methanol [31]. The selectivity to 2-MF at 120 °C was significant only for some Pd, Pt, Rh, and Ru catalysts and there was no apparent trend with the polarity of the solvent. However, as observed in the previous sections, Pt and Ru present significant ring hydrogenation activity. Therefore the lower selectivity observed in n-heptane with these catalysts might be ascribed to its further reduction to 2-MTHF as depicted in Scheme 5, for reaction 5. For Cu catalysts, at 180 °C, the selectivity to 2-MF was decreasing with increasing solvent polarity (n-heptane > diisopropyl ether> ethyl acetate) (see Figure 80). This was attributed to the low ring hydrogenation activity observed for these catalysts (reaction 5 and reaction 3 were much slower, see Scheme 5). This observation is further confirmed by the selectivity trends observed for these catalysts for THFA and 2-MTHF (see Figure 75, Figure 76, Figure 81 and Figure 82). At 180 °C, conversely, the selectivity to 2-MF observed with Cu catalysts was

quite significant, while a slight increase was observed for Pd, Pt, and Rh. Considering the selectivity to THFA at 120 °C (see Figure 75), this was much greater for almost all the catalysts with diisopropyl ether, n-heptane and ethyl acetate, while it was lower using methanol. Methanol, as previously reported, might react via the reductive etherification pathway. Therefore this trend was expected. Regarding the trends in the 2-MF selectivity with solvent polarity, the only exceptions were observed for some Ni, Pt and Rh (catalyst code: 31, 27, 33), probably because of the prevalence of the ring hydrogenation reactions.

Conversely, the apparent random trend in selectivity to THFA in diisopropyl ether, n-heptane and ethyl acetate observed at 120 °C might be ascribed to the different pathway which might be favoured in one case and not in the other. Conversely at 180 °C (see Figure 81), for almost all the catalysts, the selectivity to THFA decreases with the following order ethyl acetate > diisopropyl ether > n-heptane. The selectivity to 2-MTHF shows, instead, the same trend at 120 and 180 °C and increases with the opposite order of solvent polarity observed before (see Figure 76 and Figure 82). The amount of by-product formed at 120 °C and 180 °C is decreasing almost always in the following order n-heptane > diisopropyl ether > ethyl acetate, with the exception of methanol, which as previously reported might be attributed to the presence of additional pathway for the consumption of 2-FM, THFA (etherification pathway) and furfural (acetalization pathway).

Reporting the data of selectivity for each catalyst obtained at 180 °C with respect to the polarity of the solvent, expressed by the KTK parameters, plots like the one reported in Figure 71 were obtained, with the data for Cu catalysts family. This catalyst, as previously observed, present a simpler reaction network, given by the lower contribution of some of the pathways bring to a higher amount of by-products or less interesting products. From the data reported in Figure 71, the trends are evident. Similar trends were also obtained for other catalysts even though for some of the catalysts there was apparently no correlation with the polarity of the solvent because of the complex kinetics of the reaction.

The effect of the solvent, as observed, is complicated by different pathway for the consumption of reactant and intermediates. A further complication could be the presence of some hidden deactivation phenomena. A better way for comparing this trend, therefore, would be by kinetic analysis, but in this case, this is not possible, because of the low number of points for each catalyst and the unknown kinetic networks. However, simplifying the kinetics as described in Scheme 5, and therefore excluding methanol from this analysis, it might be possible to explain the observed selectivity trends.

The reported results appear to be in agreement with the outcomes reported by Aldosari et. al. [22], at r.t.. Nonetheless, the same authors [22] reported slightly lower conversion rates in non-polar solvents, although this difference could be explained by the fact that in the underlined study the operative conditions were slightly different (r.t., 3 barg H_2), and by the use of methanol as reference, which as previously reported is also active for the etherification and acetalization reactions [31]. Similar results were also obtained by Panagiotopoulou and coworkers [42] in a series of alcohols for liquid phase catalytic transfer hydrogenation of furfural.

As reported in the literature, hydrogenation reactions are affected by several parameters [38–40,60–62]. Among these, the solubility and thermodynamic activity of hydrogen, transport phenomena, catalyst agglomeration, the presence of inhibitors, competition for hydrogenation sites, and others [60]. Furthermore, the kinetics of competitive hydrogenation of substrates with different polarity are often influenced by the polarity of the solvent [62,63], and in some cases, the thermodynamic interaction between solvent and substrates has been shown to be the dominant factor [63,64]. More specifically, the kinetics of non-polar substrates is increased by polar solvent and vice-versa. This phenomenon has been correlated with the magnitude of the activity coefficient and has been reported as a good parameter for correlating kinetic measurement in different solvents [62].

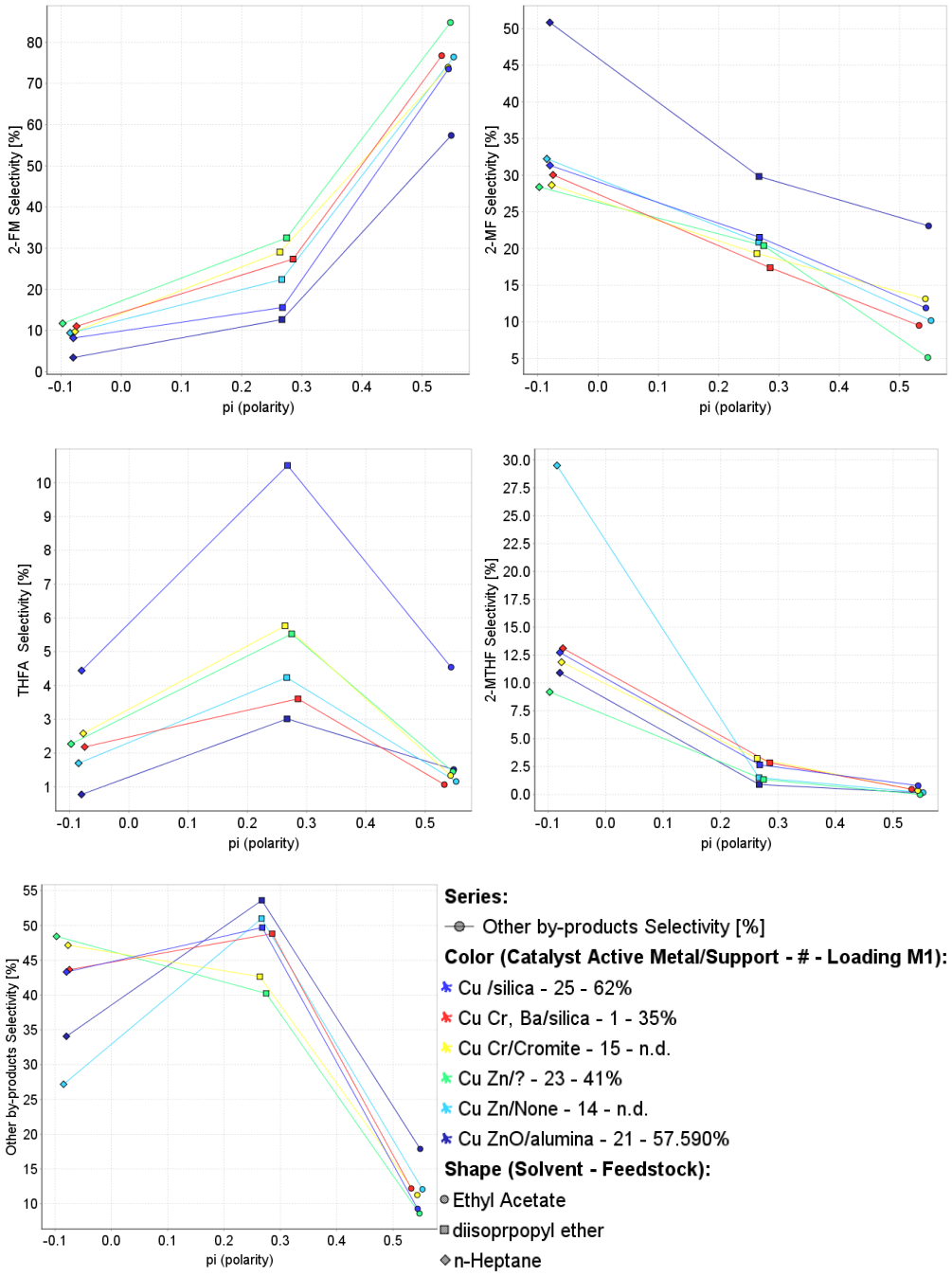

Figure 71 – Selectivity trends for the Cu catalysts with respect to the polarity of the solvent (each line represent a different catalyst)

Furthermore, the kinetics are influenced by the solubility of H_2 and its related thermodynamic activity [38–40,60–62]. Therefore, to find the reason for the reported trends in selectivity and conversion, a thermodynamic analysis was conducted (see Appendix 1 for further details). The thermodynamic activity of each species and the solubility of H_2 in each solvent were calculated. The thermodynamic study was completed by some theoretical calculations about the stabilisation effect of the solvent on each substrate.

At the end of this analysis, it was concluded that the dominant factor for explaining the observed trends in selectivity was the thermodynamic interaction between solvent and substrate, while the solubility and activity of hydrogen presented only a marginal contribution in this case. Specifically, it was observed that the thermodynamic activity of each species, in agreement with the observation of Lo et. al. [62] were higher for polar species in non-polar solvents. By computational analysis on the stabilisation effect of the solvent, instead, it was observed, in agreement with common sense that polar substrates (Furfural, 2-FM, THFA) were much more stable in polar solvents. In non-polar solvents, conversely, the effect of the stabilisation was much lower. For other less polar species like 2-MF and 2-MTHF, conversely, the effect of the stabilisation induced by the solvent was comparable in each case. Therefore, it was concluded that the most dominant factor in explaining the observed trends in selectivity is the thermodynamic interaction between each substrate and solvents. The observed increase in activity for each polar species in each solvent might be responsible for the increased kinetics of conversion of these substrates in non-polar solvents. Therefore, by decreasing the polarity of the solvent an increase in all the rate of reaction, with the exception of reaction of 5 in Scheme 5, is expected, even for the reactions leading to by-products, as confirmed by the experimental data reported in Figure 77 and Figure 83. Furthermore, for catalysts showing a considerable ring hydrogenation activity, also the kinetics of reaction 5 (see Scheme 5) can be increased, because of the increasing amount of 2-MF in the batch, explaining the trends observed by using Ni, Pd and Pt catalysts.

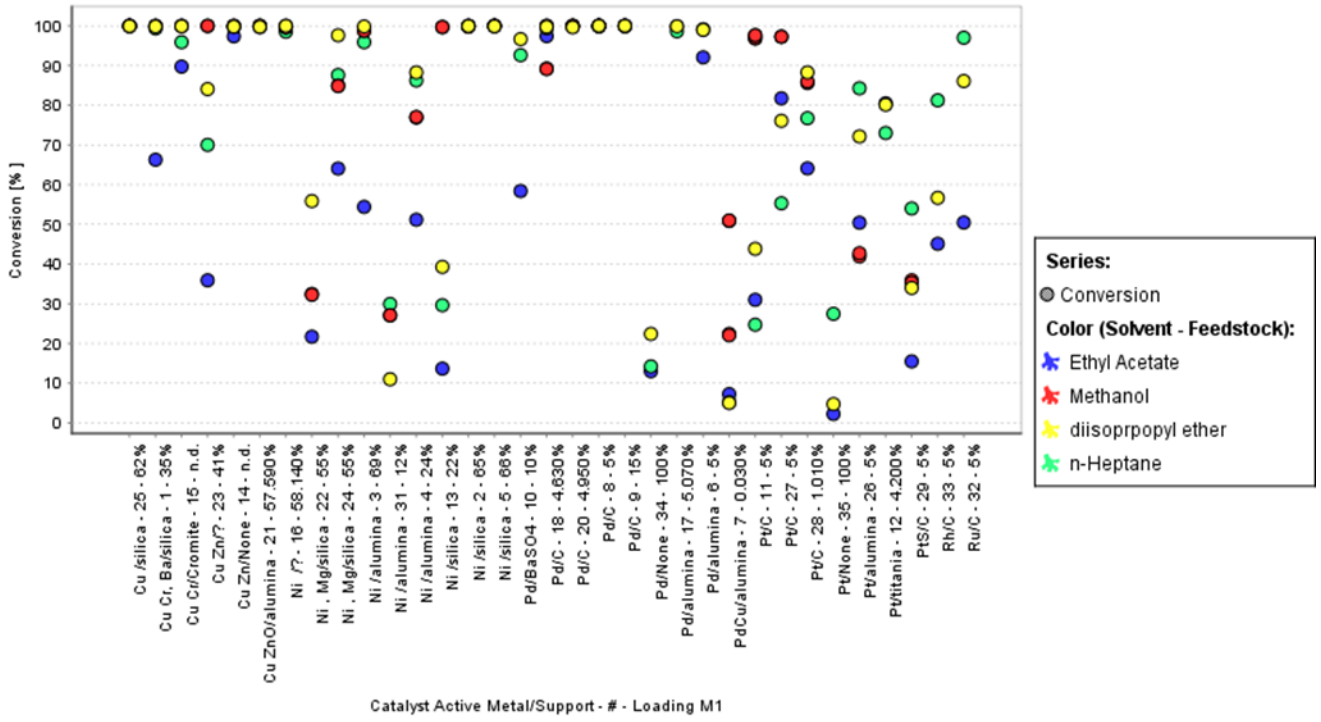

Figure 72 – Solvent effect on conversion at 120 °C in n-heptane, diisopropyl ether, ethyl acetate and methanol from [31]

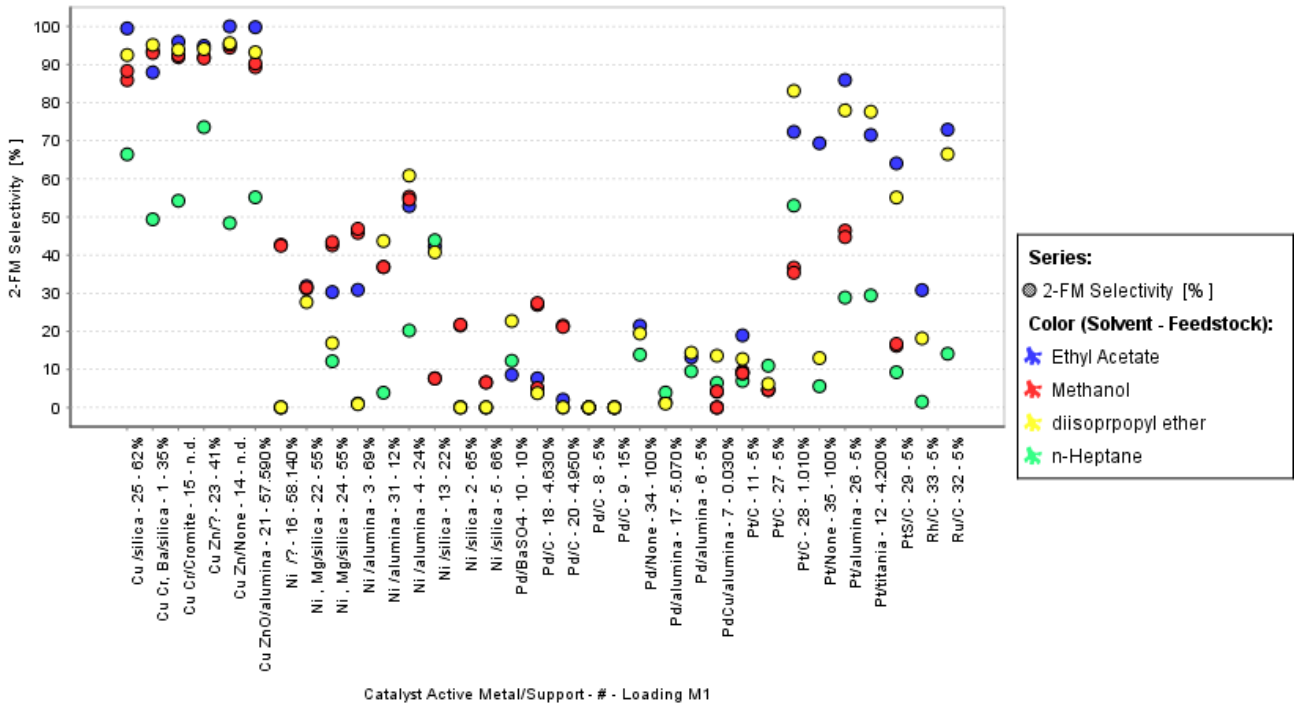

Figure 73 – Solvent effect on 2-FM selectivity at 120 °C in n-heptane, diisopropyl ether, ethyl acetate and methanol from [31]

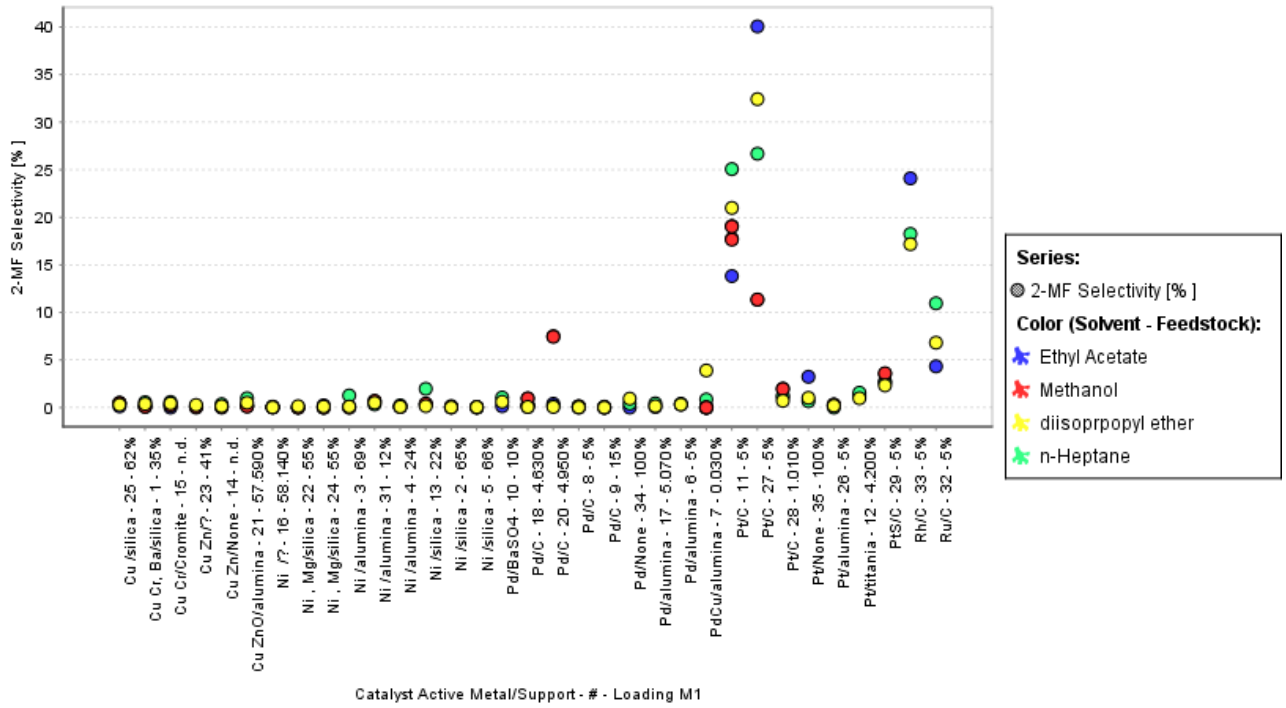

Figure 74 – Solvent effect 2-MF selectivity at 120 °C in n-heptane, diisopropyl ether, ethyl acetate and methanol from [31]

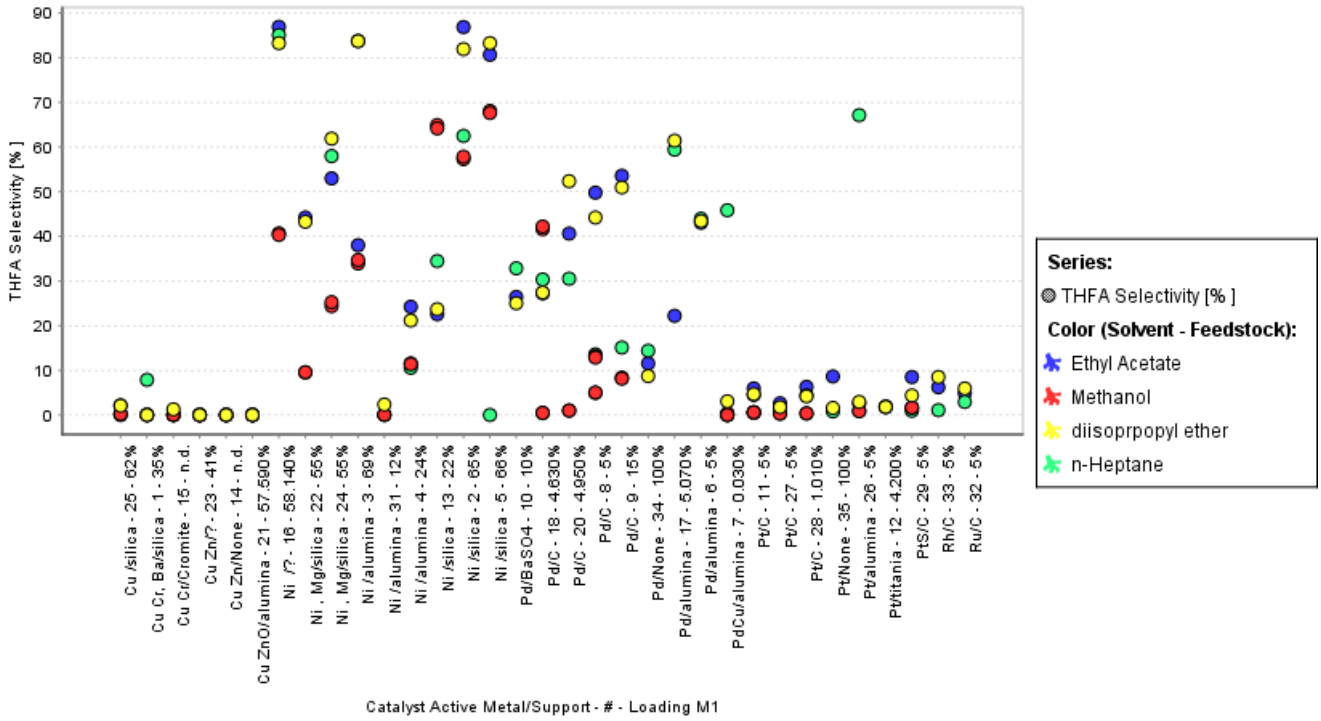

Figure 75 - Solvent effect THFA selectivity at 120 °C in n-heptane, diisopropyl ether, ethyl acetate and methanol from [31]

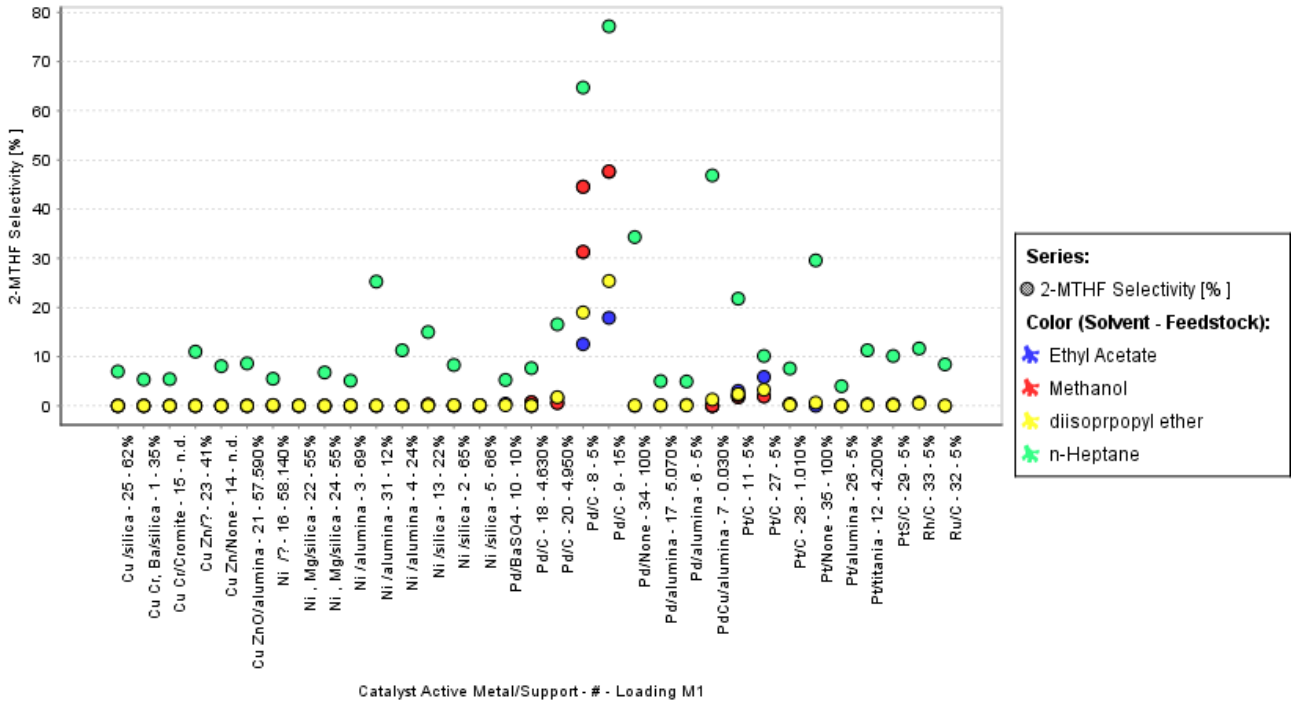

Figure 76 - Solvent effect 2-MTHF selectivity at 120 °C in n-heptane, diisopropyl ether, ethyl acetate and methanol from [31]

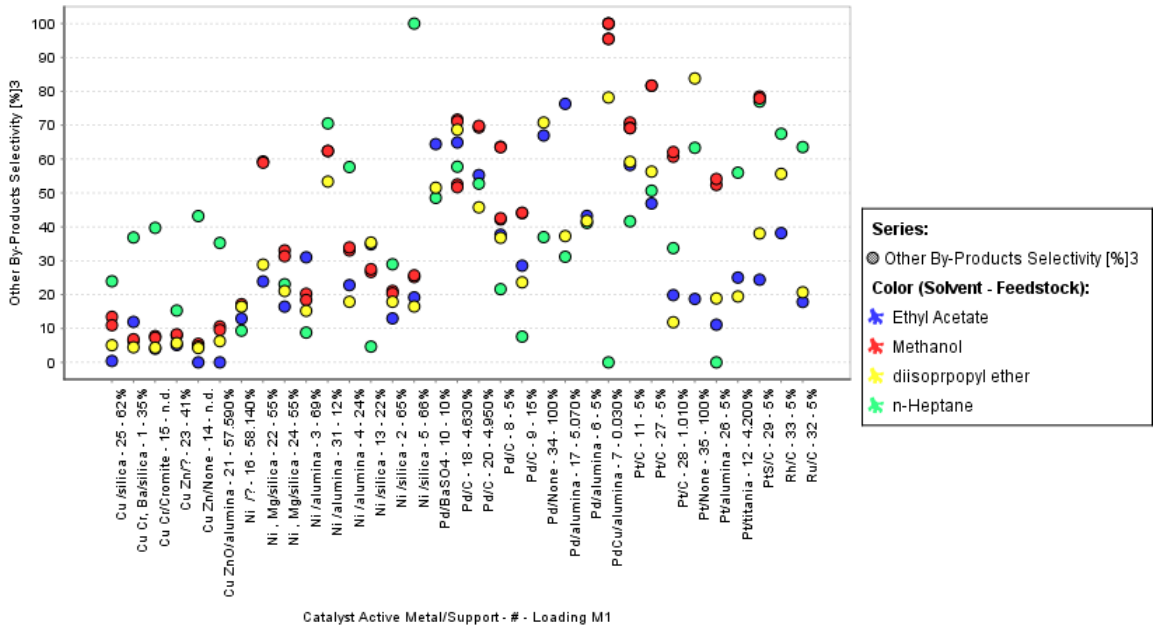

Figure 77 - Solvent effect on selectivity to by-products at 120 °C in n-heptane, diisopropyl ether, ethyl acetate and methanol from [31]

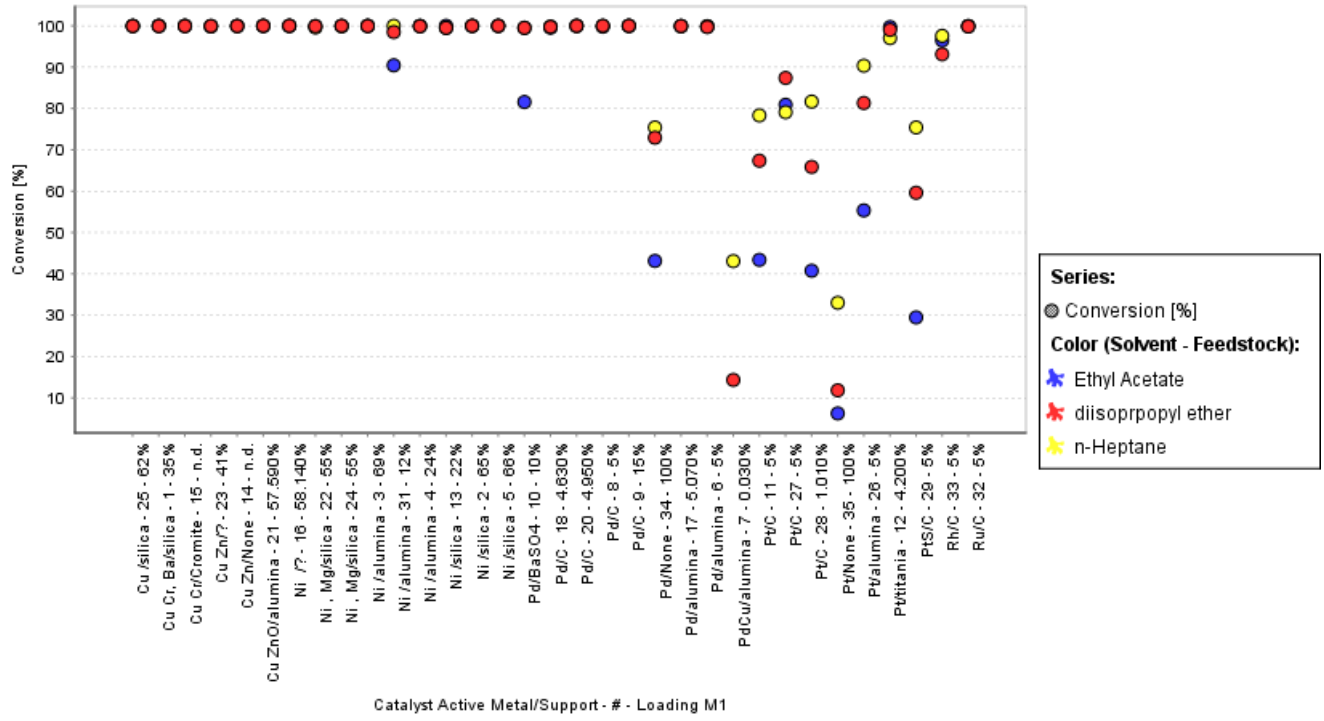

Figure 78 – Solvent effect on conversion at 180 °C in n-heptane, diisopropyl ether and ethyl acetate

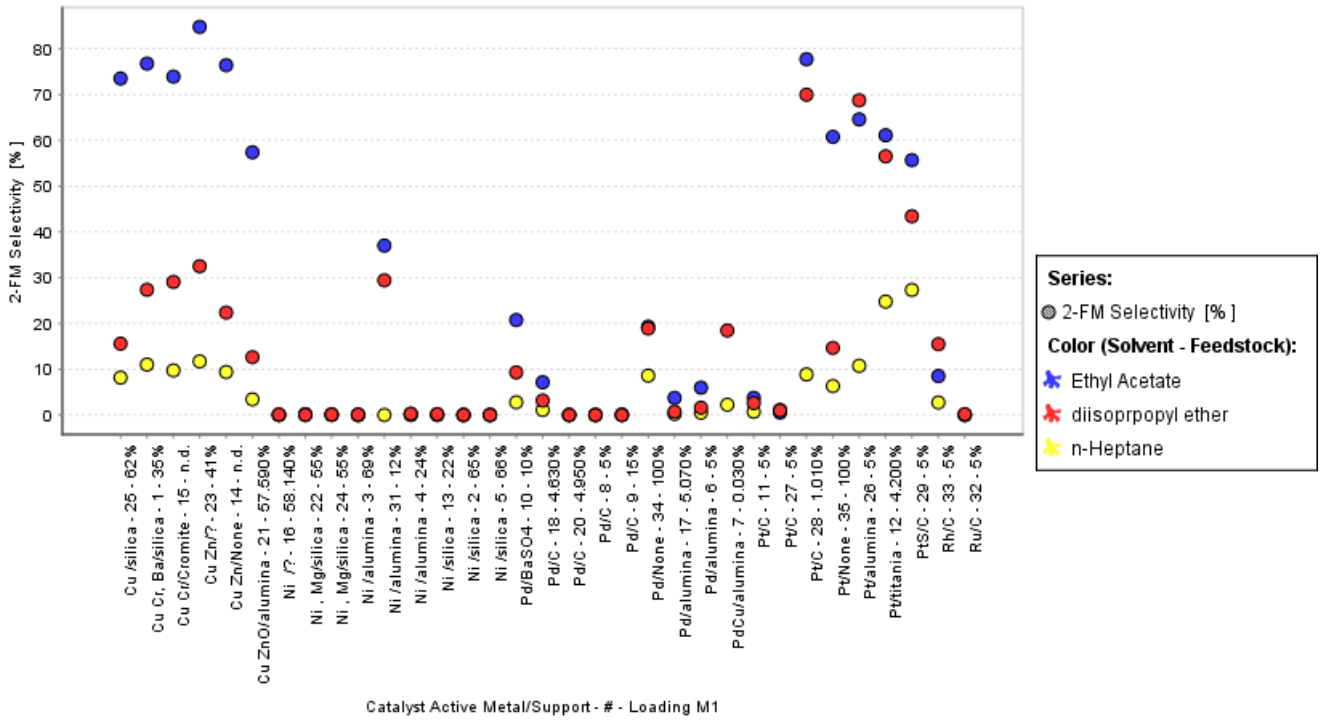

Figure 79 - Solvent effect on selectivity to 2-FM at 180 °C in n-heptane, diisopropyl ether and ethyl acetate

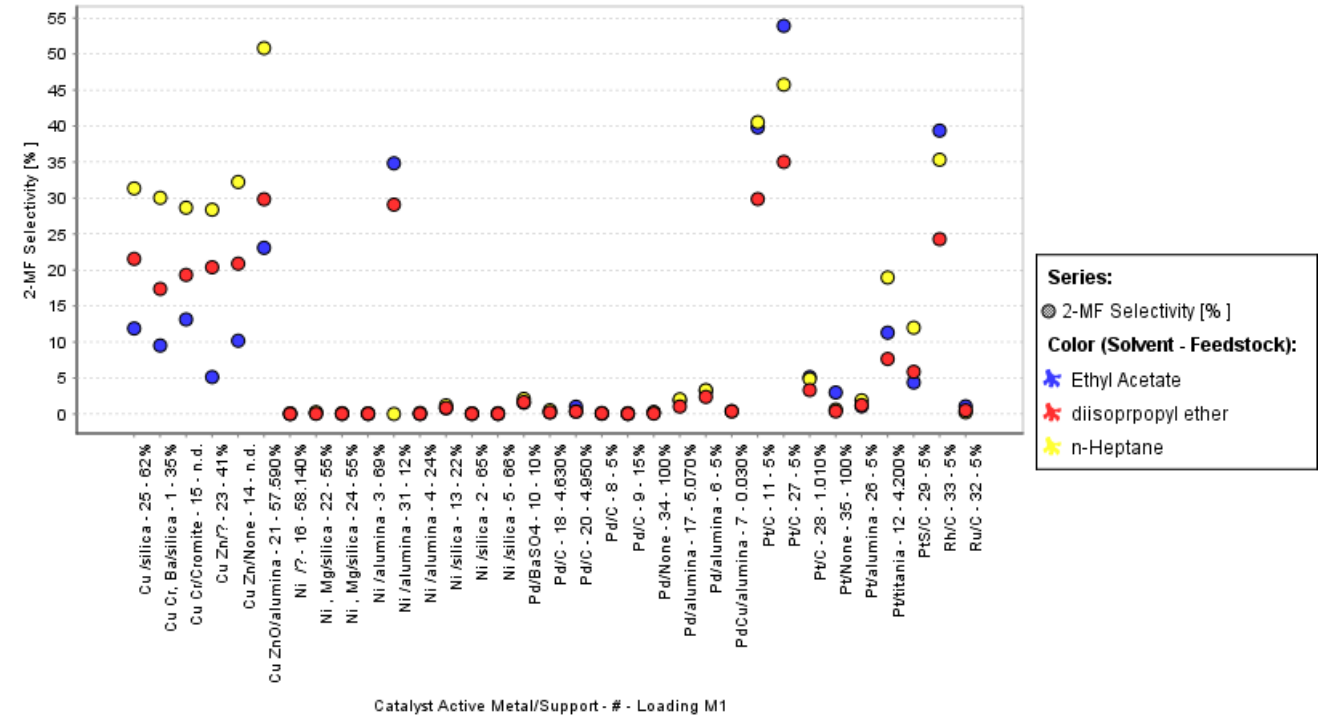

Figure 80 – Solvent effect on selectivity to 2-MF at 180 °C in n-heptane, diisopropyl ether and ethyl acetate

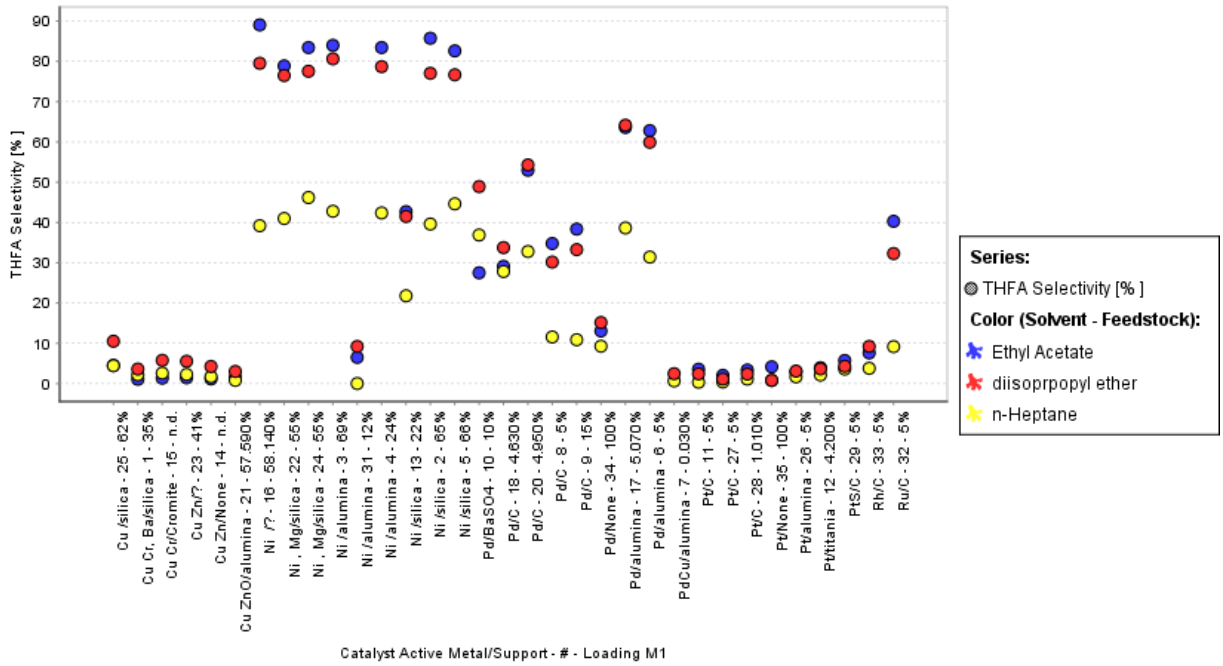

Figure 81 – Solvent effect on selectivity to THFA at 180 °C in n-heptane, diisopropyl ether and ethyl acetate

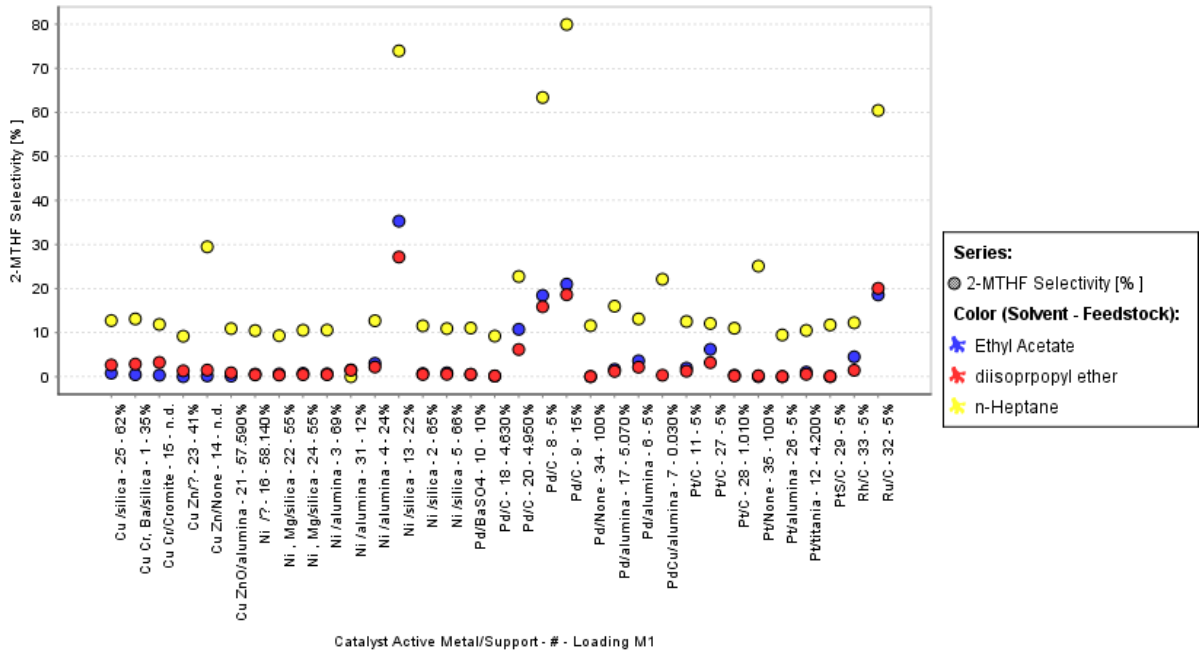

Figure 82 - Solvent effect on selectivity to 2-MTHF at 180 °C in n-heptane, diisopropyl ether and ethyl acetate

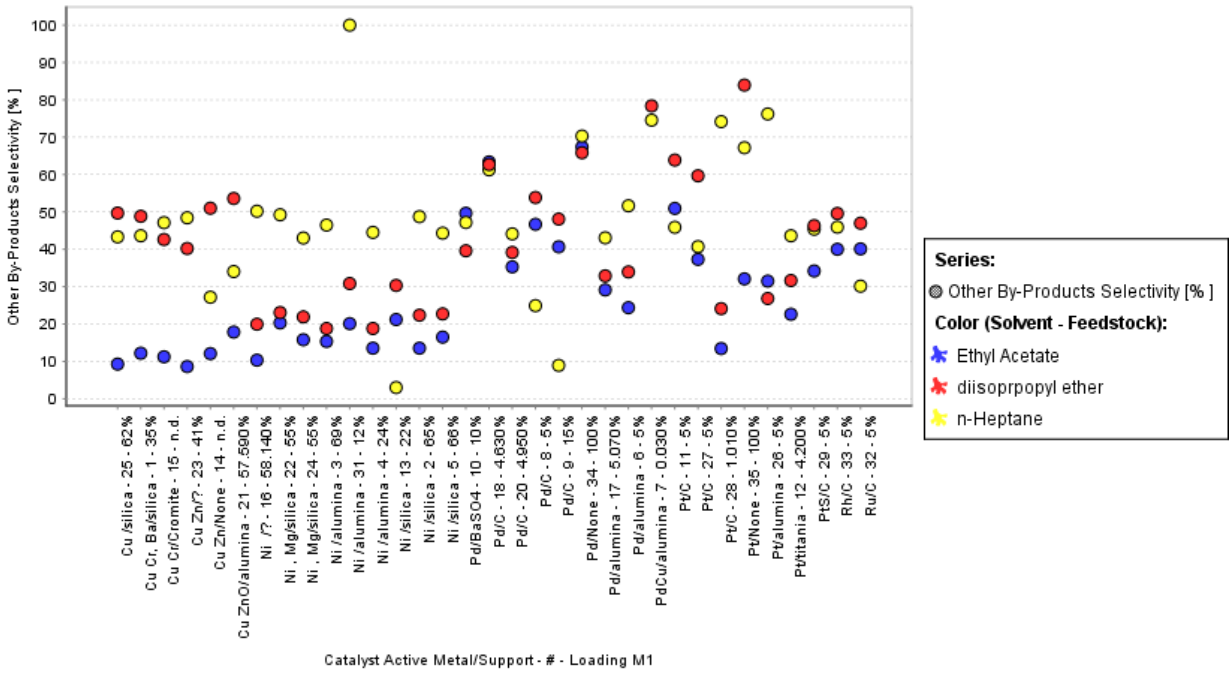

Figure 83 - Solvent effect on selectivity to other products at 180 °C in n-heptane, diisopropyl ether and ethyl acetate

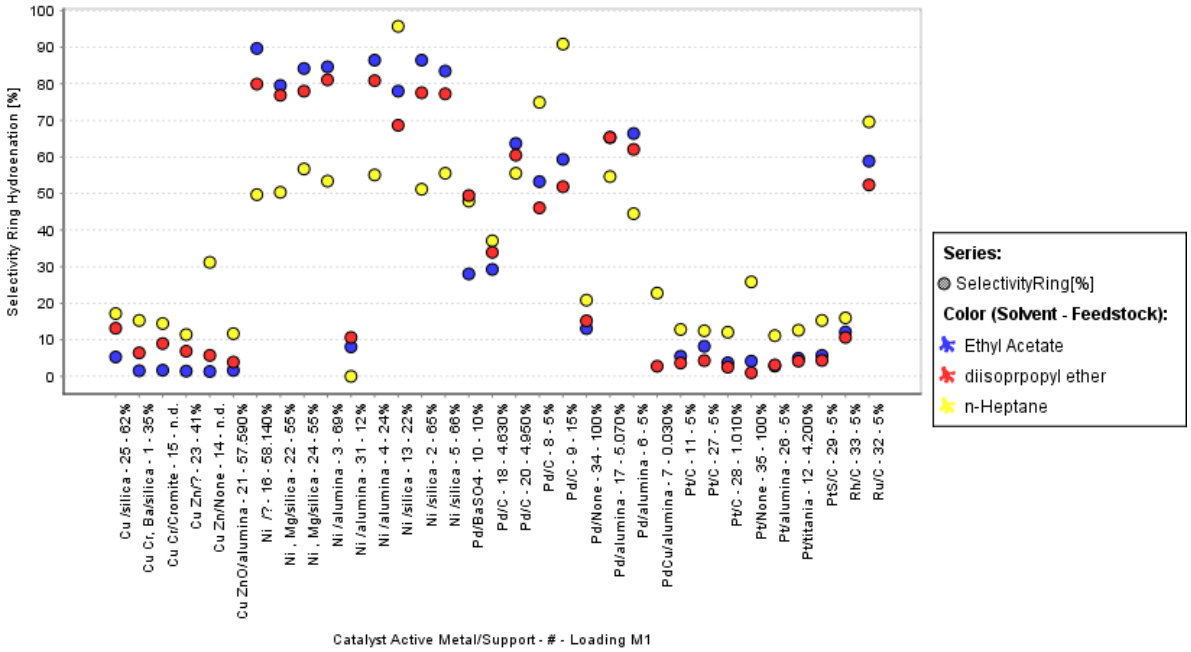

Figure 84 - Solvent effect on selectivity to ring hydrogenation (THFA + 2-MTHF selectivity) at 180 °C in n-heptane, diisopropyl ether and ethyl acetate

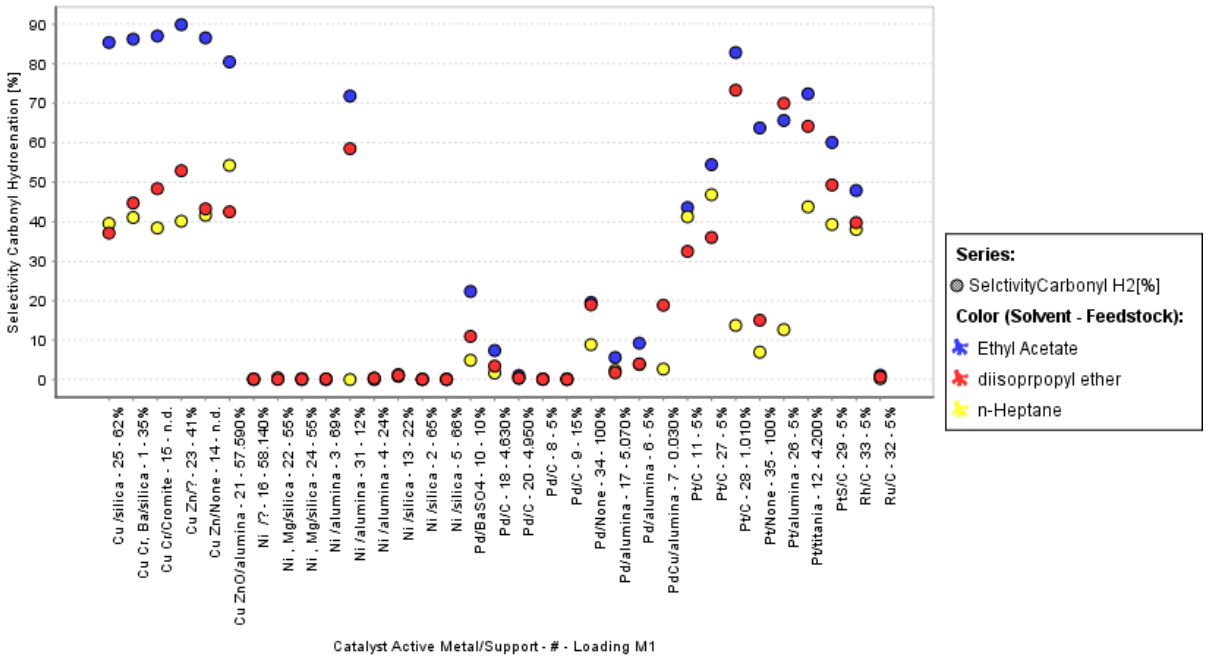

Figure 85 - Solvent effect on selectivity to carbonyl hydrogenation/hydrodeoxygenation (2-FM + 2-MF selectivity) at 180 °C in n-heptane, diisopropyl ether and ethyl acetate

4. Conclusions

The hydrogenation of furfural, as already documented in the literature, represent an interesting platform for obtaining 2-methylfuran [2,11]. In this study, several catalysts and solvents were screened. Several interesting catalysts have been found, and a base for the understanding of the effect of the solvent has been given. Furthermore, the relevance of this study is not only to be considered for the production of 2-MF but can also be extended to other high-value intermediates, giving the basis for a comparison with widely available commercial catalysts. From the analysis of the results, the temperature has been confirmed as the most critical parameter, with the best results achieved at 180 °C. Further, to optimise the selectivity to 2-MF, using non-polar solvents like n-heptane is advantageous in the presence of Cu catalysts, which are only moderately active for ring hydrogenation reactions. Conversely, in the case of Ni, Pt and Rh catalysts, the polarity of the solvent is a parameter which should be evaluated and optimised together with the residence times. In the case of metals promoting decarbonylation together with ring hydrogenation, like Pd, using non-polar solvents would also promote a higher decarbonylation rate and a higher rate to THFA, which, in non-polar solvents is further transformed in 2-MTHF. This scenario could be advantageous for the production of 2-MTHF, but the composition of the catalyst should always be optimised for minimising decarbonylation reactions. The reported results, further, confirm the role of the formulation of the catalysts, which, in this case, has shown an enormous impact on both selectivity and activity.

Appendix 1

In the literature, the solvent effect on reaction rates is classically correlated to stabilisation effects on reactants and transition states [65]. This approach can be found, practically, in most organic chemistry textbooks [39,65]. Several advanced approaches were reported for correlating solvent effect on kinetics [39,40,61,62], e.g.: 1) Červený et. al., correlated the rate of hydrogenation to specific solvent parameters [61]; 2) Murzin based on the Kirkwood and Laidler treatment for non-charged reactants, based on transition state theory, correlated the rate of reactions to solvent permittivity by using semi-empirical relationships [39]; 3) Lo et. al., based on the transition state theory and solvent-substrate interactions correlated the rate of hydrogenation for competitive substrates to the activity coefficients of the substrates and/or to activated complex in each respective solvent [40,62]. However, all these methods are based on the knowledge of reaction rates and reaction mechanisms, which in the case of screening experiments is of little value, given the little knowledge of each catalytic system. Furthermore, the effect of the solvent on specific catalytic systems might be even more subtle, as the solvent might interact directly with the active sites and, therefore, influencing the kinetics and selectivity of the reaction [40]. For instance, the interaction between solvent and catalysts have been reported to influence the relative rate of ring/carbonyl hydrogenation for 4-phenyl-2-butanone and therefore the observed selectivity [66]. However, for hydrogenation reactions, as also suggested by Lo et al. [40,62], has been demonstrated that nonpolar solvents favour the conversion of polar substrates and vice versa [40,62], a concept is further supported by thermodynamic arguments on the activity coefficient [62]. This simple approach, however, as reported by Vannice et. al. [40], present the limitation of not taking into account specific solvent-catalyst interaction and assumed identical rate expression. In this study, especially with the data at 180 °C, we observed that by using non-polar solvents increased the selectivity to non-polar species (2-MF, 2-MTHF), because of the increase conversion rate for polar species (e.g. Furfural, 2-FM, THFA). Therefore, the observed selectivity trends might be explained based on the method suggested by Lo et. al. [62]. Given the unknown kinetics, however, the reaction can only be studied qualitatively, by calculating the activity coefficient for each species, in analogy to the approach reported by Lo et. al. [62]. Other parameters reported to be of importance for hydrogenation reactions are: hydrogen solubility and related activity and transport phenomena [38,40]. Therefore, to improve our understanding, we estimated the thermodynamic activity of each species in each solvent and hydrogen solubility. Because of the lack of experimental data for several systems, and some missing groups for group contribution methods (e.g. PSRK, modified UNIFAC) for some of the key intermediates, the activity coefficient for each species were calculated by using the COSMO-SAC method. This method does not take into account the non-ideality of the vapour phase and the simple model if not specifically modified, is strictly valid at low pressure and low temperature. Therefore, the results were evaluated at 60°C and 1.013 bar at half the initial concentration of furfural. The activity coefficients for almost all the substrates were calculated by using Aspen Plus 8.4 and using the COSMO-SAC method. For 2-MF and 2-MTHF there was no data in the Aspen Plus database. Therefore, the activity coefficient for 2-MF was calculated by using COSMO-SAC-VT-2005 by calculating the sigma profile using the demo version of Turbomole ® by a standard DFT procedure [67,68]. The activity coefficient for 2-MTHF was calculated using the modified UNIFAC method. The results of these calculations were used only as a relative reference for interpreting the data. Therefore, the absolute values are not important for the final conclusions. Solubility and activity were also estimated for hydrogen in each solvent by using the equation of state (EOS) approach by regressing the binary interaction parameters to experimental data when available, and using the predictive SRK EOS when no data was available. All the results of these calculations are reported in Table 18-Table 22. Furthermore, to access also the stabilisation effect of the solvents on the reactants/products, the total energy difference between the gas phase (vacuum) and the liquid phase in each solvent was calculated by using Spartan software by using the Density functional EDF2-6-31G* method and the SM8 model for calculating solvent effects. The results of the theoretical analysis are reported in Figure 86.

From the analysis of the results, the H_2/Furfural (0.3-1) is sub-stoichiometric and with respect to the gas phase process is very low. For comparison, in the gas phase process, H_2/Furfural ratio of 2-900 were reported[12]. This, of course, could be a limit for the reaction, especially in the early stages. Furthermore, H_2 solubility at 180 °C at the final pressure (autogenous pressure at 180 °C) decreases in the following order diisopropyl ether > ethyl acetate ≥ n-Heptane, while the thermodynamic activity for H_2 decreases as ethyl acetate >diisopropyl ether > n-heptane. Both the solubility and activity do not correlate with our results. Conversely, a major effect was observed for the thermodynamic activity of the hydrogenation substrates (see Table 22). Specifically, the thermodynamic activity for polar species is higher in non-polar solvents, and therefore, in line with the observation of Lo et al. [62]. Therefore observed trends in selectivity were correlated to the increased activity of polar species in nonpolar solvents. The higher activity of polar species in non-polar solvents is expected to increase the chemisorption and hydrogenation rate of these species and vice-versa. In addition, analysing the results of the theoretical analysis (see Figure 86), we can observe as the stabilisation energy induced by the solubilization in n-heptane with respect to the gas phase is much lower for all the species. Furthermore, the stabilisation energy for the less polar species (2-methylfuran, furan) is similar in each solvent, while for the most polar species the stabilisation effect is proportional to the polarity of the solvent.

Table 18 –Activity Coefficient calculated by COSMO-SAC method at 60°C and half the initial concentration of furfural for comparison purposes calculated at 60 °C and 1.013 bar by using Aspen Plus 8.4 ® (* data not available in the Aspen Plus database, The sigma profile and activity coefficient were calculated by using, respectively Turbomole ® Demo Version and COSMO-SAC-VT-2005; ** calculation by using the modified UNIFAC method)

Solvent	**Furfural**	**2-FM**	**THFA**	**THF**	**Furan**	**2-MTHF (UNIFAC)****	**2-MF***
n-heptane	11.2	10.3	7.6	1.3	2.2	1.2	1.9
Diisopropyl ether	2.3	1.0	1.1	1.0	1.0	1.0	1.0
Ethyl acetate	1.1	0.9	1.4	1.0	0.7	1.1	0.9
methanol	1.5	0.9	1.0	1.2	2.1	5.4	2.6

The result from the thermodynamic and theoretical analysis support the observed trend in conversion and selectivity at 180 °C. Therefore, we concluded that the effect of the solvent in this reaction is mainly related to the relative stabilisation effect on each substrate. Nonetheless, the effect of specific interaction between the solvent and catalyst cannot be ruled out, and in the case of methanol, an additional pathway has been reported to influence the selectivity and conversion rates.

Table 19 – coefficient of activity of H2 calculated by EOS method in Aspen Plus 8.4 ®

H_2, Activity coefficients			
Solvent	60°C	120 °C	180 °C
Heptane	2.3	1.5	0.9
diisopropyl ether	2.6	1.5	0.8
ethyl acetate	4.9	2.7	1.4
Methanol	-	4.9	-

Table 20 – Solvent properties ranked as a function of polarity (KTK parameters retrieved from [69] and H_2 solubility data calculated with Aspen Plus at the temperature and at the autogenous pressure for the tests, using the same H_2/solvent ratio used for the testing protocol. Calculation methods validated by comparison with NIST experimental data and regression of the binary interaction parameters. *Methanol was used in a previous work [31])

KTK parameters				H_2 Solubility [mol/L] and activity coefficient			
Solvent	π (polarity)	β (basicity)	α (proticity)	60°C	120 °C	180 °C	Fluid Package
n-Heptane	-0.08	0	0	0.28	0.39	0.56	PR
diisopropyl ether	0.27	0.49	0	0.30	0.47	0.76	PSRK
ethyl Acetate	0.55	0.45	0	0.21	0.35	0.57	PSRK
methanol*	0.6	0.62	0.93	-	0.41	-	PR reg.

Table 21 – Thermodynamic activity calculated for H_2 at 60, 120 and 180 °C in all the used solvents

H_2 Activity			
Temperature	60°C	120 °C	180 °C
Heptane	0.61	0.54	0.45
diisopropyl ether	0.75	0.64	0.49
ethyl acetate	0.99	0.88	0.73
Methanol	-	1.9	-

Table 22 – Thermodynamic activity of the main species calculated by Aspen Plus and COSMO-SAC method for calculating the activity coefficients at 60°C and half the initial concentration of furfural (0.37 mol/L) for comparison purposes, ordered by dielectric constant (* activity coefficient calculated by using COSMO-SAC-VT-2005 and TmoleX [67,68], **calculated by modified UNIFAC method)

Activity, 60 °C, 1.013 bar, conc. 0.36mol/L					
Activity	n-Heptane	diisopropyl ether	Ethyl Acetate	Methanol	Dielectric constant
Furfural	**3.9**	**0.77**	0.39	0.53	38
Furfuryl Alcohol	**3.6**	0.35	0.31	0.32	18.25
Tetrahydrofurfuryl alcohol	**2.7**	0.38	0.48	0.35	13.61
Tetrahydrofuran	0.44	0.33	0.36	0.41	7.58
2-methyltetrahydrofuran**	0.43	0.35	0.41	2.00	6.97
Furan	0.74	0.33	0.25	0.74	2.90
2-methylfuran*	0.67	0.37	0.31	0.99	2.47
Solvent Dielectric constant	1.93	3.88	6.02	32.66	

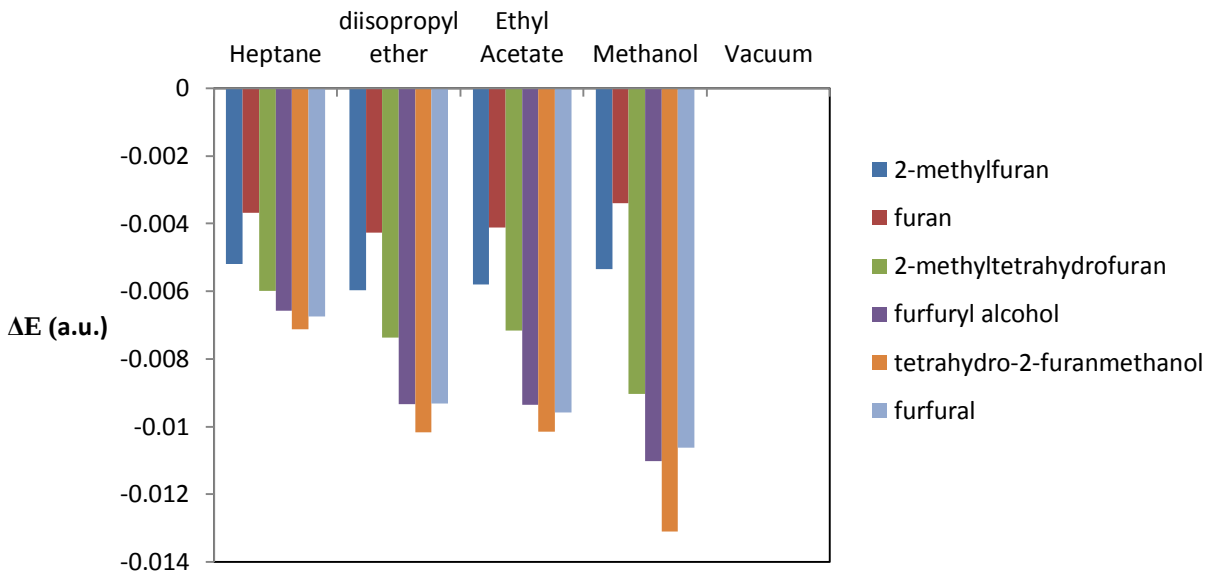

Figure 86 – Stabilisation energy by the solvent for each reactant/product/intermediate (calculation made in Spartan Wavefunction © Inc. by using the density functional EDF2-6-31G* for the gas phase and by coupling the SM8 model for the solvent calculations, $\Delta E = E^i_{solvent} - E^i_{vacuum}$)

References

1. S. De, B. Saha, and R. Luque, *Bioresour. Technol.*, 2015, **178**, 108–118.

2. D. E. Resasco, S. Sitthisa, J. Faria, T. Prasomsri, and M. P. Ruiz, in *Heterogeneous Catalysis in Biomass to Chemicals and Fuels*, 2011, vol. 661, pp. 1–33.

3. D. Scholz, C. Aellig, and I. Hermans, *ChemSusChem*, 2014, **7**, 268–275.

4. Y. Román-Leshkov, C. J. Barrett, Z. Y. Liu, and J. a Dumesic, *Nature*, 2007, **447**, 982–985.

5. F. Hoppe, U. Burke, M. Thewes, A. Heufer, F. Kremer, and S. Pischinger, *Fuel*, 2016, **167**, 106–117.

6. F. Cavani, S. Albonetti, F. Basile, and A. Gandini, Eds., *Chemicals and Fuels from Bio-Based Building Blocks - volume 1*, 2015, vol. 1542.

7. Y. Nakagawa, M. Tamura, and K. Tomishige, *ACS Catal.*, 2013, **3**, 2655–2668.

8. A. Malinowski and D. Wardzińska, *Chemik*, 2012, **66**, 987–990.

9. K. J. Zeitsch, *The Chemistry and Technology of Furfural and its many By-Products, Volume 13*, Elsevier Science, Amsterdam, 1st edn., 2000.

10. H. E. Hoydonckx, W. M. Van Rhijn, W. Van Rhijn, D. E. De Vos, and P. A. Jacobs, *Ullmann's Encycl. Ind. Chem.*, 2007, 285–313.

11. K. Yan, G. Wu, T. Lafleur, and C. Jarvis, *Renew. Sustain. Energy Rev.*, 2014, 38, 663–676.

12. R. Mariscal, P. Maireles-Torres, M. Ojeda, I. Sádaba, and M. López Granados, *Energy Environ. Sci.*, 2016, **9**, 1144–1189.

13. J. P. Lange, E. Van Der Heide, J. Van Buijtenen, and R. Price, *ChemSusChem*, 2012, **5**, 150–166.

14. A. Corma Canos, S. Iborra, and A. Velty, *Chem. Rev.*, 2007, 107, 2411–2502.

15. S. H. Pang, C. A. Schoenbaum, D. K. Schwartz, and J. W. Medlin, *ACS Catal.*, 2014, **4**, 3123–3131.

16. D. G. Manly and A. P. Dunlop, *J. Org. Chem.*, 1958, **23**, 1093–1095.

17. R. S. Rao, R. T. K. Baker, M. A. Vannice, R. Terry, K. Baker, and M. Albert Vannice, *Catal. Letters*, 1999, **60**, 51–57.

18. S. Sitthisa and D. E. Resasco, *Catal. Letters*, 2011, **141**, 784–791.

19. S. Sitthisa, T. Sooknoi, Y. Ma, P. B. Balbuena, and D. E. Resasco, *J. Catal.*, 2011, **277**, 1–13.

20. N. S. Biradar, A. A. Hengne, S. N. Birajdar, R. Swami, and C. V. Rode, *Org. Process Res. Dev.*, 2014, **18**, 1434–1442.

21. S. Bhogeswararao and D. Srinivas, *J. Catal.*, 2015, **327**, 65–77.

22. O. F. Aldosari, S. Iqbal, P. J. Miedziak, G. L. Brett, D. R. Jones, X. Liu, J. K. Edwards, D. J. Morgan, D. K. Knight, and G. J. Hutchings, *Catal. Sci. Technol.*, 2016, **6**.

23. V. Vetere, A. B. Merlo, J. F. Ruggera, and M. L. Casella, *J. Braz. Chem. Soc.*, 2010, **21**, 914–920.

24. X. Chen, H. Li, H. Luo, and M. Qiao, *Appl. Catal. A Gen.*, 2002, **233**, 13–20.

25. S. Lee and Y. Chen, *Ind. Eng. Chem. Res.*, 1999, **38**, 2548–2556.

26. H. Li, H. Luo, L. Zhuang, W. Dai, and M. Qiao, *J. Mol. Catal. A Chem.*, 2003, **203**, 267–275.

27. J. Lessard, J.-F. Morin, J.-F. Wehrung, D. Magnin, and E. Chornet, *Top. Catal.*, 2010, **53**, 1231–1234.

28. L. W. Burnett, I. B. Johns, R. F. Holdren, and R. M. Hixon, *Ind. Eng. Chem.*, 1948, **40**, 502–505.

29. M. V. Twigg, 2010, AP:GB24828.

30. M. Shimanskaya and E. Lukevits, *Chem. Heterocycl. Compd.*, 1993, **29**, 1000–1011.

31. R. Pizzi, R.-J. van Putten, H. Brust, S. Perathoner, G. Centi, and J. van der Waal, *Catalysts*, 2015, **5**, 2244–2257.

32. P. Reyes, D. Salinas, C. Campos, M. Oportus, J. Murcia, H. Rojas, G. Borda, and J. L. G. Fierro, *Quim. Nova*, 2010, **33**, 777–780.

33. H. Rojas, J. J. Martìnez, and P. Reyes, *Dyna*, 2010, **77**, 151–159.

34. S. H. Pang, N. E. Love, and J. W. Medlin, *J. Phys. Chem. Lett.*, 2014, **5**, 4110–4114.

35. M. J. Gilkey, P. Panagiotopoulou, A. V. Mironenko, G. R. Jenness, D. G. Vlachos, and B. Xu, *ACS Catal.*, 2015, **5**, 3988–3994.

36. A. J. Garcia-Olmo, A. Yepez, A. M. Balu, A. A. Romero, Y. Li, and R. Luque, *Catal. Sci. Technol.*, 2016, **6**, 4705–4711.

37. L. Grazia, A. Lolli, F. Folco, Y. Zhang, S. Albonetti, and F. Cavani, *Catal. Sci. Technol.*, 2016, **6**, 4418–4427.

38. P. J. Dyson and P. G. Jessop, *Catal. Sci. Technol.*, 2016, **6**, 3302–3316.

39. D. Y. Murzin, *Catal. Sci. Technol.*, 2016, **6**, 5700–5713.

40. U. K. Singh and M. A. Vannice, *Appl. Catal. A Gen.*, 2001, **213**, 1–24.

41. S. Xia, Y. Li, Q. Shang, C. Zhang, and P. Ma, *Trans. Tianjin Univ.*, 2016, **22**, 202–210.

42. P. Panagiotopoulou, N. Martin, and D. G. Vlachos, *J. Mol. Catal. A Chem.*, 2014, **392**, 223–228.

43. X. Chen, L. Zhang, B. Zhang, X. Guo, and X. Mu, *Sci. Rep.*, 2016, **6**, 28558.

44. Á. O'Driscoll, T. Curtin, W. Y. Hernández, P. Van Der Voort, and J. J. Leahy, *Org. Process Res. Dev.*, 2016, acs.oprd.6b00228.

45. P. Panagiotopoulou and D. G. Vlachos, *Appl. Catal. A Gen.*, 2014, **480**, 17–24.

46. G. C. A. Luijkx, N. P. M. Huck, F. Van Rantwijk, L. Maat, and H. Van Bekkum, *Heterocycles*, 2009, **77**, 1037–1044.

47. E.-J. Ras and G. Rothenberg, *RSC Adv.*, 2014, **4**, 5963.

48. S. Sitthisa, S. Crossley, and L. Lobban, *21st North Am. Catal. Soc. Meet.*, 2009, **73019**, 73019.

49. Y.-T. Tseng, W.-J. Wang, J. D. Ward, and H.-Y. Lee, *J. Taiwan Inst. Chem. Eng.*, 2015, **0**, 1–9.

50. E.-J. Ras, M. J. Louwerse, and G. Rothenberg, *Catal. Sci. Technol.*, 2012, **2**, 2456–2464.

51. N. S. Biradar, A. M. Hengne, S. N. Birajdar, P. S. Niphadkar, P. N. Joshi, and C. V Rode, *ACS Sustain. Chem. Eng.*, 2014, **2**, 272–281.

52. K. An, N. Musselwhite, G. Kennedy, V. V. Pushkarev, L. Robert Baker, and G. A. Somorjai, *J. Colloid Interface Sci.*, 2013, **392**, 122–128.

53. L. R. Baker, G. Kennedy, M. Van Spronsen, A. Hervier, X. Cai, S. Chen, L. W. Wang, and G. A. Somorjai, *J. Am. Chem. Soc.*, 2012, **134**, 14208–14216.

54. G. Li, N. Li, X. Wang, X. Sheng, S. Li, A. Wang, Y. Cong, X. Wang, and T. Zhang, *Energy and Fuels*, 2014, **28**, 5112–5118.

55. P. Gallezot and D. Richard, *Catal. Rev.*, 1998, **40**, 81–126.

56. M. Baerns, *Basic Principles in Applied Catalysis*, Springer Berlin Heidelberg, 2013.

57. J. Kijeński, P. Winiarek, T. Paryjczak, A. Lewicki, and A. Mikołajska, *Appl. Catal. A Gen.*, 2002, **233**, 171–182.

58. Q.-X. Cai, J.-G. Wang, Y.-G. Wang, and D. Mei, *AIChE J.*, 2015, **61**, 3812–3824.

59. V. V Pushkarev, N. Musselwhite, K. An, S. Alayoglu, and G. a Somorjai, *Nano Lett.*, 2012, **12**, 5196–5201.

60. P. N. Rylander, *Acad. Press inc.*, 1967.

61. V. Fajt, L. Kurc, and L. Červený, *Int. J. Chem. Kinet.*, 2008, **40**, 240–252.

62. H. S. Lo and M. E. Paulaitis, *AIChE J.*, 1981, **27**, 842–844.

63. R. A. Rajadhyaksha and S. L. Karwa, *Chem. Eng. Sci.*, 1986, **41**, 1765–1770.

64. K. F. Wong and C. A. Eckert, *Ind. Eng. Chem. Process Des. Dev.*, 1969, **8**, 568–573.

65. C. Reichardt and T. Welton, *Solvents and Solvent Effects in Organic Chemistry*, Wiley, 2011.

66. I. McManus, H. Daly, J. M. Thompson, E. Connor, C. Hardacre, S. K. Wilkinson, N. Sedaie Bonab, J. Ten Dam, M. J. H. Simmons, E. H. Stitt, C. D'Agostino, J. McGregor, L. F. Gladden, and J. J. Delgado, *J. Catal.*, 2015, **330**, 344–353.

67. E. Mullins, Y. A. Liu, A. Ghaderi, and S. D. Fast, *Ind. Eng. Chem. Res.*, 2008, **47**, 1707–1725.

68. E. Mullins, R. Oldland, Y. A. Liu, S. Wang, S. I. Sandler, C. C. Chen, M. Zwolak, and K. C. Seavey, *Ind. Eng. Chem. Res.*, 2006, **45**, 4389–4415.

69. M. J. Kamlet, J. L. M. Abboud, M. H. Abraham, and R. W. Taft, *J. Org. Chem.*, 1983, **48**, 2877–2887.